Numerical Simulations of Spirally Welded Steel Tubes Under 4-Point Bending

for the degree of:

Master of Science in Civil Engineering

Junzhi Liu
Student ID: 4274180
Email: liujunzhinl@126.com

Committee:

Prof. ir. F.S.K. Bijlaard	Delft University of Technology Steel, Hybrid, and Composite Structures Section
Ir. A.M. Gresnigt	Delft University of Technology Steel, Hybrid, and Composite Structures Section
Dr. ir. P.C.J. Hoogenboom	Delft University of Technology Structural Mechanics Section
Ir. S.H.J. van Es	Delft University of Technology Steel, Hybrid, and Composite Structures Section

Structural Mechanics Section, Department of Structural Engineering
Faculty of Civil Engineering and Geosciences
Delft University of Technology, Delft, The Netherlands

Abstract

This master thesis investigates the response of spirally welded steel tubes under 4-point bending deformation. Through the finite element simulations of a testing program undertaken at TU Delft Stevinlab II as part of the Combitube research project, the buckling behavior of sprirally welded tubes can be more clearly understood. The numerical simulation and buckling behavior of spirally welded steel tubes is discussed in this report, the existing experimental data from physical tests is compared with the help of finite elements analysis.

Linear elastic buckling analysis is carried out by finite element analysis. The results are characterized, and the response of tubes to buckling modes is investigated. the way how imperfection incorporated into non-linear analysis is explained. The results are compared to the results of the experimental data, analytical solution, and two different finite element models with ovalization-blocked supports. Statistical analyses are also performed to investigate the accuracy of the models.

Finally, parameter study is carried out in order to investigate the effect that various parameters have on the response of the tubes, in terms of both critical curvature and maximum moment. The parameters are characterized based on their influence on the tubes and their significance, recommendations for future investigation are addressed at the final chapter.

Acknowledgement

During my master research, I met a number of difficulties and problems. I am very lucky to have so many wonderful people around who helped and encouraged me. I would wish to thank my graduation committee, consisting of Prof. ir. F.S.K. Bijlaard, Ir. A.M. Gresnigt, Dr. ir. P.C.J. Hoogenboom and Ir. S.H.J. van Es. I would like to express my deep gratitude to Prof. Ir. F.S.K. Bijlaard who gave me patient guidance and comments. I would also like to also thank my daily supervisor Ir. S.H.J. van Es for continuous advice, feedback and help during the planning and progress of this research work.

Especially, I would like to thank Ir. S.H.J. van Es, who gave me guidance throughout my master research. Hope you will be succeed in continuing this project. Finally, I like to thank my parents, girlfriend and friends for their huge support and encouragement throughout my study.

Junzhi Liu
Delft, July 2015

Table of contents

List of symbols

I	-	moment of inertia	mm^4
k	-	curvature	mm^{-1}
k_{buc}	-	curvature at onset of buckling	/mm
k_{crit}	-	curvature corresponding to maximum moment	/mm
k_y	-	curvature at first yield	/mm
L	-	length of tube	/mm
M	-	section moment	kNm
M_{buc}	-	moment at onset of buckling	kNm
M_e	-	elastic moment	kNm
M_m	-	maximum moment based on currentt curvature in analytical model	kNm
M_{max}	-	maximum moment in moment-curvature relation	kNm
M_p	-	plastic moment	kNm/m
m_p	-	plate plastic moment	kNm/m
m_y	-	plate moment	kNm/m
n_p	-	plate plastic normal force	kNm/m
N_y	-	plate normal force	kNm/m
P	-	p-value (proability that regression coefficient = 0)	[-]
r	-	radius of tube from center to external layer	mm
R^2	-	coefficient of determination	[-]
S	-	arc length	mm
SE	-	standard error	[-]
SS	-	sum of squares	[-]
y	-	vertical deflection of curvature bracket	mm
ε, ε_{nom}	-	nominal (engineering) strain	[-]
ε_{true}	-	true strain	mm
$\varepsilon_{true,pl}$	-	true plastic strain	mm

a	-	horizontal half-ovalization of tube	mm
b	-	vertical half-ovalization of tube	mm
D	-	outside diameter of tube	mm
t	-	thickness of the tube	mm
ΔD	-	total horizontal ovalization of tube	mm
E	-	modulus of elasticity	MPa
f_{resid}	-	residual stress	MPa
f_y	-	nominal yield stress	MPa
$f_{y,ref}$	-	reference yield stress	MPa
f_t	-	ultimate tensile stress	MPa
F	-	observed value of F-significance	[-]
M_1	-	FEM with fix ending without ovalization	[-]
M_2	-	FEM with fix endind with longer length	[-]
ν	-	poisson's ratio	[-]
ρ	-	radius of curvature	mm^{-1}
σ_{nom}	-	nominal (engineering) stress	MPa
σ_{true}	-	true stress	MPa
d.f.	-	degrees of freedom of a statistical sample	[-]
Ap	-	the magnitude of imperfection height	mm

1 Introduction

1.1 Background

Full scale 4-point bending tests is carried out at TU Delft as part of physical testing of European research project (Combitube). Combined wall system, a parallel system, is an economical structure to resist high force as retaining wall. This system consists of tubular piles and steel sheet piling. Tubes, working as primary element of combined walls, can be longitudinally welded tube, seamless tube or more economical spirally welded tube due to much lower production cost.

Figure 1: Combined sheet and pile wall (Van Es, 2013)

The spirally welded tube is welcomed as an economical strcutural element and its application has received more and more interest, using the strain based design method. The buckling behavior of spirally welded tubes plays an important role in the area of large diameter tubes. As expected, imperfections in the spirally welded tubes are expected to be different with other tubes like longitudinal tubes due to the specific production process. The influence of imperfection on the buckling behavior on spirally welded tube and differences between the behavior of spirally welded and longitudinally welded tubes loaded in bending is an important subject.

1.2 State of current research

The first moment-curvature relationships for thin tubes under bending in the elastic phase was prompted by Brazier (1927), accounting for deformable cross sections. He also defined the instability condition, known as limit point instability: the situation when the moment-curvature relationship reaches a maximum, after the occurrence of the limit point instability, tube starts to collapse due to excessive ovalization. Further studies by Ades (1957) have extended the previous analysis into the plastic range.

Neither author considered the effect of initial imperfections, both of their work have suggested that the initial imperfections would have a significant influence on capacity as D/t ratio increases. Maximum moment and the associated curvature are determined as a function of material and geometric parameters. The curvature at which short wave-length bifurcations occur is also determined. The results are compared with behavior in the elastic range. The effect of initial imperfections were not taken into account in his study, though it is noted that for thin shells a significant reduction in load capacity due to initial imperfections would be expected, however for thicker shells the effect of the imperfections may not be quite so important. Ades introduced his method based on the total energy and work of bent and deformed tubes due to bending in plastic range can be determined by using the this method. The cross section of the tubes can be also determined based on the longitudinal curvature and the bending moment that the tubes can carry can be also calculated.

Experimental investigation into the plastic buckling of cylindrical tubes subjected to bending moments at the ends is reported by Reddy (1979). Suitable parameters characterizes and defines the buckling moment may be represented are first discussed, The tests were conducted on stainless steel and aluminum alloy tubes and results are compared with analytical results for the collapse of cylinders under pure bending, and uniform axial compression. The mode of deformation of the cylinders is discussed and the experimental strains in comparison with those of others for tests on axially compressed cylinders as well as cylinders in pure bending. He concluded that the deviation between the experimental and theoretical results was caused by the presence of imperfection.

Series of tests have been made on aluminium and steel tubes which buckle in the elastic range, under pure bending. Gellin (1980), had used as a buckling criterion the extreme fibre compression strain, rather than stress, since strain or curvature is easier to estimate in a practical situation. There is an investigation of the observed modes of deformation have led to the conclusion that the ripples, rather than the small amount of ovalization, were the primary cause of the collapse in tests. Further, the sine-wave nature of these ripples has led to the hypothesis that tubes behaved as imperfect cylinders, the imperfections in which gave rise to a steady growth of these ripples which eventually leads to collapse.

Various models were proposed in literature to describe the effect of imperfection and maximum bending moment. Most of the analysis are based on considerations of local equilibrium of the shell element. Wierzbicki (1997), introduced the alternative approach based on minimum postulate. The effect of strain hardening is also included in an iterative way, a closed form solution is derived for the moment curvature characteristic and maximum moment, which include all geometrical and material parameters. The present acquisition can be used for a rapid and accurate estimate of plastic bending response of thick metal tubes.

In 2002, Karamanos (2002) presented paper that he investigated the structural response and buckling of long thin-walled cylindrical steel shells, which are subjected to bending moments, focusing on their stability design. The cylinder response is characterized by cross-sectional ovalization, followed by buckling (named "bifurcation instability"), which occurs on the compression side of the cylinder wall. Using a nonlinear finite element technique the bifurcation moment is calculated. The post-buckling response is determined, and imperfection sensitivity with respect to the governing buckling mode is examined. The results show that the buckling moment capacity is affected by cross-sectional ovalization in contrast to Jirsa et al. (1972) and Reddy (1979) who concluded that ovalization has very little effect on the ultimate capacity of tubes in bending.

Gresnigt (1986) carried out a complete analytical design procedure for pipes of any D/t ratio and any combination of loadings, which is a strain-based design procedure, taking into account plastic deformation capacity. The limit state of the pipe is defined in terms of a maximum deformation, in the form of a critical curvature. This is much preferable to the stress-based design found in EN1993-1-6, however, the applicability of this procedure to tubes of higher D/t ratios is in doubt (Gresnigt et al. 2010), and is currently being investigated by Van Es.

In 2013, Van Es (2013), found that during the buckling tests, the tested tubes buckle at production related dimples. Although at the spiral welds also geometrical imperfections are present, they have not been the location of buckling except one tube. Also the residual welding stresses near these welds apparently did not have a decisive influence. Buckling tests have been carried out with fifteen tubes. While the buckling form of the thicker tube was clearly a plastic buckle, the failure of the thinner tube was more abrupt. The influence of geometrical imperfections, residual stresses and Bauschinger effect needs more attention. Based on the qualitative and quantitative analysis of the buckling tests, Van Es (2013) reveal that a strain based design code seems more appropriate for this type of tube in the considered D/t range. The concept of investigating post buckling behavior by angular rotation of the buckled hinge (θ) is introduced. This eliminates any influence of the test setup geometry and purely gives information of the capacity of the buckled cross section.

The differences between the behavior of spirally welded and longitudinally welded tubes loaded in bending is investigated by Van Es (2013), influence of initial imperfections, structural details and production method is studied and discussed. Except the tubes with structural details like girth welding, a comparison of the buckling location with the initial scans clearly shows that all tubes buckle at production related dimples. The study also found that the difference between critical local (curvature measured locally) and global curvature (average curvature over the middle section) is much larger for the spirally welded pipes. Spirally welded pipes seem to have a lower critical strain for thicker walled specimens. This effect is smaller when the comparison is made for local curvatures instead of global curvature. Finally, the study shows that in longitudinal direction, both spirally welded and longitudinally welded pipes may show a Bauschinger effect, but others have shown no effect at all.

With regard to the development of finite element analysis in this studied area, (Giordano et al. 2008, Guarracino et al. 2008), tried to develop a model which allows ovalization at loading support in three ways. The first approach is to increase the length of model, which will enable the ovalization at supports less restrained. Second method is to use a coupling with local coordinates. The third way is to use rigid plate by contact element to introduce the load. Lee et al. (2012) found that when diameter to thickness ratio increases the impact of girth weld is also increasing. It is also suggested by Lee et al. (2012) that the combined effect of ovalization and buckle failure occurs in thick tubes. The thermal loading and temperature dependent material is also introduced in model. , Karamanos (2005) carried out study with internal pressure, imperfection and plasticity are not included. In 2011, Karamanos (2011) extend the range of D/t ratio to 240 and 300, the buckle formed with wrinkle. He also found that imperfection reduced capacity and concluded that the behavior of inelastic extreme slenderness tube is similar as an elastic tube.

1.3 Goal of the research

The goal of the present study is to complement the physical testing that was carried out at TU Delft with finite element modeling to improve the understanding of the buckling behavior of spirally welded steel tubes with different D/t ratios (65<D/t<120).
The model for this project existed now by Pueppke (2014) is relatively accurate to predict the maximum moment and critical curvature of the tested tubes. However, the way that the loads apply to the model is not consistent with real situation, the moment is applied to the end of the tube to simulate the constant moment distribution over the length in the middle between support and the support is not correctly modelled, ovalization of the support is fully constrained. Thus, the model which is more close to the reality, allowing ovalization at support is modelled and the buckling behavior is investigated relating to the geometry and initial imperfections. This numerical model was used to answer the following questions:
1. What is the influence of initial imperfections on the local buckling capacity of the tubes?
2. Do additional parameters such as the steel yield strength, D/t ratio have significant impact on the capacity of the tubes?

2 Experimental program

2.1 Overview of test set up

The experimental program carried out at Delft University of Technology involved full scale bending tests of 13 spirally welded steel tubes and 2 longitudinally welded steel tubes. Overview of the test set up and side view can be seen in Figures 2 and 3.

Figure 2: Overview of test set up for tube in bending (Van Es, 2013)

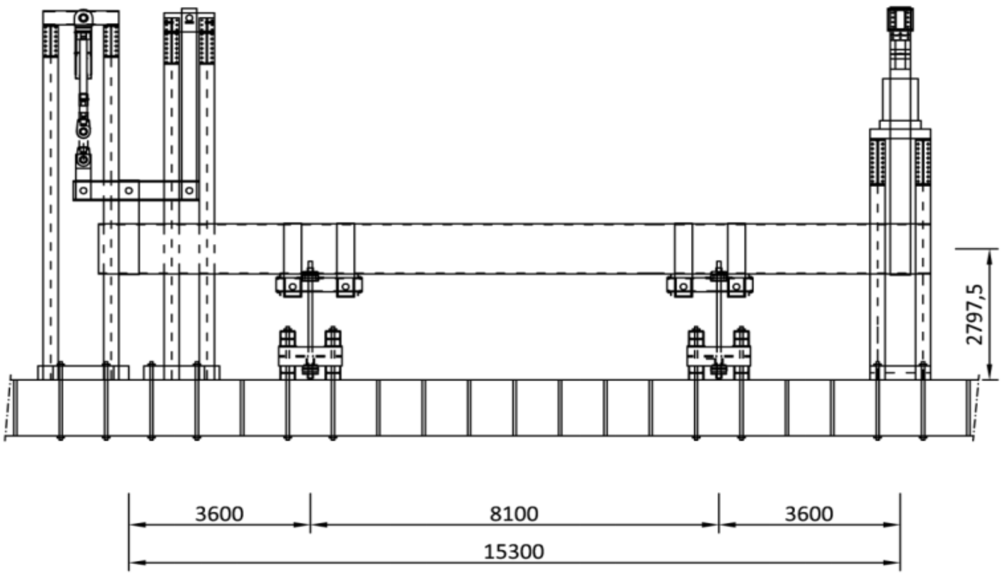

Figure 3: Schematic side view for test set up (Van Es, 2013)

The 4-point bending test consists of a specimen with two middle supports and two outer supports. For this experimental study, the middle supports were chosen to be a hinge with a fixed zero displacement while non-zero displacement would be applied to the outer supports. Hydraulic actuators applied the displacement to lift the end of the tube, two supports in the middle are fixed in vertical direction to simulate four point bending test, which allow pure bending and constant moment and curvature distribution according to the theory in the middle length between two inner support. Fifteen tests are performed at TU Delft, thirteen of these are spirally welded tubes and two additional tests were longitudinally welded tubes. An overview of the testing programme is presented in Table 1.

Table 1: Summary of tubes used in experiments

Tube	D×t [mm]	D/t [-]	Fabrication	Type	Grade
Tube 1	1066×16.4	65.1	Spiral	Plain	X70
Tube 2	1067×9.0	118.3	Spiral	Plain	X60
Tube 3	1069×9.0	118.7	Spiral	GW	X60
Tube 4	1065×9.2	116.2	Spiral	Plain	X60
Tube 5	1070×9.0	118.4	Spiral	Plain	X60
Tube 6	1066×16.3	65.3	Spiral	CCW	X70
Tube 7	1068×16.3	65.4	Spiral	GW/CCW	X70
Tube 8	1068×9.1	117.4	Spiral	Plain	X60
Tube 9	1069×16.3	65.4	Spiral	Plain	X70
Tube 10	1070×13.1	81.6	Spiral	GW/CCW	X52/X60*
Tube 11	1068×12.9	82.8	Spiral	Plain	X52/X60*
Tube 12	1069×9.1	117.1	Spiral	GW/CCW	X60
Tube 13	1070×9.2	116.3	Spiral	GW	X60
Tube 14	1068×9.8	108.8	Longitudinal	Plain	X60
Tube 15	1070×14.8	72.3	Longitudinal	Plain	X70

Each tube is featured with its diameter, type of welding/production procedure. The pictures below are some structural details by different welding process. Spirally welded tubes (see Figure 4) are produced from coil material by series of rollers, a continuous tube is welded by cold forming, new coil is connected to the former coil if the coil runs out. The coiled steel is decoiled and leveled through cold rolling before processing by rollers. The edges of the plate material are beveled and prepared for welding. The spots visible in the figure 4 are locations where thickness measurements are taken, which can be seen in the Figure 3. Girth welds (see Figure 6) are used to join two separate pipes together, coil connection welds (see Figure 5) are utilized to join two coils of steel together, connecting the former coil material with new coil by means of butt weld.

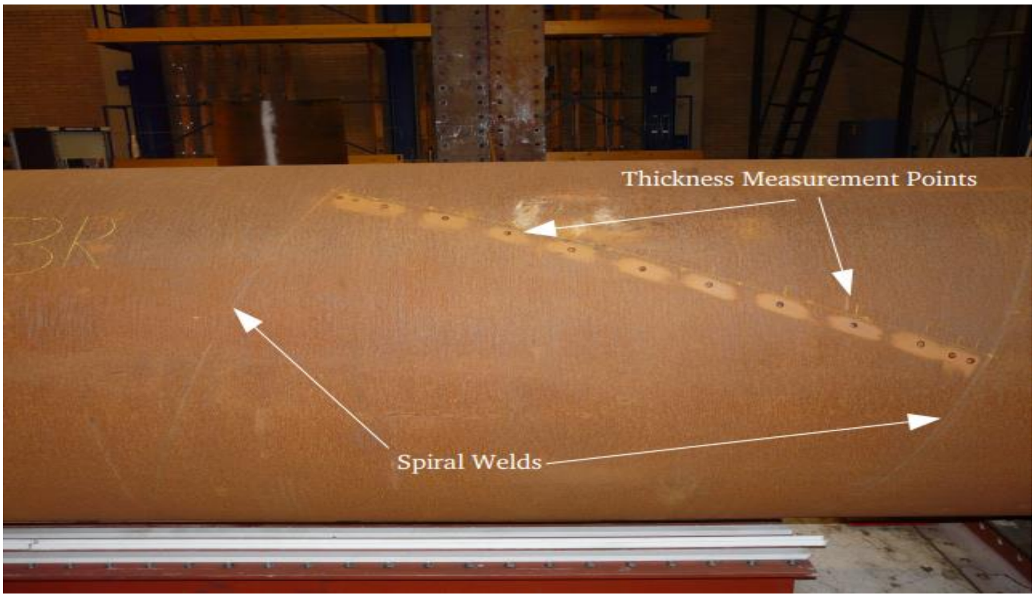

Figure 4: Spiral welds on tube surface (Van Es, 2013)

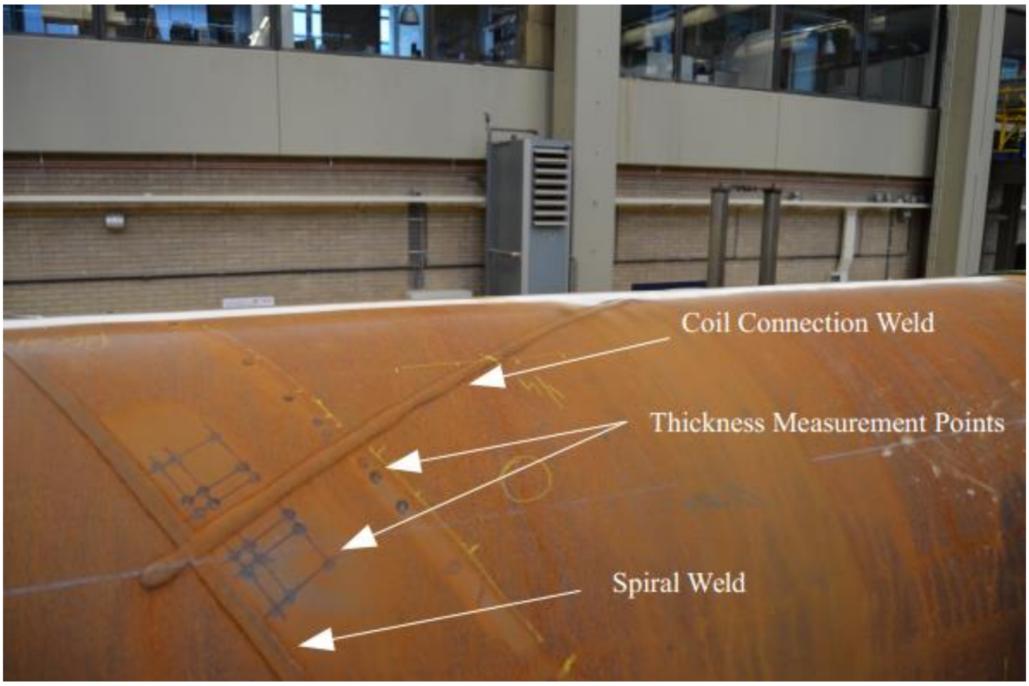

Figure 5: Structural detail at coil connection welds (Van Es, 2013)

Figure 6: Structural detail at girth welds (Van Es, 2013)

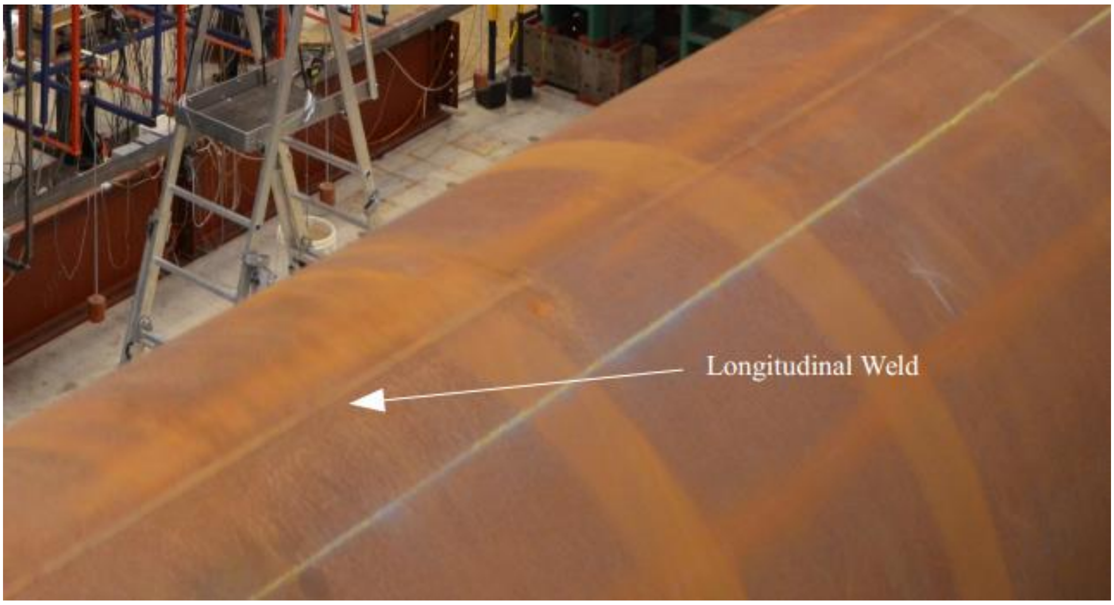

Figure 7: Example of longitudinal welds (Van Es, 2013)

2.2 Test parameters

2.2.1 Initial imperfection measurements

A special laser car in Figure 9 is used to make a line scan to obtain the tube initial geometry. The results were used to decide how to orient the tubes in the test setup. The tube surface is inspected and cleaned before scanning to obtain more relatively accurate scan result. An overview of the test set up is in Figure 9.

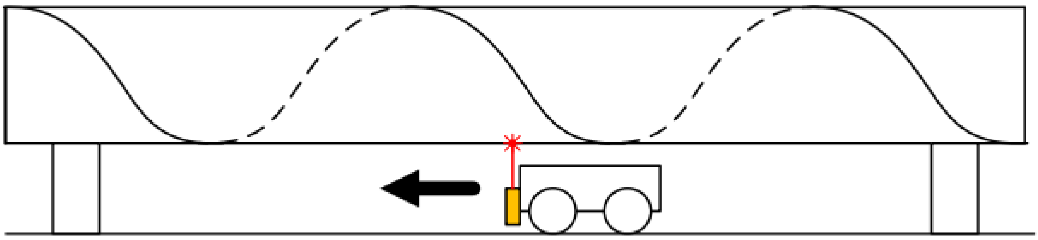

Figure 8: Initial geometric imperfection measurement (Van Es, 2013)

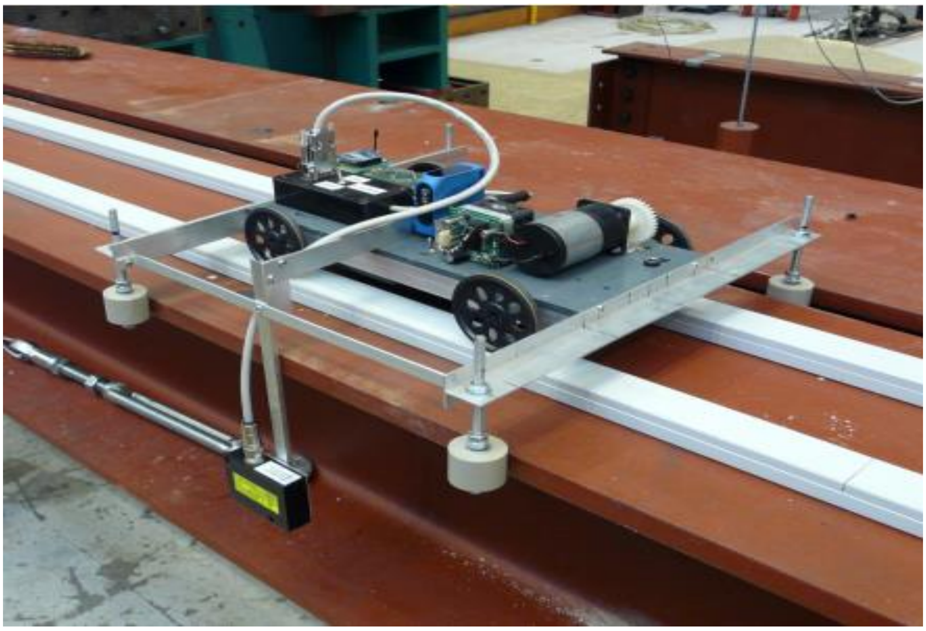

Figure 9: Laser car on suspended rail to scan initial geometric imperfection (Van Es, 2013)

2.2.2 Continuous and discrete measurements

Apart from the test for initial imperfection, other parameters including applied forces, applied displacements and measurement of ovalization at eight locations along the constant moment area of the specimen and measurement of compressive and tensile strains.

After each load step the test was paused to perform laser scans. Three laser carts performed scanning, two of them scan similar to the scans of the initial imperfections, one of them scans inside and the other one scan outside (see Figure 10). The third laser cart makes circular scans of cross sections of the tube at regular intervals. After buckling, by using this scan full 3D scan of the pipe of buckling cross section can be manifestly described.

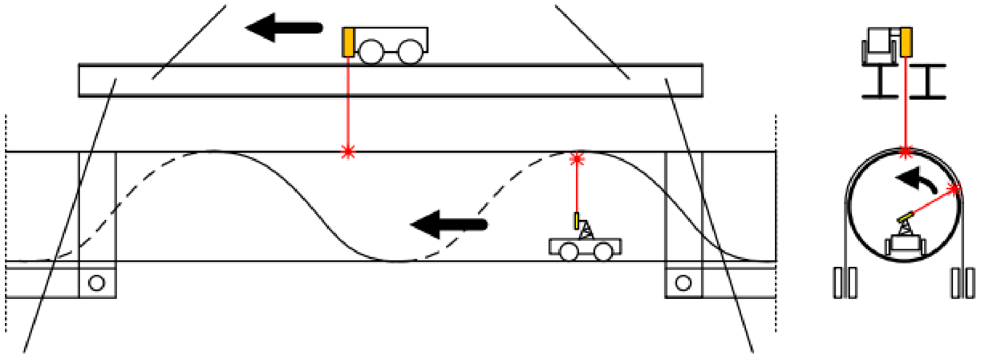

Figure 10: Laser cars scanning both outside and inside for discrete measurements (Van Es, 2013)

2.2.3 Ovalization measurements

Apart from the laser cart scanning to investigate the ovalization of the tube during experiment, ovalization bracket is also placed along the tube in the middle between two inner supports.

Figure 11: View of ovalization bracket(red)

The horizontal ovalisation of the specimen was monitored at eight locations in the area of constant moment, denoted as Ov1 to Ov8 from left to right. The side view of the ovalization bracket can be seen in Figure 11 and exact dimension is in Figure 12. The mechanism how ovalization bracket works can be seen in Figure 13.

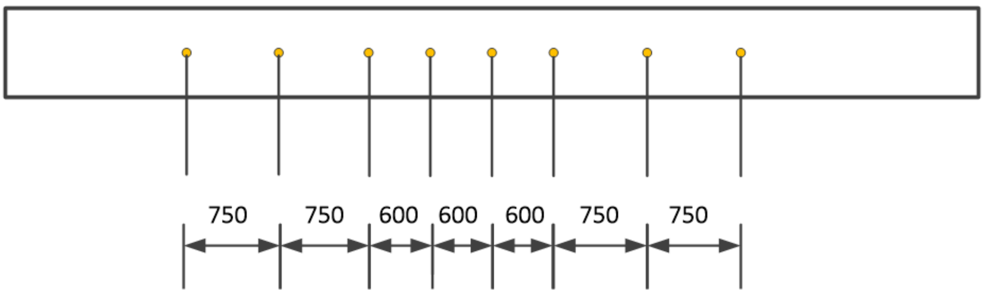

Figure 12: Horizontal ovalization bracket overview and dimensions

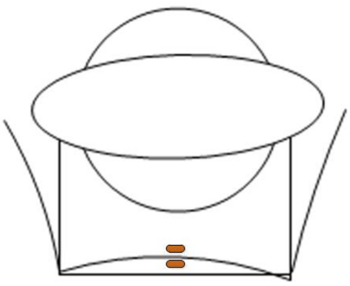

Figure 13: Lay out of the ovalization bracket and strain gauge

2.2.4 Curvature measurements

Quite amount of curvature data can be obtained from test. An average curvature (k_{avg}) over the middle section can be determined by measuring displacements of the tube at the four supports. The curvature was also measured locally by means of brackets (k_1, k_2, k_3), and one large bracket which spanned all these local measurements (k_{all}). Final results were sensitive to where the curvature localisation and local buckling occurred within the length of the bracket. Furthermore, final curvatures at brackets away from where the local buckling occurred, gave less final curvature, due to the concentration of deformation in the buckled cross section (Van Es, 2013).

Curvature can be defined in several ways. In an elastic beam, the definition is straightforward and comes from basic geometrical relationships. According to the Euler–Bernoulli beam theory, it defined as below:

$$M = EIk_{elastic} \tag{1}$$

Where:
M = section moment
E = modulus of elasticity
I = moment of inertia
$k_{elastic}$= elastic curvature

The central angle is equal to the total rotation of the middle section, the central angle of an arc θ divided by the arc length is defined as curvature ,where ρ is the radius of curvature. S is the length of middle tube where the curvature is calculated. Elastic curvature can be derived by following (see Figure 14)

$$S = \rho\theta \tag{2}$$

$$k_{elastic} = \frac{1}{\rho} \tag{3}$$

$$k_{elastic} = \frac{\alpha_1 + \alpha_2}{S} \tag{4}$$

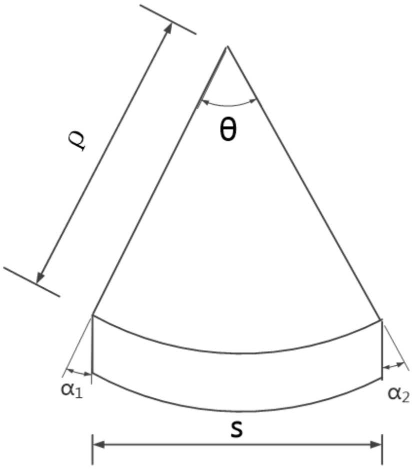

Figure 14: Definition of curvature

Curvature bracket along the tubes can be seen in Figure 15, and schematic view of dimensions of curvature brackets (see Figure 16).

Figure 15: Curvature bracket overview along the tubes neutral line (blue)

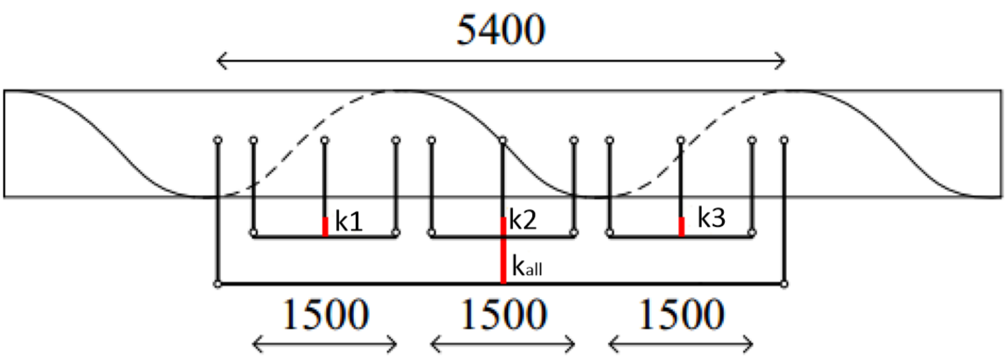

Figure 16: Schematic view of dimension of curvature brackets (Van Es, 2013)

With regard to the two outer curvature brackets, the method to calculate the curvature, calculated by distance change between bracket as defined as y here, bracket length is defined as b, thus the curvature is obtained as following in Figure 17, because $y^2 << b^2$, therefore the curvature can be obtained as follows:

$$(\rho\text{-}y)^2+(\frac{b}{2})^2=\rho^2 \tag{5}$$

$$2\rho y=y^2+\frac{b^2}{4} \tag{6}$$

Because $y^2 << b^2$, then formula 6 can be simplied as,

$$\rho=\frac{b^2}{8y} \tag{7}$$

$$k=\frac{1}{\rho}=\frac{8y}{b^2} \tag{8}$$

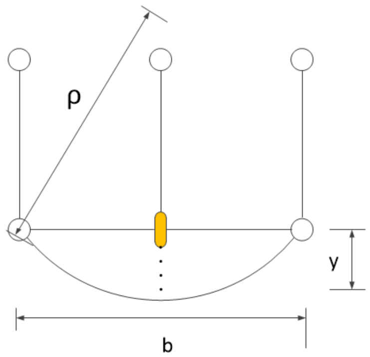

Figure 17: Geometry of the curvature brackets

3 Bending and ovalization model

3.1 Ovalization models

Ovalization is defined as the change in diameter of an initially round tube during bending, ΔD is defined as 2a or 2b as shown in Figure 18. Elastic ovalization model has been derived by Reissner and Weinitschke (1963), plastic ovalization models has been derived by Gresnigt in 1986.

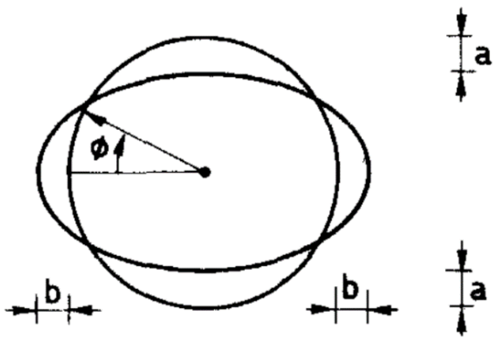

Figure 18: Ovalization of tube due to bending (Gresnigt, 1986)

3.1.1 Elastic ovalization

The ovalization model is given in the following series. The exact ovalization value can be obtained for any given curvature. However, such a model is only valid in elastic stage, derived by Reissner and Weinitschke (1963), parameter a and b is the half amount of ovalization of tube horizontally and vertically (see Figure 16).

$$a_{i,elastic}=r(\frac{\alpha_i^2}{12}+\frac{\alpha_i^4}{960}-2059\frac{\alpha_i^6}{168*7200}+..\ ) \quad (9)$$

$$b_{i,elastic}=r(\frac{\alpha_i^2}{12}+71\frac{\alpha_i^4}{8640}+44551\frac{\alpha_1^6}{7560*7200}+..) \quad (10)$$

$$\alpha_i=\frac{k_i r^2}{t}\sqrt{12} \quad (11)$$

3.1.2 Plastic ovalization

The plastic part of ovalization can be calculated according to (EN1993-4-3, Pipelines).

$$a_{pl}=\left(a_{qd\text{-}pl}+a_{qi\text{-}pl}+a_{c\text{-}pl}\right)\bullet(1+\frac{3a}{r}) \quad (13)$$

where
$a_{qd\text{-}pl}$ is the plastic part of the ovalisation caused by direct soil load including rerounding.
$a_{qi\text{-}pl}$ is the plastic part of the ovalisation caused by indirect soil load including reronding.
$a_{c\text{-}pl}$ is the plastic part of the ovalisation caused by the applied curvature including rerounding.

$$a_{c\text{-}pl}=-2\frac{r^3}{t}\bullet\varphi\bullet(k-ke) \quad (14)$$

where

$$\varphi=1-(\frac{0.5\cdot c_2}{g})^2 \quad (15)$$

The plastic ovalization is same as in elastic stage, the displacement of the horizontal displacement is same as vertical displacement:

$$a_{i,plastic}=b_{i,plastic} \quad （16）$$

3.2 Bending models

An analytical solution for the bending moment of the tube is given in EN1993-4-3, Pipelines. Yield moment of the pipe cross section is:

$$M_e=\pi r^2 t f_y \quad （17）$$

The plastic moment is :

$$M_p=4r^2 t f_y \quad (18)$$

The resistance under pure bending is given by :

$$M_m=M_{pr}\sqrt{1-(\frac{V}{V_{pr}}+\frac{M_t}{M_{tpr}})^2} \quad （19）$$

$$M_{pr} = g\,h\,M_{pl} \tag{20}$$

$$M_{tpr} = g\,M_{tp} \tag{21}$$

$$M_{tp}= \frac{2}{\sqrt{3}}\,\pi r^2 t f_y \tag{22}$$

$$h=1-\frac{2}{3}\frac{a_i}{r} \tag{23}$$

$$g=\frac{c_1}{6}+\frac{c_2}{3} \tag{24}$$

$$c_1=\sqrt{4-3\left(\frac{n_y}{n_p}\right)^2-2\sqrt{3}\cdot\left|\frac{m_y}{m_p}\right|} \tag{25}$$

$$c_2=\sqrt{4-3\left(\frac{n_y}{n_p}\right)^2} \tag{26}$$

n_p is the plastic normal force per unit width of shell wall

$$n_p = tf_y \tag{27}$$

The yield axial force n_y per unit width of shell wall due to earth pressure and internal pressure,

$$n_{y,i}=n_{yq}+n_{yk}+n_{yp} \tag{28}$$

m_p is the full plastic moment per unit width of shell wall,

$$m_p = 0.25t^2 f_y \tag{29}$$

The yield moment m_y per unit width of plate due to directly transmitted earth pressure Q_d and the indirectly transmitted earth pressure (support reaction) Q_i is defined as m_{yq}, and the m_{yp} is the yield moment per uint width of plate due to internal pressure, k is the curvature of the tube.

$$m_y = m_{yq} + m_{yk} + m_{yp} \tag{30}$$

The yield moment m_y per unit width of plate related to full plastic bending resistence,

$$m_{yk}=0.071 \cdot M_m \cdot k \cdot \eta \tag{31}$$

$$\eta=1+\frac{a}{r} \tag{32}$$

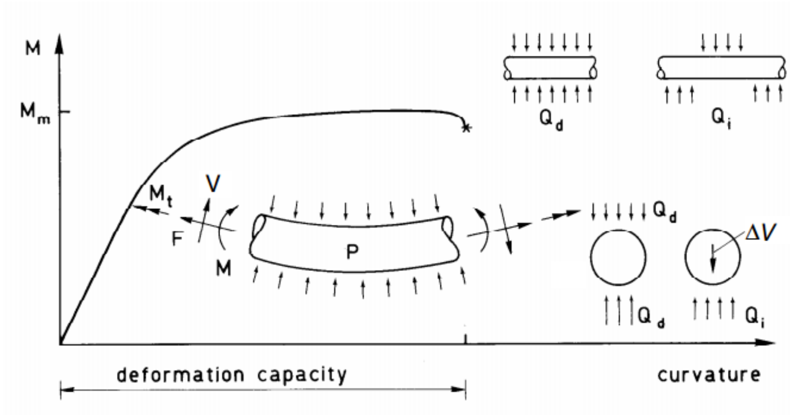

Figure 19: Tube under combination loads (EN1993-4-3)

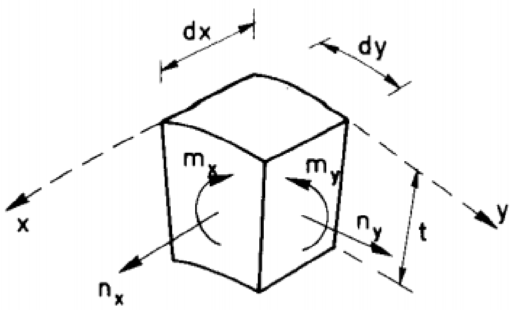

Figure 20: Plate forces sign direction definition

The critical value of the compressive strain could be obtained by the follows:

$$\varepsilon_{cr}=0.5\ \frac{t}{D}-0.0025 \tag{33}$$

The curvature correspond to this strain is

$$k_{crit} = \frac{\varepsilon_{cr}}{\frac{D}{2}} \tag{34}$$

In the section 5 , the results of the tested tubes from numerical models are discussed and comparison is made. It is note that the moment-curvature diagrams and ovalization-curvature diagrams are fomulated based on Matlab syntax provided by Pueppke (2013). They are used as a reference line in section 5. The simplified bending and ovalization model is given in this section, which can be used in future research.

4 Full scale finite element model

A finite element analysis is employed to investigate the buckling and post-buckling behaviour of the tubes under 4-point bending. For this purpose, a numerical model using the finite element package ABAQUS is established. The displacement control and the force applications in the numerical model is built in consistent with experimental situations.

The tube features a length of 16500 mm, supported by four supports, with two supports at the end of the tube and two inner supports in middle, each of them was divided into two parts in order two avoid stress concentration and pre-mature buckling near middle supports (discussed in section 4.2). When building the numerical model, outside diameter of the entire tube is constant, in case of the tubes with structural details averaged diamater based on the geometric dimensions of the tube cross section of the real tubes. The girth and coil connection welds were incorporated by partitioning the tube geometry into sections and applying the corresponding material and geometric properties separately. The material properties of the welds themselves were not considered. Both girth and coil connection welds were modeled as being normal to the longitudinal axis by the partition the tube along the cross section, perpendicular to z-axis. Full measured material models were applied as well as residual stress distributions. Geometrical imperfection should be applied on the perfect tube as the initial imperfection before the nonlinear analysis, imperfections were applied by performing elastic buckling analyses scaled to the height of the measured imperfections.

4.1 Material properties

After construction of the tube geometry, material properties should be applied first to determine the physical properties of the objective. The process of building the FEA model, true stress and true strain are required to fill in the material property section. Since the results from the steel tensile and compression specimen test are the engineering stress and engineering strain, and should be converted as input for the numerical models. The true stress and true strain can be obtained from the equation listed below:

$$\sigma_{true}=\sigma_{engineering}\left(1+\varepsilon_{engineering}\right) \quad (35)$$

$$\varepsilon_{true}= ln\left(1+\varepsilon_{engineering}\right) \quad (36)$$

$$\varepsilon_{true,pl}=\varepsilon_{true}-\frac{\sigma_{true}}{E} \quad (37)$$

The material test is carried out at TU Delft, both tensile and compression test is performed for test specimen, four directions of specimen is tested: longitudinal direction, circumferential direction and parallel and perpendicular to the spiral weld. All tubes engineering stress strain relation has been listed in Appendix 1 based on averaging the stress strain relation in four direction. In order to obtain a more accurate comparison, there is also python formed syntax to get more smooth material data averaged from four directions which can be seen in Appendix 3.

4.2 Initial imperfection and linear elastic buckling analysis

4.2.1 Approach and method

The measurement approach has been described in the initial imperfection measurement section before. In this part, it is mainly focused on the method of how to introduce the initial imperfection to ABAQUS. Imperfections are analyzed and divided into several categories.

4.2.2 Initial imperfection results

Initial geometry of the spirally welded tubes show regular dimple pattern and can be linked to the spiral welding production process (Van Es, 2013). This regular behaviour can also be seen in the lines of tube 1 in Figure 21. The figure clearly shows the sharp peaks of the spiral welds. The characteristic imperfection was taken as the height of this dimple near buckling, which was then introduced into the numerical models by scaling one of the elastic buckling modes as an initial assumption. The imperfection height incoporated in non-linear buckling analysis can be seen in Figure 21.

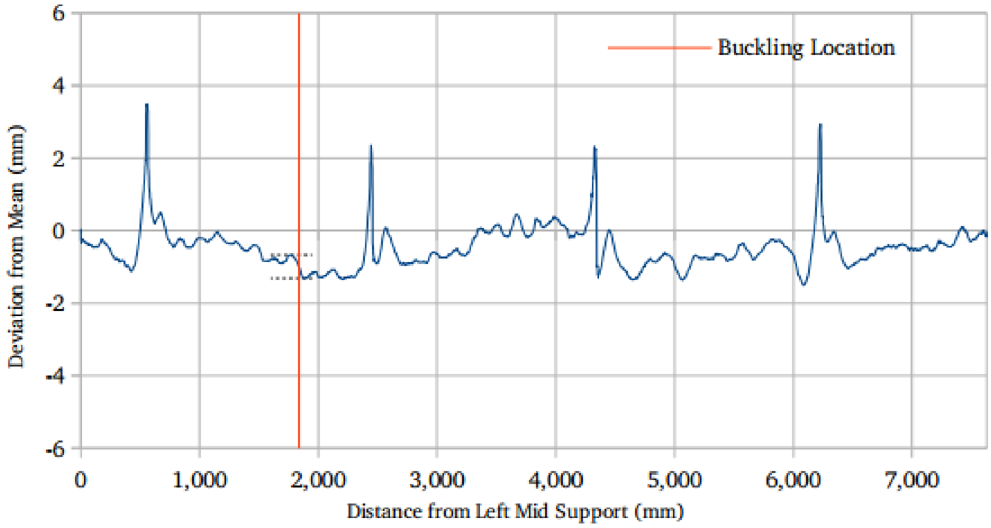

Figure 21: Initial imperfection and buckling location for tube 1

In figure 22, it can be seen that the intial geometry pattern for tube 6 is different from tubes with regular dimple pattern. This can be caused by structural details such as girth welds or coil connection welds. The intermediate imperfection is chosen between two largest imperfection near place where buckling occurs (see Figure 22).

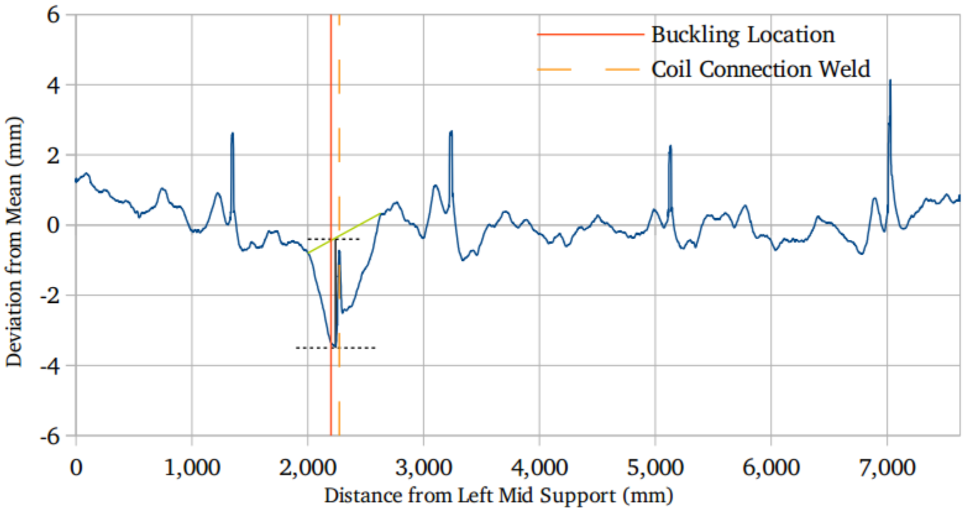

Figure 22: Initial imperfection and buckling location for tube 6

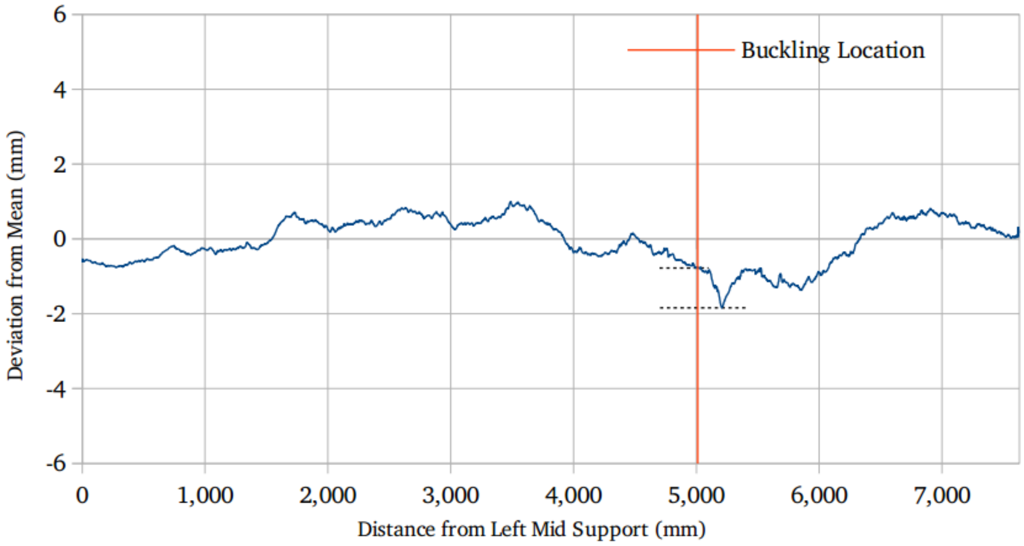

Figure 23: Initial imperfection and buckling location for tube 14

Tubes 1, 2, 4, 8, 11, failed at production related dimple induced by processing technique used to bend coiled plates into a tubular shape. Such dimple height will be incorporated by scaling corresponding critical representative linear buckling mode. With regard to the tubes which featured with girth weld and coil connection weld, tubes 3, 10, 13 failed at girth weld feature, and tube 6 failed at coil connection weld tube 12 failed at technique related dimple. For these tubes failed at coil connection weld, the imperfections were taken as the height of the intermediate imperfection between largest imperfection near buckling. The initial profiles of Tubes 14 and 15 are different from the other tubes because the production process is quite different. There are no any welds or tooling marks in the profiles. The profile of Tube 14 does not appear to have a regular pattern (see Figure 23), while Tube 15 is characterized by a series of regular waves caused by manufacturing process (see Figure 24). For tubes 14 and 15, imperfection near buckling location is incoporated in non linear analysis.

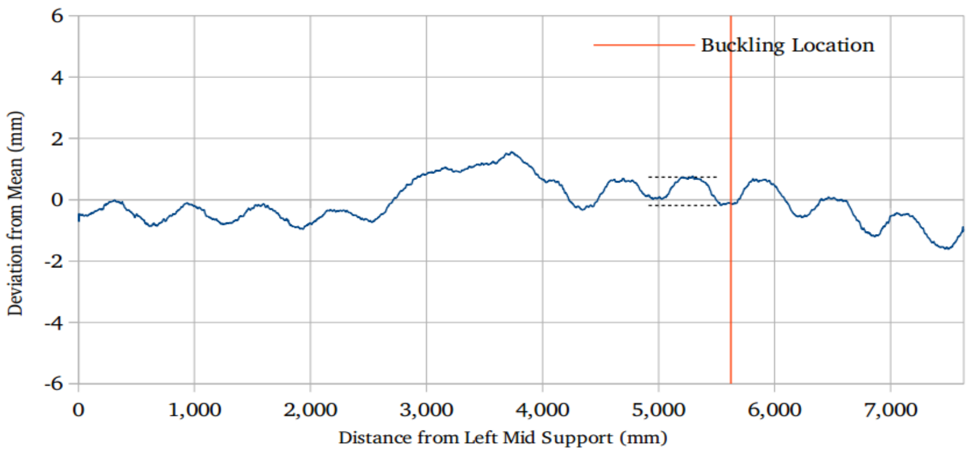

Figure 24: Initial imperfection and buckling location for tube 15

4.2.3 Imperfection value chosen in model

In this section, the imperfections measured in the tubes were analyzed, and the characteristic imperfections were described for each type tube (see Table 2). For the plain spirally welded tubes, the imperfections were introduced into the numerical models based on characteristic dimple height imperfections observed near the buckling locations. For the tubes 3, 6, 10, and 13, three different kinds of imperfection are calculated and the intermediate imperfection is incorporate into non linear analysis based on the measured imperfections at the welds. For tube 12, an imperfection was introduced based on the characteristic dimple imperfection observed at the buckling location. Finally, for the longitudinally welded tubes, imperfections were simply introduced based on the initial profiles observed near the buckling location.

Table 2: Imperfection values for different kinds of tubes

Tube	**Type**	**Imperfection height (mm)**	**Imperfection/thickness**
1	Plain	0.645	0.039
2	Plain	0.871	0.097
3	GW	2.820	0.310
4	Plain	0.636	0.069
5	Plain	0.718	0.078
6	CCW	3.100	0.191
7	GW/CCW	2.450	0.150
8	Plain	1.070	0.117
9	Plain	2.010	0.123
10	GW/CCW	2.850	0.218
11	Plain	0.465	0.036
12	GW/CCW	1.160	0.127
13	GW	1.780	0.193
14	Plain	1.066	0.109
15	Plain	0.926	0.063

4.2.4 Elastic buckling analysis

Before the nonlinear buckling analysis of the full scale model, the elastic buckling behavior of thin wall tube is obtained with shell finite element analysis in ABAQUS. Imperfections in the form of elastic buckling modes are typically used for analysis purposes because structures are generally most sensitive to imperfections in the form of a eigenmode. The buckling load or shape is generally used to determine the nonlinear buckling strength and final deformation of structures. An important aspect should be mentioned that the imperfection shape from linear elastic buckling analysis should be representative enough. It means if the geometry and dimension of node and element size are fit well with the imperfection displacement, a smooth amplitude of imperfection shape can be obtained by distributed nodes and elements (see Figure 25), if the element size or node geometry are not matched well with displacement of linear elastic buckling mode, some information of buckling mode will not correcty expressed and incoporated in non-linear buckling analysis, as shown in Figure 25, imperfection shape fomulated based on coarse distribution of hollow circle simply reflect main trend. It is noticeable that in the figure of first eigenmode of tube 9, the node is not perfectly matched with imperfection displacement, but it is acceptable due to clear explanation of elastic buckling tendency without losing decisive information.

The nature of the eigenmodes and eigenvalues was qualitatively observed for all tubes and investigated in detail for tube 9. This was done by incorporating imperfections to neutral line model of tube 9 in the form of several critical buckling modes. Imposed imperfections were scaled based on the actual measured imperfections. Linear buckling analysis can obtain the linear, elastic solutions of buckling shapes with respect to various buckling modes. Usually, the buckling shape is used for the description of the imperfections when the maximum amplitude of the imperfection is known but its distribution is not known. This shape is result in a displacement distribution normalized with 1 mm as the maximum value.

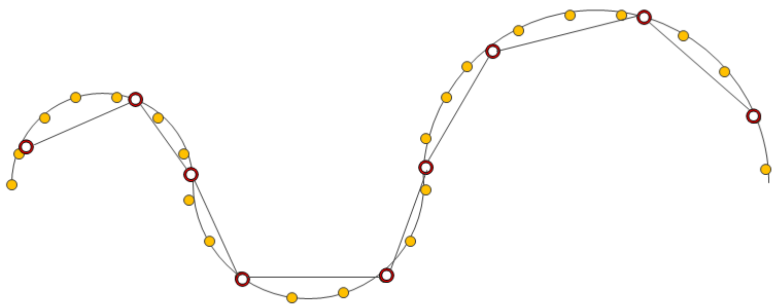

Figure 25: Node fitting situation in elastic buckling displacement

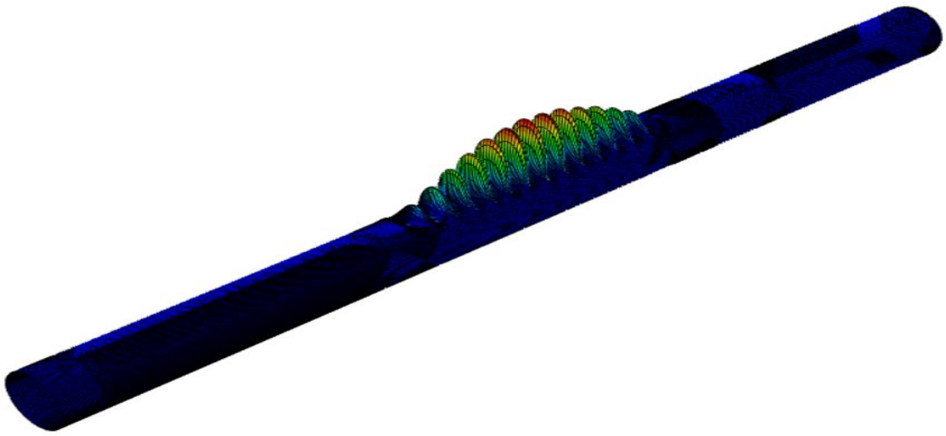

Figure 26: 1st eigenmode of Tube 9

As can be seen in Figure 26, the eigenmode obtained from linear elastic analysis featured with long length appearance between two inner suppors of middle supports. It is one of the most critical and typical shape depending on the final deformed shape after incoporating this imperfection shape. Final deformed shape followed with one buckling location in the middle of the tube is required. Except for tubes which includes structural details, the suitable imperfection shape from linear elastic buckling mode should be incoporated into non linear buclking analysis in consistent with the real situation where buckling occurs.

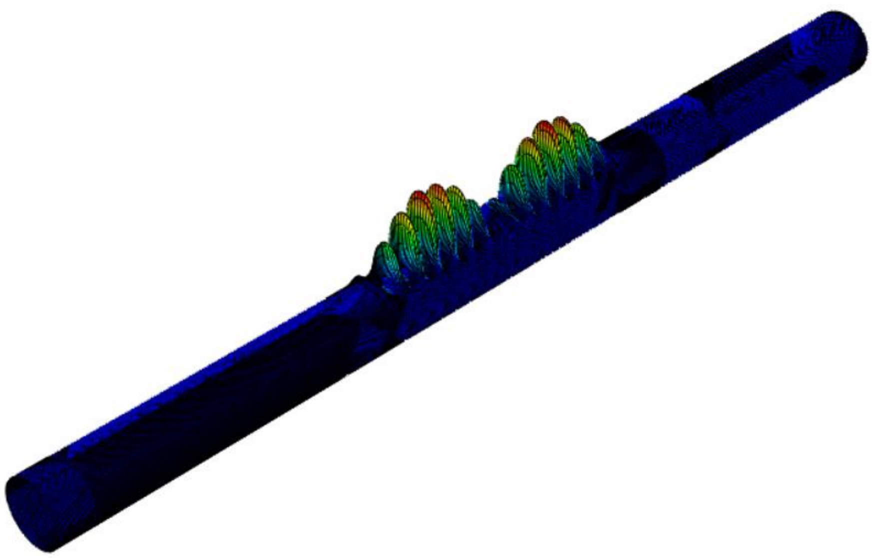

Figure 27: 5th eigenmode of Tube 9

Figures 27 and 28 show diffenrent linear elastic buckling imperfection shapes. Two higher peaks are included in 5th eigenmode, while three higher peaks are located in the middle of 6th eigenmode from linear elastic imperfection shape, the length between the seprerate peaks depends on the imperfection shapes and wavelength, the eigenmode is chracterized with sine and cosine function with different phases.

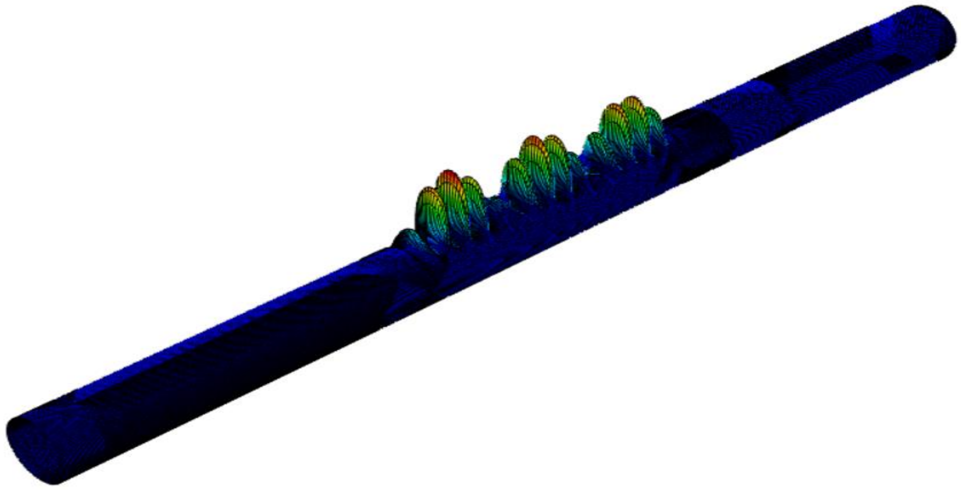

Figure 28: 6th eigenmode of Tube 9

The x-axis line represents the center of the compression face of the tube, and the blue lines represent the deviation from the centerline, normalized to a amplitude of 1mm. The orange line represents the center of the tube. Other plain tubes were found to have similar buckling modes. The first 6 buckling modes of tube 9 are shown in detail in Figure 29.

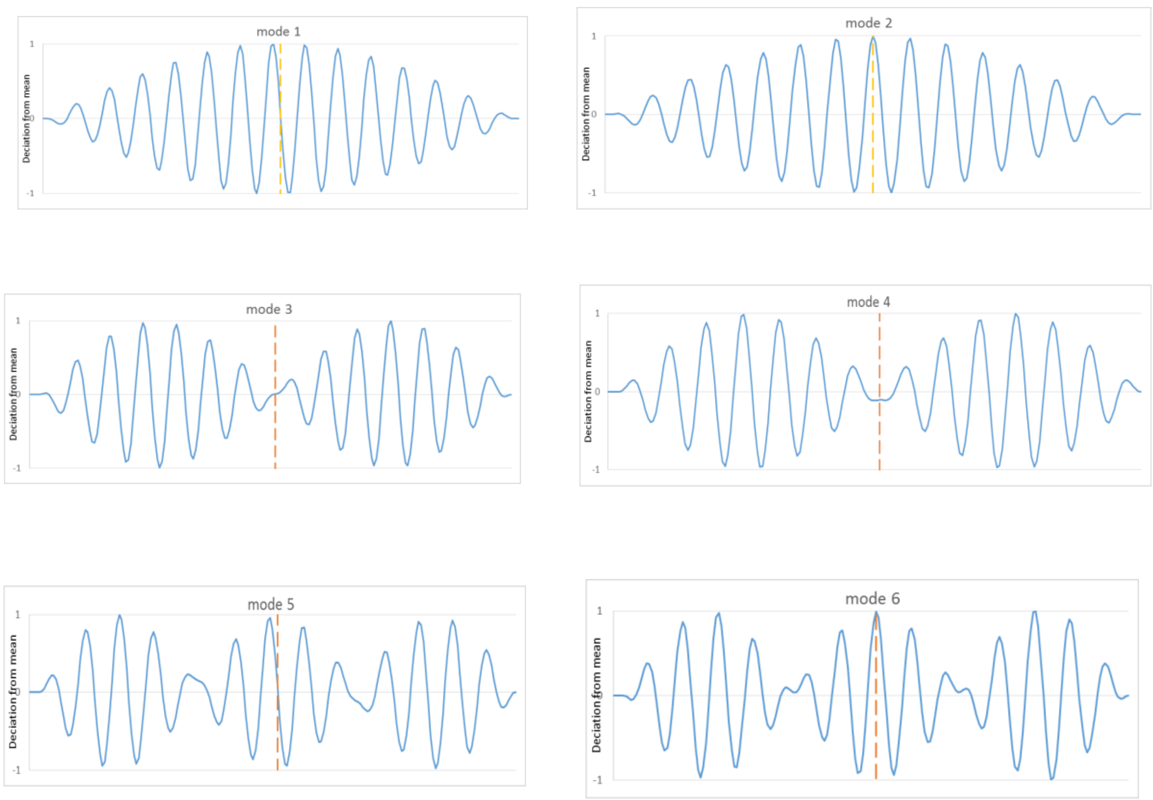

Figure 29: Buckling modes of the Tube 9

4.2.5 Discussion

In this case the length of the imperfection shape incorporated in non-linear buckling analysis is short between two inner supports of middle supports, which features with one large amplitude in the middle is the one incoporated in non linear analysis. In fact, most experimental tubes generally failed at middle of tubes from experiment, suggesting that the antisymmetric buckling mode is dominant, which can result in one buckling occuring in middle. An important aspect is one buckling mode was found to be a cosine function, which is an even (symmetric) function and one was found to be a sine function, which is odd (antisymmetric).

In this report, the antisymmetric buckling mode described by sine function will be used for clear and reasonable imperfection shape.

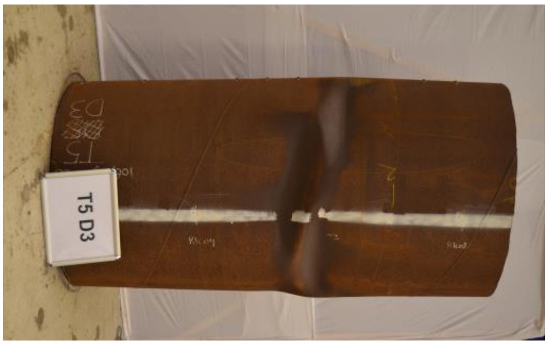

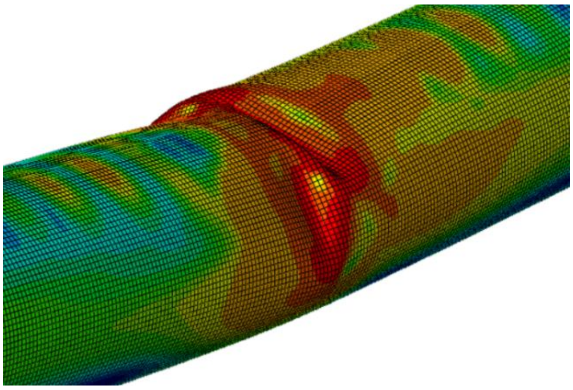

Figure 30: Deformed shape from experiment

In this section, the influences of various elastic buckling modes on the buckling behavior of tube 9 have been investigated. Based on the results, it is concluded that tube 9 is not sensitive to the imperfection combinations, the antisymmetric mode is the most realistic and clear one. It was further assumed that this analysis was valid for all of the other plain spirally welded and longitudinally welded tubes.

4.3 Support condition refinement

The deformation required for bending is applied at the two outer supports in four-point bending test. Loads are applied by a strap which evenly spreads the applied force. At the middle supports each load is introduced by two straps. The outer strap of these two introduces ⅔ of the load, while the inner strap introduces ⅓ of the load (see Figure 31). By doing this, the risk of buckling at the load introduction is minimized. Therefore, numerical model is modelled according to the real situation that each of the middle supports is divided into two supports in consistent with experimental set up .

Such supports modelling can be seen more clearly in section above. During the experiment, it is observed that the opening and closing of strap lead to large ovalization at the support where the load is applied than ovalization in middle for first test of tube 1. Since the problem has been adjusted in experiment by setting up parallel supporting system, it indicates that the support which allow free ovalization is required in numetical simulation.

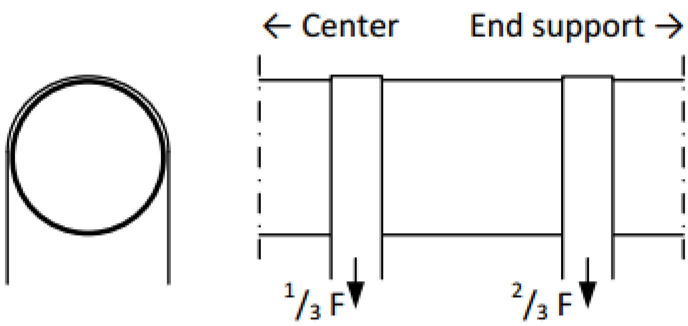

Figure 31: Force application at middle support

4.3.1 Approach and method

In the experimental program, the displacement of the tube was fixed by using thin steel straps which support the tube at the middle support. This thin straps are strong enough to act as supports, but flexible enough to allow the tube to ovalize. There are two ways to account for condition at middle supports in a finite element model. By coupling the movement of the surface to the control point same as reference point through continuum distributing coupling, which allows relative movement of the surface coupled. Continuum distributing coupling constraint between the reference point and a set of nodes is used to simulate the behaviour of the straps. By using this constraint conditions, the straps can rotate themselves as well.

Two coupling approach is discussed here,the first coupling approach is to make a circle by partition the surface of tube, after that the movement of the circle (red line in Figure 33) is coupled to the control point in the centroidal of the tube, and this control point also called reference point is positioned at 2/3 distance from inner support and 1/3 distance from outter support. (named “ring coupling method”, see Figure 32). Three-dimension view can be seen in Figure 33.

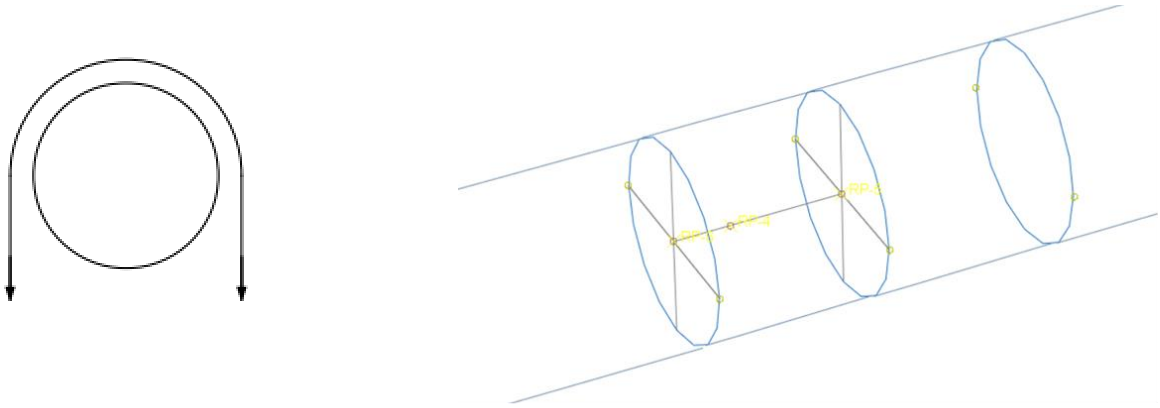

Figure 32: First coupling method "ring coupling"

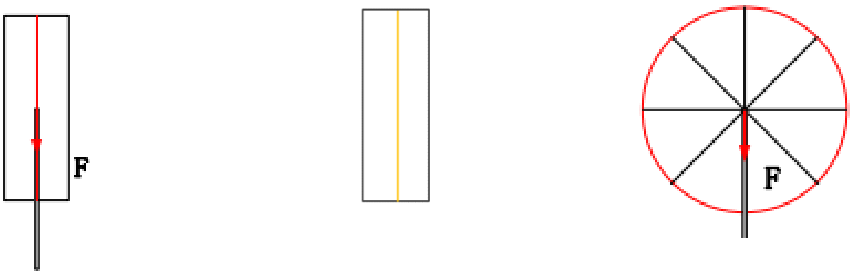

Figure 33: From left to right is front view top view and sectional view for ring coupling

The second coupling way which can be seen Figure 34 is to mark out two short line at the location of neutral line of the tube. The length of the short line is equal to the width of the strap couple to the control point locating in centroidal of the tube. Three dimension view of this approach can be seen in Figure 35.

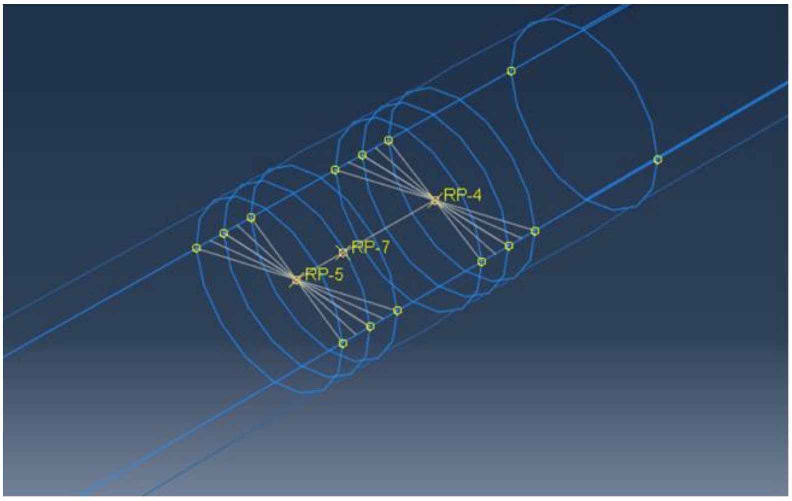

Figure 34: Second coupling method "Neutral line coupling"

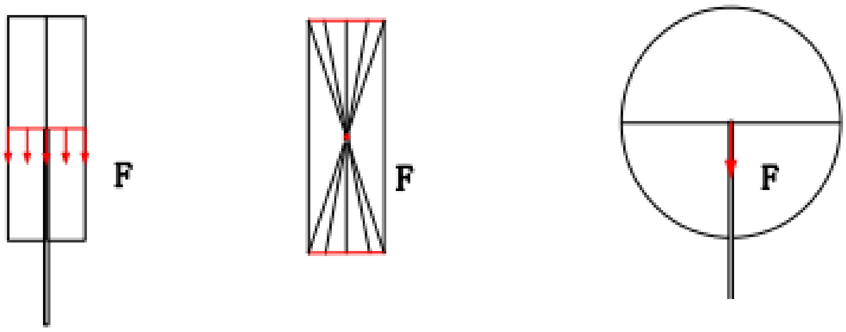

Figure 35: From left to right is front view top view and sectional view for neutral line coupling

4.3.2 Support modelling analysis

In this section, some comparison groups are made to determine suitable linear buckling imperfection shape which can be incorporated into non-linear analysis which can modify the stress concentration situation near the load introduction support in the middle for two coupling methods. Imperfections in the form of elastic buckling modes are often used for analysis purposes because shell structures are most sensitive to imperfections in the form of a buckling mode. Another important subject is discussed here, the influence of the geometry of the elastic imperfection.

The first and second comparison group are built using the first coupling method, (named by the author "ring coupling method") while, the third and fourth group using second coupling method (named by the author "neutral line coupling") .

***ring couple**: 1st Group*

Figure 36: Non linear analysis without imperfection for tube 1

Figure 36 shows that when elastic linear imperfection is not incoporated into non-linear buckling analysis, there are two bucklings taking place in the middle of the tube near supports where loads are applied. The results of the Von Mise stress also indicates that the place near middle supports suffers stress concentration which negatively influence the stability of the structure, and the final deformed shape is not the targeting deformed shape.

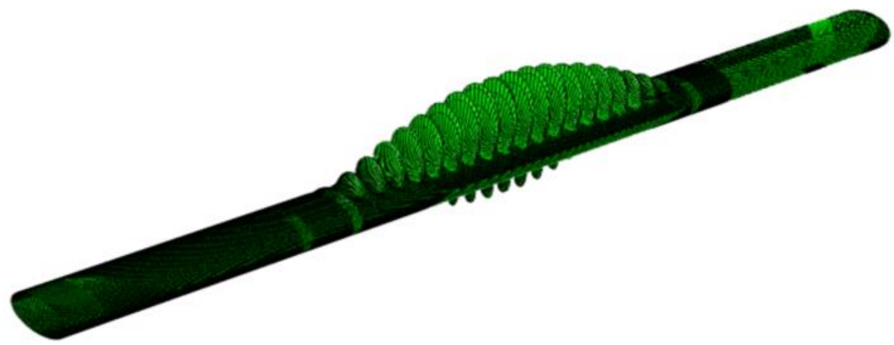

Figure 37: Linear analysis of Imperfection zone right between supports for tube 1

It is hard for a perfect shell element to compute convergence during instability analysis in finite element analysis. The elastic linear buckling analysis is used to predict the initial imperfection of thin shell and the corresponding buckling shapes. After elastic linear buckling analysis, the imperfection mode is obtained and incoporated in non-linear buckling analysis. Since the first eigenmode features with one highest peak along the length of imperfection shape right between the middle supports (see Figure 37), the first eigenmode is introduced in non-linear buckling analysis.

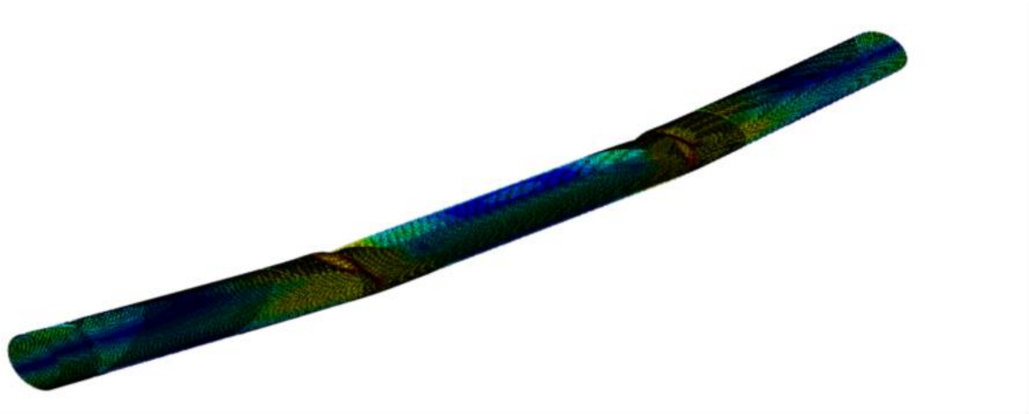

Figure 38: Deformed shape by non linear analysis for tube 1

From the analysis above for the first group, it can be observed that buckling still occur at the middle supports (see Figure 38) even after incoporating the linear elastic imperfection shape and stress concentration at load introduction support still exists, it is concluded that linear buckling mode right between middle support possibly lead some negative effect in terms of stress concentration, because it is too close to the middle support due to relative longer length of imperfection shape, and another possibility is that the impact of such coupling method is more governing than the introduced imperfection.

ring couple: *2nd Group*

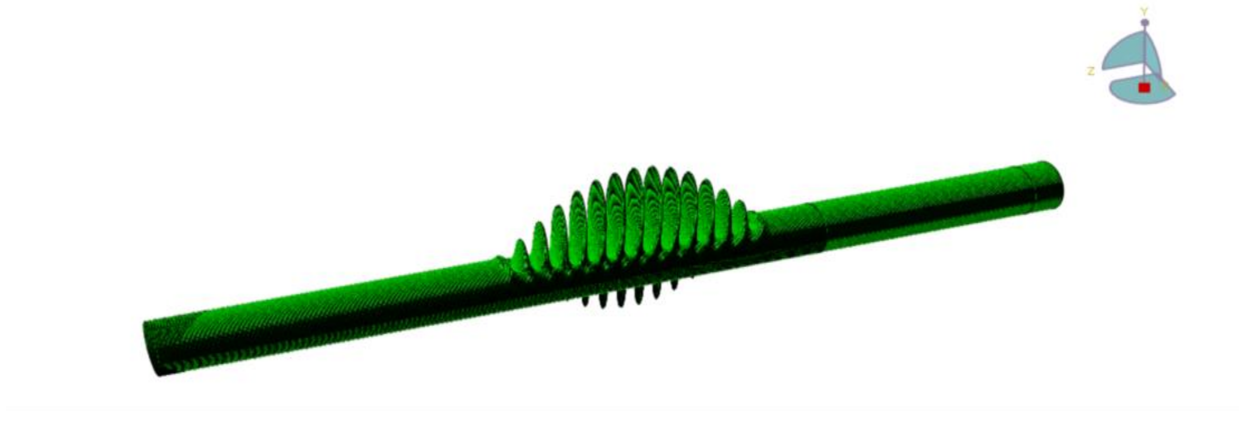

Figure 39: Linear analysis of Imperfection zone shorter between supports for tube 1

With this problem in mind, some adjustments have been made to elastic linear buckling model, the control point (explained before) where the boundary condition assigned is moved along U3 direction to make the length of imperfection shorter than the length in first case, which the length is right between the middle supports. It is a necessary assumption when the imperfection shape is more shorter between supports, more clear linear buckling mode concentrating in middle will result in final deformed shape with one buckling in middle.

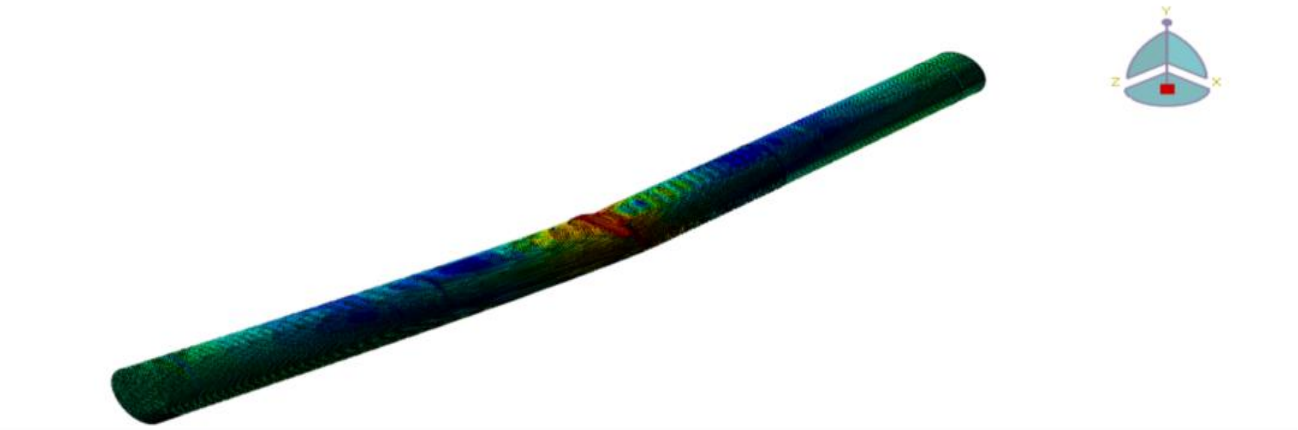

Figure 40: Deformed shape by non linear analysis for tube 1

By comparing second group it can be clearly seen that by adjusting the geometry of the control point where the boundary condition is assigned to get a shorter imperfection eigenmode with shorter length in the middle between middle support, the problem of stress concentration is modified properly, and the buckling position is more reasonable (see Figure 40), taking place in the middle. However, the stress concentration is still noticeable, another possiblility to modify this problem is the second coupling method which has been introduced above, then the third and fourth group is compared below.

Neutraline couple: *3_{rd} group*

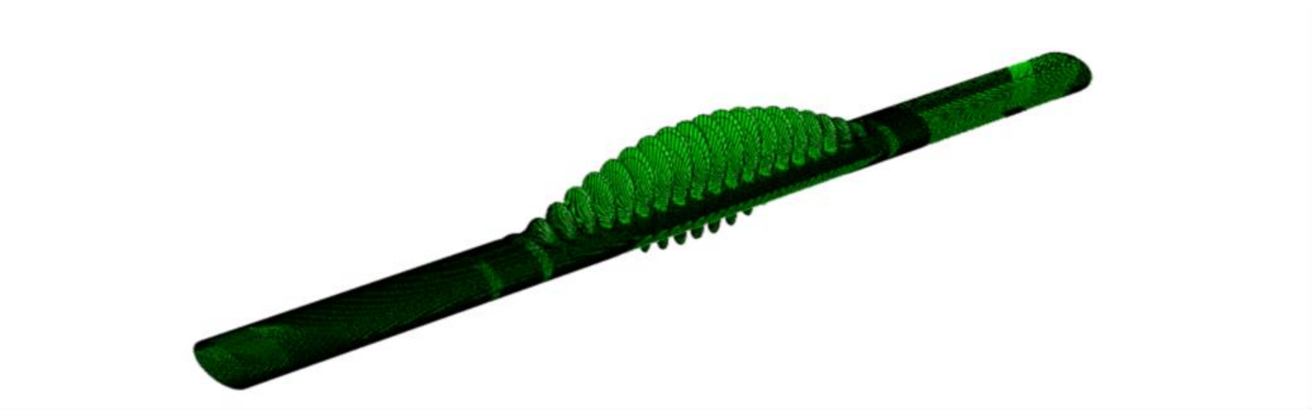

Figure 41: Linear analysis of Imperfection zone right between supports for tube 1

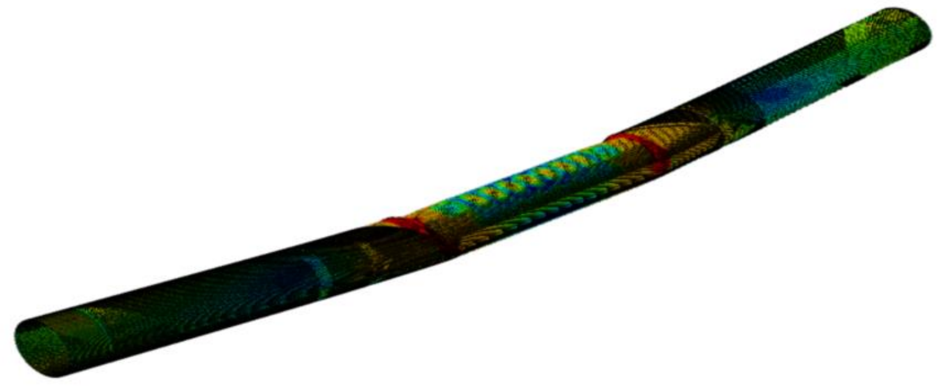

Figure 42: Deformed shape by non linear analysis for tube 1

For the third comparison group it can be observed stress concentration is significantly reduced by neutral line coupling, however the buckling position is not correct, two buckling occurs in the middle between middle support (see Figure 42). In fact, there is considerable modification for problem of stress concentration. The method used here is similar as the method used for ring coupling, moving the control point more close to middle to obtain a shorter linear buckling mode. Finally, as expected, one reasonable buckling shape is obtained (see Figure 44).

Neutral line couple: *4_{rd} group*

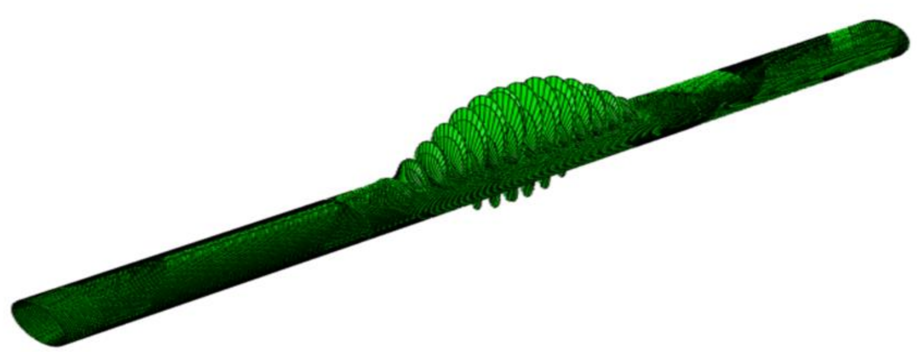

Figure 43: Linear analysis of Imperfection zone right between supports for tube 1

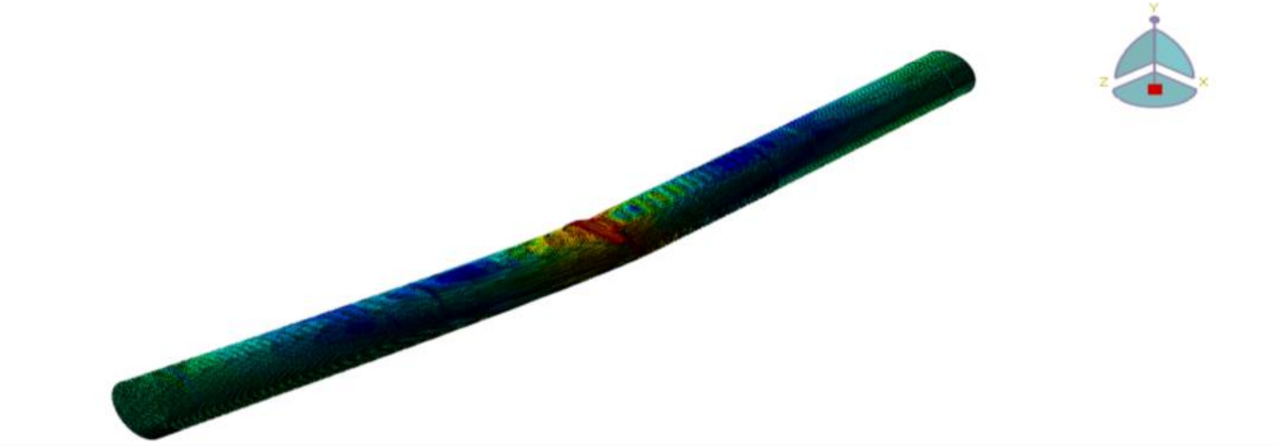

Figure 44: Deformed shape by non linear analysis for tube 1

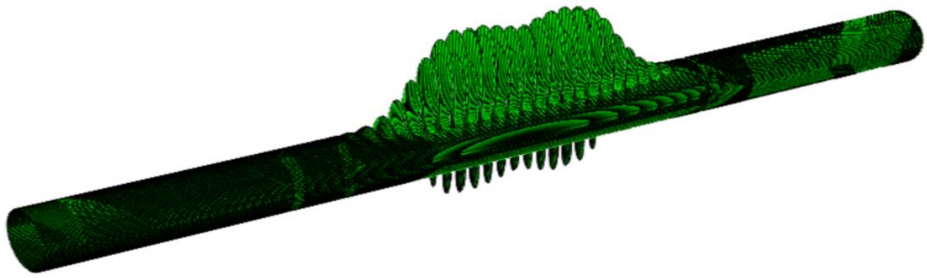

Figure 45: Improper Linear analysis of Imperfection zone by neutraline coupling method

There is a need to pay attention that the linear buckling mode from neutral line coupling method is not correct there are two humps in the middle (see Figure 45). As long as the mesh size and node numbering of the model analyzed in linear and non-linear buckling analysis are kept the same, the imperfection shape obtained from linear buckling analysis can be incorporated into non linear analysis. Thus, the linear buckling mode from ring couple is corporated into non linear analysis by neutral line coupling.

Linear buckling mode incorporated in non-linear analysis is the shorter imperfection buckling shape between middle supports, which can not only get more reasonable result, it also modifies stress concentration and makes it closer to the real situation. Therefore, neutraline model will be used further.

4.4 Boundary condition and loading

Models in this report feature displacement controlled boundary conditions, two displacement are applied at the end of the tube, and controlled to lift the tube moving upwards. Aaccording to the real situation, two supports in the middle are fixed in the vertical U2 direction and the displacement is applied at the end of the tube in U2 direction perpendicular to the x-z plane to obtain 4-point bending situation.

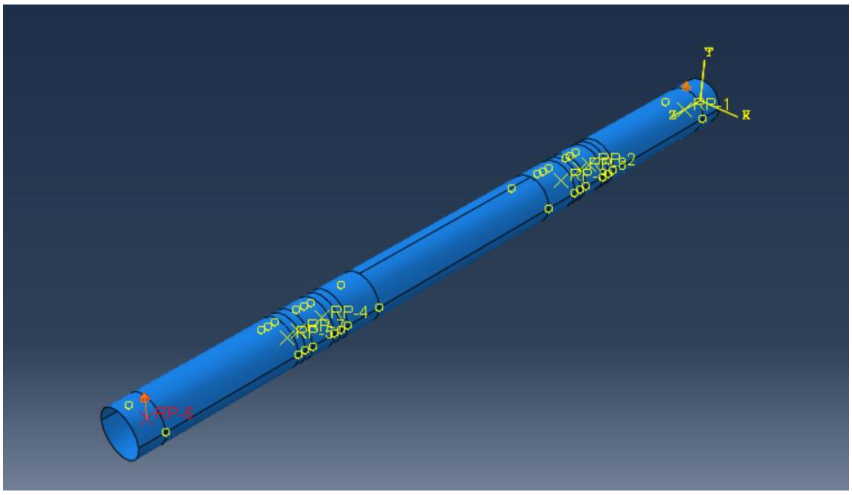

Figure 46: Boundary condition of the model

Figure 47: Simplified view of the boundary condition for middle supports

The middle of tube can simplified in Figure 47. When the ends of the tube are lifted up, the two supports in middle are fixed in U2 direction to have static equilibrium in U2 direction. Since the model is a three dimensional model, both supports in middle should rotate freely around U1 axis, UR1 is set to be free for both middle supports. Right support in middle is allowed to slide along U3 direction. The tube is also restrained from rotating about the y and z axes at both supports. The displacement is set in U2 direction at end support to the actual dimension according to the real test or the displacement leading to buckling occurs. Continuum distributing coupling is applied at all supports, as explained in detail in section 4.3.

4.5 Element type and mesh size

4.5.1 Approach and method

Convergence study plays an important role to ensure the actual mesh size for the further analysis. There are two aspects for mesh convergence study, the mesh size and total calculation time of analysis. The results can be viewed in the following graphs.

Neutral line coupling of Tube 1, meshed with S4R elements (Linear quadrilateral S4R, a 4-node doubly curved thin or thick shell, reduced integration) was used to investigate the influence of mesh size, including the full material model, the residual stresses, and the measured imperfection height. Imperfection was introduced in non-linear buckling analysis, both M_{max} and k_{crit} were used as convergence criteria.

It is important to note that the size distribution is constant along the full tube, and shell element is used. Compared with other two dimensions of the tube, length and diameter of the tube, thickness is very small, therefore, shell element is used and studied in this report. Shell elements are used to model structures in which one dimension, the thickness, is significantly smaller than the other dimensions. (ABAQUS/Standard Analysis User' s Manual, 6.12)

4.5.2 Comparison of convergence for mesh size

Mesh convergence is a crucial factor for the finite element model and is closely related to the accuracy of the entire simulation. Finer mesh size means the more numbers of element and the more calculation memory storage and time. The influence of mesh size on the tube capacity shown in Figure 48. These figures show a logarithimically decreasing trend for both k_{crit} and M_{max}. Mesh size was found to influence k_{crit} significantly more than M_{max} .

I t was found that changing mesh size from 25mm to 20mm result in a less than 1.1% decreasing, k_{crit} value obtained from models are very close. However, computing time increases. Observing mesh size 35mm, it is noticed that the error of result is also not large but less computing expenses, when the mesh size goes to 45mm, there is significant error comparing with 20mm size (see Figure 49). It is concluded that the increasing in accuracy was not worth the additional computing time, especially considering the fact that simply switching from S4 to S4R elements also result in a change in k_{crit} , 25mm or 35mm are both acceptable. Balancing between accuracy and computing time, 25mm size mesh is chosen.

It was found that changing mesh size from 25mm to 20mm result in a less than 1.1% decreasing, k_{crit} value obtained from models are very close. However, computing time increases. Observing mesh size 35mm, it is noticed that the error of result is also not large but less computing expenses, when the mesh size goes to 45mm, there is significant error comparing with 20mm size (see Figure 49). It is concluded that the increasing in accuracy was not worth the additional computing time, especially considering the fact that simply switching from S4 to S4R elements also result in a change in k_{crit} , 25mm or 35mm are both acceptable. Balancing between accuracy and computing time, 25mm size mesh is chosen.

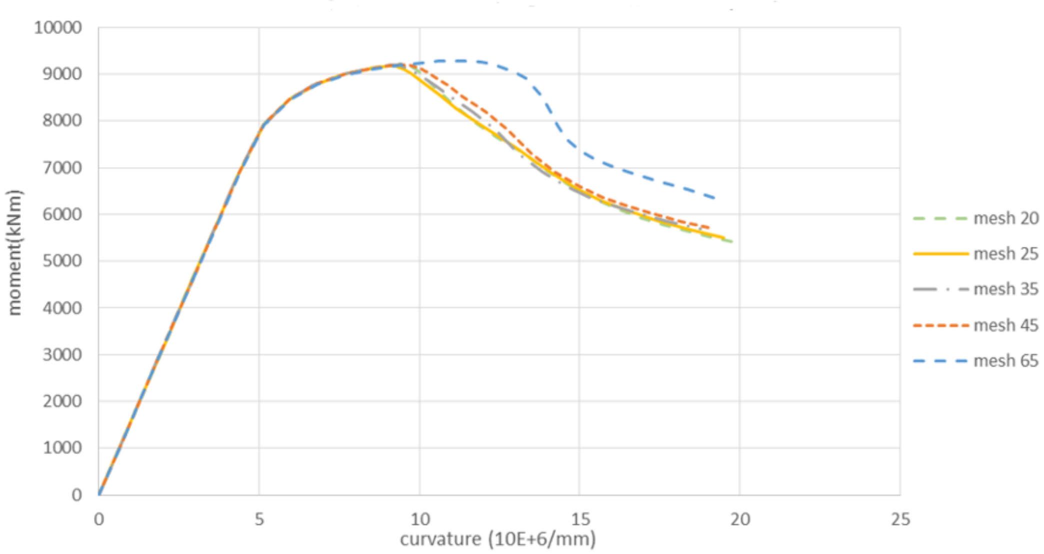

Figure 48: Convengence comparison for neutraline coupling of Tube 1

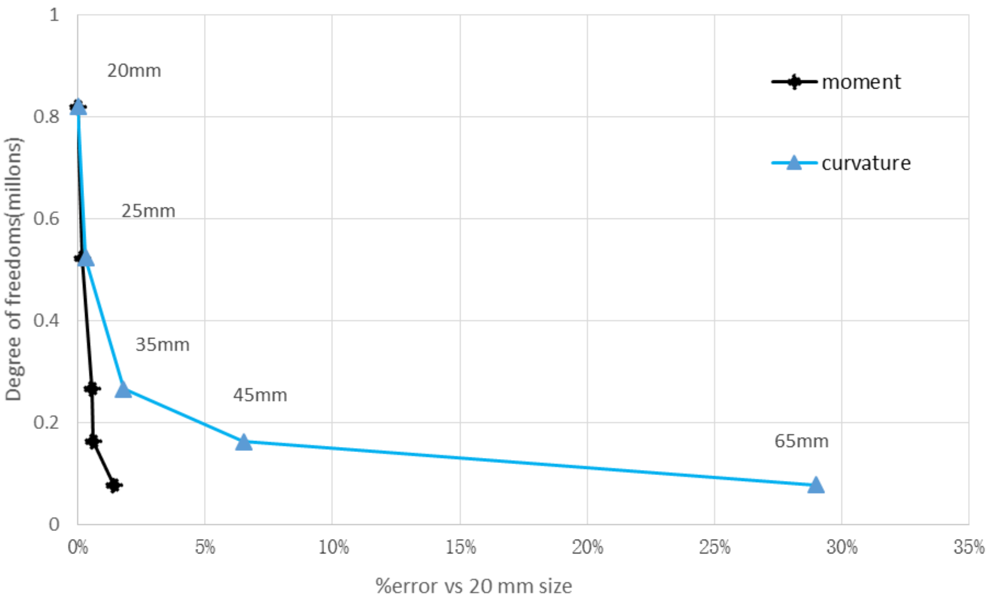

Figure 49: Mesh refinement study of neutraline coupling for tube 1

4.5.3 Element type analysis

With regard to the element type which will be used in ABAQUS, convergence analysis is also made for three kinds of element type among S4, S4R, S3 (for more clear explaination see Figure 50). These elements allow transverse shear deformation. They use thick shell theory as the shell thickness increases and become discrete Kirchhoff thin shell elements as the thickness decreases; the transverse shear deformation becomes very small as the shell thickness decreases (ABAQUS manual 6.12).

For element CPS8, it has advantages in analysing problems with stress concentration, and can obtain relative accurate result without shear locking problem. However, in terms of analysing plastic problems, it is likely to have volume locking if the material is incompressible. For element of CPS8R, it is not sensitive to hour glass control problem, and it is also not sensitive to self-locking issues, but is not suitable for large strain analysis. Therefore, CPS8R will not be used in this numerical simulations. From the Figure 51, it is concluded that S4R could have a relatively closing result with other two elements, while decreasing calculating time.

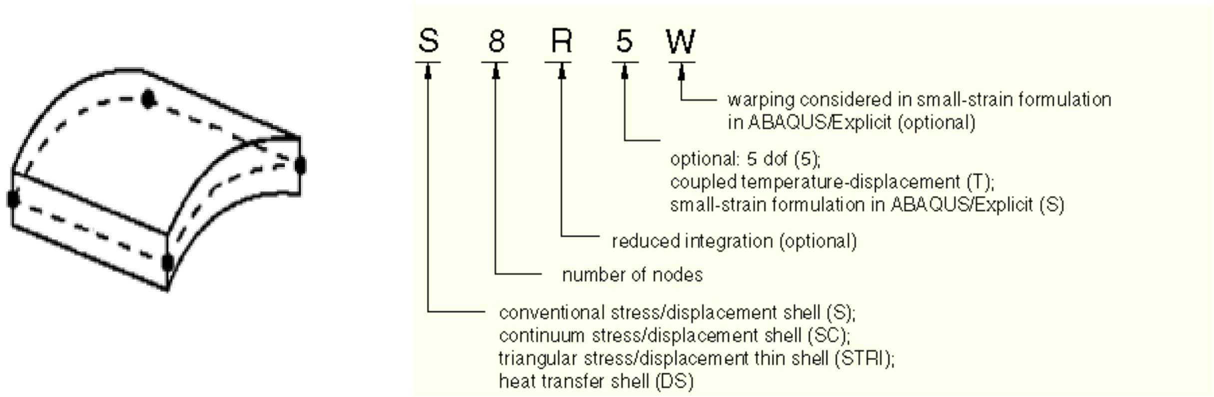

Figure 50: S4R element (ABAQUS/Standard Analysis User' s Manual, 6.12)

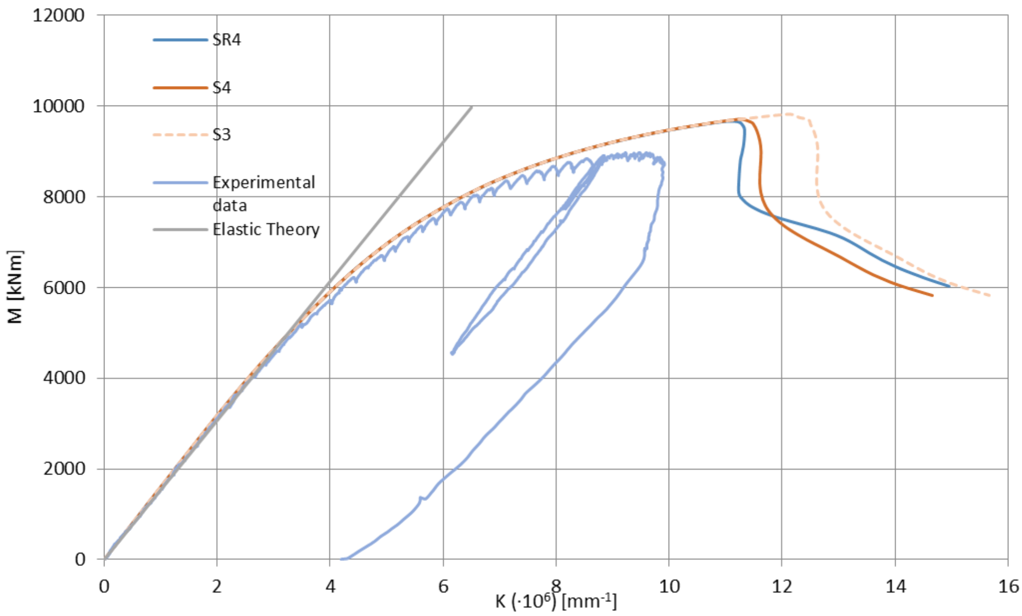

Figure 51: Effect of element type on buckling behavior of Tube 9

4.6 Thickness layers in model

The number of section points through the thickness of each layer can be specified. The default number of section points should be sufficient for routine thermal-stress calculations and nonlinear applications. The default number of section points is five for a homogeneous section and three in each layer for a composite section.

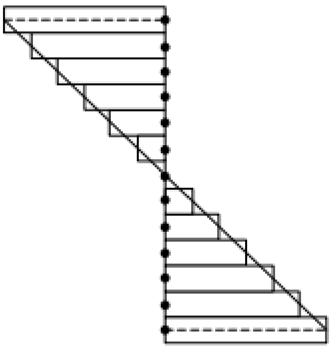

Figure 52: Section integration points along shell thickness

5, 7, 9, 11, 13, 15 and 17 shell integration points are applied separately in model for tube 9 to see the difference values of their finite element analysis in terms of critical curvature and maximum moment (see Figure 53). 15 shell section integration points included in the thin wall means there are 15 layers through the thickness of the tube see (Figure 52). The larger number of integration points the more layers divided through the thickness, one side is tension and the other side is compression. The output of the data obtained from the numerical model is the intermediate value of these shell integration points to avoid the local force components impact from the shell bending itself. Simpson's integration rule should be used if results output on the shell surfaces or transverse shear stress at the interface between two layers of a composite shell is required and must be used for heat transfer and coupled temperature-displacement shell elements.(Abaqus manual 6.12). From the requirement of the test simulation, Simpson's integration rule was chosen for defining section properties.

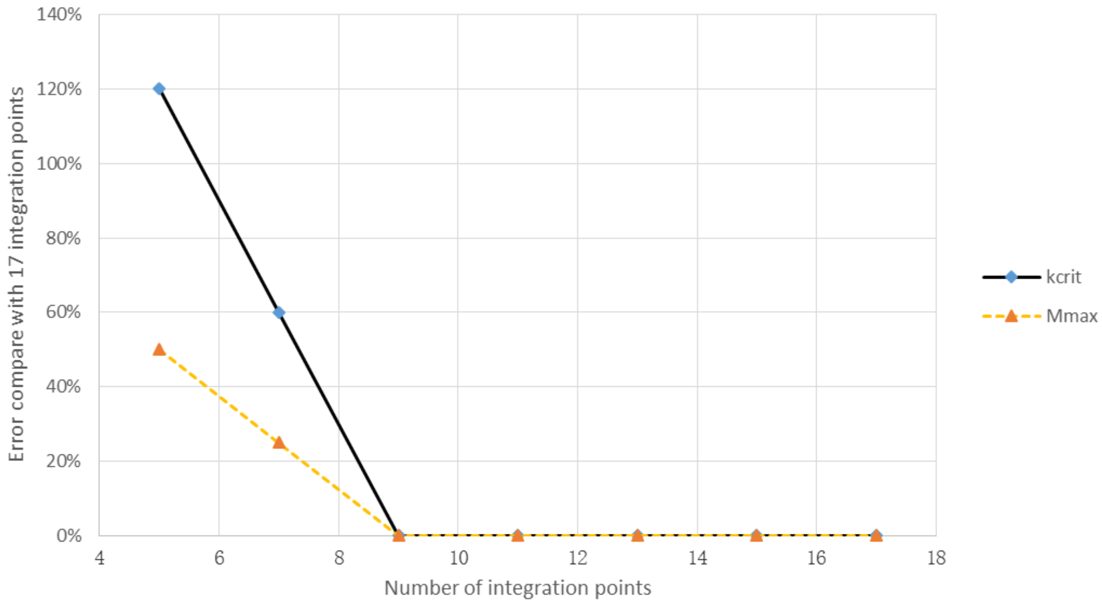

Figure 53: Effect of integration points on the behavior of Tube 9

The impact of number of integration points can be seen in Figure 53, more integration points means there will be more layers and the calculation will be more accurate but it will require more calculating time as well. As can be seen in the Figure 53, with different shell integration points, the difference values compared to the shell element with 17 points is getting larger with decreasing number of integration points. When there is need to achieve high accuracy, integration need to increase correspondly. Since the residual stress distribution was calculated by using 15 thickness integration points for compatibility, the integration points is chosen to be 15.

4.7 Residual stress model

The presences of residual stresses have many sources for spirally welded steel tubes: production process, uneven heating, cooling and later uncoiling of the plate material. Several attempts have been made to measure and characterize the residual stresses by different
research partners within the research project. Unfortunately, there is still no clear conclusive result.

The process of bending a plate into a tubular shape was modeled in ABAQUS by Vasilikis and Karamanos (2014). The result is a normalized residual stress distribution across the thickness of the tube, which was adapted to each specific tube by multiplying by the yield stress and assign to the 15 thickness layers. In this case, the average stress at 0.2% plastic strain was used. This distribution could then be applied directly to each tube as an initial stress state. The table 3 below has been modified. The integration points are numbering from inside to outside of the tube thickness.

Table 3: Residual stress distribution (from inner surface to outer surface)

Integration points	Normalized Thickness	NormalizedAxial Stress	NormalizedHoop Stress
1	0	-0.018	0.598
2	0.071	-0.096	0.354
3	0.143	-0.171	0.114
4	0.214	-0.248	-0.139
5	0.286	-0.312	-0.392
6	0.357	-0.342	-0.641
7	0.429	-0.262	-0.862
8	0.5	0.01	-0.017
9	0.571	0.284	0.875
10	0.643	0.343	0.646
11	0.714	0.307	0.398
12	0.786	0.241	0.146
13	0.857	0.165	-0.106
14	0.929	0.089	-0.345
15	1	0.01	-0.59

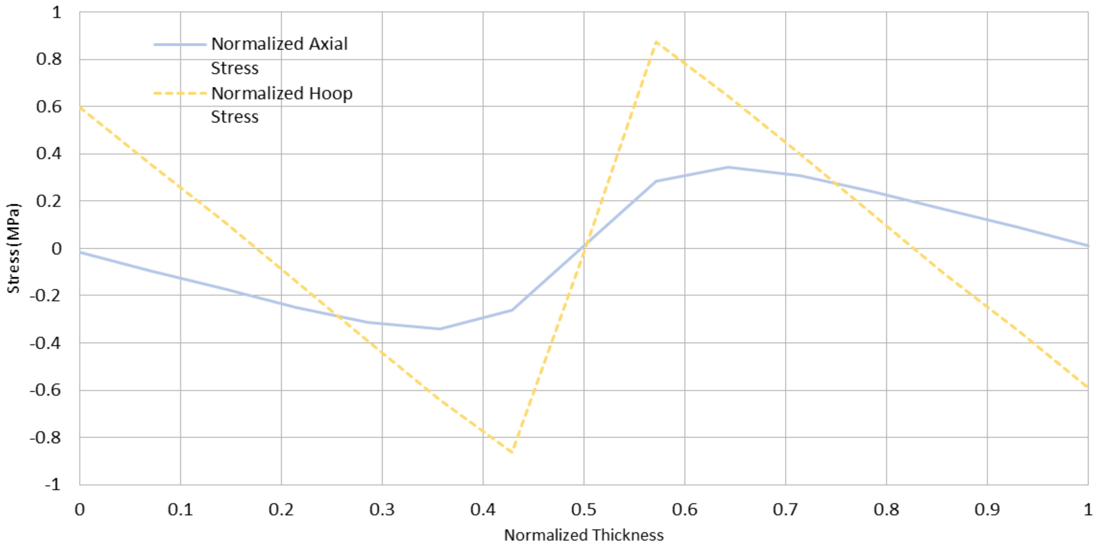

Figure 54: Residual stress distribution

4.8 Non-linear buckling analysis

When geometric nonlinearity and material nonlinearity are involved in the analysis, a pre and post buckling analysis is needed to investigate buckling behaviour. Several convergence approaches are possible to analysis the buckling problmes with different algorithm solution. In finite element analysis involving post buckling analysis the Riks method is applied, which is generally used to predict unstable collapse of a structure up to failure. The Riks method is an algorithm that gives effective solution of non-linear geometric induced failure. When there is need to concern about material nonlinearity, geometric nonlinearity prior to buckling, or unstable post buckling response (Riks) analysis must be performed to investigate the problem further (ABAQUS manual 6.12).

The nonlinear analysis Riks method solves simultaneously for loads and displacements. Because it uses the arc length “l” along the static equilibrium path in load-displacement space to find equilibrium. This approach can perform the analysis regardless of whether the response is stable or unstable. While the standard static solution procedure, when used with displacement control, was often able to find the limiting moment, but was generally not able to trace the post-buckling equilibrium path, depending on its stability. Therefore the first step is to create general static step to apply the residual stress, after applying residual stress as initial condition, Riks solution is created for non-linear analysis to trace full equilibrium path.

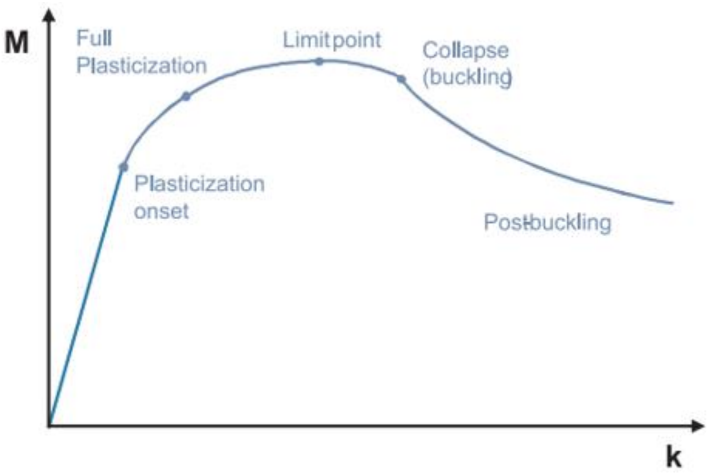

Figure 55: M-K relations stage formming

5 FEM modelling results

5.1 Plain tubes

In this section, test tubes are simulated themselves and compared with not only analytical and experimental data, but also compared with the other existing FEM models with fix ends without ovalization. Model 1 (which will named “M1” for simplicity) represents the middle section of each tube only, with a length of 8,100mm. Bending moments were applied to each end of the tube to simulate the constant moment situation created by the 4-point bending tests. This model accurately represents the geometry of the physical tubes, but does not allow ovalization at the tube ends. Therefore, a second model was created (named “M2” for simplicity), which is a tube with length 12500mm. In this model, the middle span of the physical tubes is represented by an 8100mm section in the center of the model. The ends of the tube are still restrained but due to the additional length of the ends of the 8,100mm central section are much less restrained. Both tubes (Nicolas, 2014) have the same loading situation, with a constant moment along the entire length of the model.

The curvature has been calculated based on the rotation of the node locating at neutraline at each support, the length between the measuring point is 8100mm. This curvature is defined as critical curvature which is listed in the table. Since the finite element analysis only determine the maximum value of bending moment, the buckling curvature is set equal to critical curvature.

Local curvatures are curv1, curv2 and curv3, which have been calculated in the way described in Section 2.2.4. During the experiments, these curvatures were calculated directly based on the deflection of the curvature brackets. These local curvatures are only plotted for plain tubes. In numerical models, the corresponding locations of the brackets first had to be calculated, based on the difference between the buckling location observed during testing and the buckling location in the models. Because the bucklings does not occur in the same location in the models and in the test setup, for some tubes, the corrected location of the curvature brackets was beyond the end of the tube. Therefore, not all curvatures are presented for all tubes. With regard to the ovalization measurement, the locations of the brackets were related to the location of the buckle in the physical tube, and this information was used to locate the measuring points correctly in the models.

5.1.1 Tube 1 results

Tube 1 is plain tube without structural detail, featured with D/t = 65, f_y = 540MPa, imperfection value incoporated in non-linear buckling analysis is 0.646mm. The results of tube 1 can be seen in Table 4.

Table 4: Tube 1 results

	k_{buc} (10^6 mm^{-1})	**k_{crit} (10^6 mm^{-1})**	**M_{buc} (kNm)**	**M_{crit} (kNm)**
FEM	10.40	10.40	9159	9159
Gresnigt	-	9.741	-	9280
Experimental	10.08	9.61	8430	8840
M1 (8.1m)	9.62	9.62	9072	9072
M2 (12.5m)	10.55	10.55	9143	9143

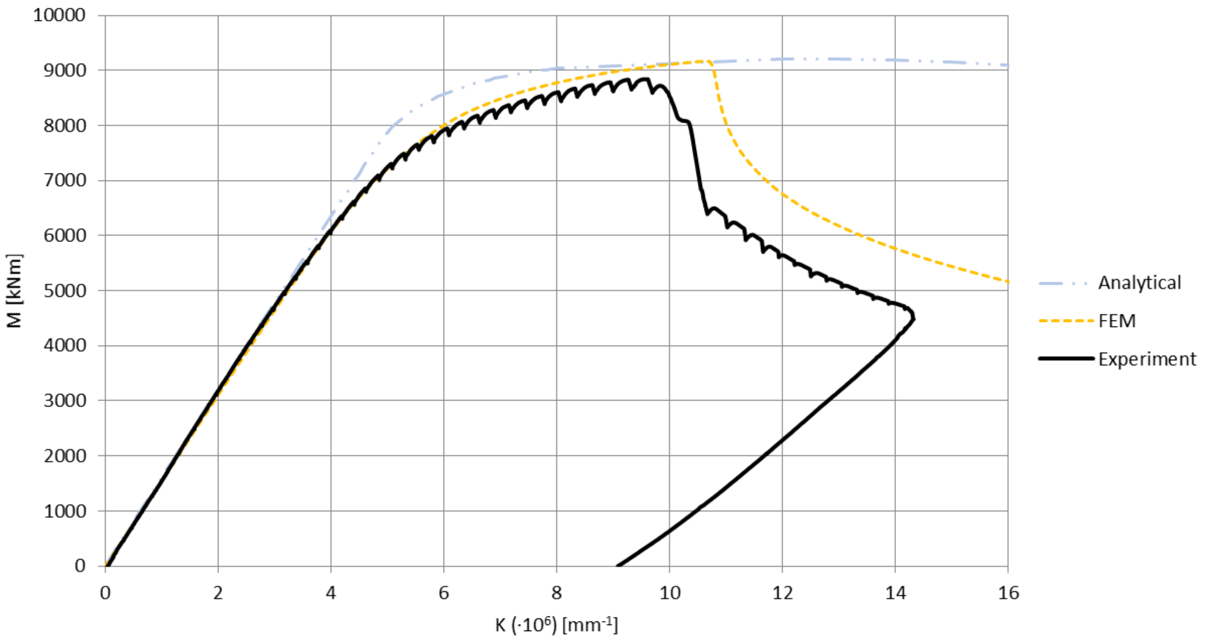

Figure 56: M-K relations of Tube 1

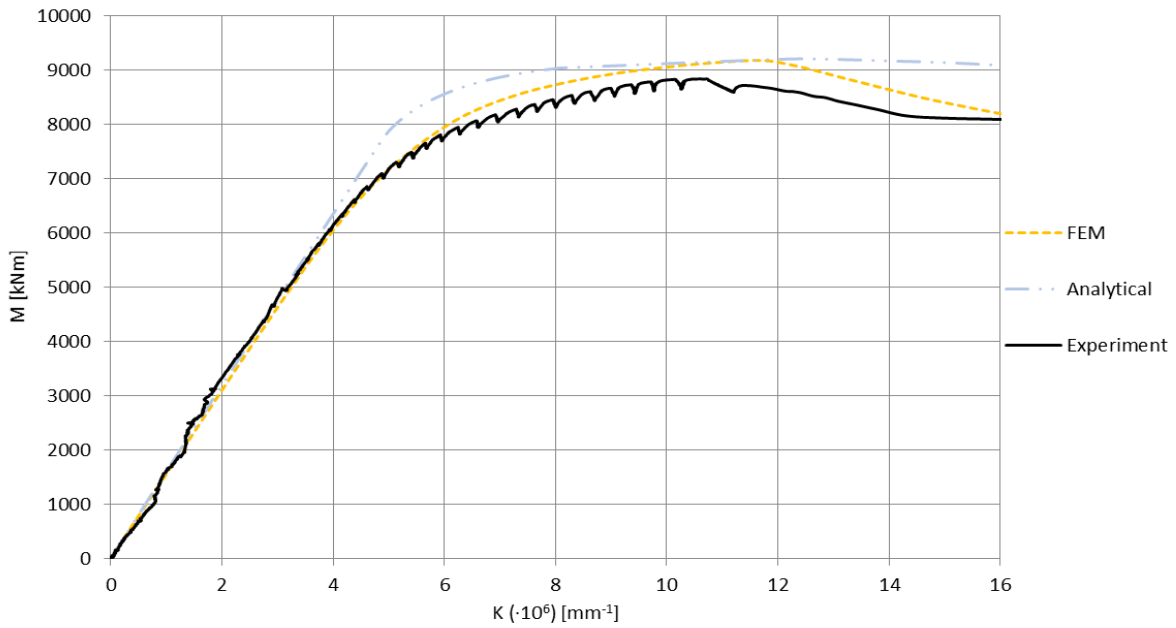

Figure 57: M-K relationships forTube 1 of curvature 1

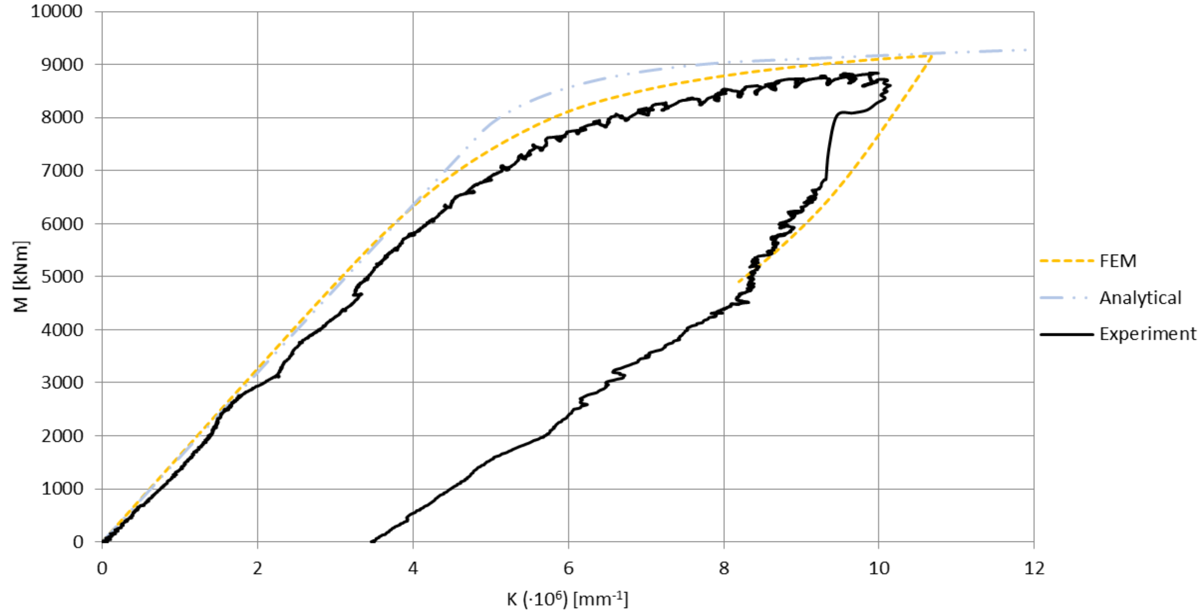

Figure 58: M-K relations for Tube 1 of curvature 2

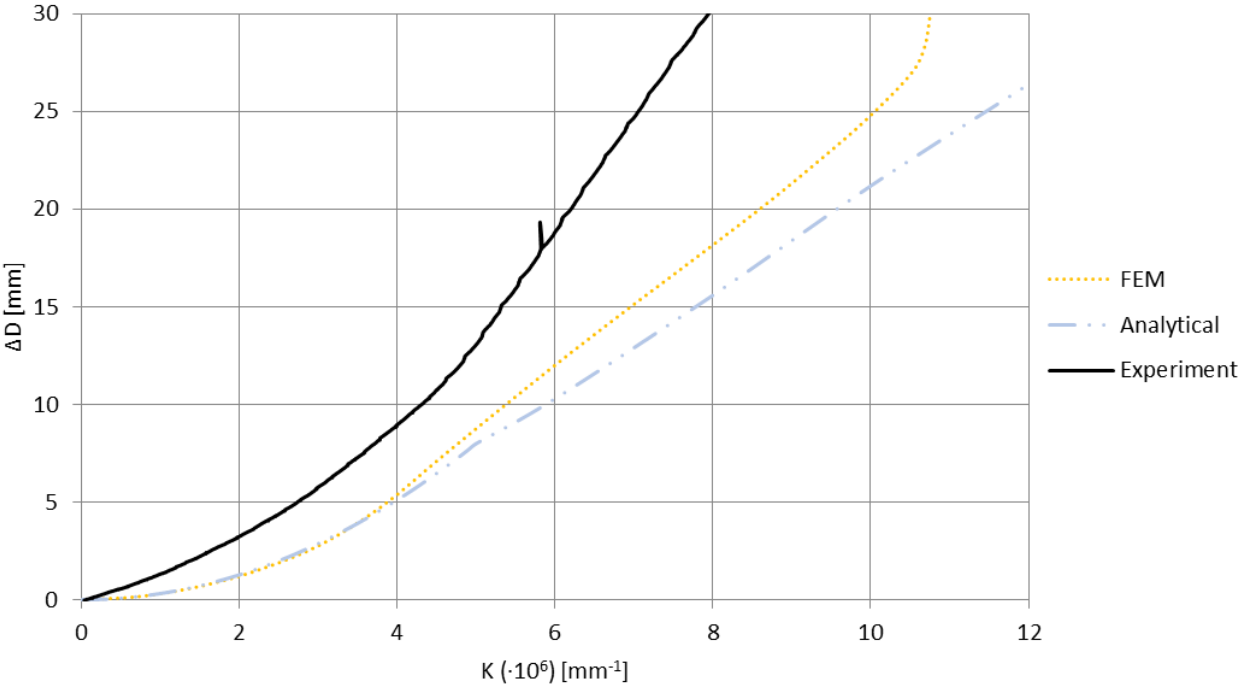

Figure 59: ΔD-K relations for Tube 1

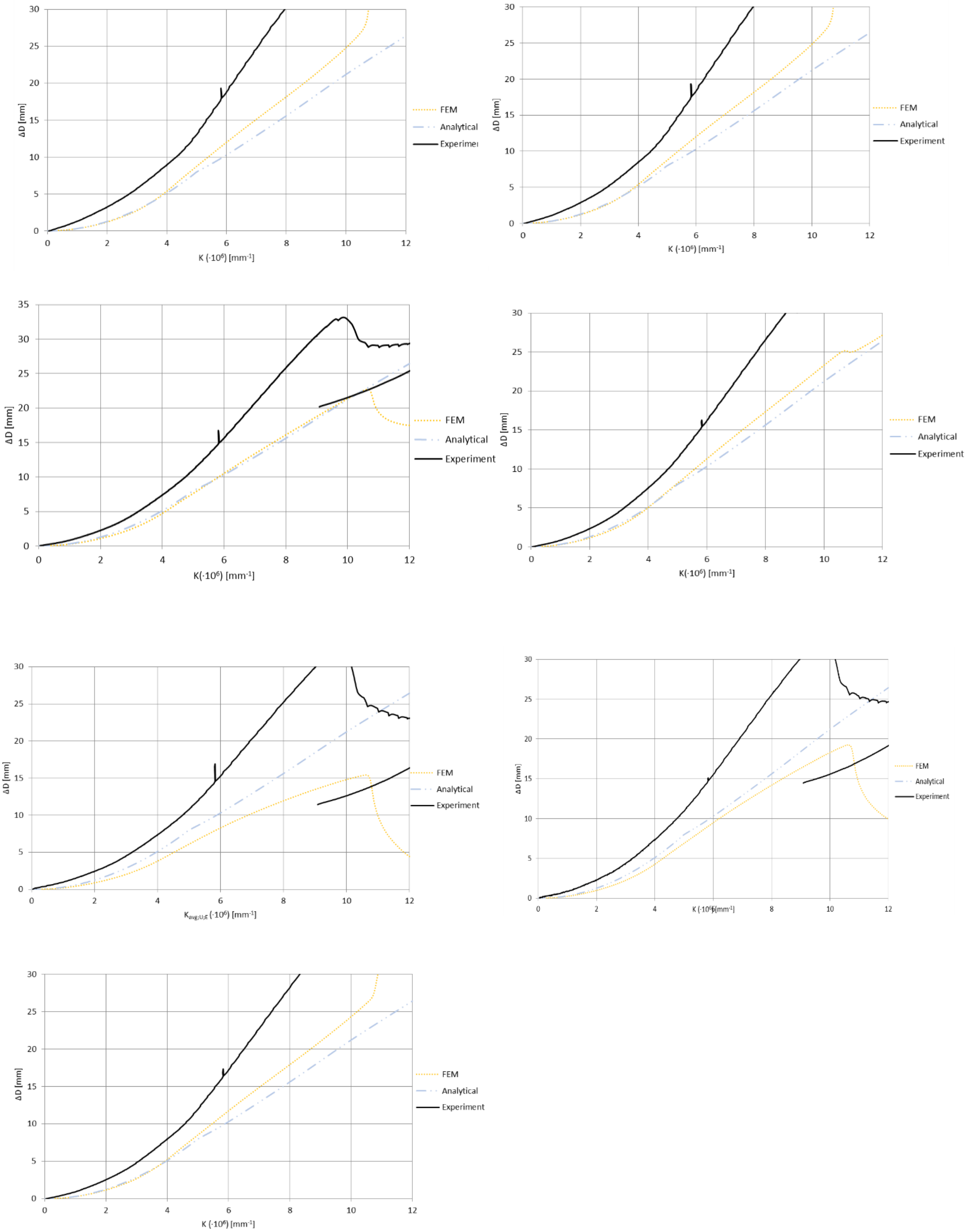

Figure 60: ΔD-K relations for Tube 1 at Ovalization bracket from OV1 to OV 7

For tube 1 there is one buckling occurs in the middle of the tube in final deformed shape, and there is excellent agreement between the neutral line model and the experimental data, especially significant agreement in pre-buckling path. Neutral line model shows good agreement both in terms of M_{max} and k_{crit}. Both values obtained from neutral line model are slightly higher than experimental data. The buckling point is slightly overestimated by numerical model. This is possibly due to the imperfection introduced to the model is underestimated. As explained before, some curvatures can not measure due to the curvature shifting along the neutral line. With regard to the curv1 and curv2, there is also great agreement between model and experimental data, the buckling point of curv1 is closer than curv 2, which the M_{max} and k_{crit} were both overestimated. In terms of ovalization, the result from neutral line model matches the analytical solution almost perfectly in elastic part, strating to deviate in the later plastic stage, while compare with the experimental data, the numerical model underestimates the ovalization from experiment data, this can caused by the force that the support indtroduced to the support is less than the actual force introduced in the real situation. Apart from the neutral line model which allows free ovalization at support in this paper, there are other two model which simulated in different ways, the one with fix end (named “M1”), the other one extend the length to 12500mm, in order to modify the support of tube restrained by coupling method (named “M2”). Compare with M1, neutral line model has higher critical curvature and moment, while the critical curvature is significantly close to M2, which indicates that it might be also suitable to use the M2 in order to realize less restrained tube. In terms of ovalization, FEM model perform better which allow more ovalization and more close to experimental data. Another aspect that can be observed that the measured curvature from curvature bracket 1 is higher than curvature obtained from curvature bracket 2. Because the final results of the curvature are sensitive the the localisation of curvature and the curvature away from where buckling occurs gives lower curvature.

5.1.2 Tube 2 results

Tube 2 is a plain spirally welded tube characterized by D/t = 119, f_y= 390 MPa, and introduced imperfection is 0.871mm. The results of Tube 2 can be seen in Table 5.

Table 5: Tube 2 results

	k_{buc} (10^6 /mm)	k_{crit} (10^6 /mm)	M_{buc} (kNm)	M_{crit} (kNm)
FEM	4.85	4.85	3296.2	3296.2
Gresnigt	-	7.9	-	3615.9
Experimental	4.94	4.51	2812.5	3046.7
M1 (8.1m)	4.53	4.53	3248.2	3248.2
M2 (12.5m)	4.77	4.77	3381.6	3381.6

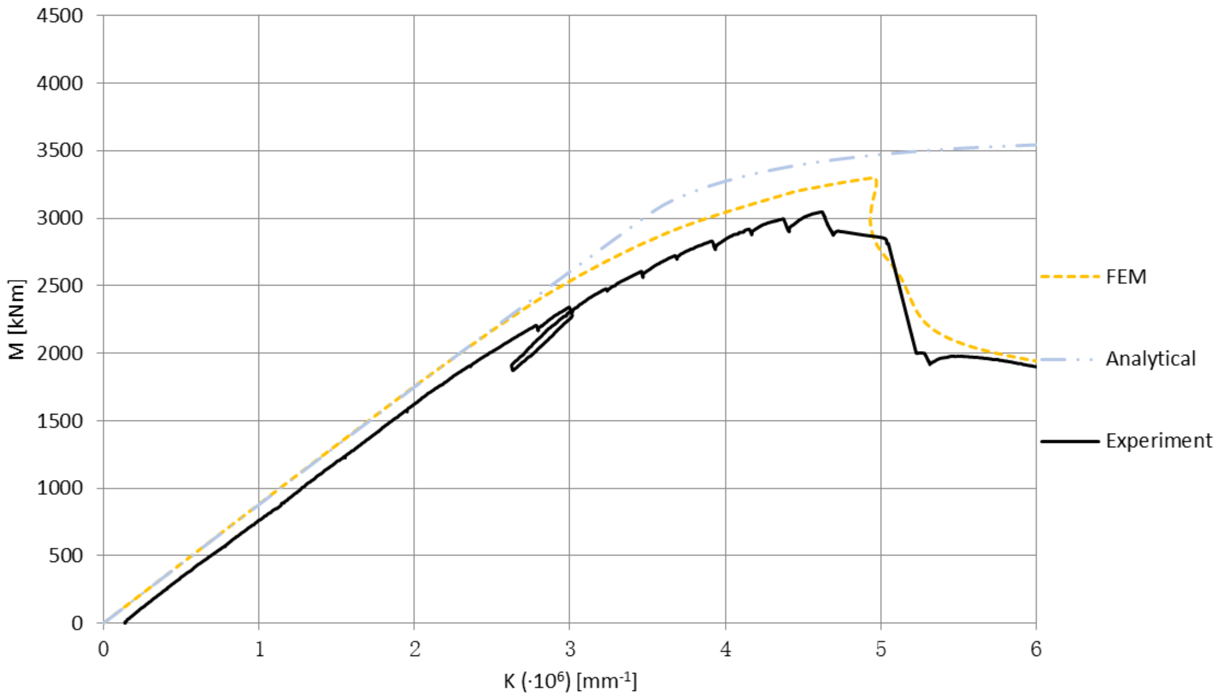

Figure 61: M-K relations of Tube 2

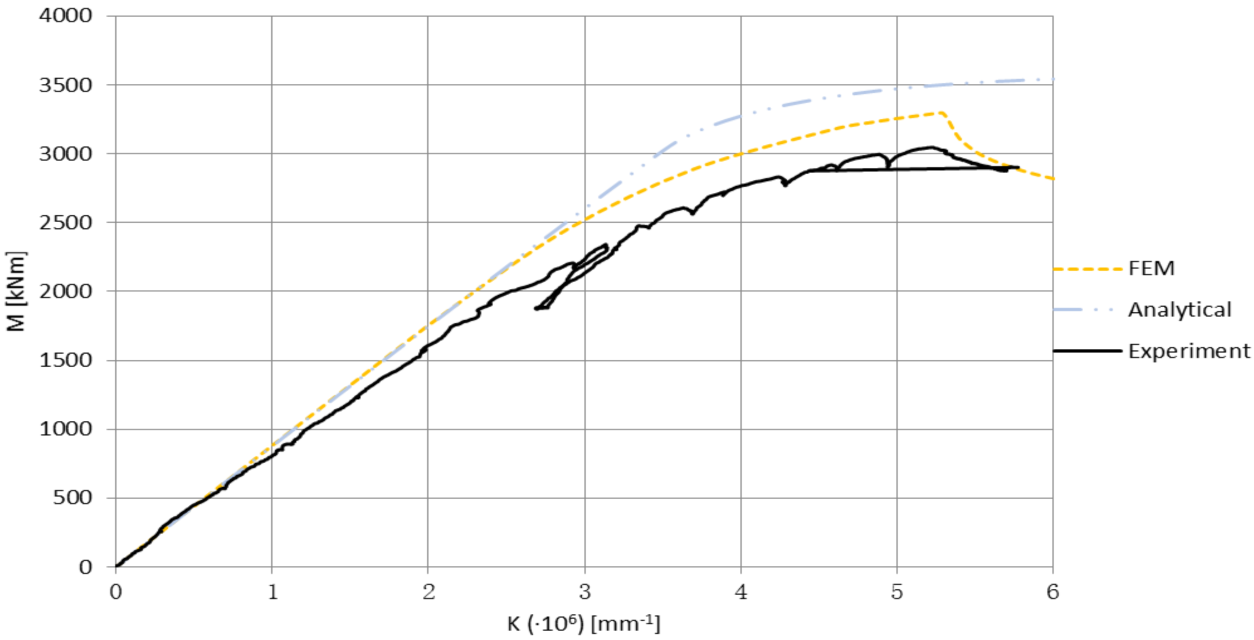

Figure 62: M-K relationships forTube 2 of curvature 1

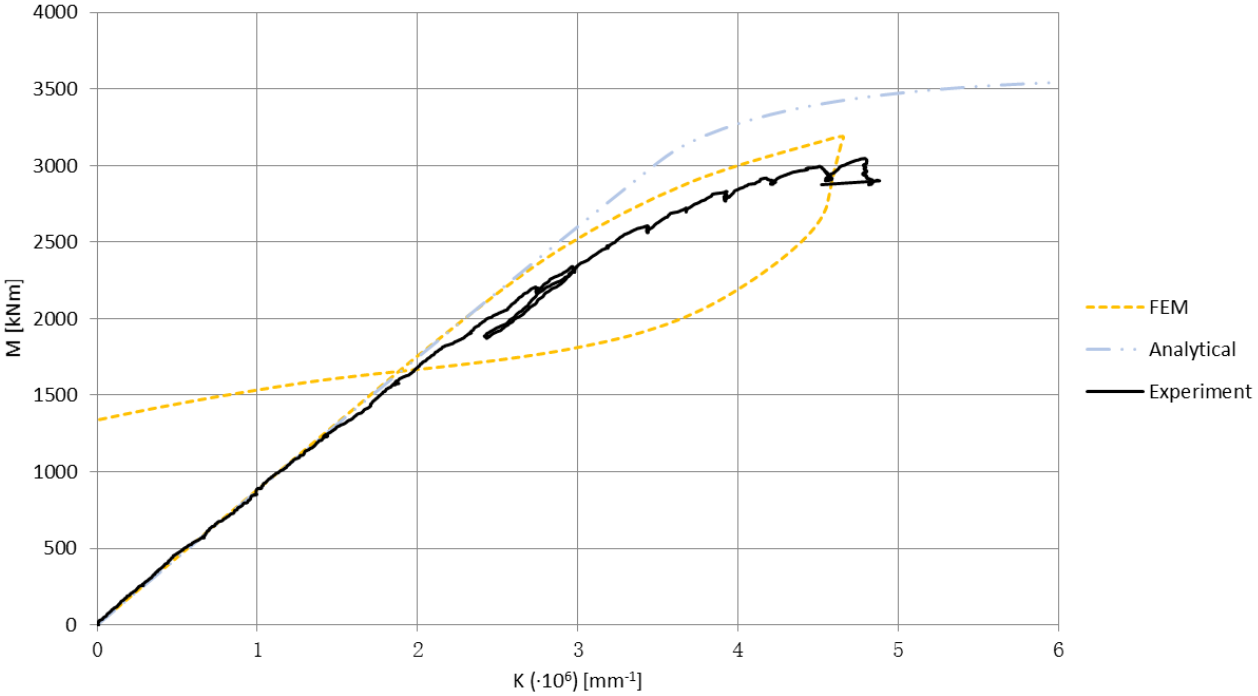

Figure 63: M-K relationships forTube 2 of curvature 2

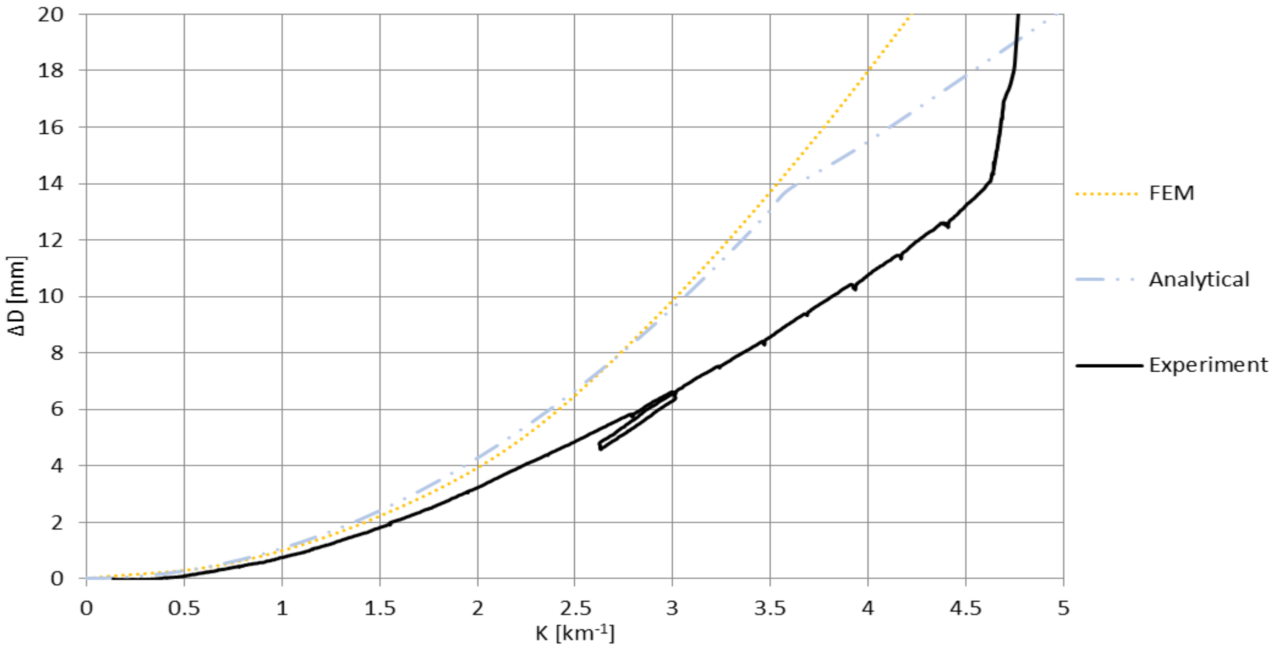

Figure 64: ΔD-K relations for Tube 2

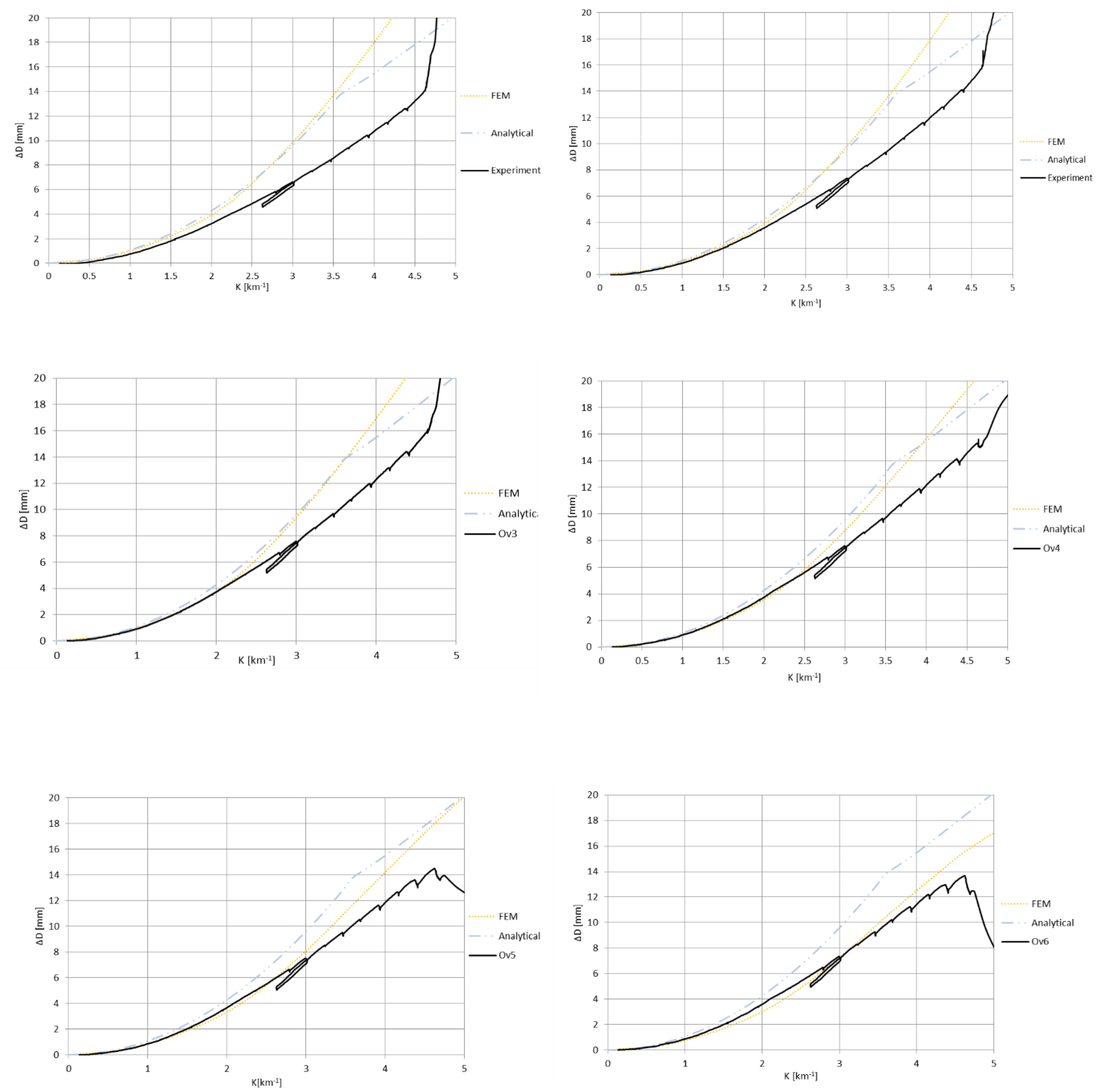

Figure 65: ΔD-K relations for Tube 2 at Ovalization bracket from OV1 to OV 7

For tube 2, the results obtained from neutral line model is relatively good in terms of the moment and curvature, there is good agreement in the pre-buckling equilibrium path, and slightly deviate in the post-buckling equilibrium path. However, both moment and curvature are slightly overestimated by neutral line model. The agreement is excellent for curvature bracket 1. For curvature bracket 2, the maximum moment is slightly overestimated but the curvature is underestimated. In terms of ovalization for Tube 2, it can be seen that, compared with Tube 1, the ovalization of Tube 2 is much more restrained, ovalization of Tube 2 is less than analytical, the model match the analytical solution perfectly. This could be that the Tube 2 characterised with higher D/t ratio and relatively lower strength. It has tendency to be more restrained. Compared with experimental data, all ovalization bracket overestimate the actual overlization. When comparing with model M1 and M2, neutraline model obtain higher critical curvature than both M1 and M2, while the moment is almost equal to M1 but less than M2. Taking look at ovalization, neutral line model performs best among these three, M1 is the worst, it is greatly restrained by model, already deviate from linear branch. Still, the curvature from curvature bracket 1 is higher than curvature obtained from curvature bracket 2. Because the final results of the curvature are sensitive the the localisation of curvature and the curvature away from where buckling occurs gives lower curvature.

5.1.3 Tube 4 results

Tube 4 is a plain spirally welded steel tube characterized by D/t = 116, f_y= 420 MPa, and introduced imperfection is 0.636mm. The results of Tube 4 can be seen in Table 6.

Table 6: Tube 4 results

	k_{buc} (10^6 /mm)	**k_{crit} (10^6 /mm)**	**M_{buc} (kNm)**	**M_{crit} (kNm)**
FEM	6.22	6.22	3607.9	3607.9
Gresnigt	-	8.4	-	3949.5
Experimental	6.31	6.27	3730.9	3716.4
M1 (8.1m)	5.71	5.71	3582.4	3582.4
M2 (12.5m)	6.19	6.19	3639.4	3639.4

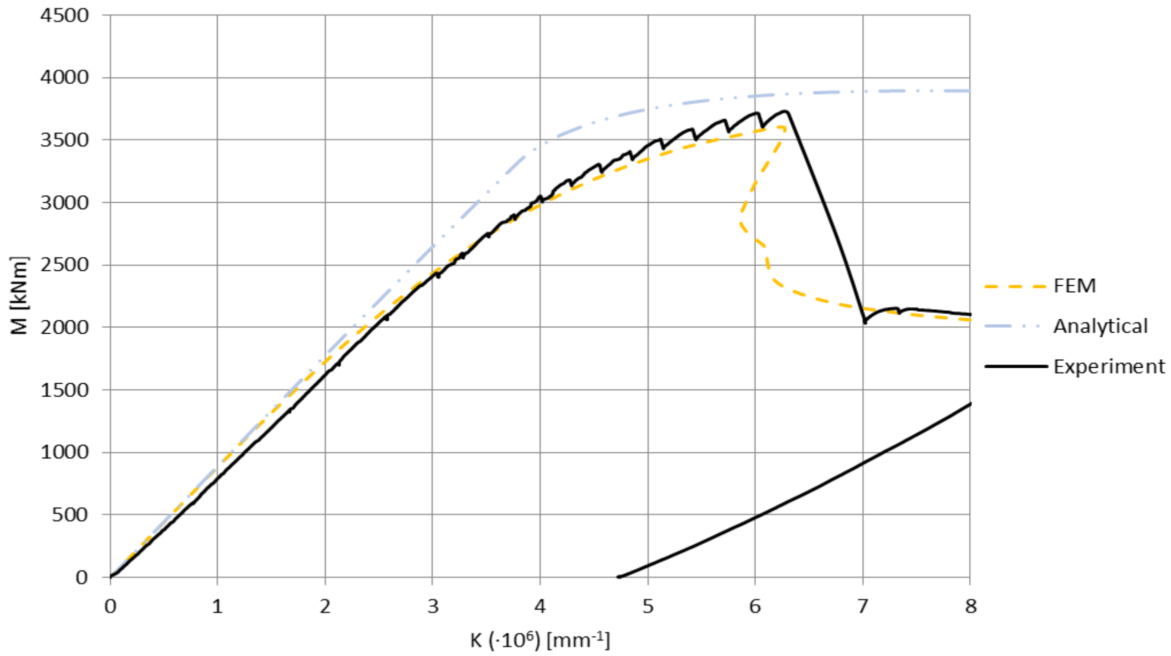

Figure 66: M-K relations of Tube 4

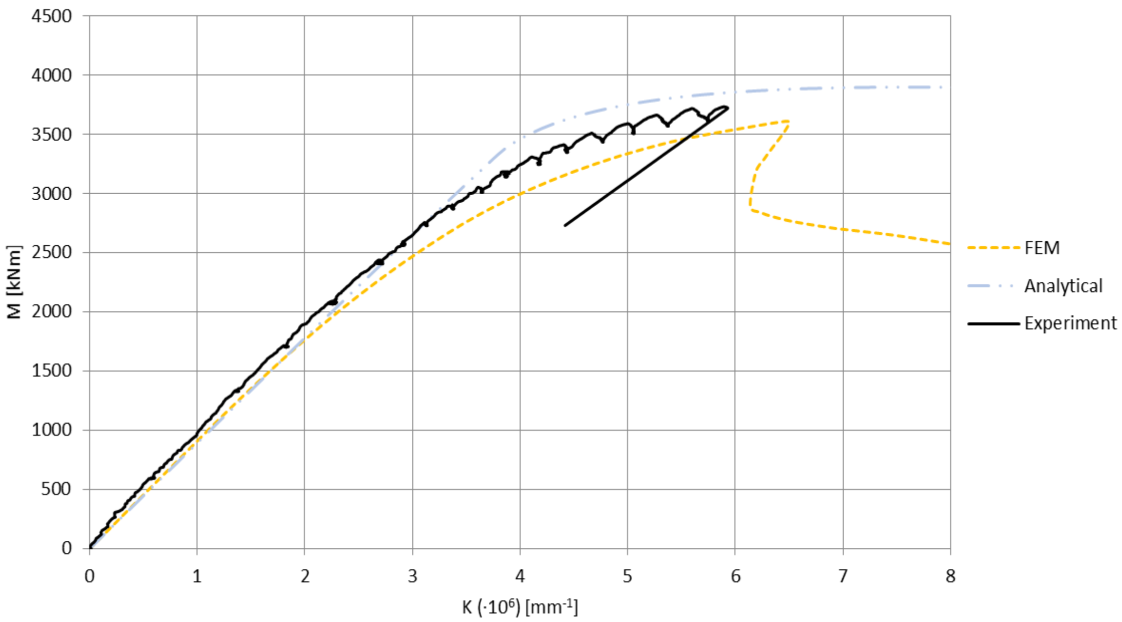

Figure 67: M-K relations forTube 4 of curvature 1

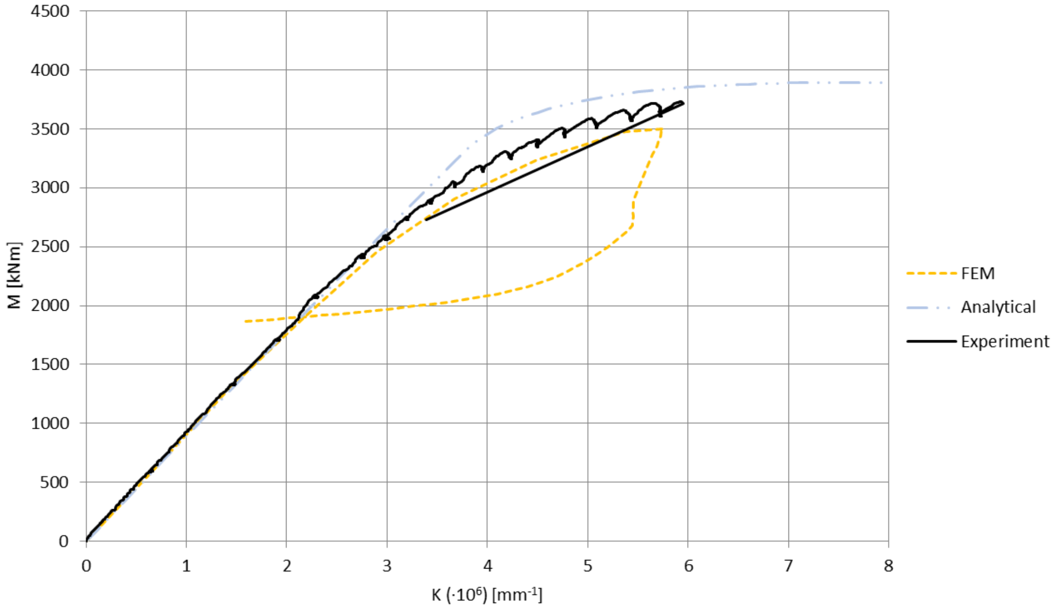

Figure 68: M-K relations forTube 4 of curvature 2

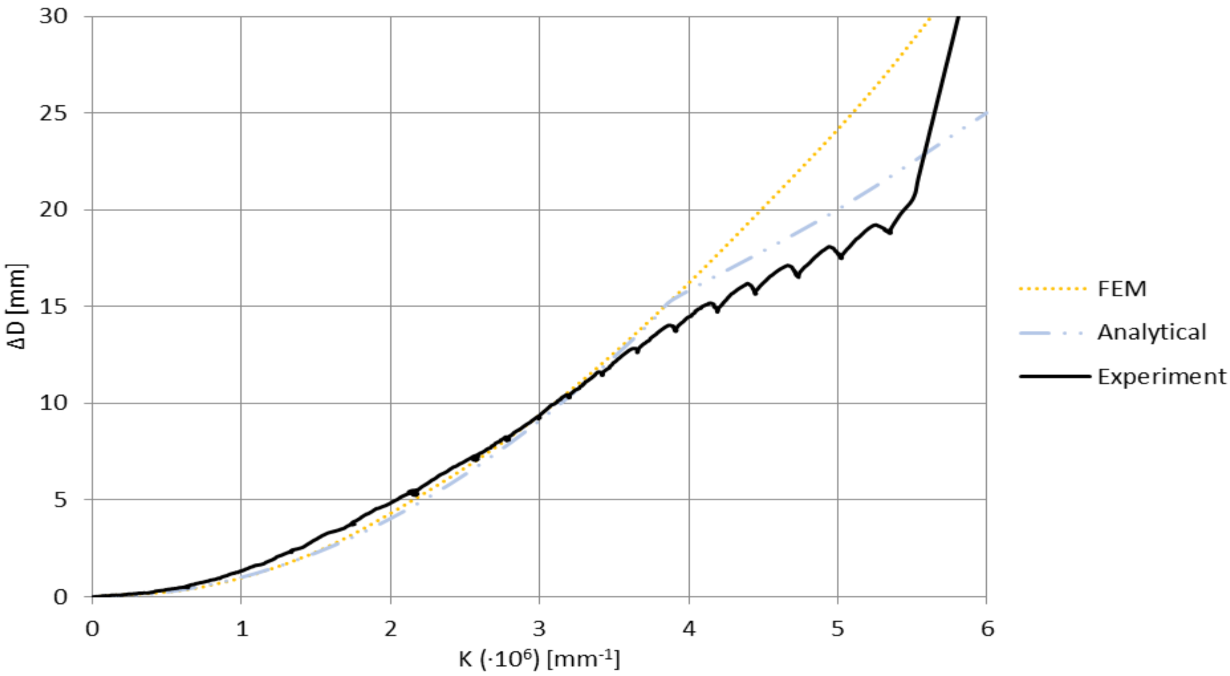

Figure 69: ΔD-K relations for Tube 4

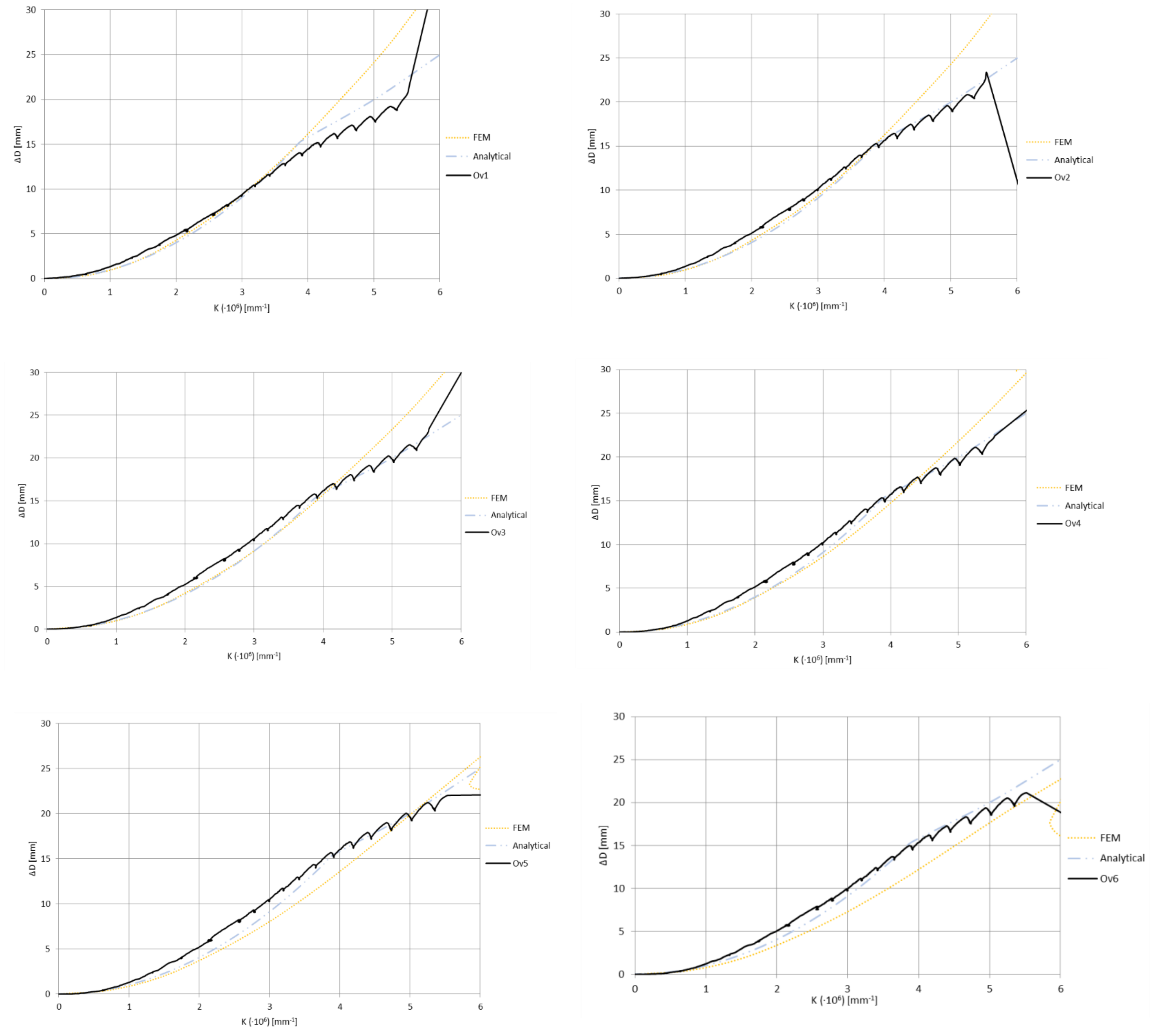

Figure 70: ΔD-K relations for Tube 4 at Ovalization bracket from OV1 to OV 6

For Tube 4, it shows excellent agreement in the pre-buckling equilibrium path, and very good agreement with the maximum moment and the critical curvature. About curvature bracket, it can be seen that the maximum moment is both underestimated by the models, while critical curvature is accurately predicted by the model. Taking look at the ovalization of Tube 4, the model shows quite good agreement with ovalization-curvature graph. It matches analytical and experimental data very well, slightly overestimated when plasticity onset. With regard to the ovalization bracket of 5 and 6, the ovalization is underestimated. While compare with M1, the critical curvature and moment from M1 are both lower than neutral line model, it is noticeable that neutral line model has same critical curvature as M2, in terms of ovalization, again as before, neutral line model predicts best results.

5.1.4 Tube 5 results

Tube 5 is a plain spirally welded tube characterized by D/t = 119, fy= 400MPa, imperfection is equal to 0.718mm. The results of Tube 5 can be seen in Table 7.

Table 7: Tube 5 results

	k_{buc} (10^6 /mm)	**k_{crit} (10^6 /mm)**	**M_{buc} (kNm)**	**M_{crit} (kNm)**
FEM	6.37	6.37	3432.5	3432.5
Gresnigt	-	8.0	-	3721.0
Experimental	5.47	5.51	3238.5	3338.2
M1 (8.1m)	6.06	6.06	3431.7	3431.7
M2 (12.5m)	6.37	6.37	3443.5	3443.5

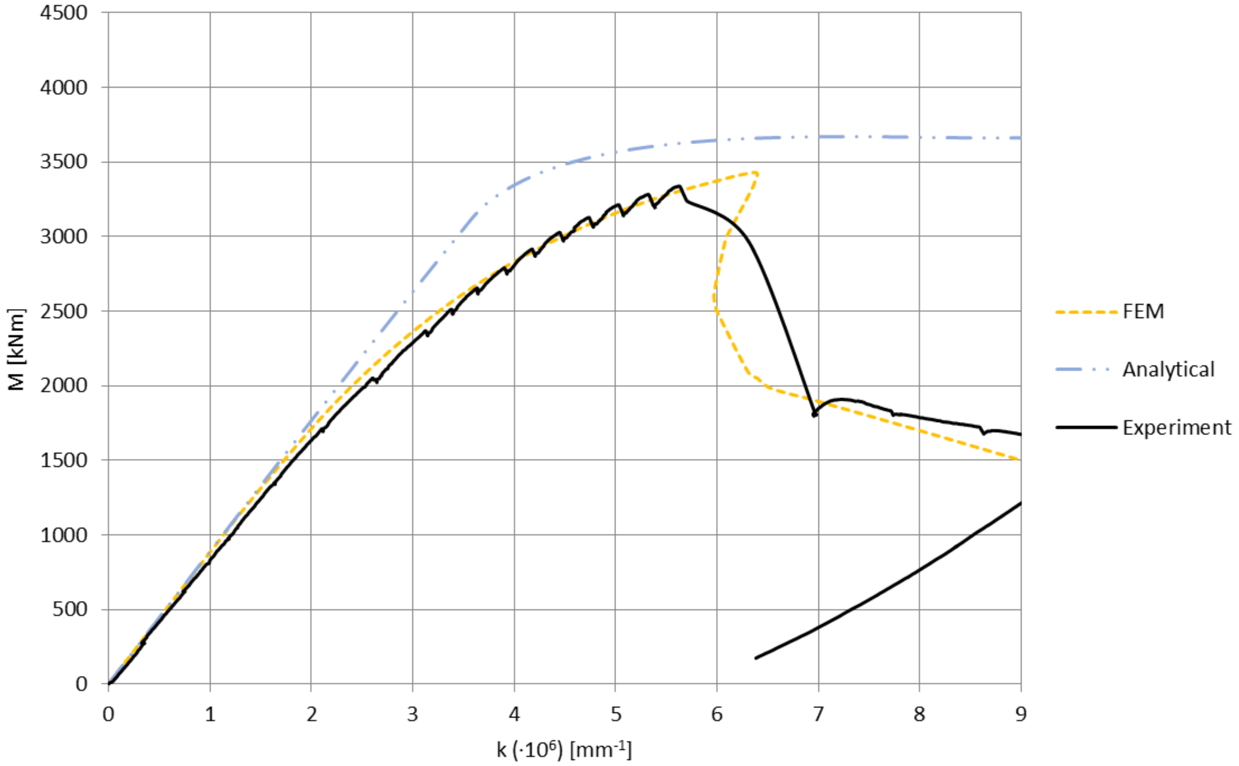

Figure 71: M-K relations of Tube 5

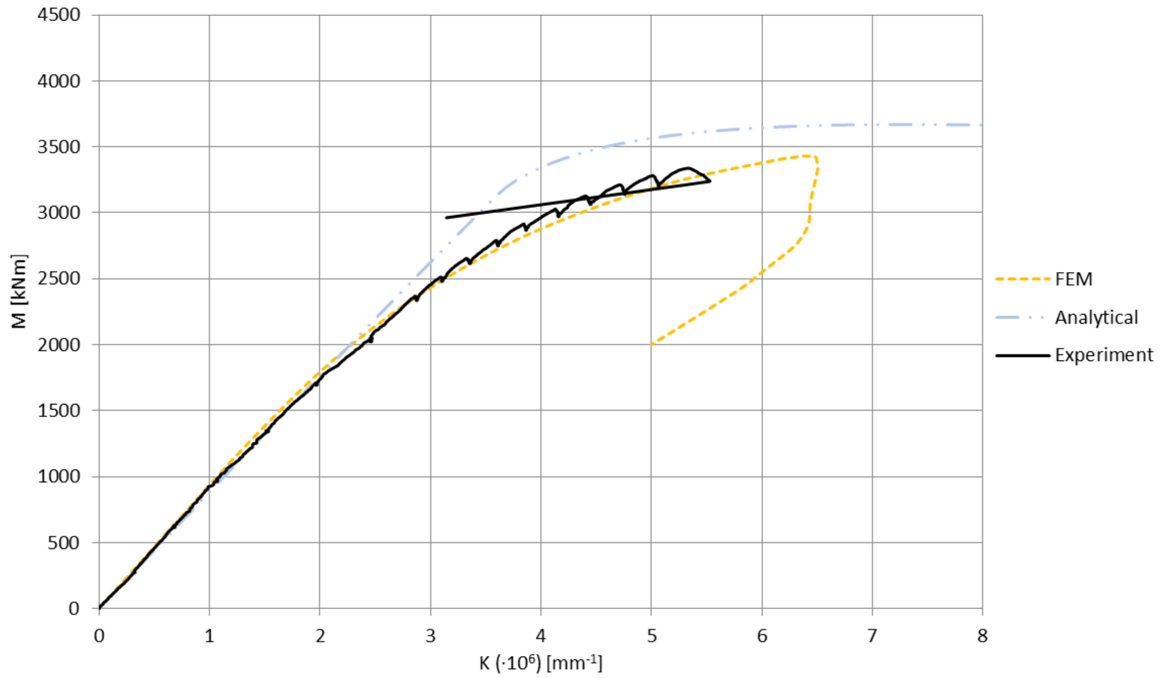

Figure 72: M-K relations forTube 4 of curvature 2

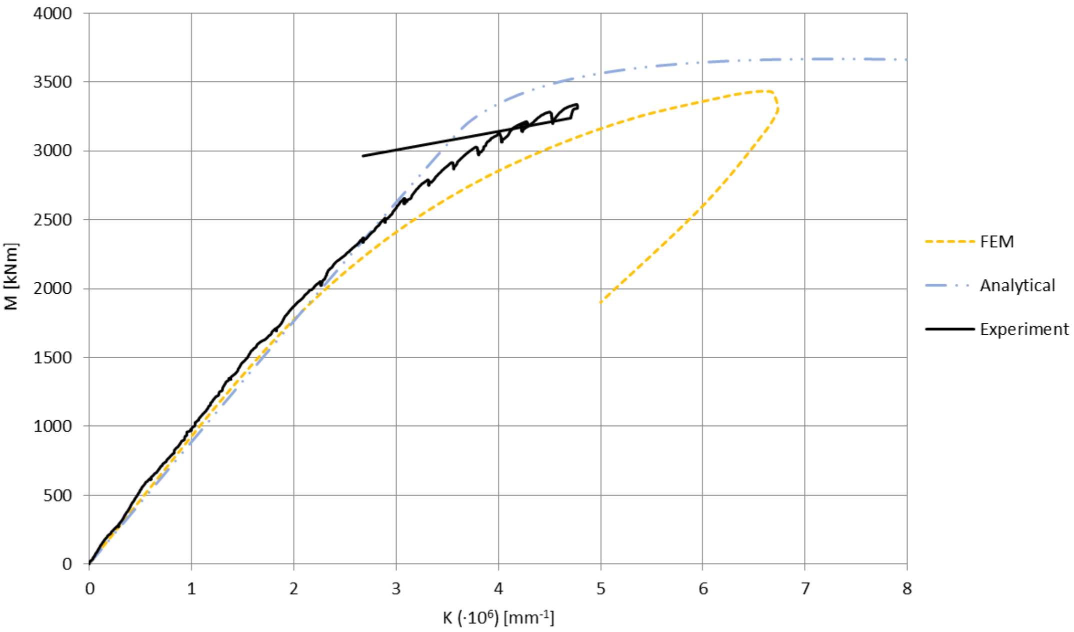

Figure 73: M-K relations forTube 4 of curvature 3

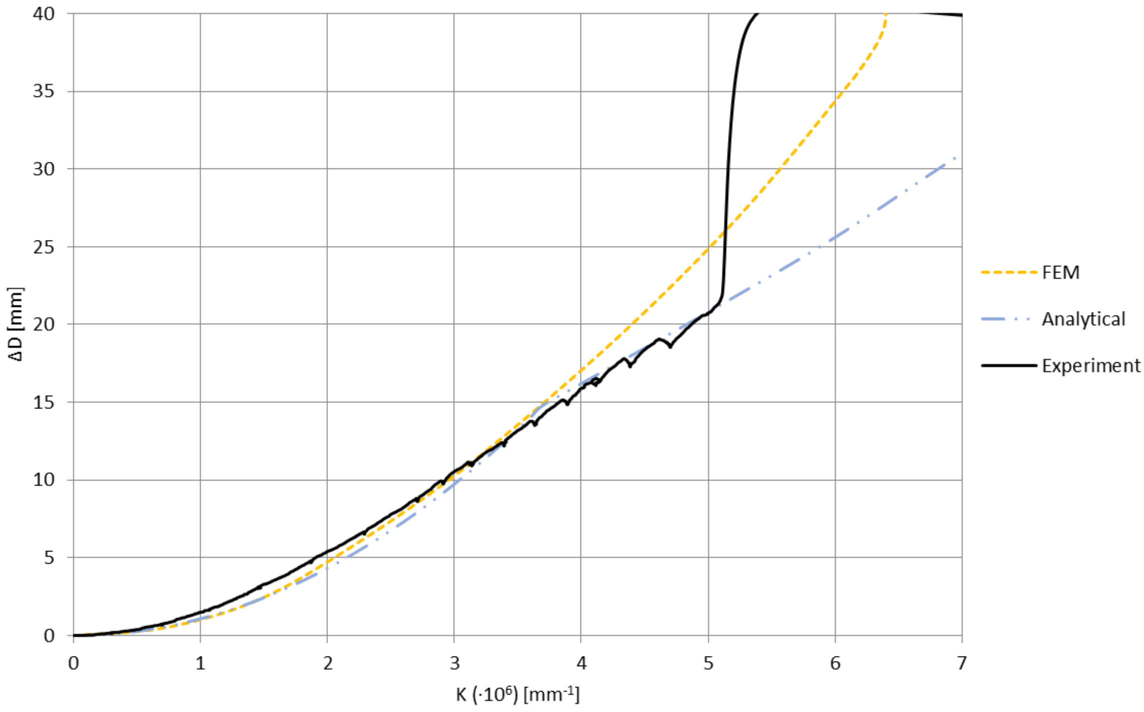

Figure 74: ΔD-K relations for Tube 5

For Tube 5, the neutral line model shows great agreement with experimental in pre-buckling path, the critical curvature obtained by model is relative accurate compare with experimental data, the curvature is slightly higher compare with the experimental data and the moment is more closer to the experiment. It can be noticed that duing elastic branch, the elastic line of experimental data deviated from analytical elastic line, that is due to the situation that the bending stiffness in real tubes has weakness which relative reduce the capacity of deformation. In terms of ovalization the model matches the analytical solution very well in elastic branch, and the model deviates a little bit when plasticity onset. Among all models, neutral line model has higher curvature than M1 but same as M2. Maximum moment obtained from neutral line model is higher than M1 but lower than M2, which indicates that in this case, M2 might suffer from geometric influence. Observing ovalization, it is again that neutral line model has the best performance.

5.1.5 Tube 8 results

Tube 8 is a plain spirally welded tube characterized by D/t = 117, f_y= 435 MPa, and imperfection value is equal to 1.070mm. The results of Tube 8 can be seen in Table 8.

Table 8: Tube 8 results

	k_{buc} (10^6 /mm)	k_{crit} (10^6 /mm)	M_{buc} (kNm)	M_{crit} (kNm)
FEM	5.30	5.30	3594	3594
Gresnigt	-	8.5	-	4052.4
Experimental	5.70	5.66	3469.1	3347.1
M1 (8.1m)	5.14	5.14	3579.1	3579.1
M2 (12.5m)	5.36	5.36	3599.5	3599.5

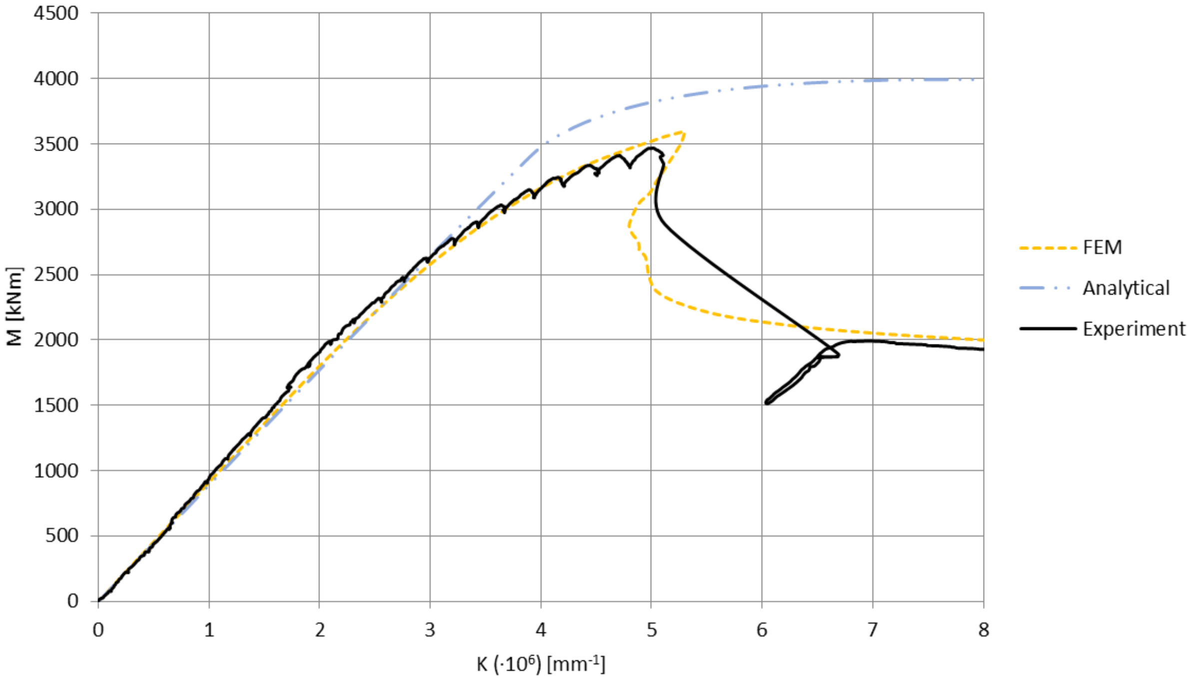

Figure 75: M-K relations of Tube 8

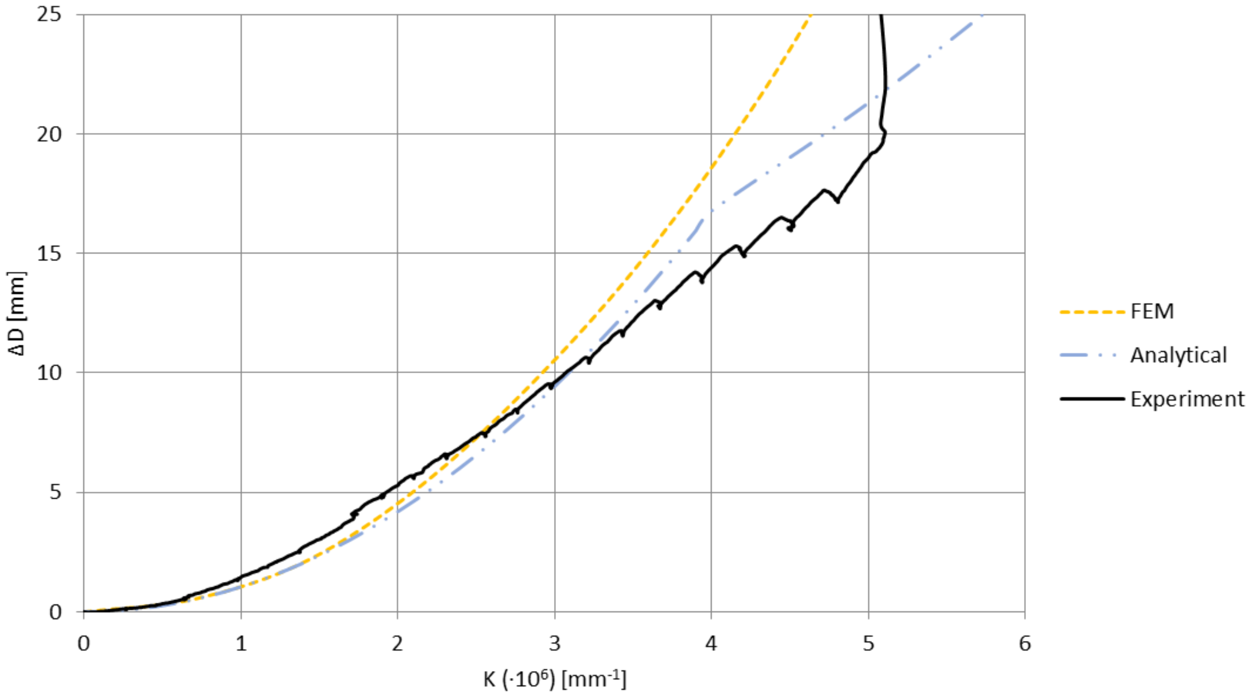

Figure 76: ΔD-K relations for Tube 8

For Tube 8, the neutral line model shows great agreement with experimental in pre-buckling path, the critical curvature obtained by model is relative accurate compare with experimental data, the curvature is slightly higher compare with the experimental data and the moment is more closer to the experiment. The deviation of experimental data from linear elatic line is due to the mistake of test. In terms of ovalization the model matches the analytical solution very well in elastic branch, and the model deviates a little bit when plasticity onset. Since Tube 8 also featured high D/t ratio, the ovalization is also restrained during experiment. Among all models, neutral line model has higher curvature than M1 but lower than M2, maximum moment has the same situaction as critical curvature, which indicates that in this case, M2 might suffer from geometric influence. Observing ovalization, it is again that neutral line model has the best performance.

5.1.6 Tube 9 results

Tube 9 is a plain spirally welded tube characterized with D/t = 65 and f_y= 570 MPa and the imperfection introduced in non-linear analysis is 2.01mm.

Table 9: Tube 9 results

	k_{buc} (10^6 /mm)	k_{crit} (10^6 /mm)	M_{buc} (kNm)	M_{crit} (kNm)
FEM	11.82	11.82	9680.2	9680.2
Gresnigt	-	12.4	-	9816.5
Experimental	9.90	9.22	8770.0	8978.0
M1 (8.1m)	10.85	10.85	9665.4	9665.4
M2 (12.5m)	12.04	12.04	9808.2	9808.2

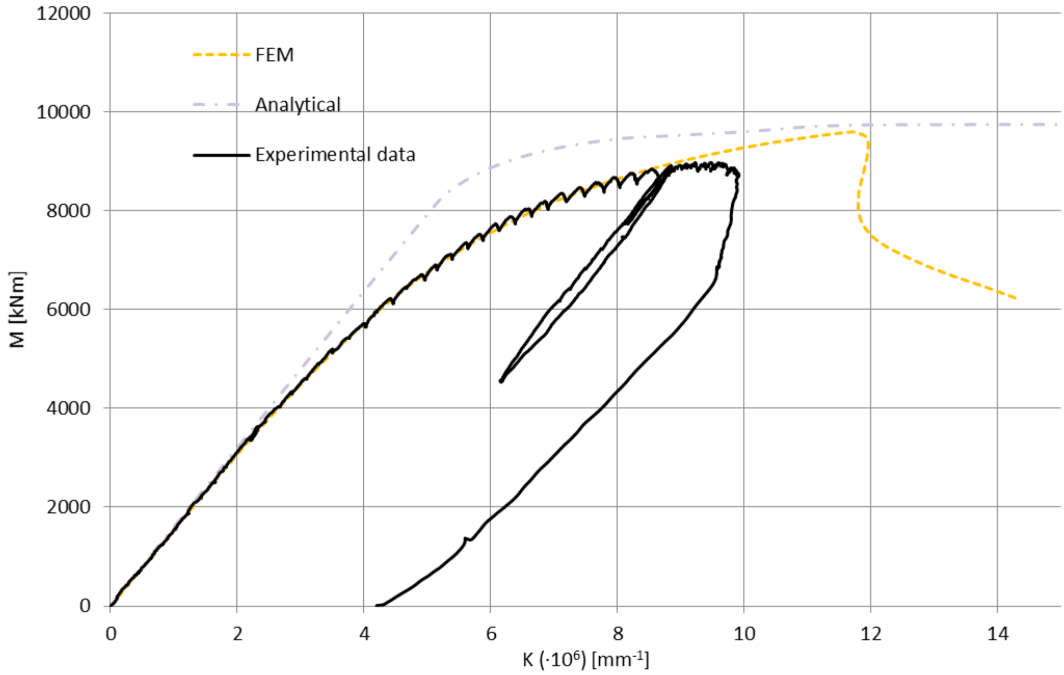

Figure 77: M-K relations of Tube 9

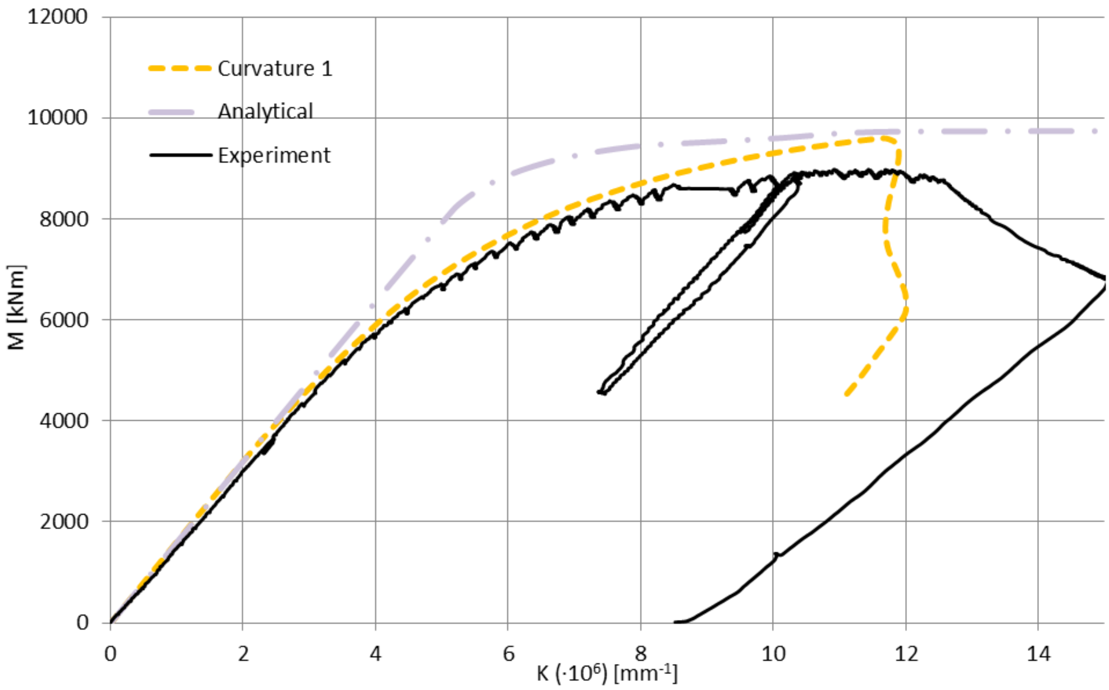

Figure 78: M-K relations forTube 9 of curvature 1

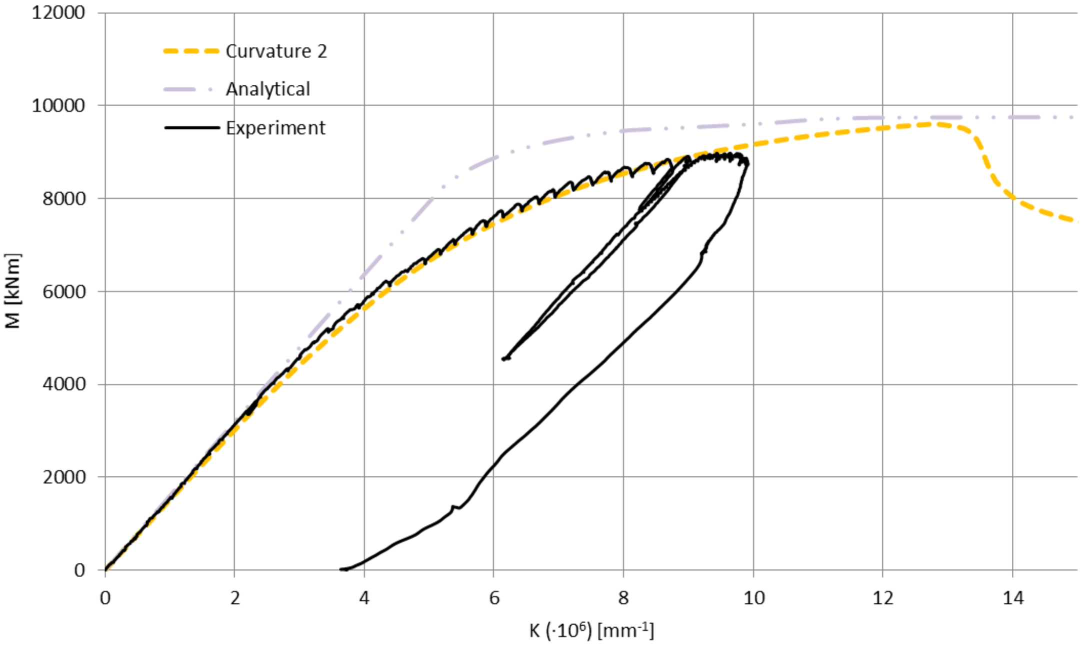

Figure 79: M-K relations forTube 9 of curvature 2

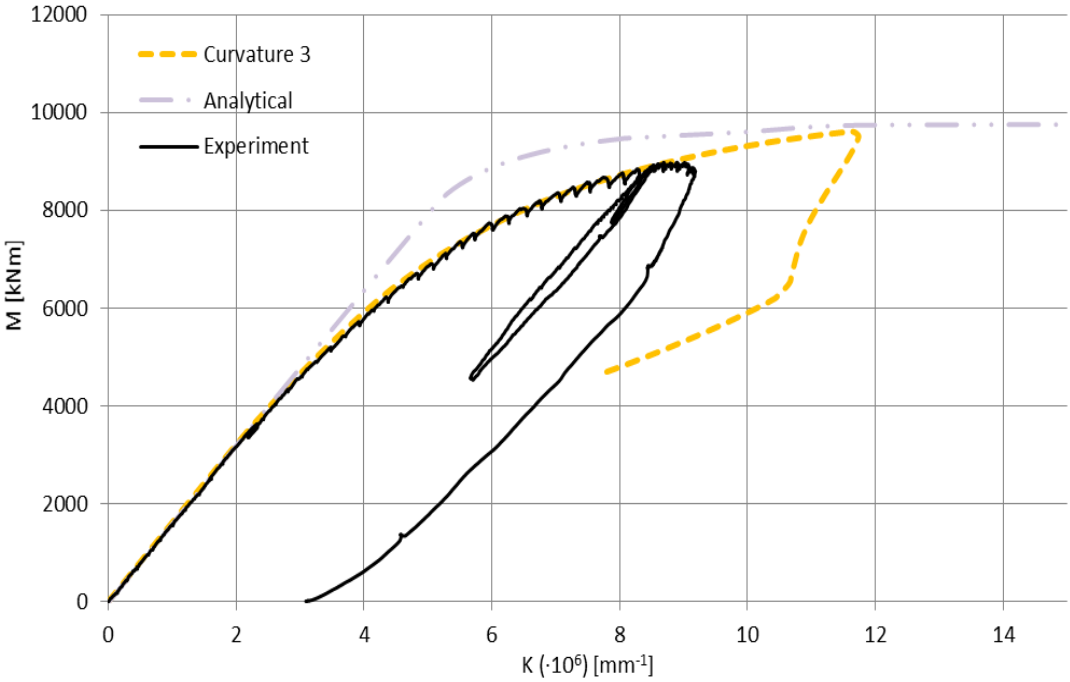

Figure 80: M-K relations forTube 9 of curvature 3

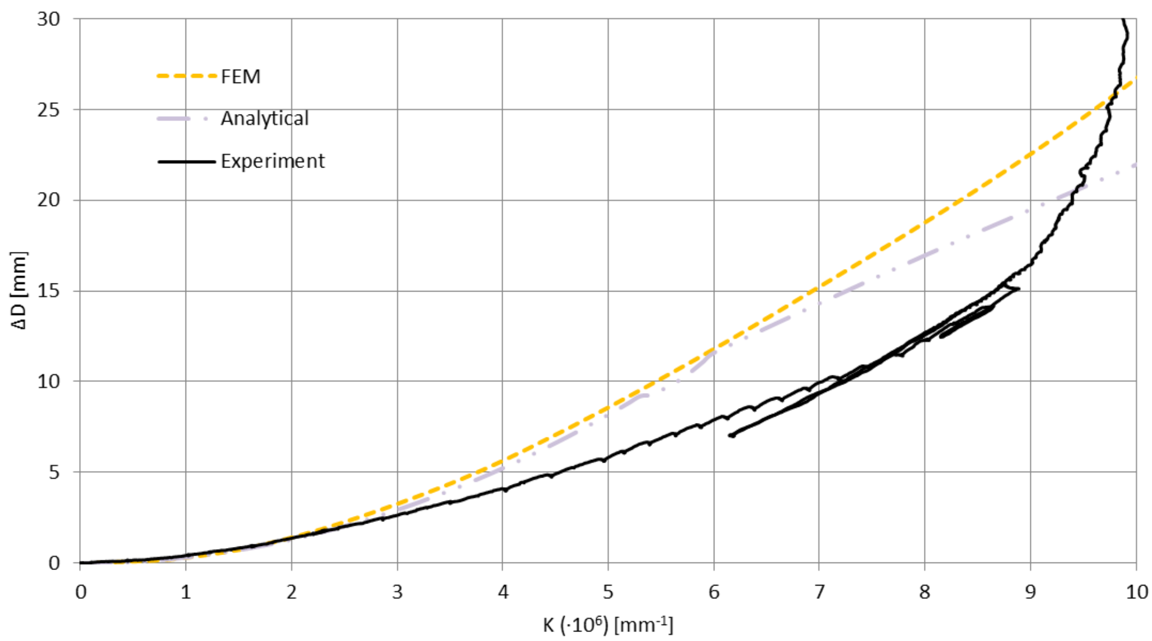

Figure 81: ΔD-K relations for Tube 9

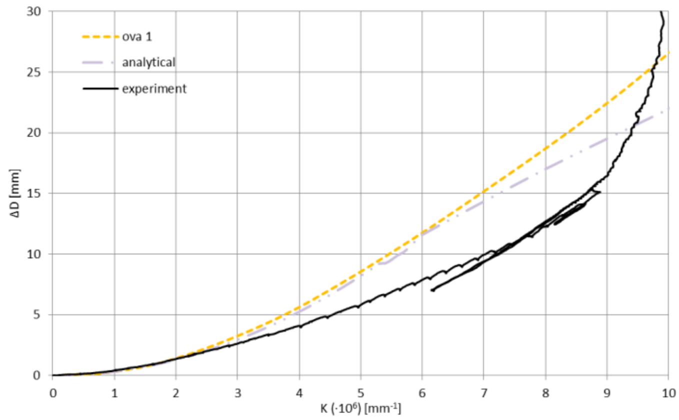

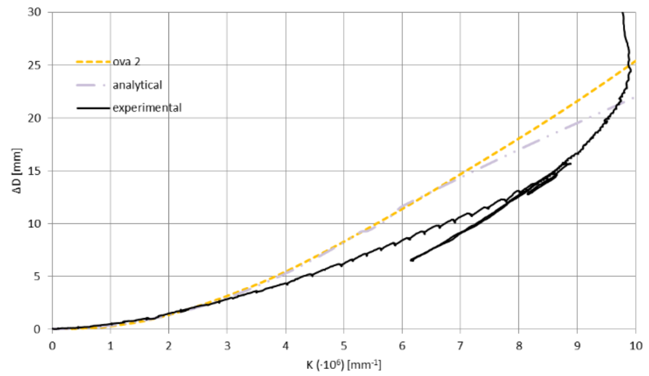

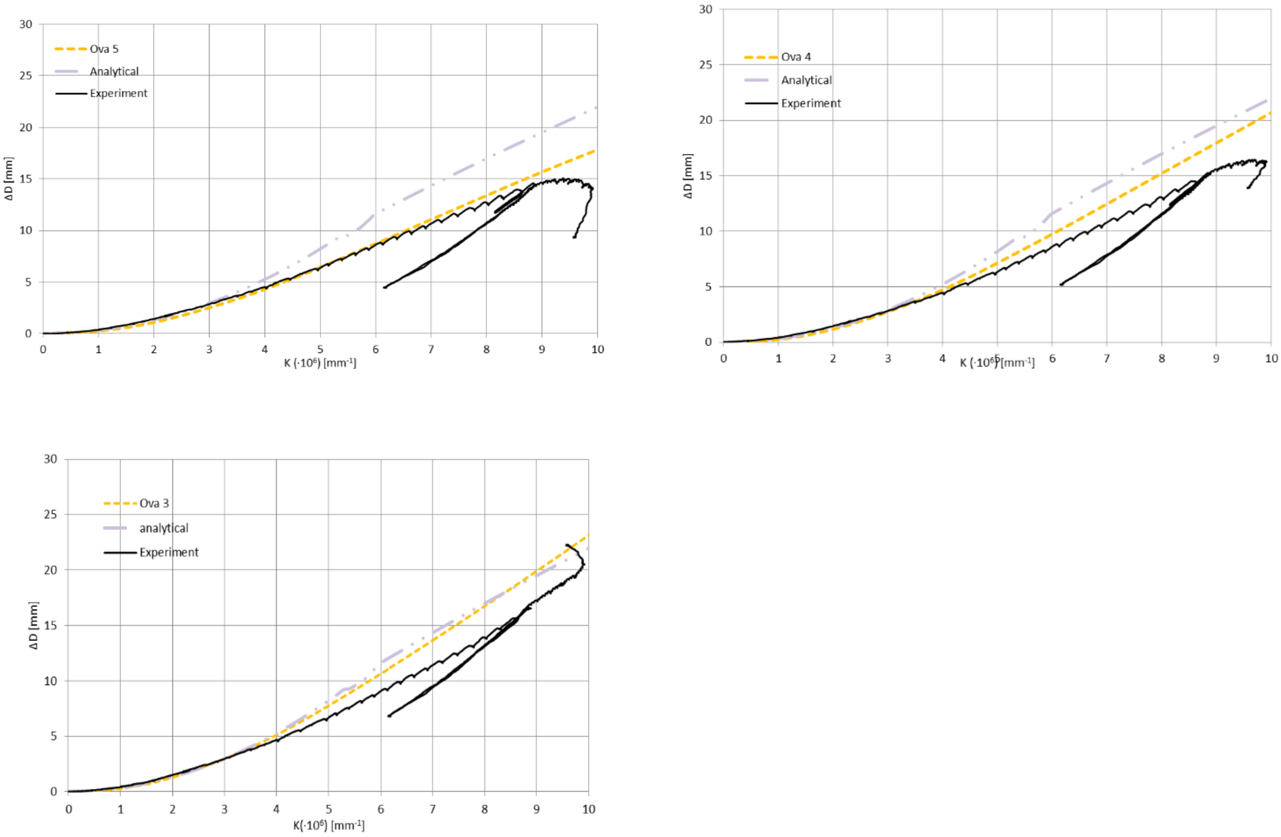

Figure 82: ΔD-K relations for Tube 11 at Ovalization bracket from OV1 to OV 5

For Tube 9, the neutral line model shows great agreement with experimental data in pre-buckling path, the critical curvature obtained by neutral line model is higher than experimental data, which is possibly caused by underestimated imperfection. Both critical curvature and moment is slightly higher than experimental data. In terms of ovalization the numerical model matches the analytical solution very well in elastic branch, and the model deviates a little bit when plasticity onset. The ovalization of Tube 9 is also restrained during experiment. Among all models, neutral line model has higher curvature than M1 but lower than M2, moment has the same situaction as critical curvature, which indicates that in this case, M2 might suffer from geometric influence. Observing ovalization, it is again that neutral line model has the best performance.

5.1.7 Tube 11 results

Tube 11 is a plain spirally welded tube characterized by D/t = 83, f_y= 340 MPa, and introduced imperfection is 0.465mm. The results of Tube 11 can be seen in Table 10.

Table 10: Tube 11 results

	k_{buc} (10^6 /mm)	k_{crit} (10^6 /mm)	M_{buc} (kNm)	M_{crit} (kNm)
FEM	9.47	9.47	4684.3	4684.3
Gresnigt	-	8.1	-	4677.9
Experimental	9.03	9.53	3724.5	4172.9
M1 (8.1m)	8.06	8.06	4649.7	4649.7
M2 (12.5m)	9.26	9.26	4687.0	4687.0

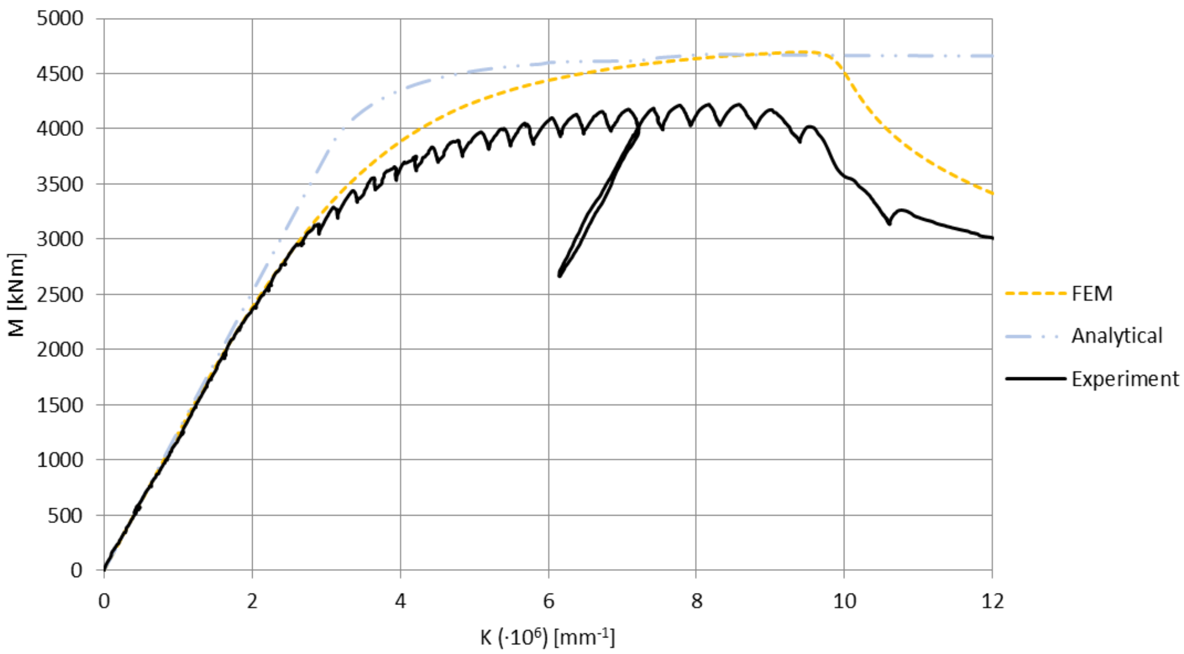

Figure 83: M-K relations of Tube 11

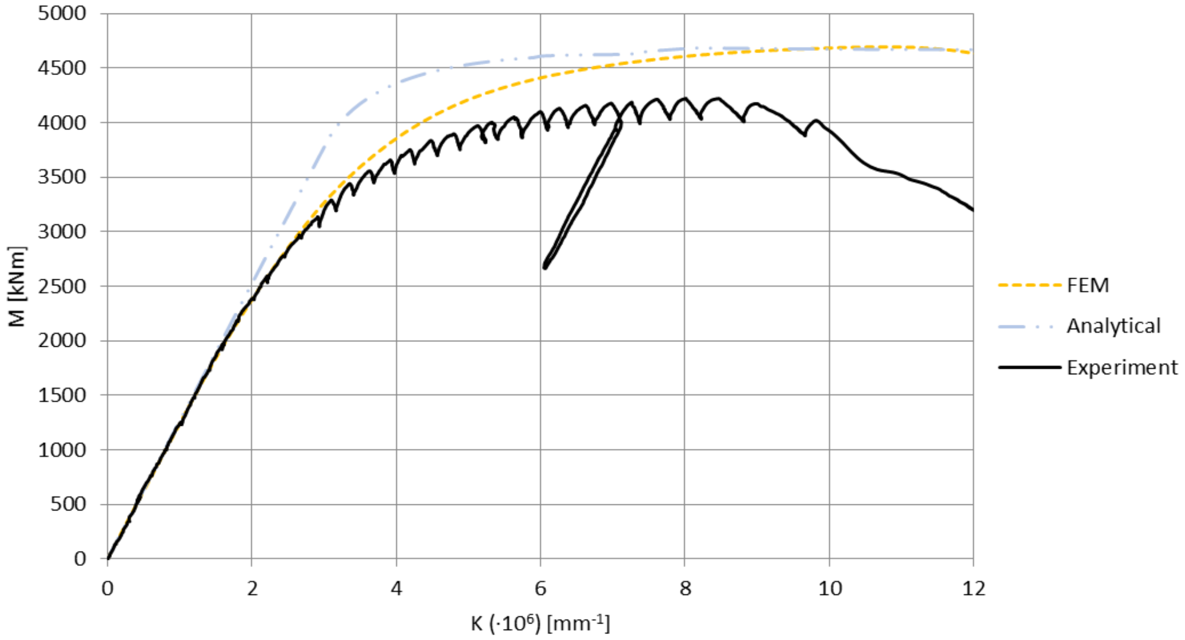

Figure 84: M-K relations forTube 11 of curvature 1

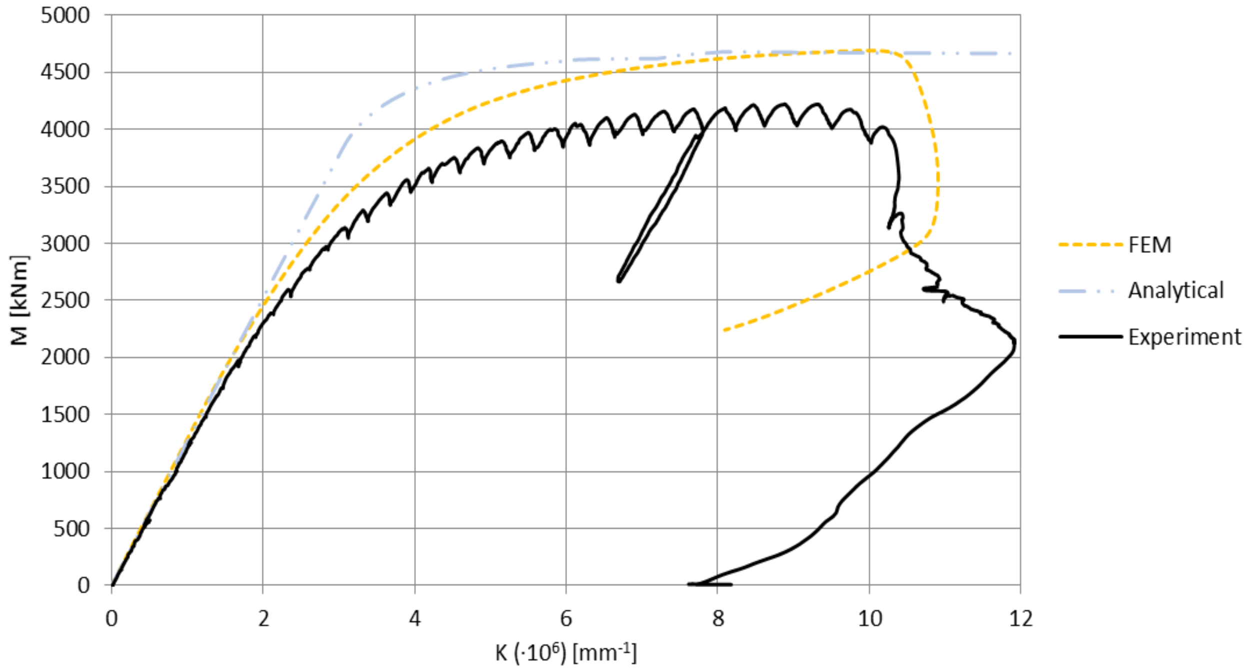

Figure 85: M-K relations forTube 11 of curvature 2

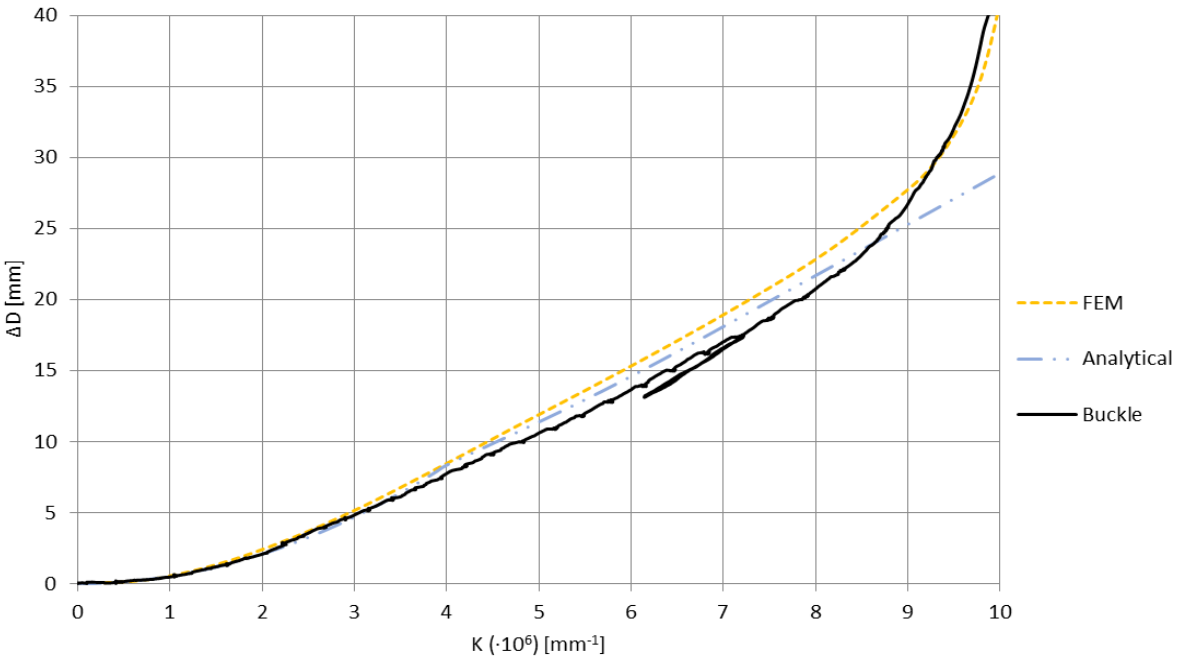

Figure 86: ΔD-K relations for Tube 11

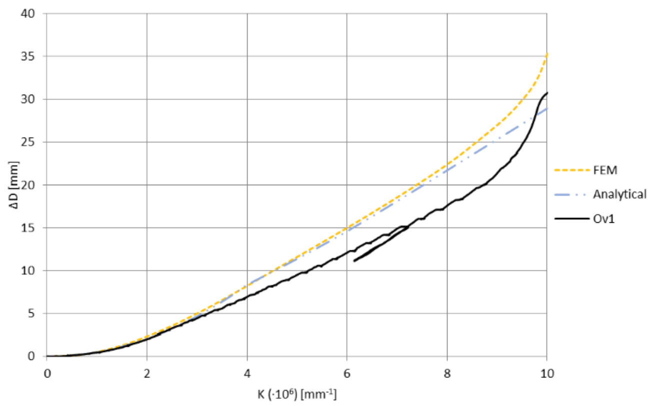

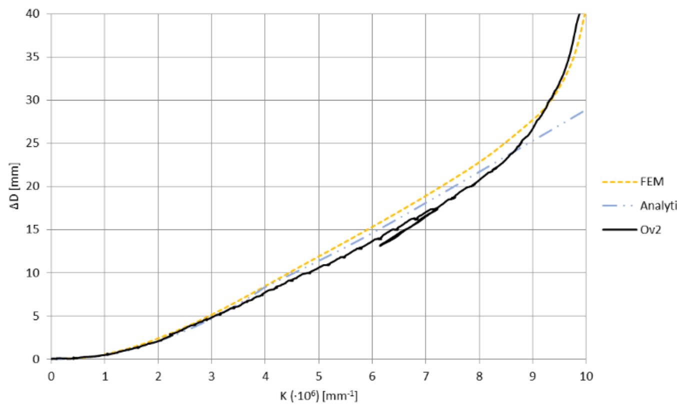

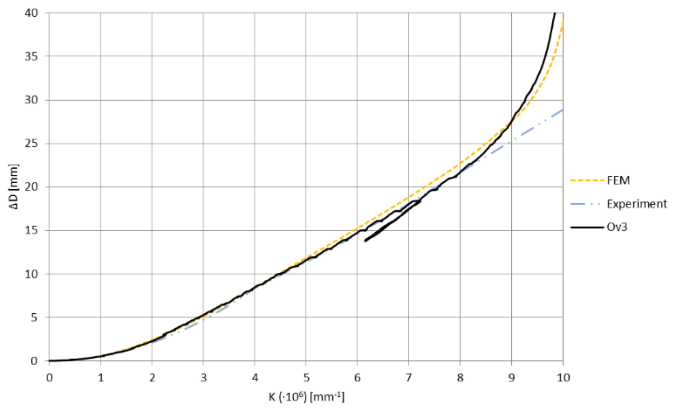

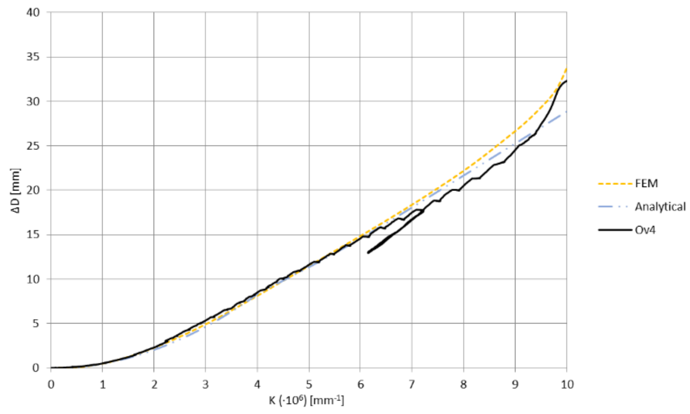

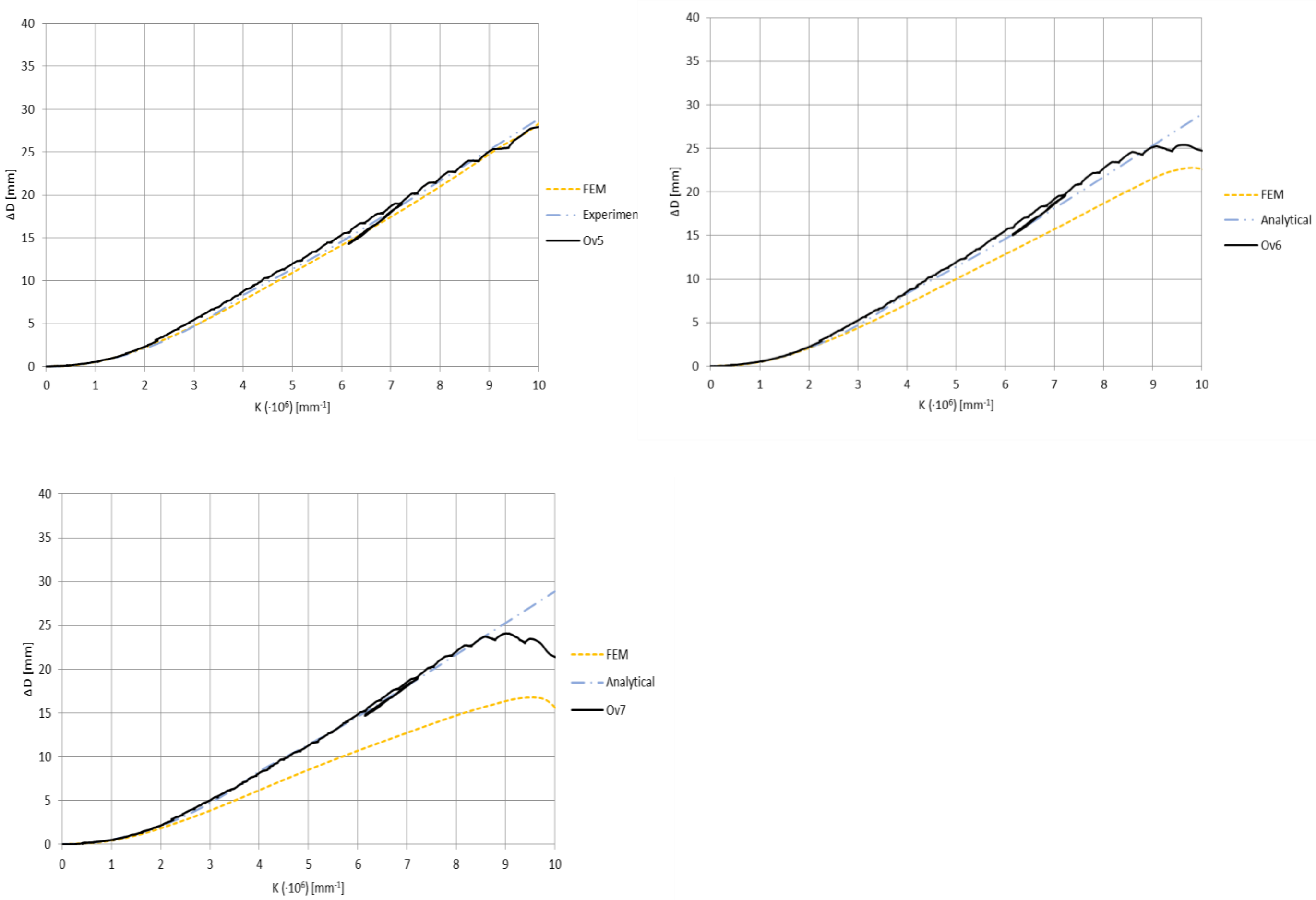

Figure 87: ΔD-K relations for Tube 11 at Ovalization bracket from OV1 to OV 7

For Tube 11, there is a great agreement for pre-buckling equilibrium path, the maximum moment is overestimated, while the critical curvature is significant obtained by neutral line model, with regard to the post-buckling equilibrium path, the model and experiment data have similar shape, which means the simulation performing very well, analytical solution has bigger maximum moment than experimental maximum moment, it is interesting that analytical solution underestimate the critical curvature without introducing the imperfection. With regard to the curvature bracket, bracket 1 overestimate both curvature and maximum, while curvature bracket 2 only overestimate moment, but relatively accurate critical curvature. In terms of ovalization, there is significant agreement between both analytical, experiment and neutra lline model. Compare with the other two model M1, M2, neutral line model has higher critical curvature than M2, almost equal to M1. The maximum moment of neutral line model is between M1 and M2. The ovalization of neutral line model has similar results as M2.

5.2 Tubes with welded feature

5.2.1 Tube 3 results

Tube 3 is a plain spirally welded tube with a girth weld in the center of the tube. The left side is characterized by D/t = 121 and f_y = 375 MPa, and the right side is characterized by D/t = 116 and f_y = 410 Mpa. The girth weld is characterized by an imperfection of 3.41mm. The results of Tube 3 can be seen in Table 11.

Table 11: Tube 3 results

	k_{buc} (10^6 /mm)	k_{crit} (10^6 /mm)	M_{buc} (kNm)	M_{crit} (kNm)
FEM	4.29	4.29	2797	2797
Gresnigt	-	8.0	-	3647.2
Experimental	3.44	3.41	2809.9	2878.7
M1 (8.1m)	5.20	5.20	3139.4	3139.4

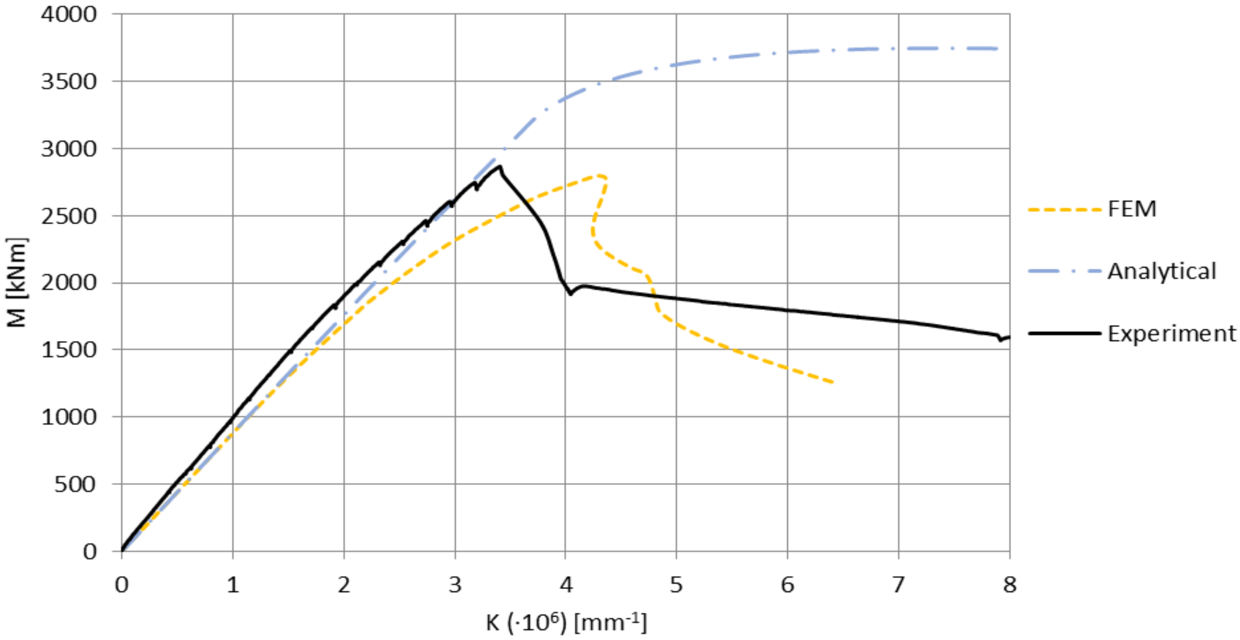

Figure 88: M-K relations of Tube 3

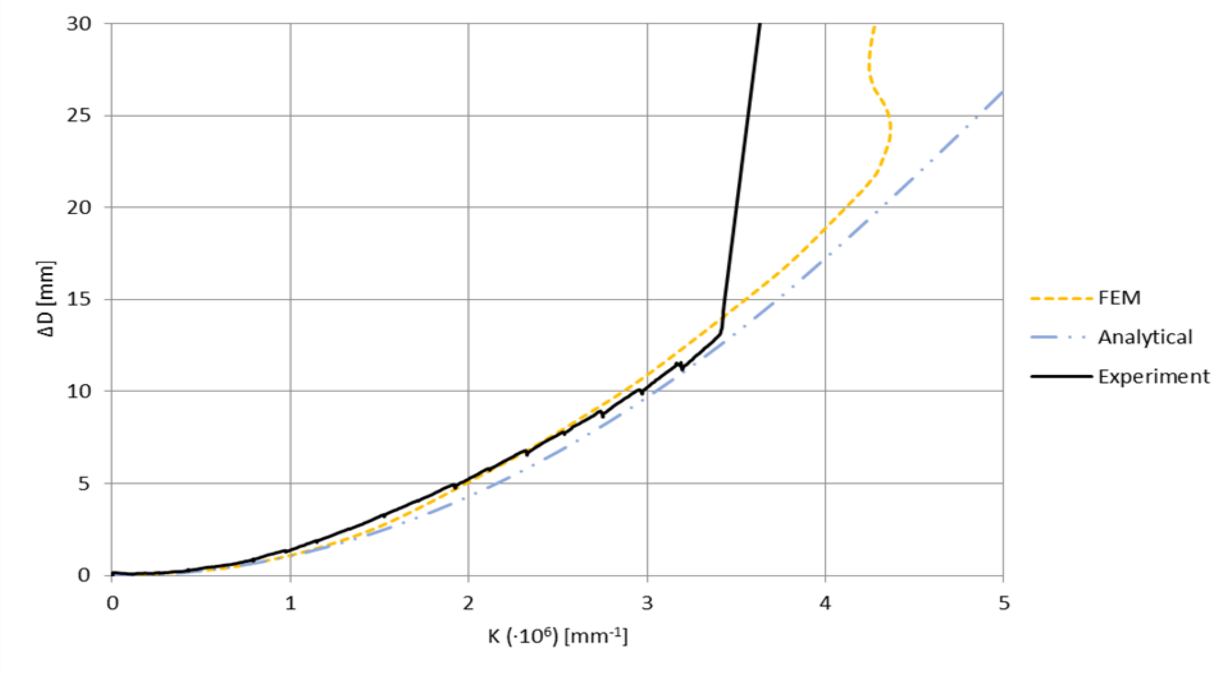

Figure 89: ΔD-K relations for Tube 3

For tube 3, the neutral line model deviates from experimental data at relatively low curvature, but it follows well with the analytical solution during elastic stage, because analytical cannot represent tube with weld feature, it makes sense that when plasticity onset, deviation will definitely appear. It is interesting that the moment obtained by neutral line model is close to the experimental data. The deviating of curvature could explaine by the material data and the thermal mechanical interation on the either side of the girth weld. The ovalization of neutral line model is greatly agree with the path of experiment until buckle point happens. Tube 3 featured welded feature, only M1 is modelled, compare with M1, critical curvature and maximum moment are both lower than M1, which more close to the experimental data, it is interesting that when considering tube with weld features, neutral line model obtain more accuracy result than the model with fix ends (M1).

5.2.2 Tube 6 results

Tube 6 features a coil connection weld but no girth weld. The left side is characterized byD/t = 66 and f_y = 525 MPa. The right side is characterized by D/t = 65 and f_y = 545 MPa. The results of Tube 6 could be seen in Table 12.

Table 12: Tube 6 results

	k_{buc} (10^6 /mm)	k_{crit} (10^6 /mm)	M_{buc} (kNm)	M_{crit} (kNm)
FEM	6.34	6.34	7826.22	7826.22
Gresnigt	-	11.8	-	9151.5
Experimental	9.30	8.84	7667.9	8160.4
M1 (8.1m)	8.09	8.09	6490.7	6490.7

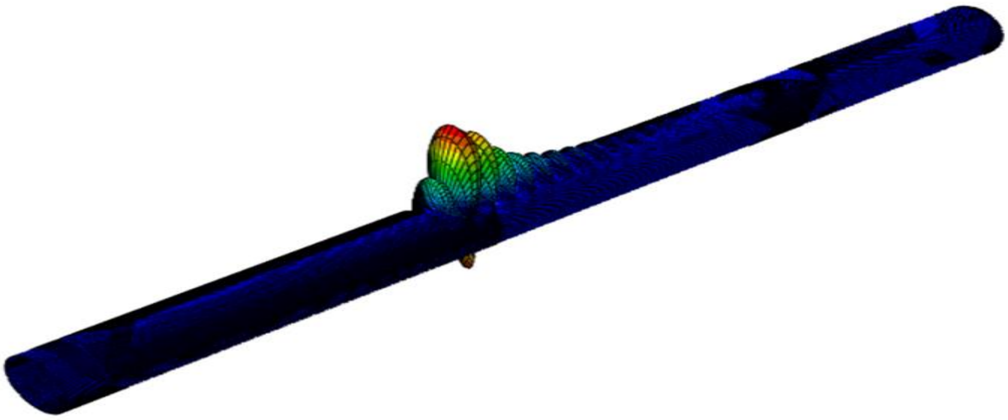

Figure 90: Linear imperfection shape of tube 6

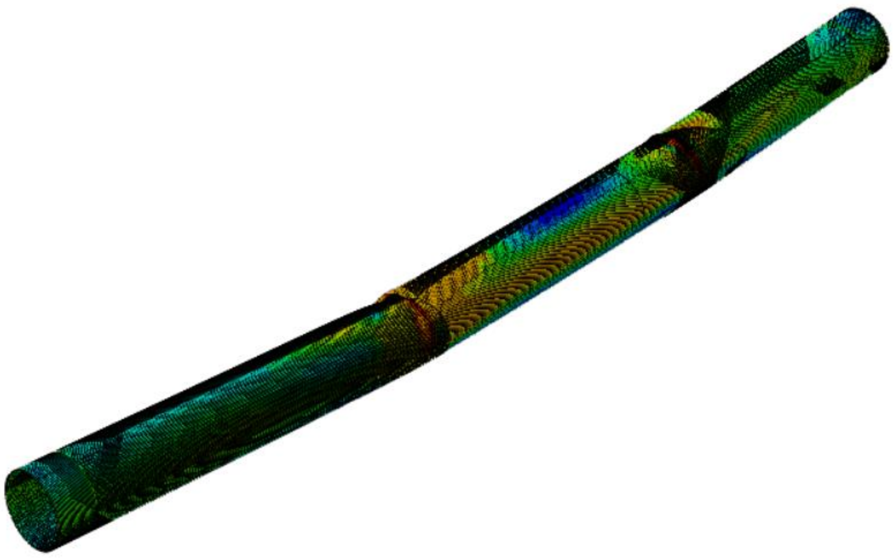

Figure 91: Non-linear deformed shape of tube 6

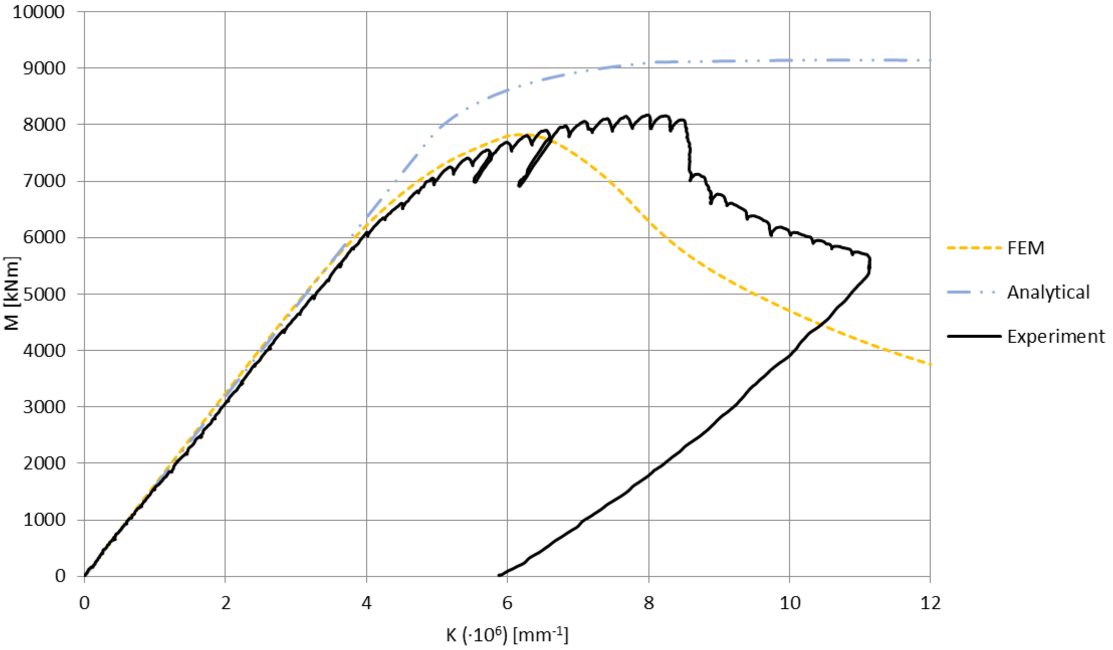

Figure 92: M-K relations of Tube 6

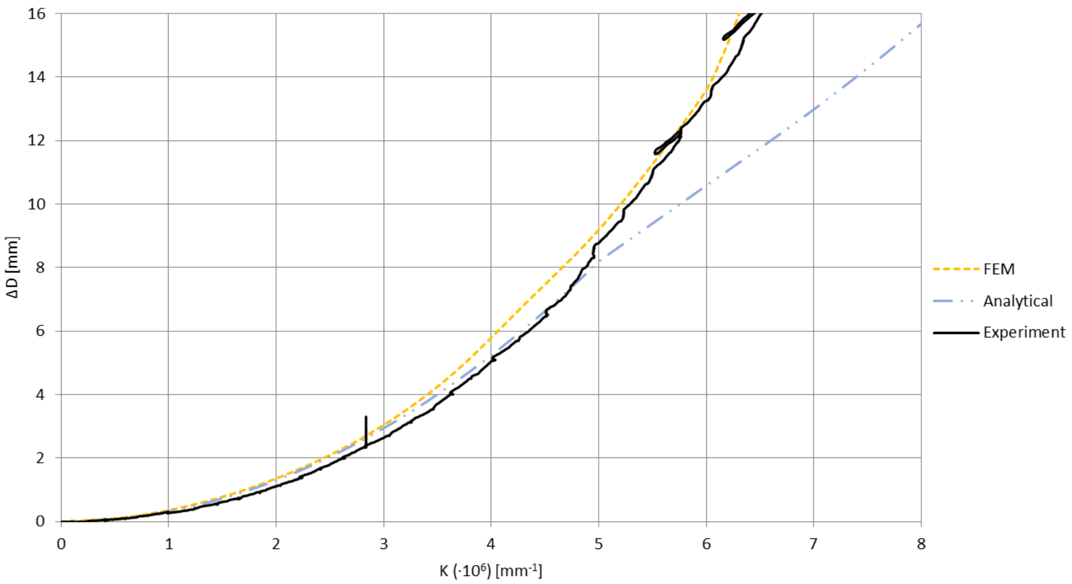

Figure 93: ΔD-K relations for Tube 6

For tube 6, which featured coil connection weld, the imperfection is chosen by intermediate imperfection, observing the buckle point which underestimate the experimental data shows that the imperfection value might be overestimate, however neutral line model shows great agreement with pre-equilibrium path with both experiment and analytical solution. Analytical solution greatly overestimates both maximum moment and curvature, while neutral line model predict relatively accurate maximum moment. Apart from the property of material could not be well explained by the matrial model, the interaction of welding is also a big influence factor. It can be noticed that the ovalization is excellent predict by neutral line model, even the buckle point is underestimated, the ovalization path shows a great agreement with both analytical and experimental data. M1 has better predicting in terms of critical curvature, but worse in predicting maximum moment. Finally, it should be pay attention to the linear buckling imperfection shape for tube 6, it features with incorrected shape, it might be caused by the asymmetrical geometry and material property with different parts. It can be also caused by wrong modelling approach for tube 6 with coil connection welds. It was found that in simulation of the tube 6, diameter of different part varies, which lead to negative influence on buckling behavior, and this problem should be resloved in future study.

5.2.3 Tube 7 results

Tube 7 is a tube featuring a girth weld and a coil connection weld. All sections are characterized by D/t = 65. The left section is characterized by f_y= 545 MPa, the middle section by f_y = 575 MPa, and the right section by f_y = 560 MPa. The imperfection introduced to model is 2.45mm and occured in the left section. The results of Tube 7 can be seen in Table 13.

	k_{buc} (10^6 /mm)	**k_{crit} (10^6 /mm)**	**M_{buc} (kNm)**	**M_{crit} (kNm)**
FEM	10.14	10.14	9411.2	9411.2
Gresnigt	-	12.5	-	9736.5
Experimental	8.20	7.88	8092.6	9736.9
M1 (8.1m)	10.64	10.64	9649.2	9649.2

Table 13: Tube 7 results

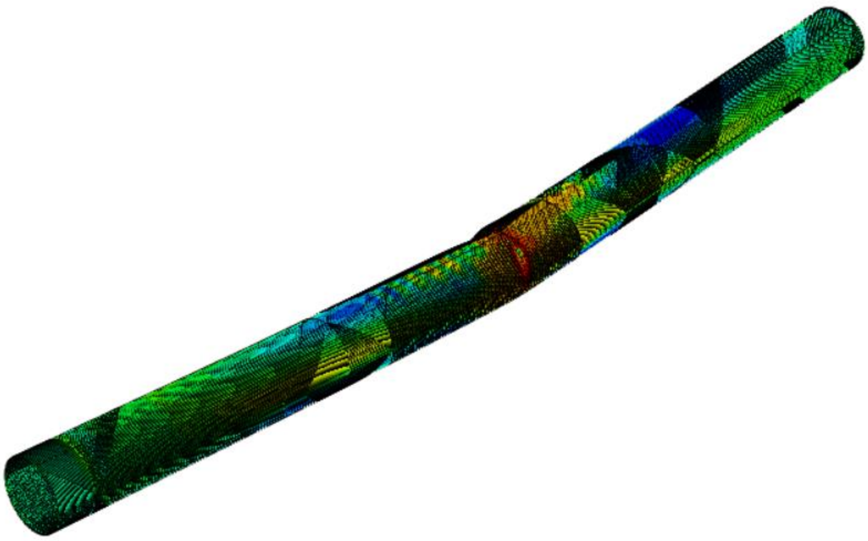

Figure 94: Non-linear deformed shape of tube 7

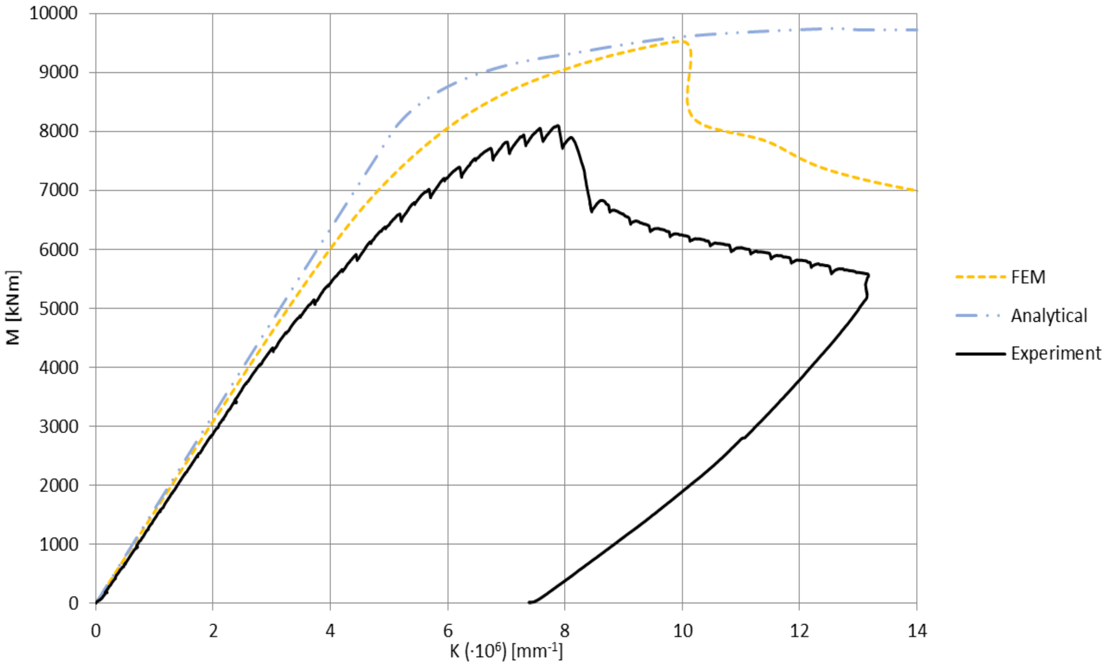

Figure 95: M-K relations of Tube 7

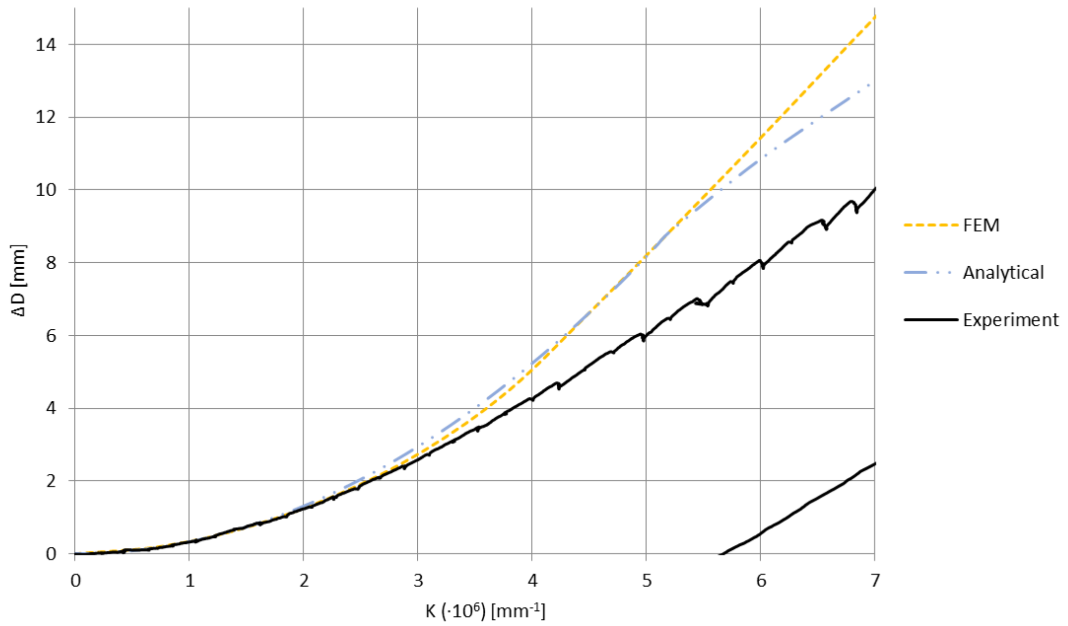

Figure 96: ΔD-K relations for Tube 7

For tube 7, which includes both girth welds and coil connection welds, the final deformed shape can be seen in Figure 84, observing the peak point of bending moment which underestimate the experimental data shows that the imperfection value might be overestimated, however before neutral line model shows plasticity, experimental diagram already deviate from linear branch. It indicates that apart from the property of material could not be well explained by the matrial model, the interaction of welding is also a big influence factor. The residual stress might also not correctly modelled in numerical model. It can be noticed that the ovalization is excellent predict by neutral line model, which follows analytical solution quite well, even the buckling point is overestimated. The ovalization path shows that the ovalization of tube 7 is restrained during physical experiment. Neutral line model has better performance in predicting critical curvature, but worse in predicting maximum moment.

5.2.4 Tube 10 results

Tube 10 includes both girth and coil connection welds. The left section is characterized by D/t = 80 and f_y= 525 MPa, the mid section is characterized by D/t = 80 and f_y= 485 MPa, and the right section is characterized by D/t = 84 and f_y= 325 MPa.. The results of Tube 10 can be seen in Table 14.

Table 14: Tube 10 results

	k_{buc} (10^6 /mm)	k_{crit} (10^6 /mm)	M_{buc} (kNm)	M_{crit} (kNm)
FEM	6.41	6.41	4230.1	4230.1
Gresnigt	-	9.8	-	6155.2
Experimental	6.02	5.57	3982.9	4270.2
M1 (8.1m)	7.20	7.20	4445.8	4445.8

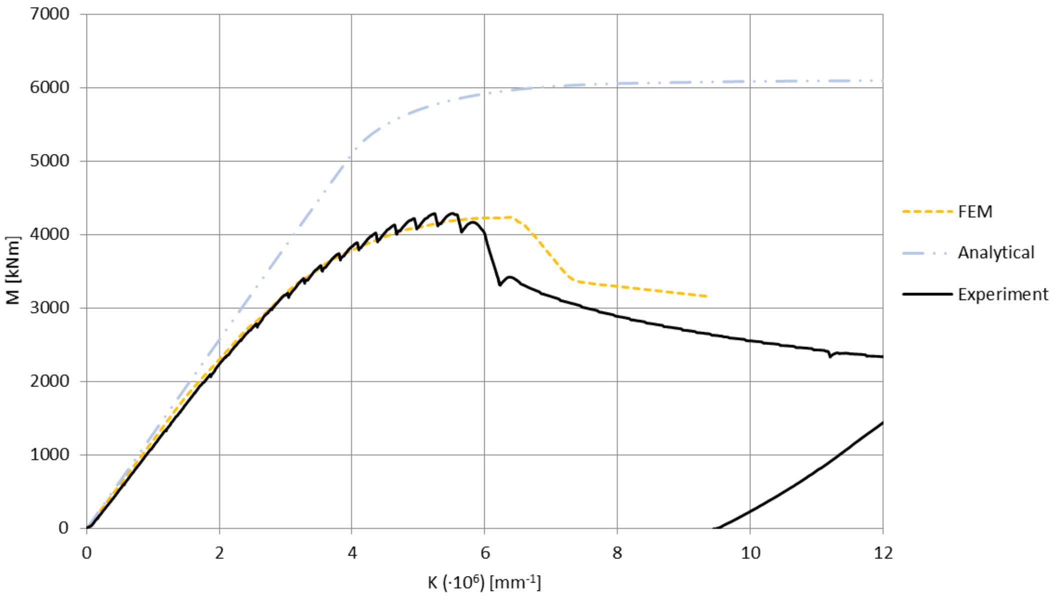

Figure 97: M-K relations of Tube 10

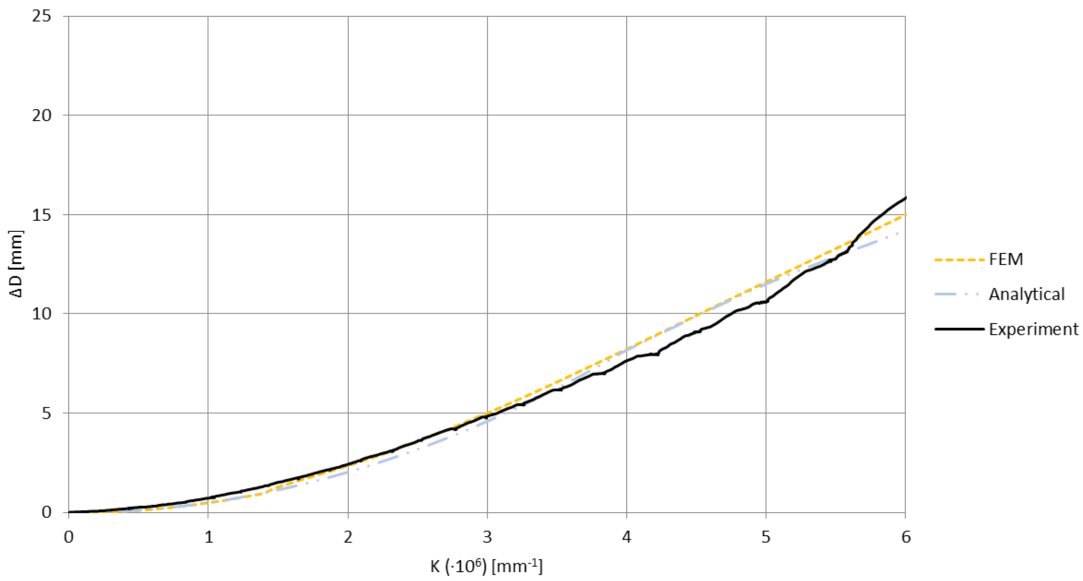

Figure 98: ΔD-K relations for Tube 10

Tube 10 is well simulated by neutral line model in terms of pre-buckling path, even the critical curvature is a little bit overestimate by neutral line model, the maximum moment obtained by neutral line model is very close to the experiment data, this could be that the imperfection introduced to the neutral line is a little bit overestimate, and the residual stress ratio is relative good enough since they have similar equilibrium shape. With regard to the analytical solution, it is again overestimated both curvature and moment because of limiting property that it cannot take into account two different yield strengths. In terms of ovalization, neutral line model again shows a great agreement with experimental data and the analytical solution. The results obtained by neutral line model are more close to the experimental results.

5.2.5 Tube 12 results

Tube 12 features both girth and coil connection welds. The left section is characterized by D/t = 117 and f_y= 430 MPa, the mid section is characterized by D/t = 116 and f_y = 426 MPa, and the right section is characterized by D/t = 117 and f_y = 430 MPa. An imperfection was introduced into the left section with 1.16mm. The results of Tube 12 can be seen in Table 15.

Table 15: Tube 12 results

	k_{buc} (10^6 /mm)	**k_{crit} (10^6 /mm)**	**M_{buc} (kNm)**	**M_{crit} (kNm)**
FEM	4.91	4.91	3557	3557
Gresnigt	-	8.5	-	4054.3
Experimental	4.82	5.59	3435.3	3435.3
M1 (8.1m)	6.03	6.03	3722.8	3722.8

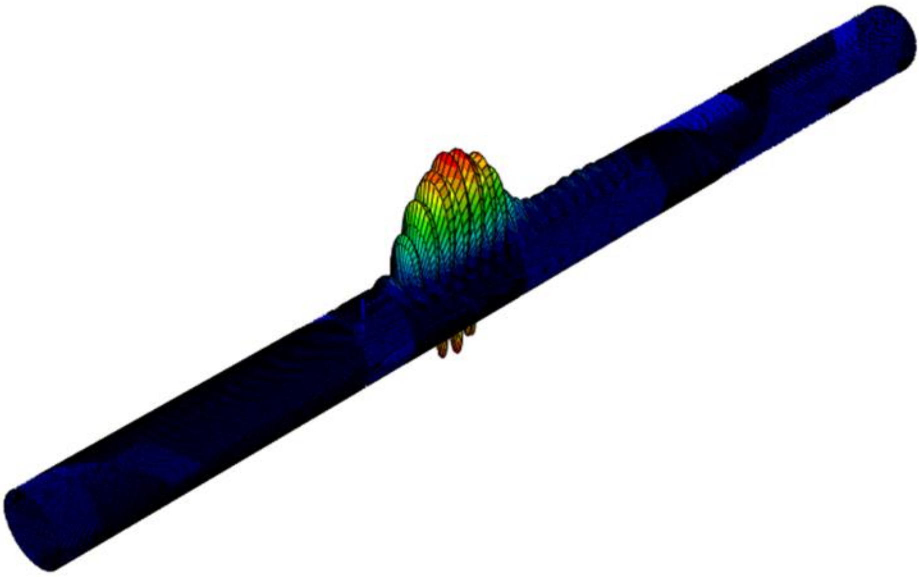

Figure 99: Linear imperfection shape of tube 12

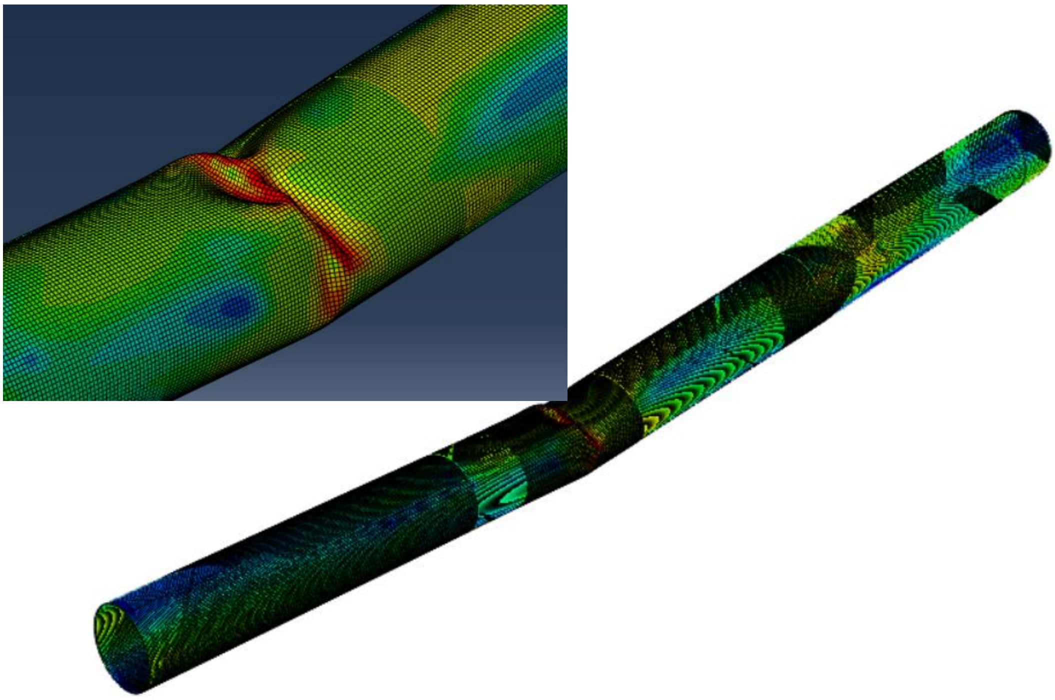

Figure 100: Non-linear deformed shape of tube 12

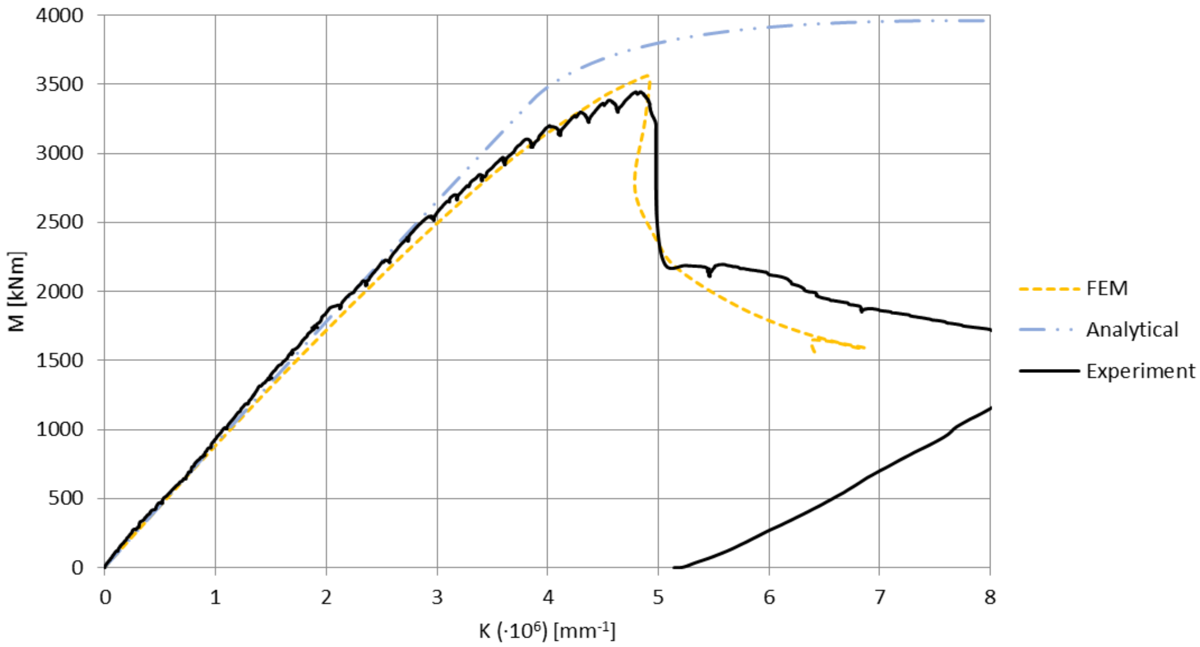

Figure 101: M-K relations of Tube 12

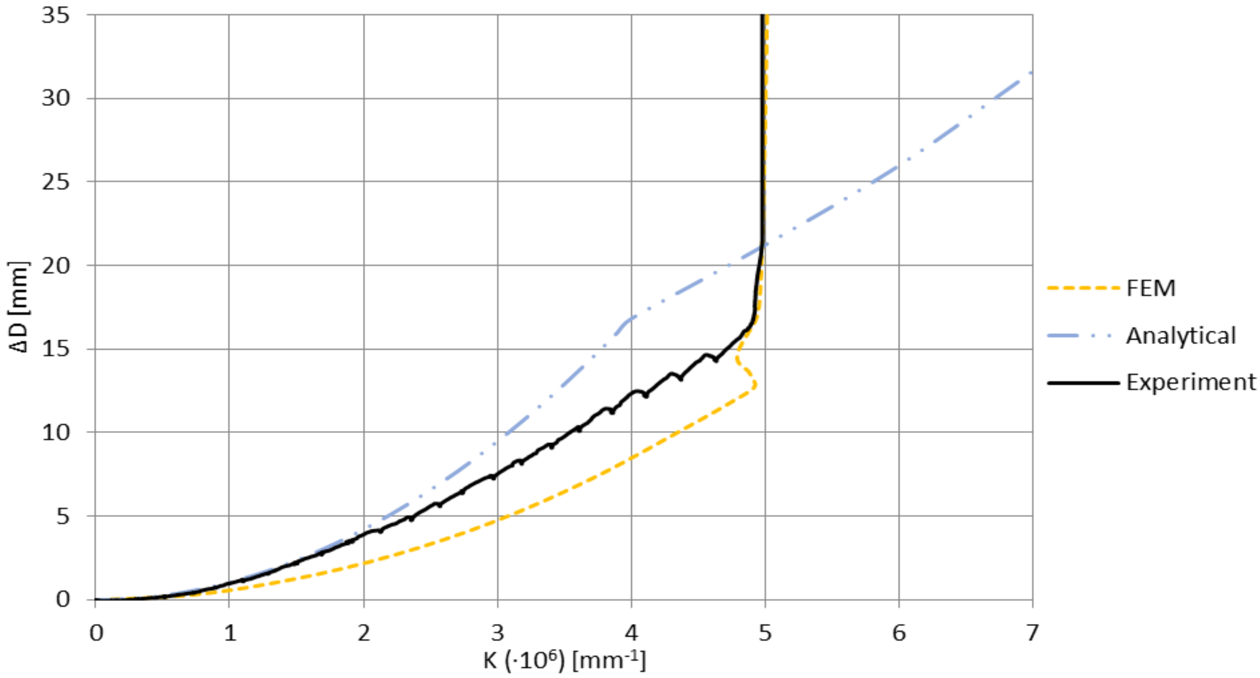

Figure 102: ΔD-K relations for Tube 12

Tube 12 featured both girth welds and coil connection welds, the final deformed shape can be seen in Figure 89, which occurs to the left of middle. The results from numerical model show great agreement with experimental data, following well in terms of pre-buckling path. The critical curvature is accurately predicted by neutraline model, the maximum moment obtained by neutral line model is also very close to the experiment data. In terms of ovalization, the results of neutraline model is greatly deviated from both experimental data and analytical solution. It is noticeable that tube 12 also obtained incorrect imperfection shape, the reason is similar as tube 6, the asymmetrical material properties and geometrical dimension. In further numetical study, this problem should be corrected.

5.2.6 Tube 13 results

Tube 13 is a spirally welded tube with a girth weld in the center. The left side is characterized by D/t = 118 and f_y = 425 MPa, and the right side is characterized by D/t = 116 and f_y = 445 Mpa. The imperfection amplititude that introduced to the model is 1.645mm. The results of Tube 13 can be seen in Table 16.

Table 16: Tube 13 results

	k_{buc} (10^6 /mm)	k_{crit} (10^6 /mm)	M_{buc} (kNm)	M_{crit} (kNm)
FEM	4.81	4.81	3382.6	3382.6
Gresnigt	-	8.5	-	4094.7
Experimental	5.15	5.15	3393.2	3435.3
M1 (8.1m)	5.54	5.54	3628.0	3628.0

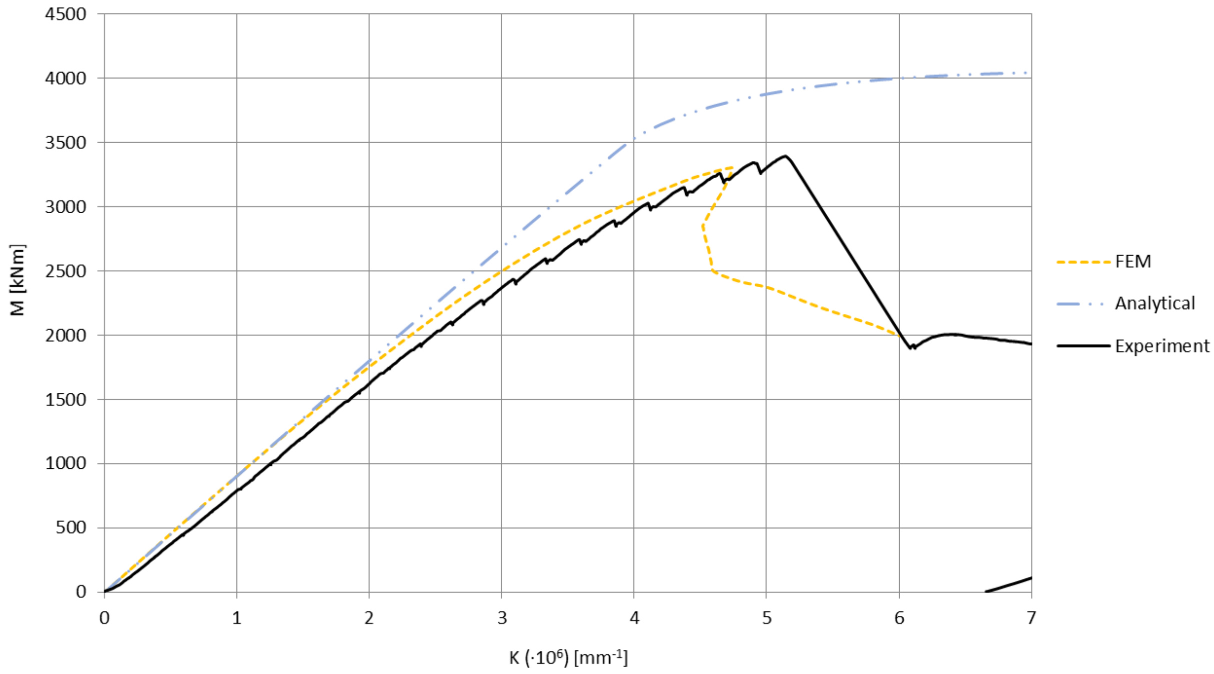

Figure 103: M-K relations of Tube 13

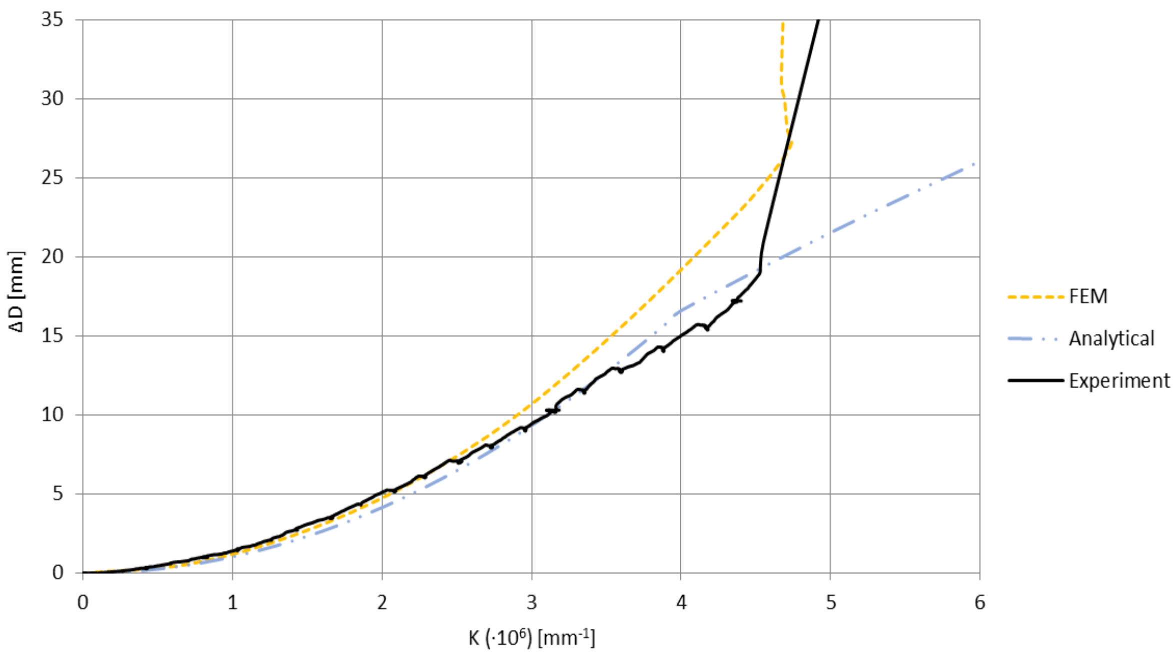

Figure 104: ΔD-K relations for Tube 13

For tube 13, the curvature obtained by neutral line model is slightly underestimated, while the maximum moment is relatively close. Analytical greatly overestimate curvature and moment. With regard to the ovalization, neutral line model follows well with experimental data, it start to deviate when plasticity onset. Compare with the model with fix ends, neutral line model has the same critical curvature as M1, and the maximum obtained by neutral line model is lower than M1, which is more close to experimental data.

5.3 Longitudinal welded tubes

5.3.1 Tube 14 results

Tube 14 is a longitudinally welded tube characterized by D/t = 109, f_y = 525 MPa, and the imperfection value that introduced into the FEM model is 1.066mm. The results of Tube 14 can be seen in Table 17.

Table 17: Tube 14 results

	k_{buc} (10^6 /mm)	k_{crit} (10^6 /mm)	M_{buc} (kNm)	M_{crit} (kNm)
FEM	5.86	5.86	4501.30	4501.30
Gresnigt	-	9.9	-	5212.2
Experimental	5.75	5.75	4357.5	4357.5
M1 (8.1m)	6.65	6.65	4532.8	4532.8
M2 (12.5m)	6.90	6.90	4533.1	4533.1

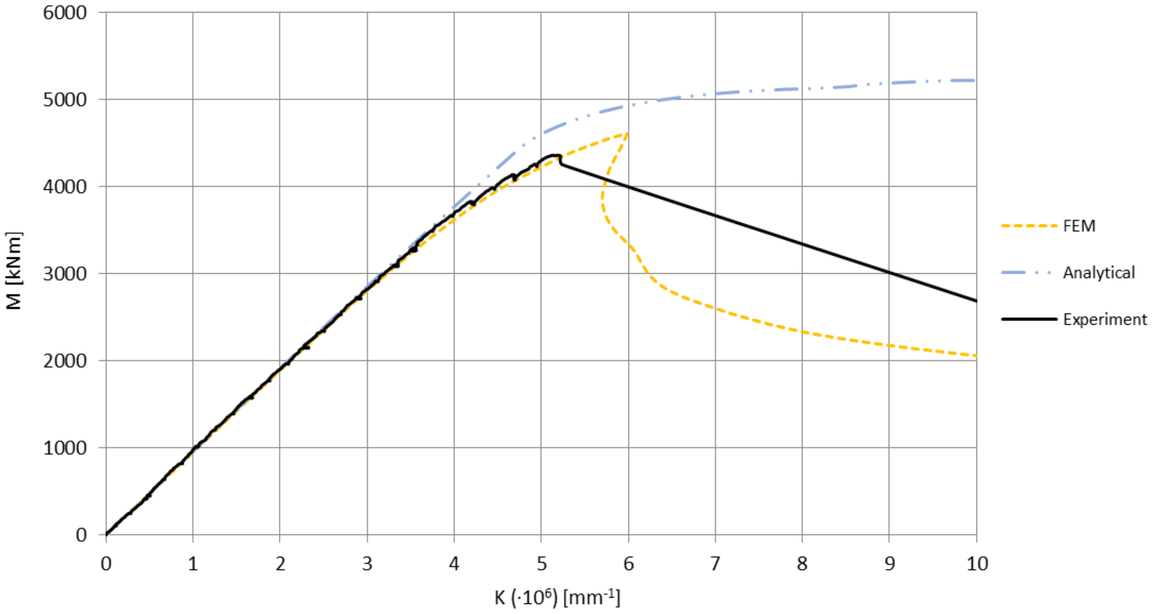

Figure 105: M-K relations of Tube 14

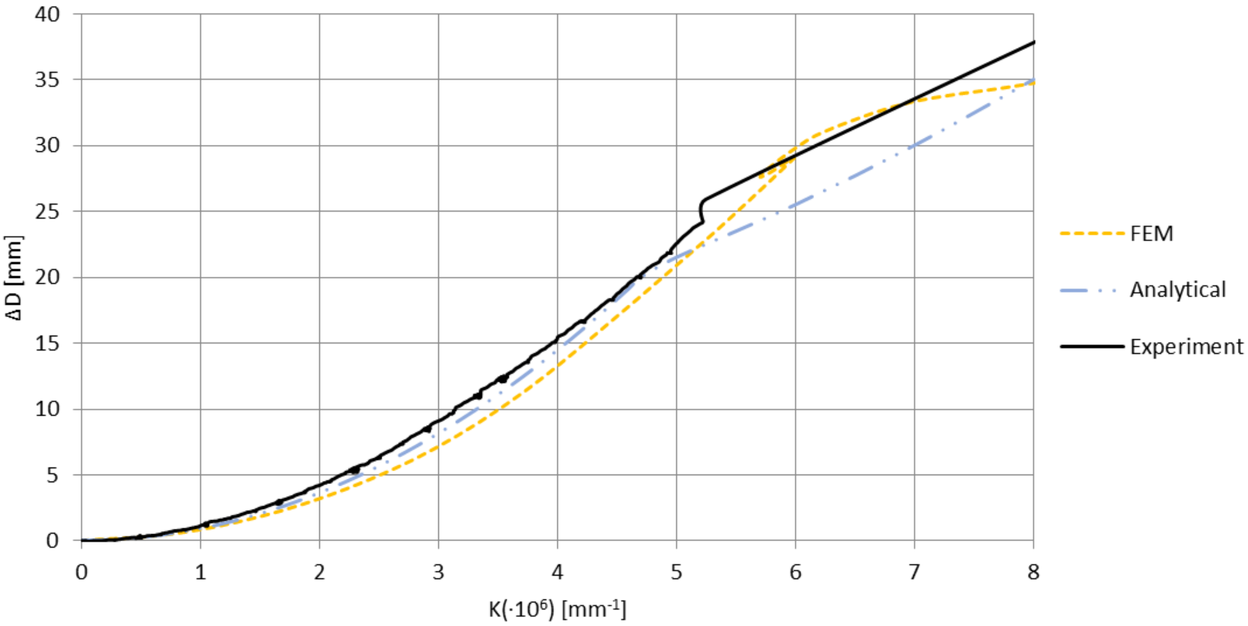

Figure 106: ΔD-K relations for Tube 14

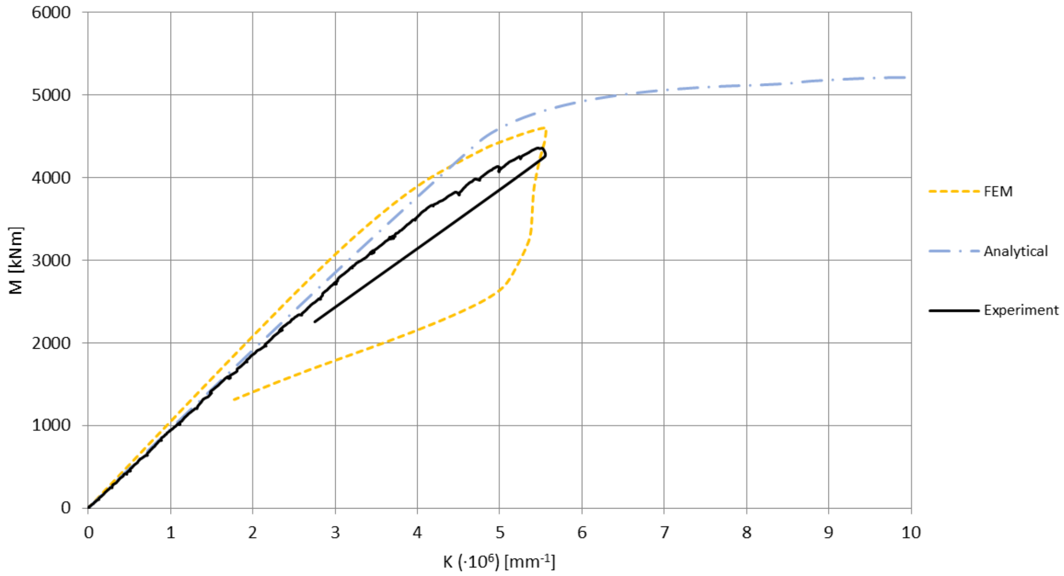

Figure 107: M-K relations forTube 14 of curvature 1

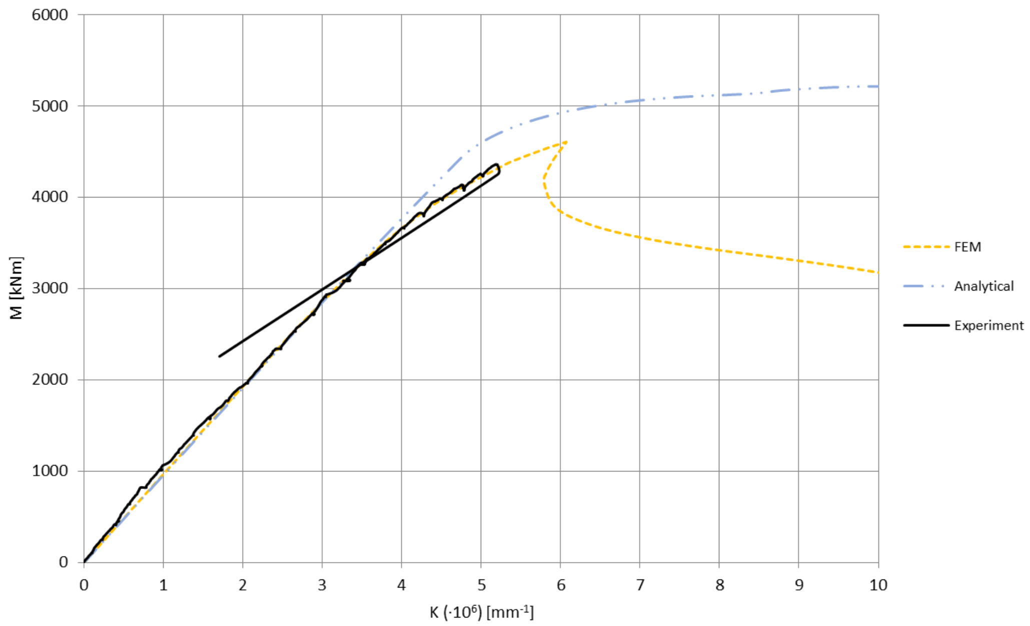

Figure 108: M-K relations forTube 14 of curvature 2

For tube 14, there is good agreement between neutral line model and experiment in terms of pre-buckling equilibrium path, the critical curvature obtained by neutral line model is slightly lower than the experimental data, the moment is more closely. The ovalization shows good prediction compared with experimental data, although it starts to deviate after elastic stage. Both critical curvature and maximum moment predicted by neutral line model is more closely to experimental data compare with M1.

5.3.2 Tube 15 results

Tube 15 is a longitudinally welded tube characterized by D/t = 72, f_y = 535 MPa, and the imperfection value that introduced to the FEM model is 0.996mm. The results of Tube 15 could be seen in Table 18.

Table 18: Tube 15 results

	k_{buc} (10^6 /mm)	k_{crit} (10^6 /mm)	M_{buc} (kNm)	M_{crit} (kNm)
FEM	11.50	11.50	8192.3	8192.3
Gresnigt	-	11.50	-	8308.9
Experimental	12.50	12.11	7305.5	7665.7
M1 (8.1m)	10.26	10.26	8076.8	8076.8
M2 (12.5m)	11.66	11.66	8196.5	8196.5

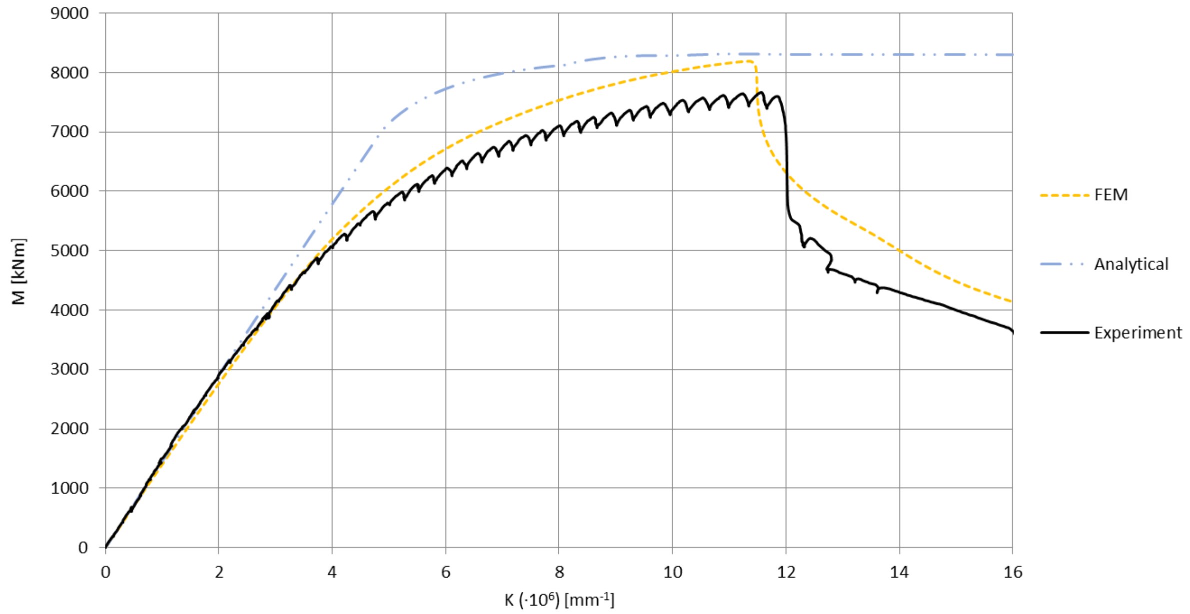

Figure 109: M-K relations of Tube 15

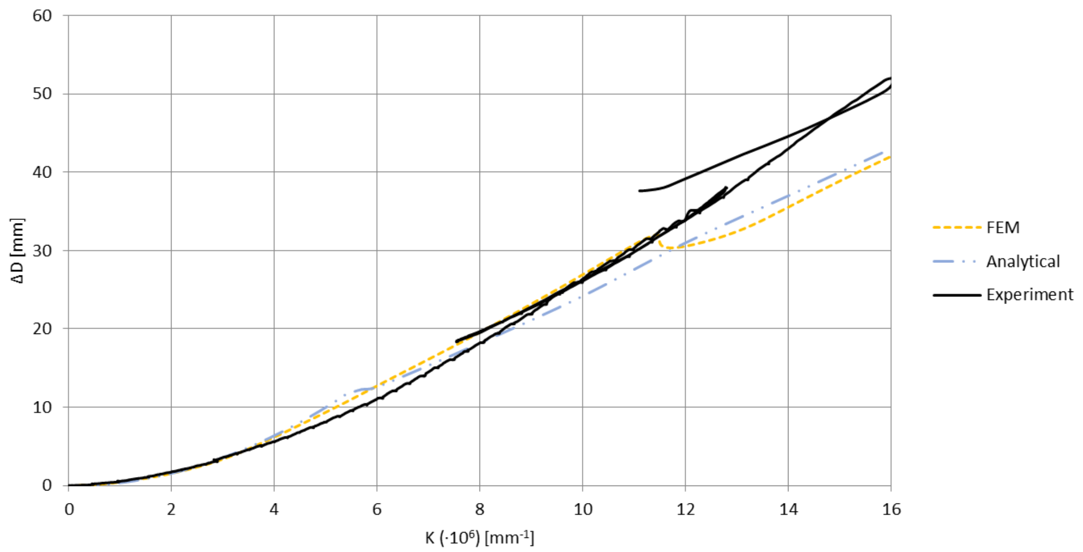

Figure 110: ΔD-K relations for Tube 15

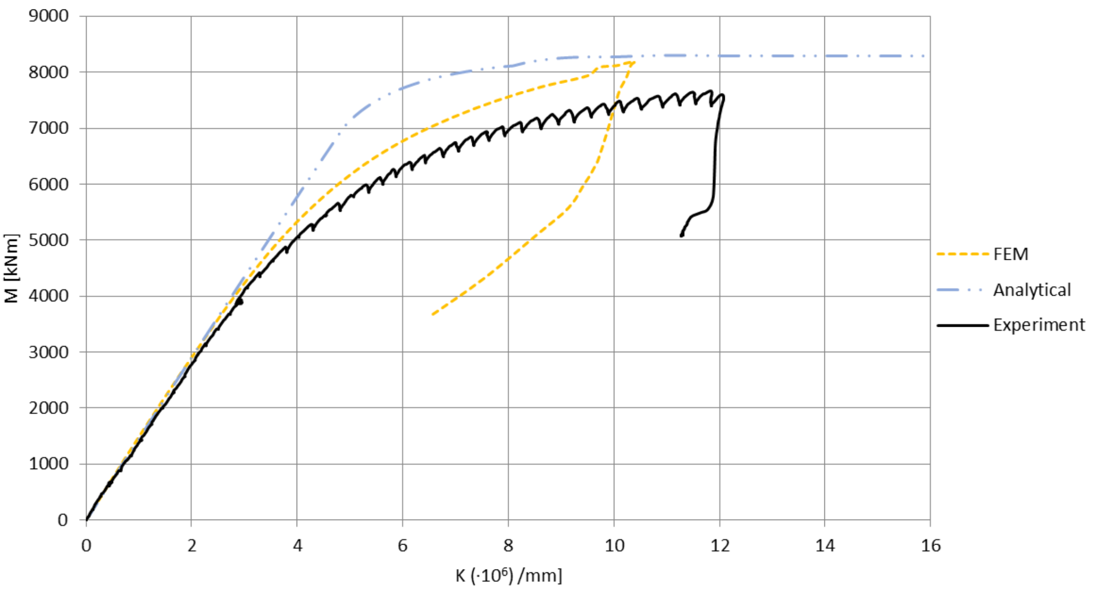

Figure 111: M-K relations forTube 15 of curvature 2

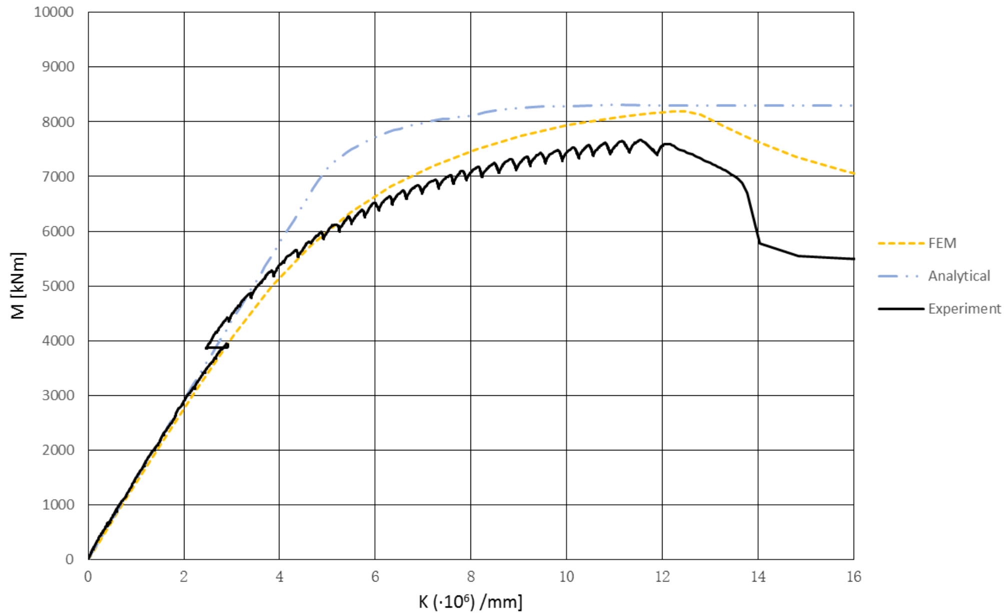

Figure 112: M-K relations forTube 15 of curvature 3

For Tube 15, the critical curvature obtained by neutral line model is underestimated compare with exerimental data, however, the moment is overestiamted. Analytical solution overestimate both curvature and momen.The deviation of experimental data and numerical results when plasticity onset indicates that the material model is not fully representative for this tube. With regard to ovalization,neutral line model shows great agreement with the analytical solution, it deviates from experimental data, the ovalization is restrained by experiment. Critical curvature from neutral line model is better than M1, but worse than M1 in terms of maximum moment.

5.4 Discussion and recommendation

From the results above, it can be seen that the numerical model can accurately predict critical curvature and maximum moment for most tubes except some tubes like tubes6, 7 and 9. The underestimated and overestimated critical curvature for these tubes indicates initial imperfection introduced to the model is not fully representative, especially for the tubes with weld features which the property of welds itself might also influence the result a lot. A representative imperfection close to the reality should be used for further study. Another infuencing factor is residual stress, since residual stress have many sources. Apart from forming process, uneven heating and cooling, later uncoiling of the plate material also introduces the residual stress. Therefore, residual stress should be introduced from more sources. Material model is also one crucial factor which impact the moment-curvature curves, tubes 7 and 11 start to deviate at relatively low curvature in pre-buckling equilibrium, while for other tubes which already deviate from elastic branch like tube 3 could caused by the mistake of the experiment, because the geometry and Young's modulus of the tubes are correctly measured.

Considering all the models, including the model with fix ends, it is interesting that for plain tubes only, the model which simply modelled based on middle part of the tube can obtain more accurate curvature closed to experimental data. In most cases, the critical curvature value from neutral line model is between M1 and M2, while in terms of maximum moment, neutral line model predict similar results as M1, M2 performs worst among these three models. The critical curvature with neutral line model is lower than M2 in most cases. It is suggested that if the curvature is used as determining parameter, M1 is the best and M2 is better in predicting plain tubes. However, the ovalization is far from reality, the difference between neutral line model and experimental data can be compensated by introducing more representative imperfection without losing ovalization affect. Comparing neutraline model with M1, it is concluded that by blocking the end ovalization will get more conservative estimates. Even M2 suffers geometrical impact, it underestimates both critical curvature and maximum moment. When compring ovalization for plain tubes, neutral line model predicts better than M1, at the expense of losing capability in accurately predicting critical curvature and moment.

5.5 Statistical analysis of results

In this section, the accuracy of the neutral line model is investigated. The figures below show the predicted value of critical curvature versus experimental value for each tubes.

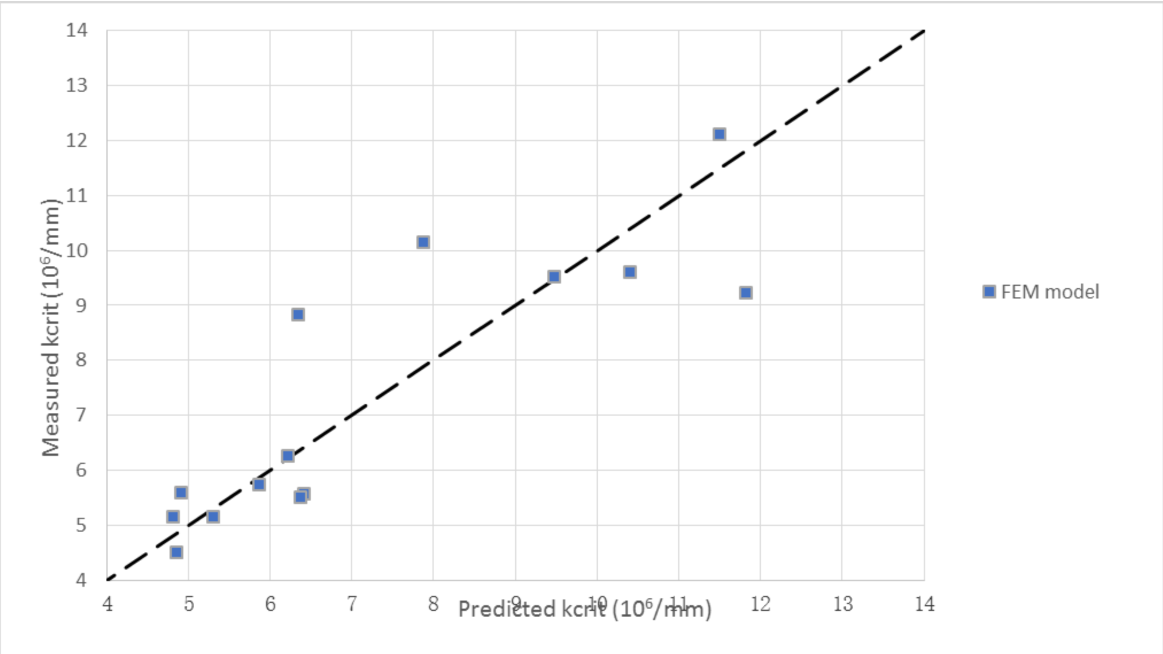

Figure 113: Accuracy of Model for k_{crit}

Table 19: Regression analysis for k_{crit} : all tubes

	FEM Model	**M1**
R^2	0.803	0.722
Standard Error(10^6/mm）	1.21	1.32

Table 20: Regression analysis for k_{crit} : plain tubes

	FEM Model	**M1**	**M2**
R^2	0.549	0.818	0.562
StandardError10^6/mm）	1.69	1.18	1.67

The data for maximum bending moment is also plot below,

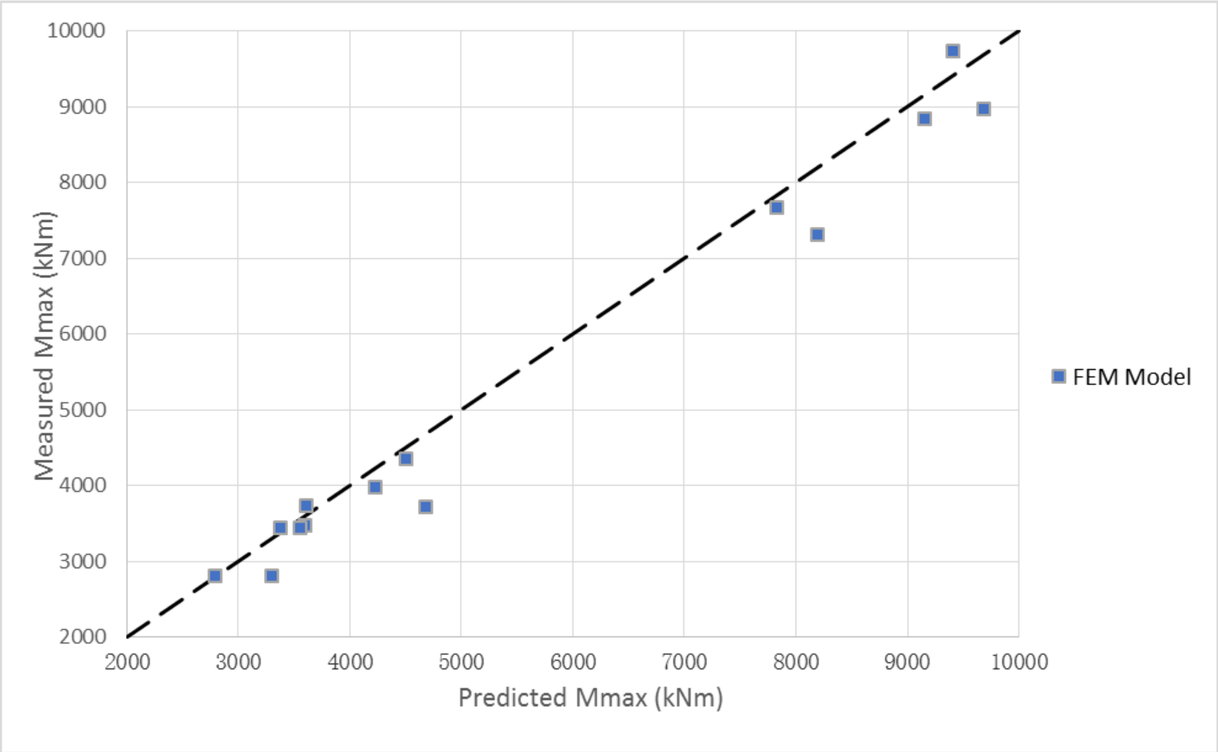

Figure 114: Accuracy of Model for M_{max}

Table 21: Regression analysis for M_{max} : all tubes

	FEM Model	**M1**
R^2	0.973	0.928
Standard Error(kNm)	355.81	666.4

Table 22: Regression analysis forM_{max} : plain tubes

	FEM Model	M1	M2
R^2	0.972	0.987	0.986
Standard Error(kNm)	312.3	309.3	314.6

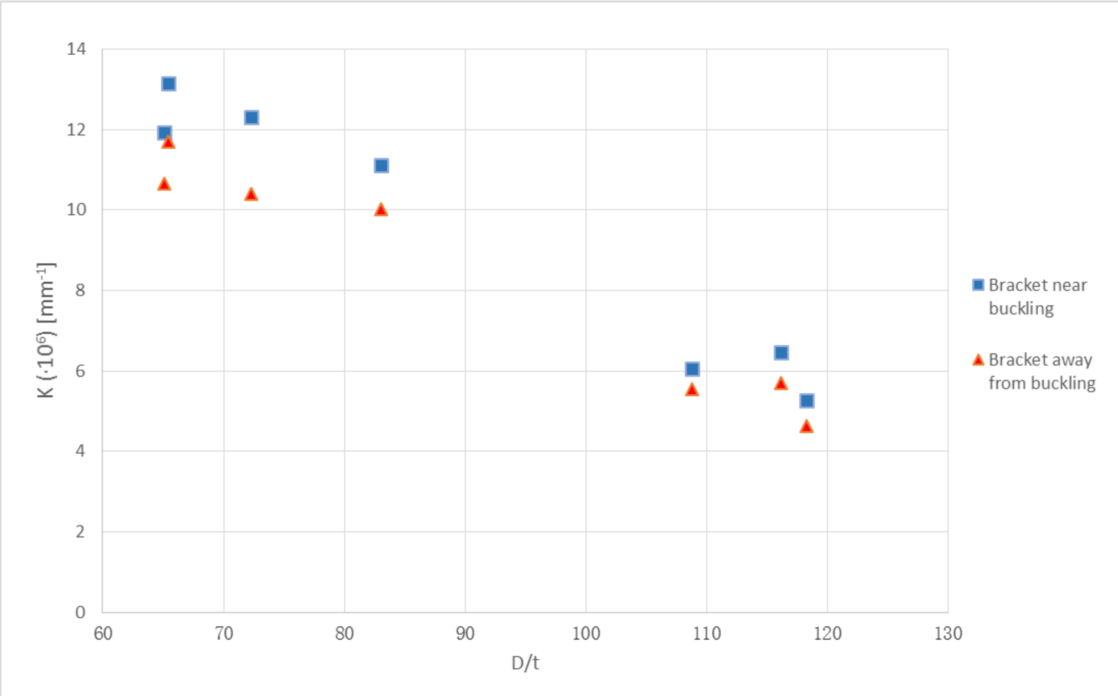

Figure 115: Local curvature differences between curvature measuring brackets for plain tubes

5.6 Chapter conclusion and discussions

From statistical analysis, it can be seen that experimental data like critical curvature and maximum moment can correctly predicted by neutral line model. The value predicted by neutral line model closely distribute along the accuracy line, except tubes 6, 7 and 9, if these tubes are leave out, the correlation factor will be significantly improved. When all tubes are considered, it can be seen that critical curvature have been improved from 0.722 with M1 to 0.803 with neutral line model, and the standard error is reduced from 1.32 (10^6/mm) with M1 to 0.927 (10^6/mm) with neutral line model. However,considering only plain tubes, M1 is the most accurate model in predicting critical curvature with correlation factor R^2 0.818, significant higher than 0.554 obtained from neutral line model and 0.562 with M2 model (see Table 20). The standard error is reduced from 1.67 (10^6/mm) with M2 model to 1.18 (10^6/mm) with M1 model, neutral line model have not make any improvement in terms of critical curvature for plain tubes. It is interesting that when all tubes are considered, neutral line model perform better than M1 both in aspects of critical curvature and maximum moment. Observing the accuracy analysis of maximum moment, it is noticeable that M1 has best correlation compare with neutral line model, the standard error is reduced from 312.3 (kNm) with neutral line model to 309.3 (kNm) with M1. There is no improvement made by M2 (see Table 22). When it comes to the maximum moment of all tubes, it is again that neutral line model has the best prediction, the improvement of correlation factor R^2 has been made from 0.928 with M1 to 0.973 with neutral line model, the standard error is reduced from 666.4 (kNm) with M1 to 355.81 (kNm) with neutral line model.

It is concluded that by using free ovalization end support will obtain more accurate results in terms of critical curvature and maximum moment for tubes with welded features. If the tubes with welded feature and rust material is leave out like tube 6 and tube11, the results of M1 will be more accurate. However, blocking the ovalization of support is far from reality, it is suggested to use this model as tool to predict critical curvature for plain tubes. As said before, if more representative approach is used for introducing imperfection, neutral line model is more closed to real situation. By observing from the results for regression analysis, it can be seen that although by enlarging the length of the tube can indeed make tube less restrained by support, the results obtained by M2 still overestimate the experimental data. Even it allows more ovalization than M1, it is still a risk to use it, because neutral line model can predict more accurate ovalization without suffering geometric effects. If analytical design formula is put in the figure of accuracy analysis, the data points obtained from design formula will below the accuracy line.

Finally, the curvature differences between curvature measuring brackets are plotted for plain tubes. It can be seen that the final results of the curvature are sensitive not only to the the localisation of curvature and it also relate to where local buckling occurred within the length of the bracket. the curvature away from where buckling occurs gives lower curvature (see Figure 115). According to the theory that the curvature in the middle under constant bending moment should be same. However, by comparing the result of the local curvature measuring brackets, there is considerably difference between local curvatures.

6 Parameter study for combination of variable parameters

6.1 Approach and methods

Three variables parameter study is designed here in order to investigate the sensitivity of the tubes to these variable parameters. Residual stress is not included in first three variable parameters investigation, because the way that introducing residual stress is based on the manufacturing sources which is related to the yield strength.

Investigating the influence of imperfection size, imperfection value varied from 0.01 to 0.2 times of thickness. Because most imperfection values for the tubes in experiment range from 0.05 to 0.15, so it seems that 0.05 and 0.2 is good preliminary assumption for studying the influence of imperfection size. Thus three D/t ratios (one lower one, one large one, and the middle one) and three yield strengths (same as D/t ratios), and five imperfection sizes. Based on the similar theory, investigating the influence of D/t ratios, most tubes range from 65 to 118, for parameter study of D/t ratios, the range is extended to 60 to 140. Same as before, the influence of yield strength is obtained from five yield strength, three imperfection values and three D/t ratios.

Table 23: Factors used in parameter investigation

f_y (Mpa)	**Imperfection/thickness ratio**	**Diameter/thickness ratio**
320	0.01	60
420	0.05	90
520	0.1	120
600	0.15	140
-	0.2	-

The the first step is to define the material model which can be used to investigate 3 variable parameters study. Based on the fact that the diameter and thickness of the tube were both varied, therefore D/t is used as an independent variable, with regard to the yield strengh, in order to obtain the same shape of material model, Both stress and strengh were normalized by yield strength and yield strain. Diameter could be changed by changing the thickness of tube, inputing the corresponding material model, and imperfection value.

At the end of the three variable parameters study, regression analysis of predicting model is carried out to investigate the capacity of tubes with different parameters.

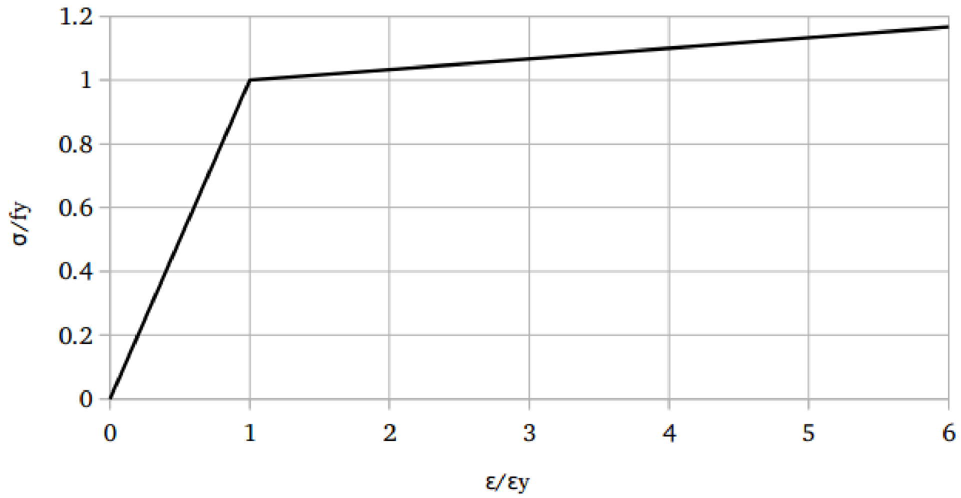

Figure 116: Material model for parameters study

The basic setup is a tube with middle length with 8100mm, D=1,068mm, and a material model as shown in Figure 116. The elastic branch has E=205,000 MPa, while linear strain hardening is assumed in the plastic branch with H=E/30.
This method can make it very easy to change the parameters independently of each other. D/t could be changed by changing the thickness of the shell elements, and the material model could be scaled by changing f_y without changing the shape of the stress-strain curve. Note: The effective range in the trendline is between the minimum and maximum critical point, the extended tendency of trendline is plotted for reference but not valided. For parameters f_y = 420MPa and D/t = 140, imperfection to thickness value only varies 0.05, 0.1 and 0.2.

6.2 Influence of imperfection size

In this section, the results are presented to show the influence imperfection value on critical curvature with regard to the different D/t ratios corresponding to different yield strengths. The graphs are obtained and listed respectively with different yield strengths. The model to describe the relationship between critical curvature and imperfection value is:

$$y=a*\ln(x)+b \tag{38}$$

The coefficient of regression formula is listed in the tables, the regression is plotted in the figures for each tubes.

Table 24: Regression analysis for yield strength f_y=320Mpa

D/t	**a**	**b**	**R^2**
60	-0.639	0.5832	0.995
90	-0.209	0.7771	0.997
120	-0.132	0.757	0.998
140	-0.071	0.752	0.998

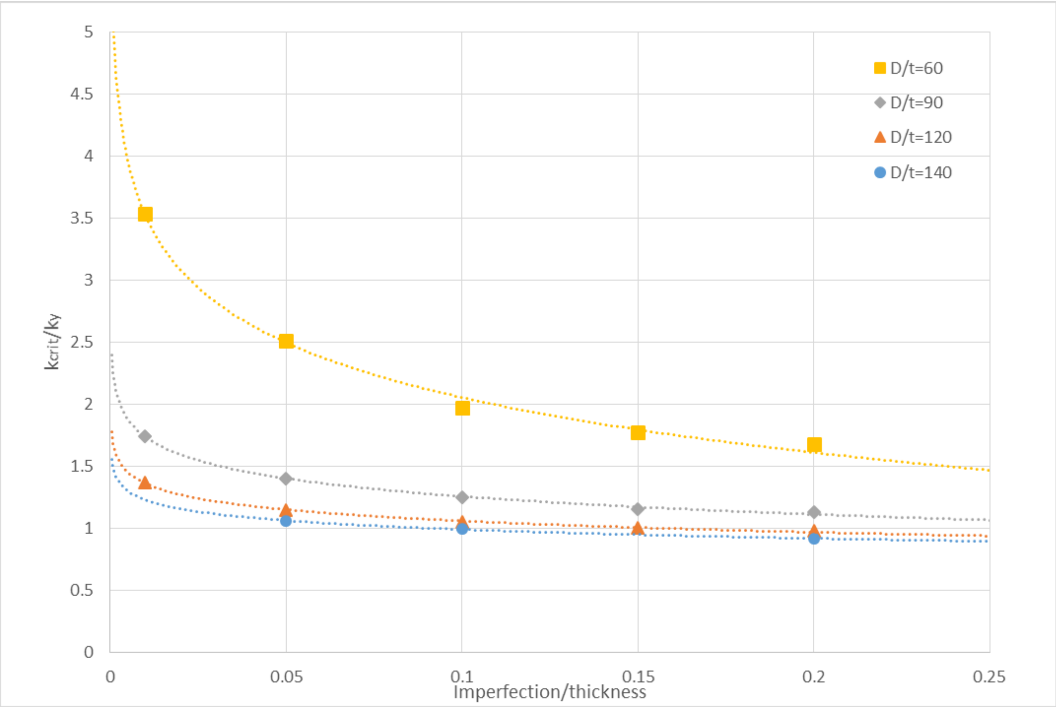

Figure 117: Effect of imperfection value on k_{crit} (f_y=320Mpa)

Table 25: Regression analysis for yield strength f_y=420Mpa

D/t	**a**	**b**	**R^2**
60	-0.261	0.8611	0.938
90	-0.126	0.8392	0.987
120	-0.071	0.752	0.995

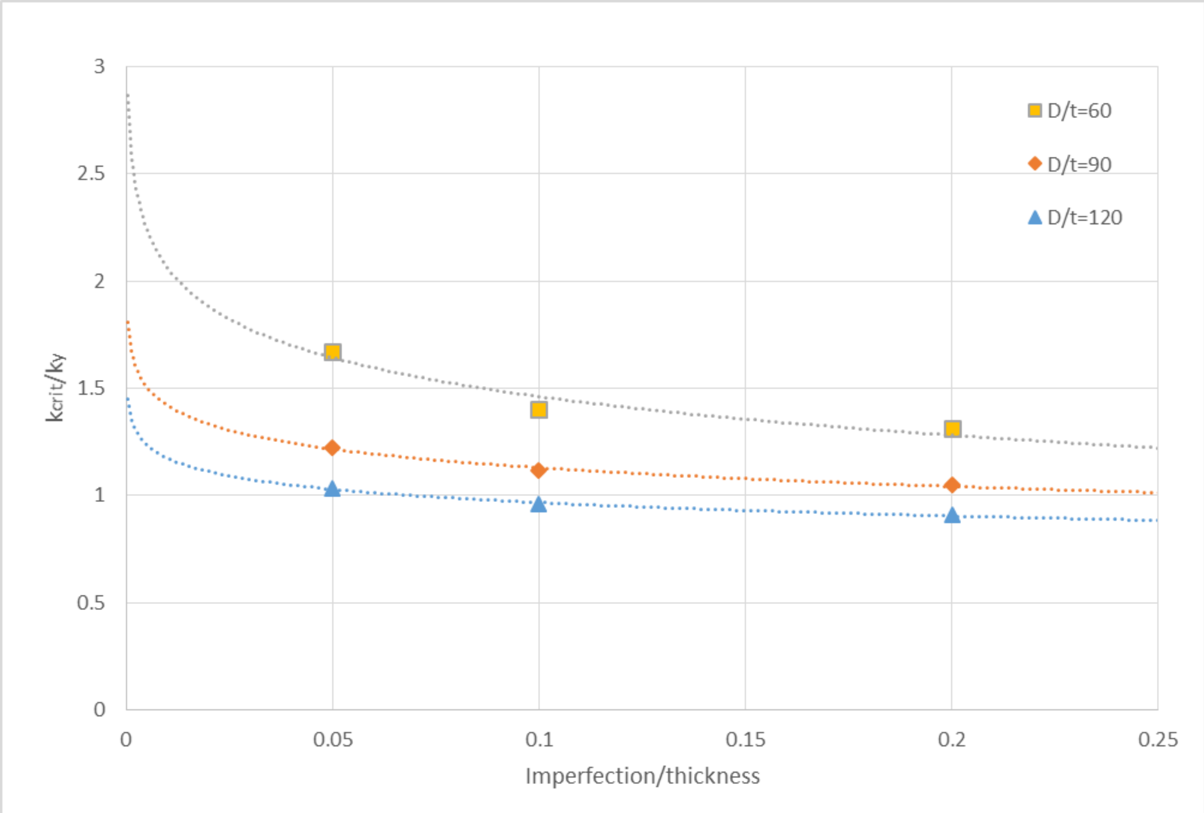

Figure 118: Effect of imperfection value on k_{crit} (f_y=420Mpa)

Table 26: Regression analysis for yield strength f_y=520Mpa

D/t	**a**	**b**	**R^2**
60	-0.254	0.8195	0.997
90	-0.109	0.795	0.999
120	-0.063	0.7858	0.995
140	-0.048	0.7719	0.976

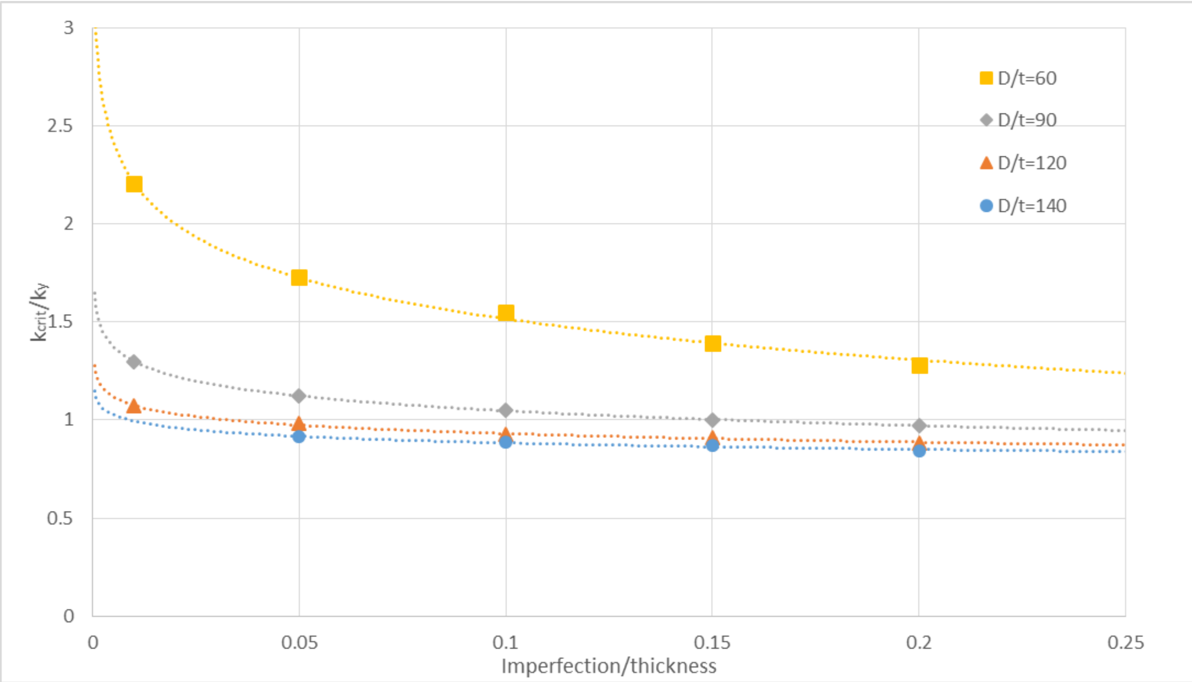

Figure 119: Effect of imperfection value on k_{crit} (f_y=520Mpa)

Table 27: Regression analysis for yield strength (f_y=600Mpa)

D/t	**a**	**b**	**R^2**
60	-0.247	0.8345	0.989
90	-0.077	0.8201	0.998
120	-0.053	0.7724	0.994
140	-0.038	0.7765	0.974

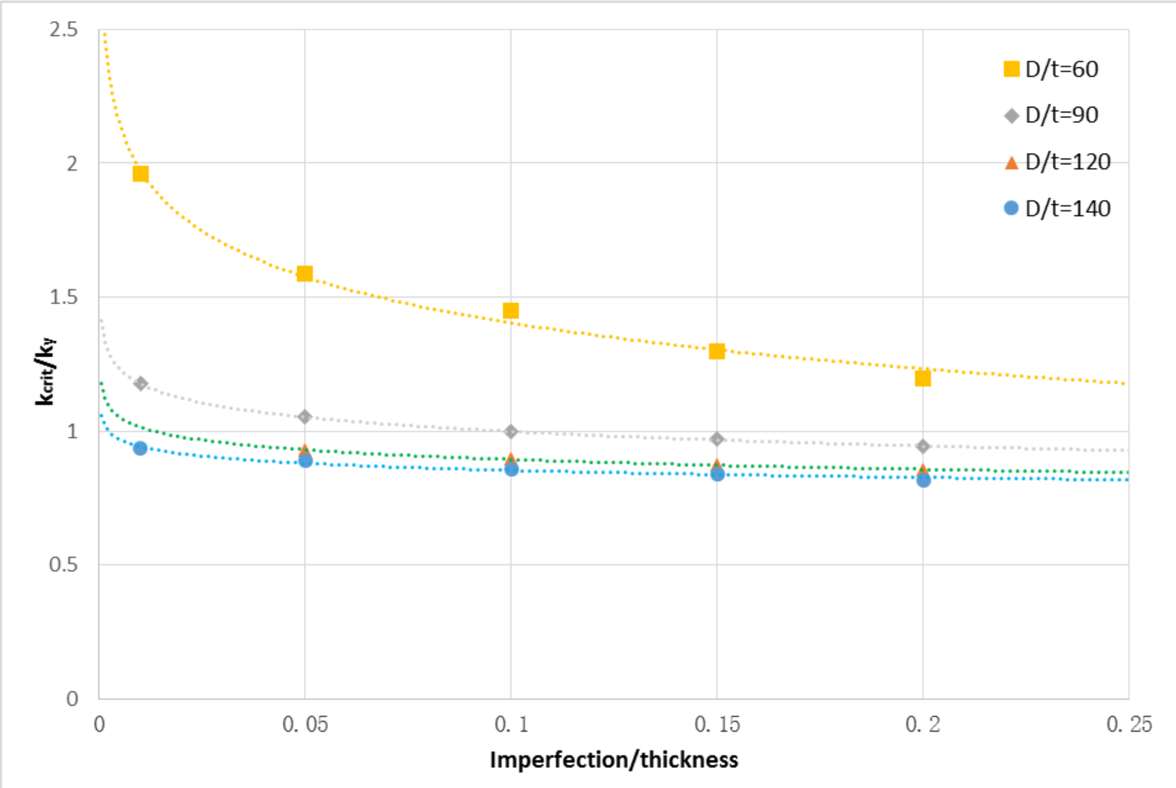

Figure 120: Effect of imperfection value on k_{crit} (f_y=600Mpa)

For maximum bending moment, the linear relationship is used to take account between moment-imperfection relation as below:

$$y = ax + b \tag{39}$$

The result is plotted in the following figures corresponding to different yield strengths.

Table 28: Regression analysis for yield strength (f_y=320Mpa)

D/t	**a**	**b**	**R^2**
60	-0.2184	0.9475	0.988
90	-0.2864	0.8681	0.9952
120	-0.3346	0.8329	0.9653
140	-0.4735	0.8229	0.999

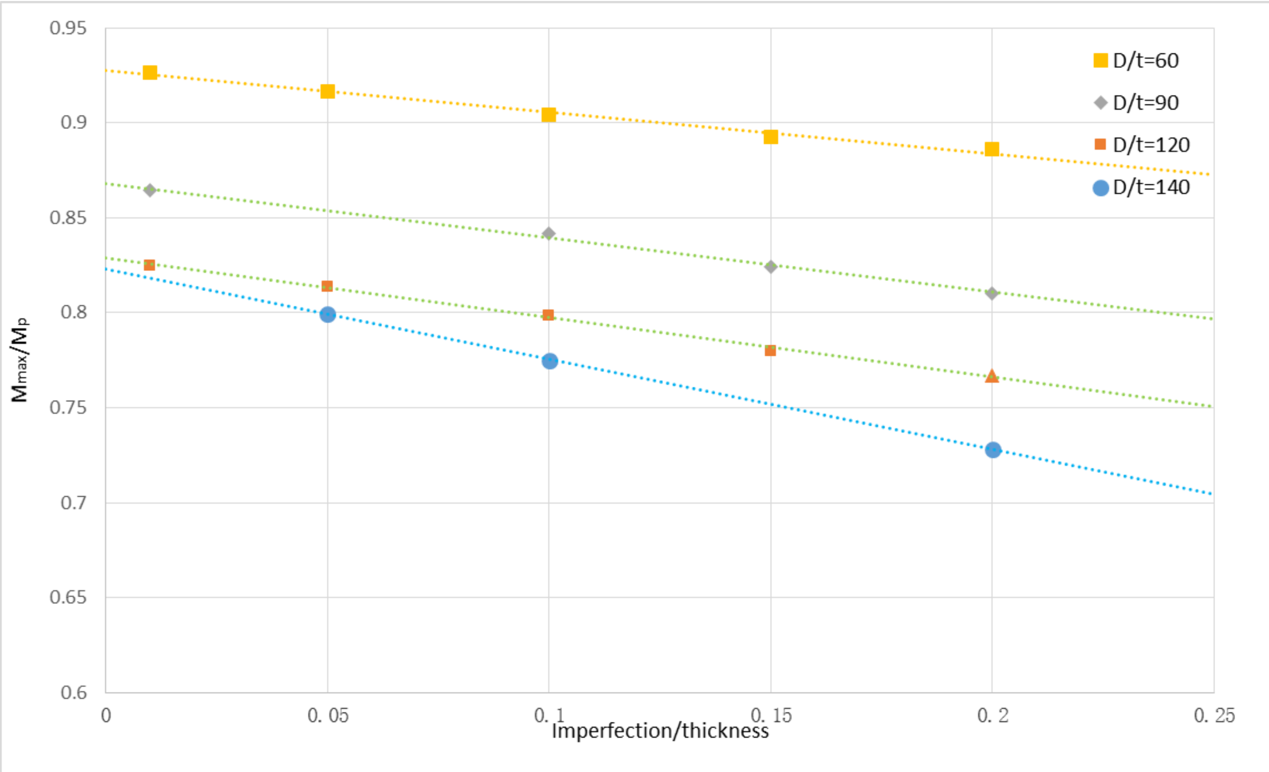

Figure 121 : Effect of imperfection value on M_{max} (f_y=320Mpa)

Table 29: Regression analysis for yield strength (f_y=420Mpa)

D/t	**a**	**b**	**R^2**
60	-0.3325	0.8966	0.991
90	-0.349	0.8915	0.990
120	-0.393	0.8029	0.980

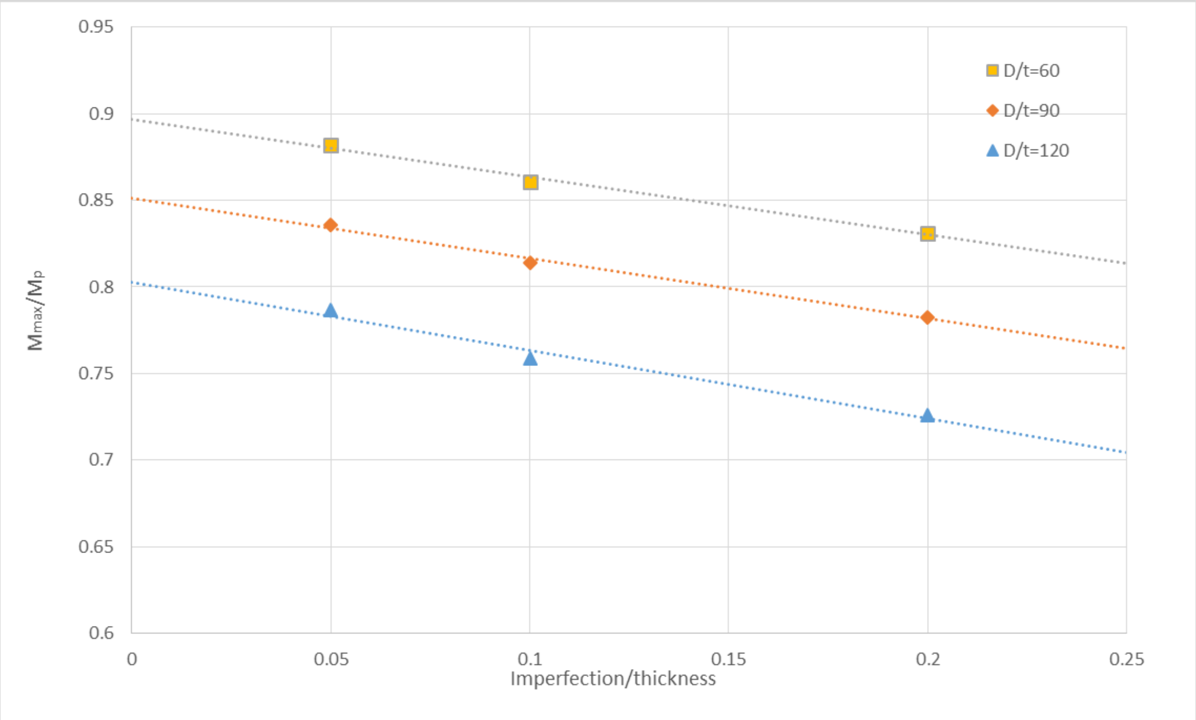

Figure 122: Effect of imperfection value on M_{max} (f_y=420Mpa)

Table 30: Regression analysis for yield strength (f_y=520Mpa)

D/t	**a**	**b**	**R^2**
60	-0.1964	0.8999	0.9916
90	-0.4156	0.8339	0.9952
120	-0.281	0.7621	0.9982
140	-0.325	0.7409	0.999

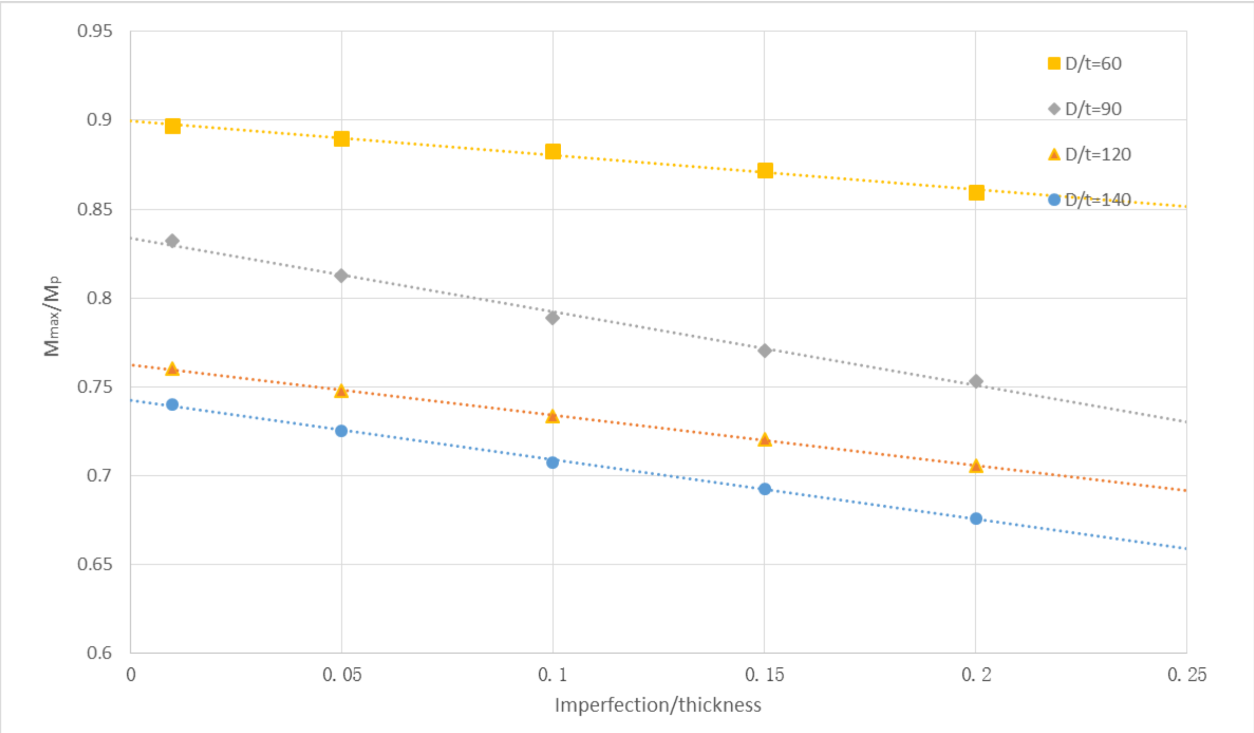

Figure 123: Effect of imperfection value on M_{max} (f_y=520Mpa)

Table 31 : Regression analysis for yield strength (f_y=600Mpa)

D/t	**a**	**b**	**R^2**
60	-0.2367	0.8752	0.9942
90	-0.3232	0.8031	0.9982
120	-0.3403	0.7437	0.9958
140	-0.3643	0.7198	0.9998

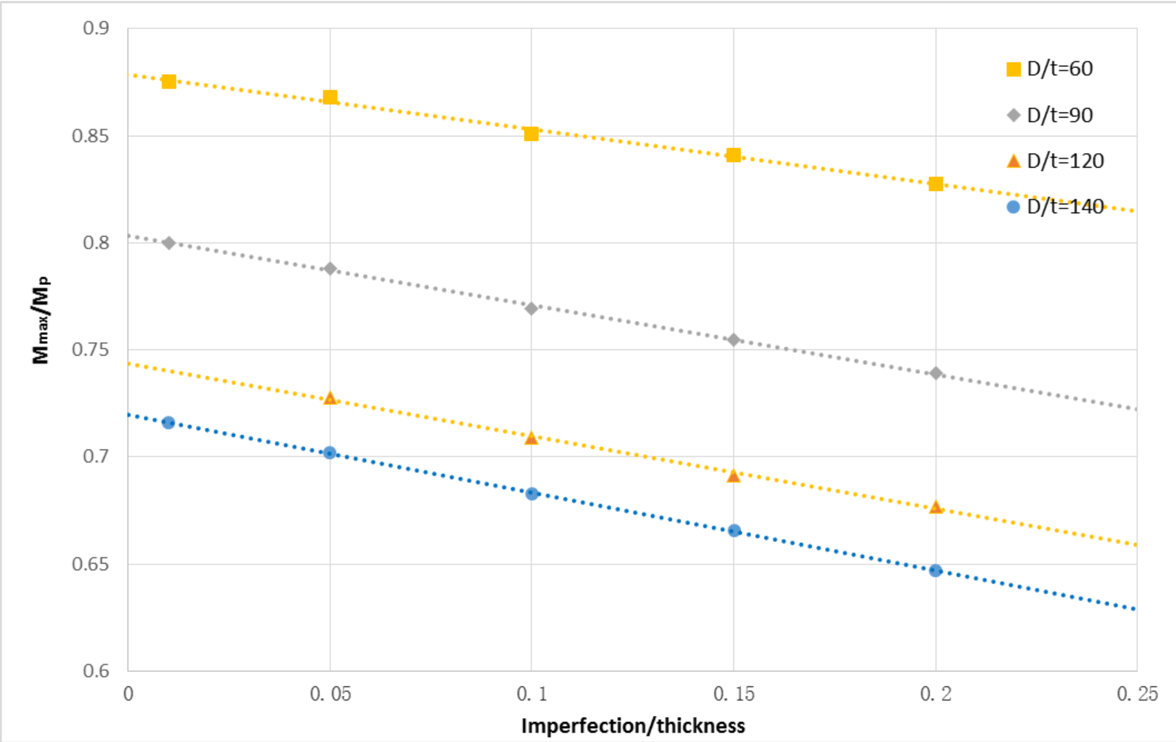

Figure 124: Effect of imperfection on M_{max} (f_y=600Mpa)

6.3 Influence of diameter to thickness ratio

In this section, the influence of D/t ratio on the critical curvature and the maximum moment is plotted with regard to different imperfection vaules as below, the relation between D/t ratio and the critical curvature can be described as following relation:

$$y=ax^b \tag{40}$$

Table 32: Regression analysis for D/t (imperfection/thickness 0.05)

f_y	a	b	R^2
320	182.81	-1.05	0.991
520	38.948	-0.765	0.993
600	28.297	-0.707	0.988

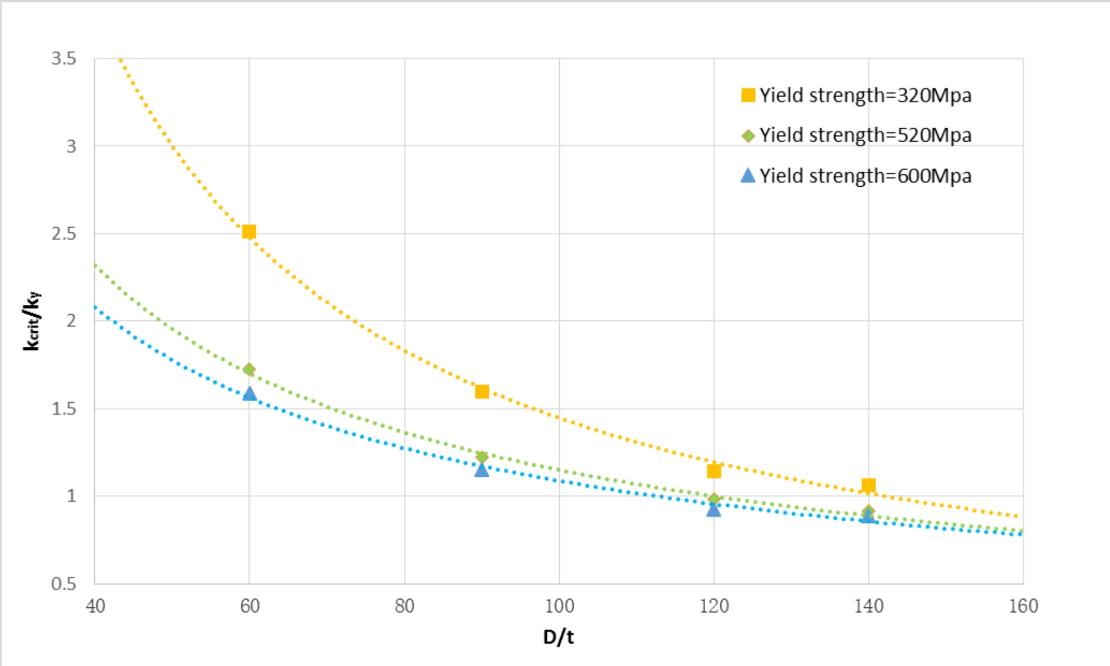

Figure 125: Effect of diameter/thickness ratio on k_{crit} (imperfecion/thickness=0.05)

Table 33: Regression analysis for D/t (imperfection/thickness 0.1)

f_y	a	b	R^2
320	60.092	-0.839	0.989
520	24.652	-0.679	0.989
600	19.469	-0.637	0.990

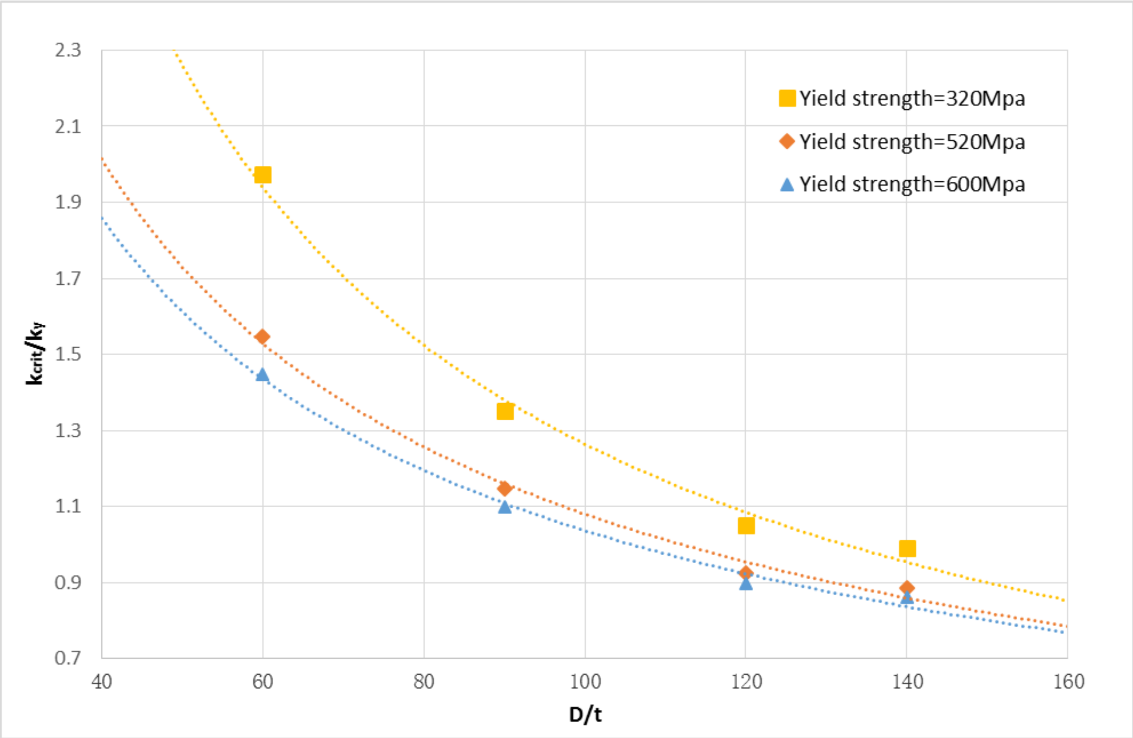

Figure 126: Effect of diameter/thickness ratio on k_{crit} (imperfecion/thickness=0.1)

Table 34: Regression analysis for D/t (imperfection/thickness 0.2)

f_y	a	b	R^2
320	-0.0017	1.0353	0.989
520	-0.0021	1.0088	0.981
600	-0.0020	0.9785	0.987

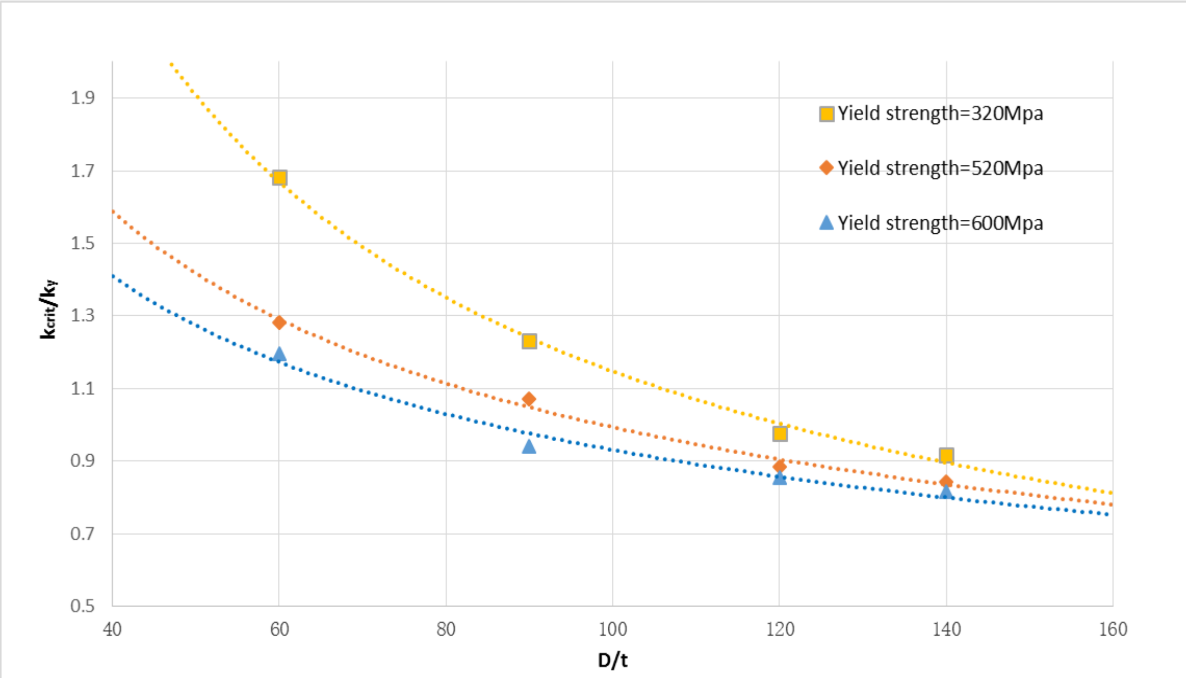

Figure 127: Effect of diameter/thickness ratio on k_{crit} (imperfecion/thickness=0.2)

For M_{max}, linear regressions have been used of the following form:

$$y=ax+b \tag{41}$$

Table 35 : Regression analysis for D/t (imperfection/thickness 0.05)

f_y	a	b	R^2
320	33.581	-0.733	0.994
520	10.483	-0.512	0.989
600	7.4484	-0.451	0.974

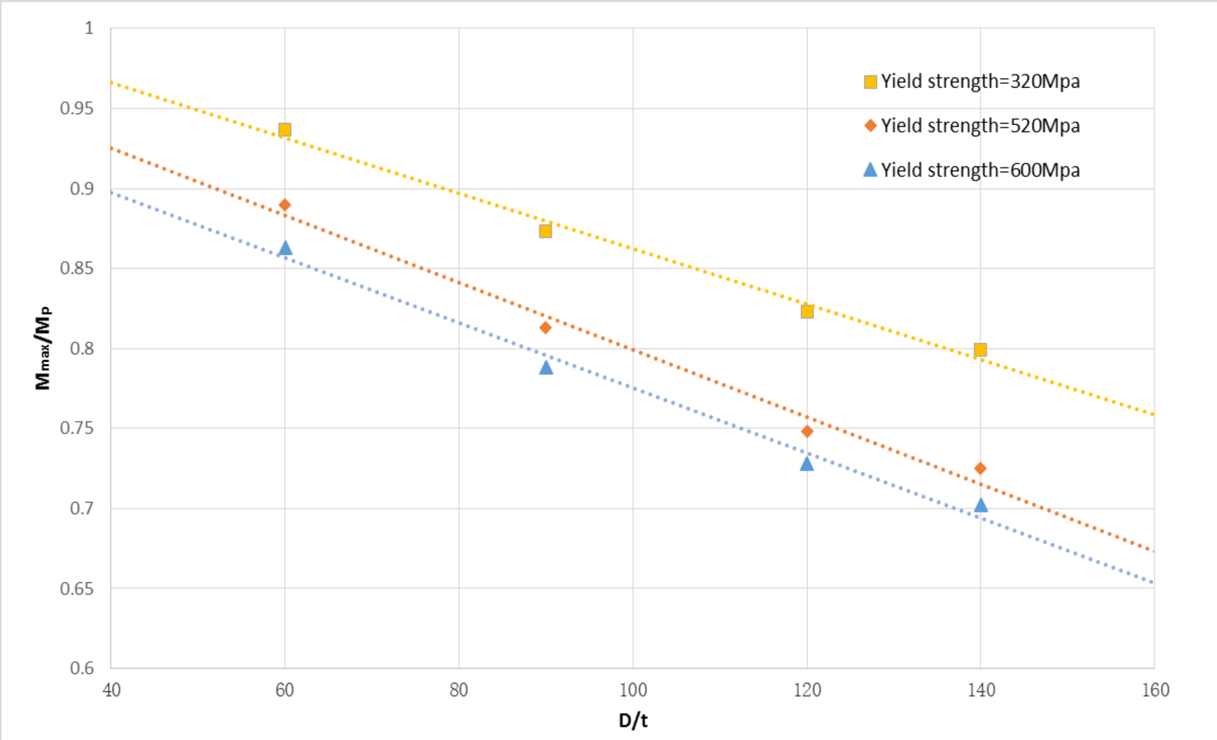

Figure 128: Effect of diameter/thickness ratio on k_{crit} (imperfecion/thickness=0.05)

Table 36 : Regression analysis for D/t (imperfection/thickness 0.1)

f_y	a	b	R^2
320	-0.0018	1.0235	0.987
520	-0.0022	1.0009	0.970
600	-0.0021	0.9694	0.9814

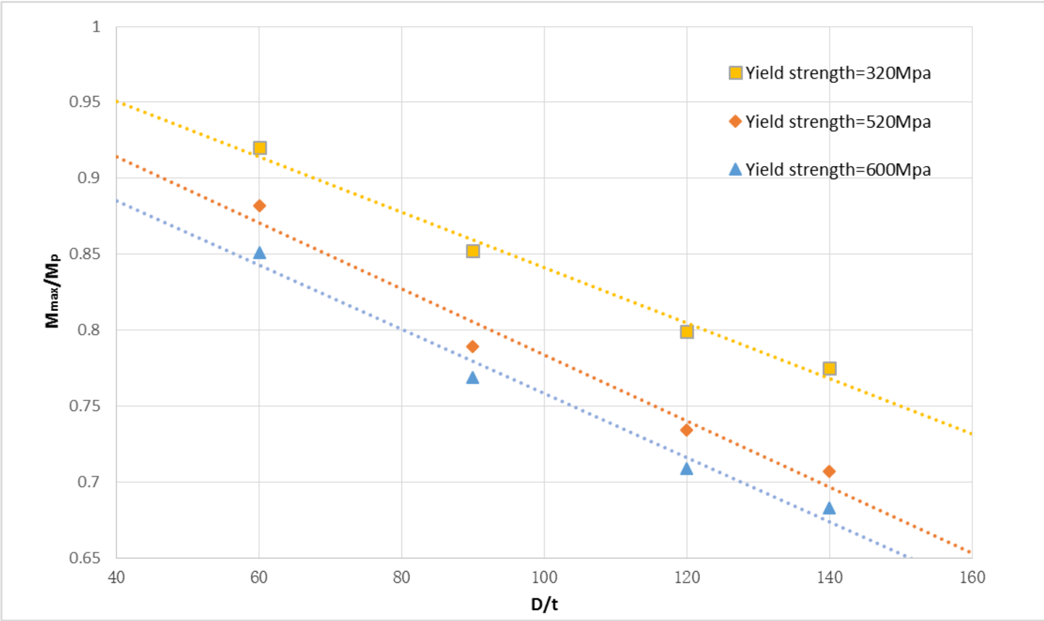

Figure 129: Effect of diameter/thickness ratio on k_{crit} (imperfecion/thickness=0.1)

Table 37 : Regression analysis for D/t (imperfection/thickness 0.2)

f_y	a	b	R^2
320	-0.0019	1.4722	0.986
520	-0.0023	1.7032	0.987
600	-0.0023	1.6508	0.983

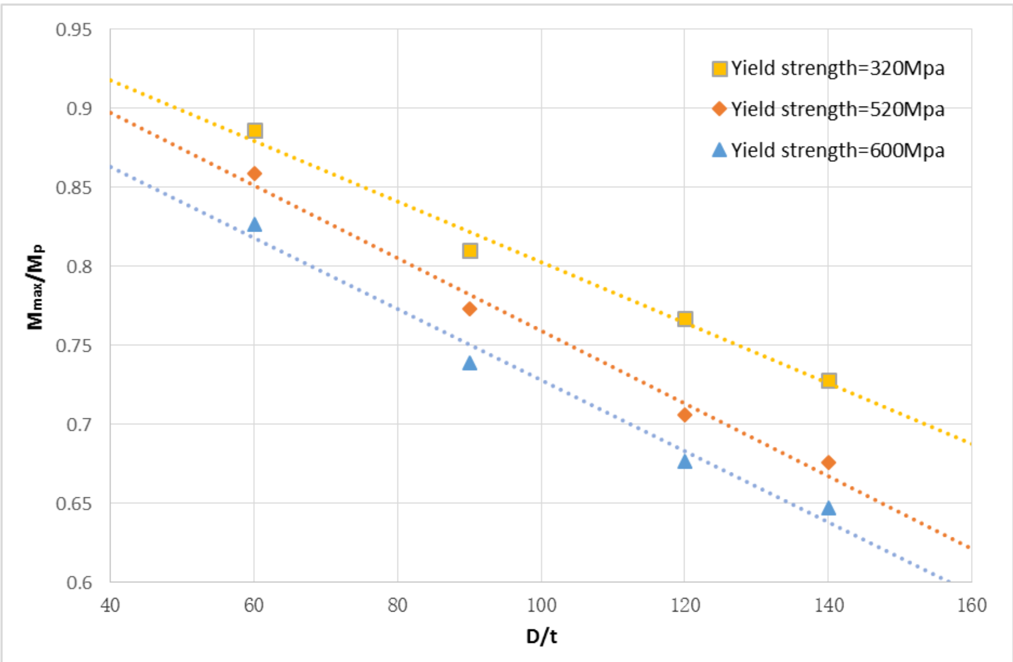

Figure 130: Effect of diameter/thickness ratio on k_{crit} (imperfecion/thickness=0.2)

6.4 Influence of yield strength

It is found that the influence of yield strength on the critical curvature can be described by power model as following:

$$y=ax^b \tag{42}$$

Table 38: Regression analysis for yield strength (imperfection/thickness 0.05)

f_y	a	b	R^2
320	181.88	-0.743	0.998
520	19.248	-0.455	0.997
600	7.2909	-0.322	0.991

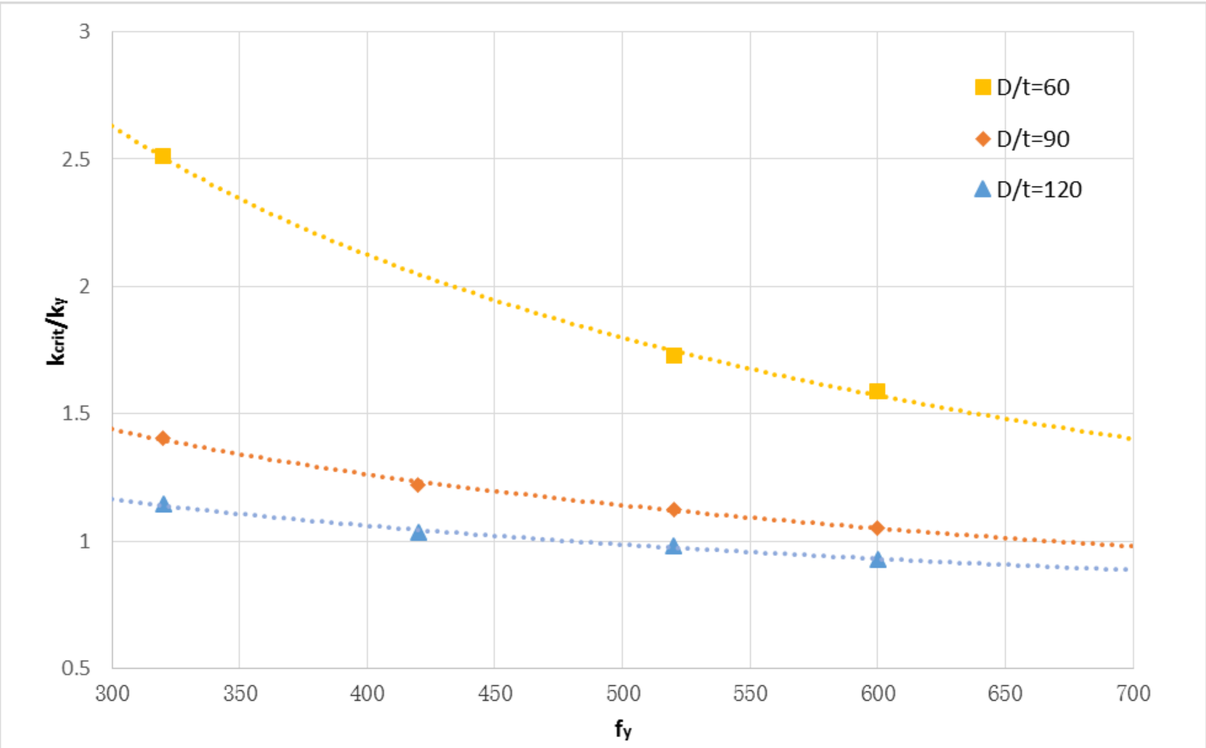

Figure 131: Effect of diameter/thickness ratio on k_{crit} (imperfecion/thickness=0.05)

Table 39 : Regression analysis for yield strength (imperfection/thickness 0.1)

f_y	a	b	R^2
320	34.62	-0.497	0.997
520	9.9456	-0.36	0.994
600	4.5267	-0.254	0.978

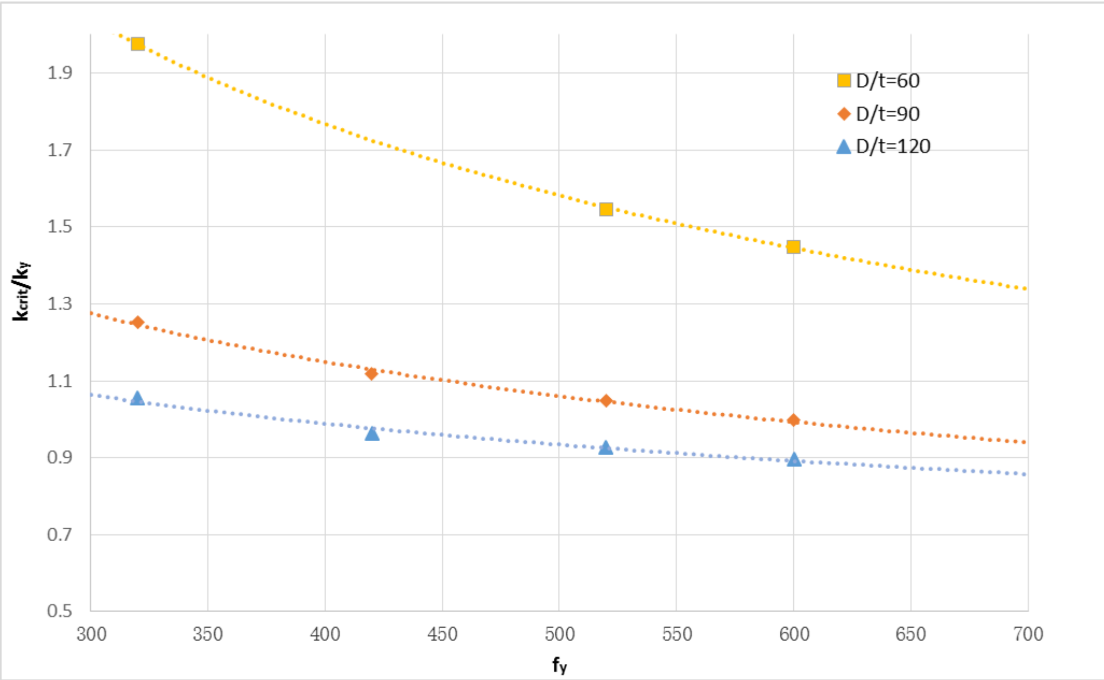

Figure 132: Effect of diameter/thickness ratio on k_{crit} (imperfecion/thickness=0.1)

Table 40: Regression analysis for yield strength (imperfection/thickness 0.2)

f_y	a	b	R^2
320	36.648	-0.536	0.9911
520	6.4578	-0.302	0.9969
600	3.1966	-0.206	0.9756

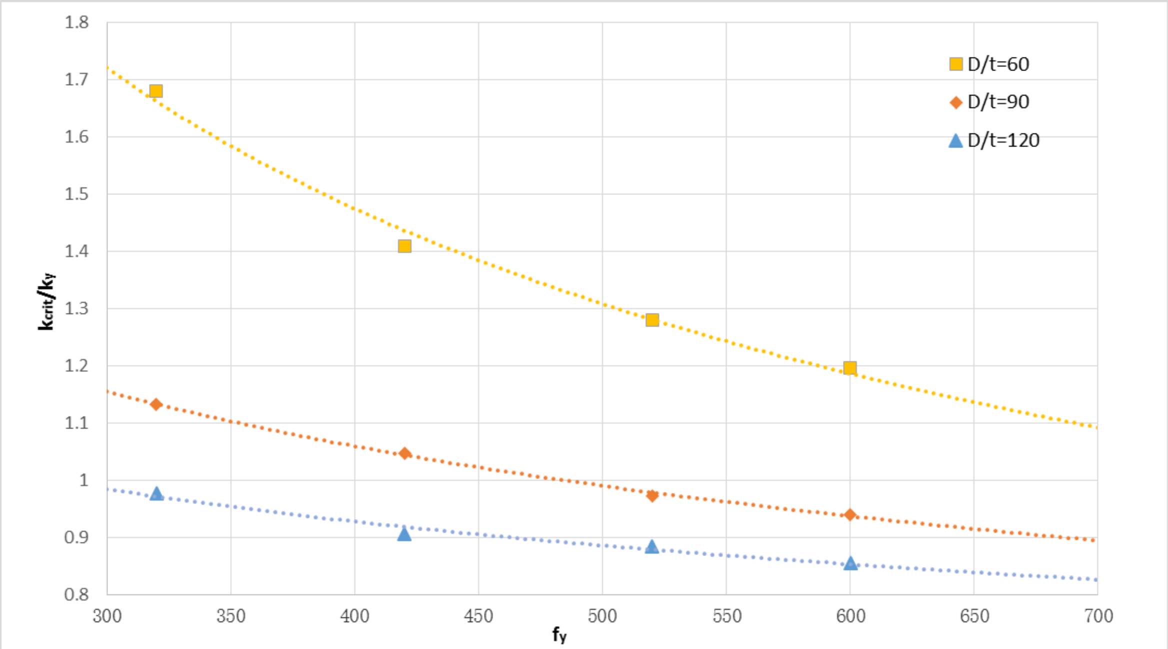

Figure 133: Effect of diameter/thickness ratio on k_{crit} (imperfecion/thickness=0.2)

For M_{max}, the trendline is describe as linear relations between the M_{max} and yield strength as following:

$$y = ax + b \tag{43}$$

Table 41 : Regression analysis for yield strength (imperfection/thickness 0.05)

f_y	a	b	R^2
320	-0.0003	1.0174	0.998
520	-0.0002	0.9297	0.983
600	-0.0004	0.9346	0.995

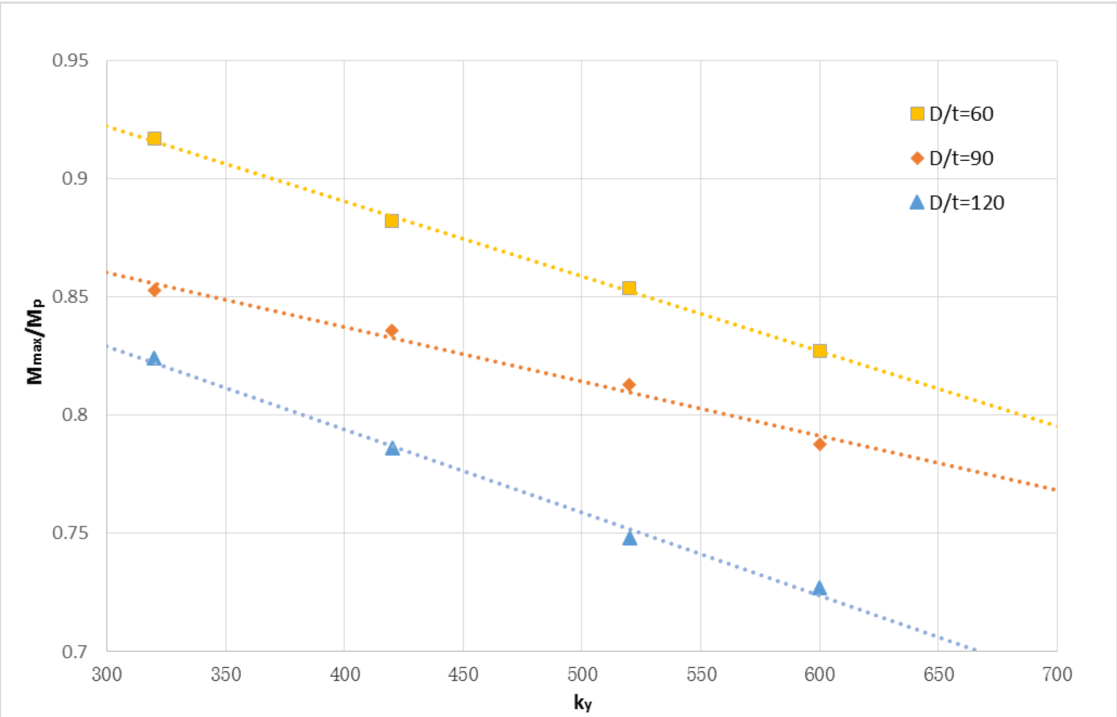

Figure 134: Effect of diameter/thickness ratio on k_{crit} (imperfecion/thickness=0.05)

Table 42: Regression analysis for yield strength (imperfection/thickness 0.1)

f_y	a	b	R^2
320	-0.0002	0.9601	0.892
520	-0.0003	0.9218	0.999
600	-0.0003	0.9918	0.992

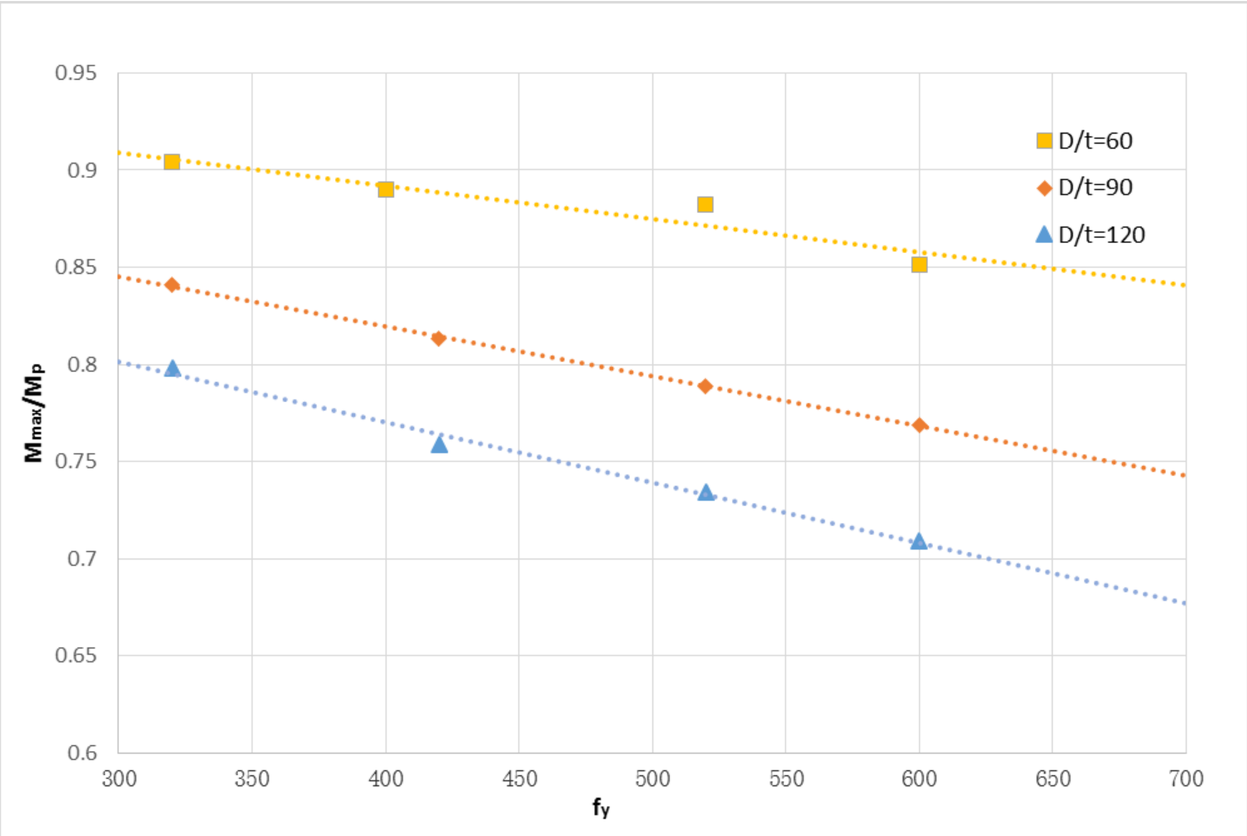

Figure 135: Effect of diameter/thickness ratio on k_{crit} (imperfecion/thickness=0.1)

Table 43: Regression analysis for yield strength (imperfection/thickness 0.2)

f_y	a	b	R^2
320	-0.0002	0.9379	0.885
520	-0.0003	0.892	0.992
600	-0.0003	0.9828	0.983

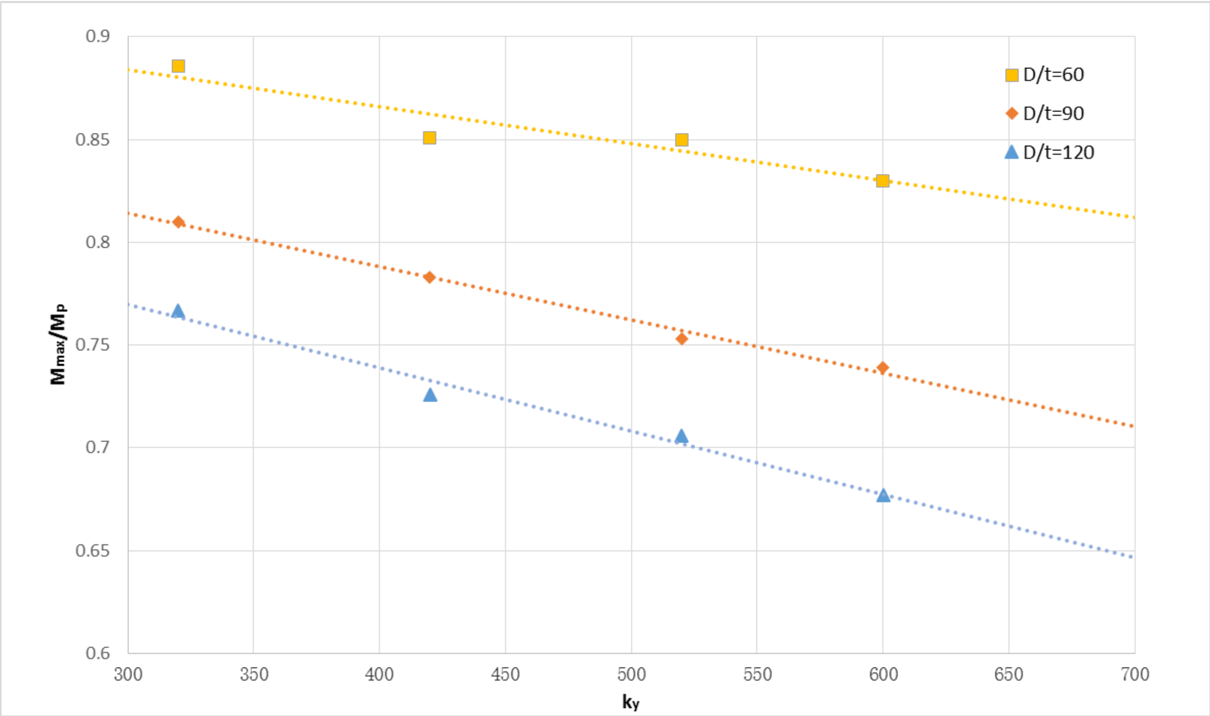

Figure 136: Effect of diameter/thickness ratio on k_{crit} (imperfecion/thickness=0.2)

6.5 Influence of residual stress

Residual stresses were investigated by varying the yield stress to obtain different residual stress distribution. For each tube, the residual stress ratios $f_{residual}/f_y$ were varied at 0.2, 0.8, 1, 1.2. In some welding cases, the residual stress is even higher than yield strength, it is not so common, but 1.2 is a necessary assumption for parameter trial study. The actual material properties of the tubes were not varied. It is similar as the approach for imperfection investigation. First, a selection of results has been used to plot moment-curvature and ovalization-curvature pictures for each tube in order to qualitatively illustrate the effect of residual stresses. Thus, the effects of residual stresses on k_{crit} and M_{max} are shown by plotting the residual stress ratios $f_{residual}/f_y$ against k_{crit}/k_y and M_{max}/M_p.

The result of this study shows that among the tubes in the experiment, residual stress has a great effect on equilibrium path, it can be seen that the influence on tube 1 (see Figure 137), is most significant, the critical curvature will increase greatly when the residual stress increase. Tube 1 increase faster than tube 2 (see Figure 139) and tube 11 (see Figure 141). With regard to the maximum moment, only tube 1 increases as residual stress increasing, the other two tubes tend to decrease as residual stress increasing. From figure 137 and 139 it can be clearly seen that the higher residual stress the more smooth equilibrium path for M-k curve when plasiticity onset. The trendline of influence of residual stress is plotted in the figure of 143, and 144 in following relation:

$$y = ax + b \tag{44}$$

Table 44: Effect of residual stress on tubes in experiment

	$\mathbf{k_{crit}}$		$\mathbf{M_{max}}$			
Tube	**a**	**b**	**a**	**b**	**D/t**	**fy**
1	0.6495	1.4533	0.0126	0.9334	65	540
2	0.2699	1.079	-0.0008	0.8172	118	390
11	0.2339	0.7244	-0.0055	0.9694	83	340

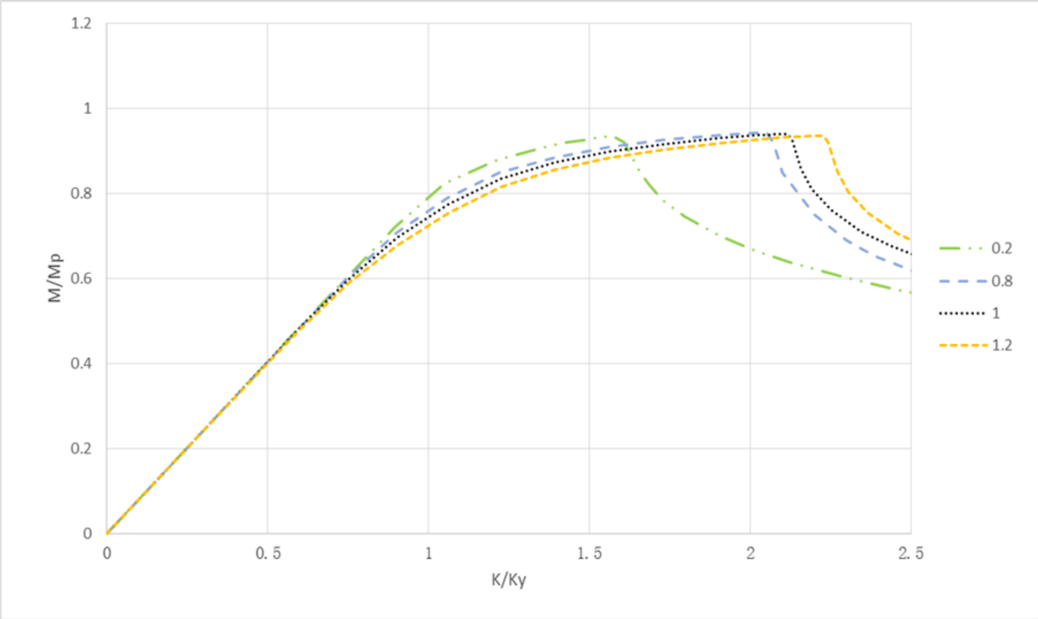

Figure 137: Effect of residual stress on the equilibrium path of Tube 1

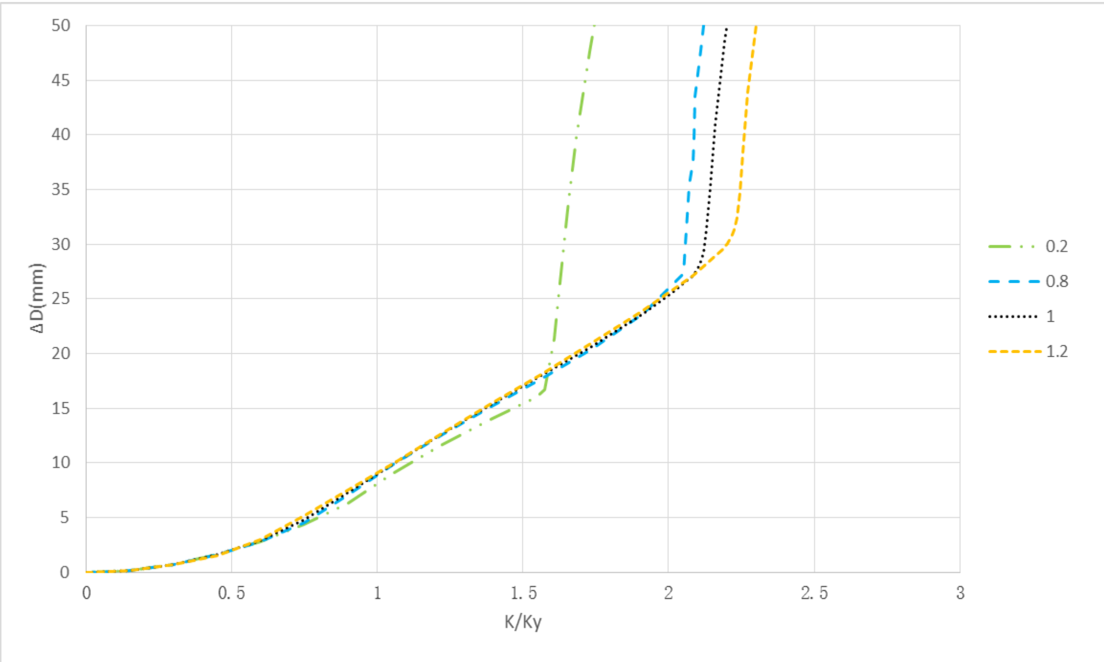

Figure 138: Effect of residual stress on the ovalization of Tube 1

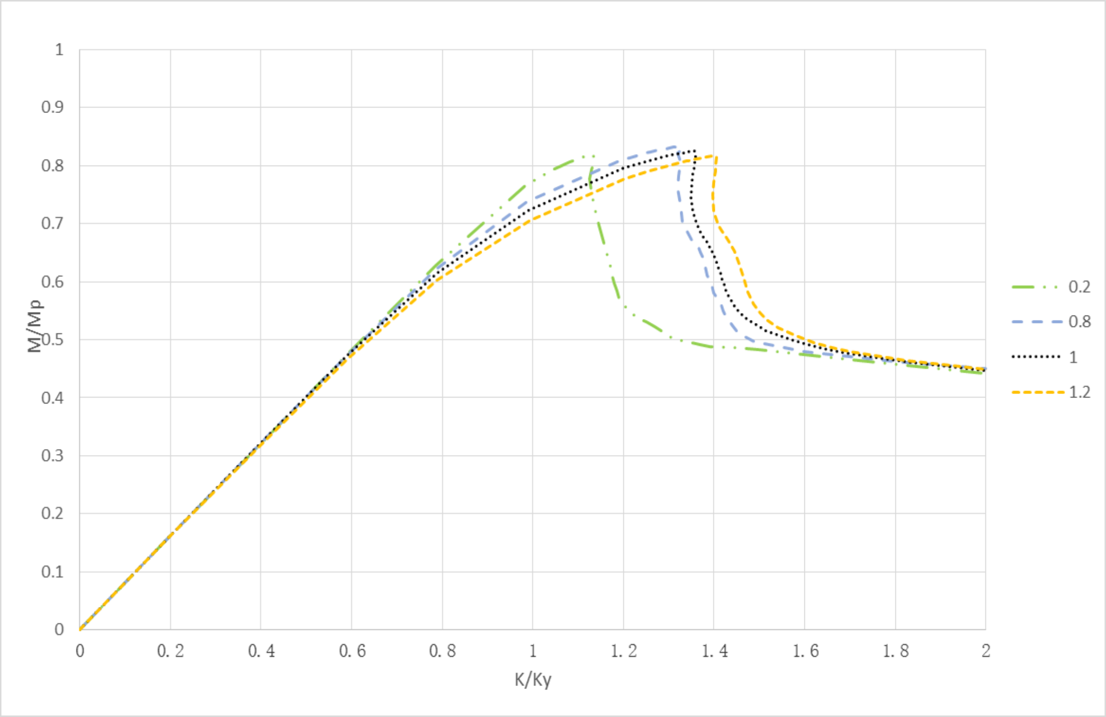

Figure 139: Effect of residual stress on the equilibrium path of Tube 2

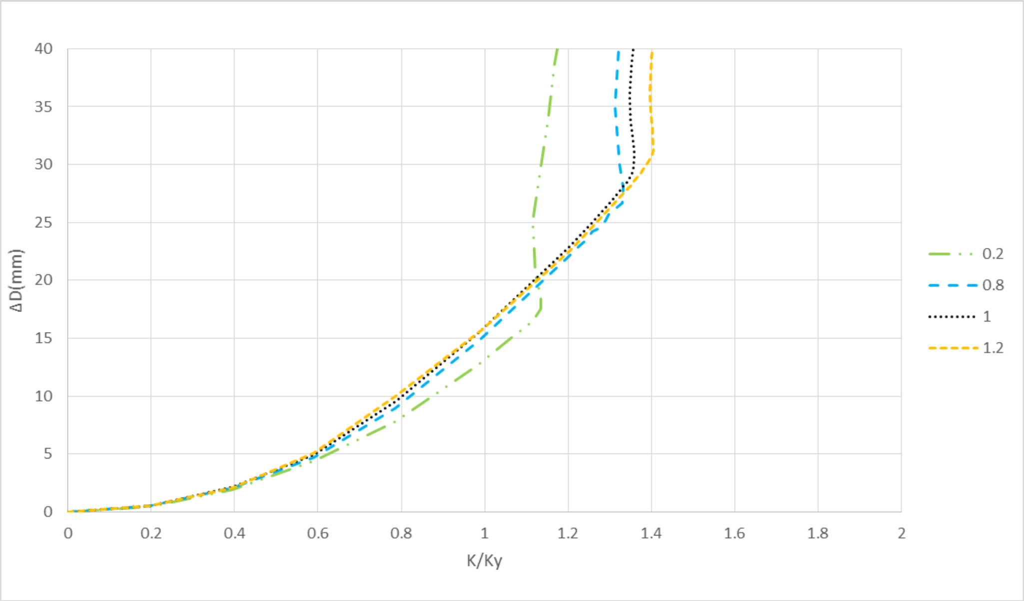

Figure 140: Effect of residual stress on the ovalization of Tube 2

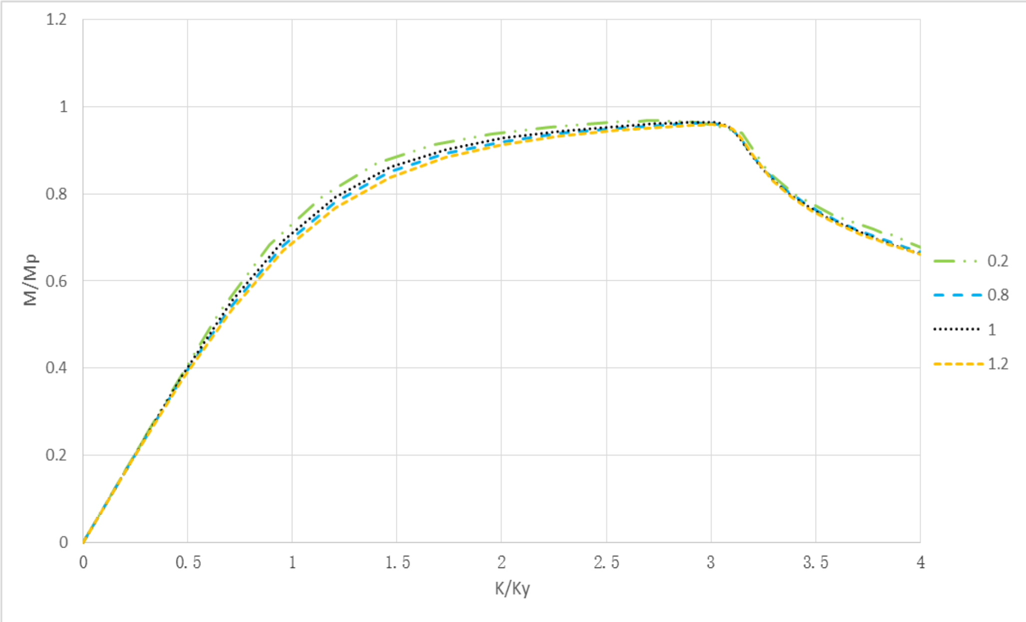

Figure 141: Effect of residual stress on the equilibrium path of Tube 11

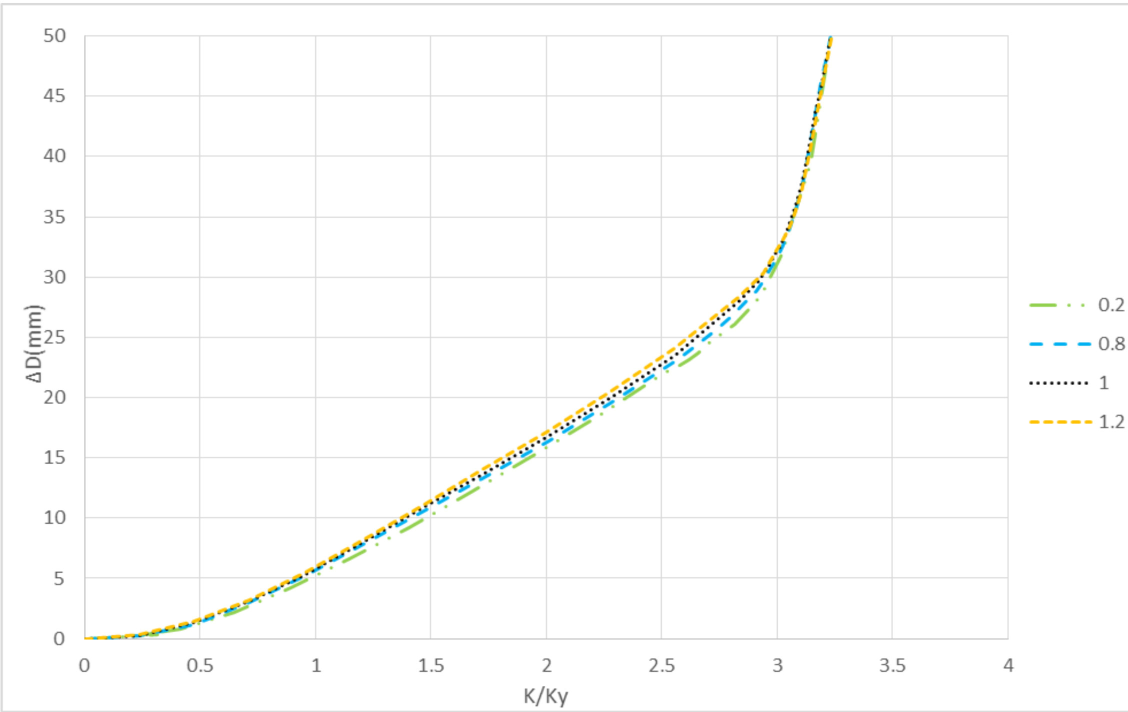

Figure 142: Effect of residual stress on ovalization of Tube 11

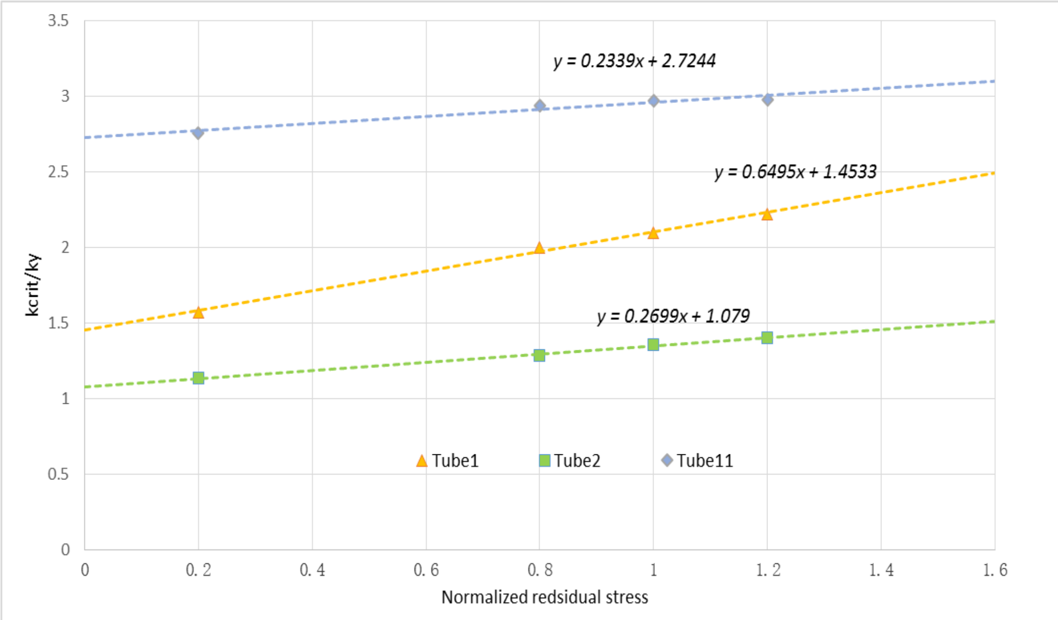

Figure 143: Effect of residual stress on k_{crit} of Tubes

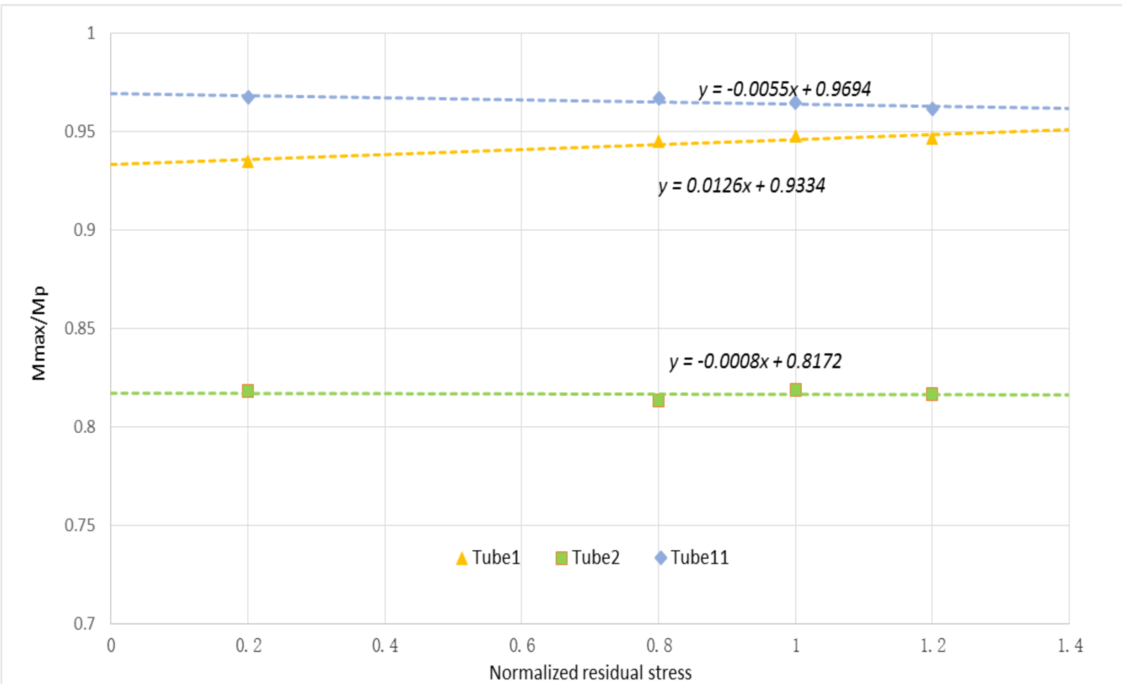

Figure 144: Effect of residual stress on M_{max} of Tubes

From the table, it can be seen that the critical curvature is influenced more than maximum moment, critical curvature of all tubes is positively influenced by residual stress, the higher residual stress, the higher critical curvature, Tube 1 is influenced most than the other two tubes. Since Tube 1 featured low D/t ratio, it is thought that low D/t ratio tubes have tendency to be influenced by residual stress more. Tube 2 and Tube 11 have a similar tendency of increasing.

Overall, the critical curvature of all tubes benefit from higher residual stress, since the increasing speed of Tube 1 is the highest, which featured lowest D/t ratio, Tube 2 is faster than Tube 11, featured with highest D/t ratio, but they were both featured higher D/t ratio, therefore, it is thought that residual stress have higher effect for lower D/t ratio. In Figure 144, it is noticeable that Tube 1 have an increasing tendency while the other two start to decrease as residual stress increase. From the result above it is assumed that the effect of residual stress depend on D/t ratio, since Tube 1 features lower D/t ratio, it has significant plasticity and higher ductility, while the other two tubes feature with higher D/t ratio have less ductility. When the tubes is under external loading, the interactions between residual stress and external load might lead to partial plastic deformation in tubes, and the residual stress is redistributed. Thicker tubes like tube 1 with sufficient plasticity might benefit from residual stress in terms of maximum moment. It is assumed that when the D/t ratio decrease to certain value, the declined trendline might start to increase. Another possibility is that the deformation capacity of thicker tubes is influenced more severe than thinner tubes by varying magnitude of parameters, it indicates thicker tubes might show unstable behavior. However, only three tubes were investigated, and there are other differences between the tubes, such as the imperfection heights and the material models, conclusion based on these three tubes is not objective enough and lacking theoretical support. Further work is needed to exclude these variables and confirm the relationships between residual stresses and D/t.

6.6 Statistical analysis of parameter study

In this section, regression analysis is performed based on the result of the parameter study.The regression relation between the critical curvature, D/t, imperfection and yield strength can be described as linear by logimath transforming, and the M_{max} is introduced by linear relation with regard to these three parameters.

$$M_{max} = a_0+a_1(Ap)+a_2(D/t)+a_3(f_y) \tag{45}$$

Table 45: Regression analysis for M_{max}

	a_0	a_1	a_2	a_3
Coefficient	7635.966	-38.09	-70.4162	9.3323
Standard Error	511.5201	101.5181	3.389781	0.758085
P-Value	3.56318E-21	0.1328	5.45631E-28	1.45024E-17
Upper 95%	8660.66379	165.275	-63.62562	10.8509
SignificanceF	4.29287E-30			
F	203.74758			
$SS_{Regression}$	2.6E+08	23853586	2.84E+08	
df	3	56	59	
R^2	0.916			
SE	652.6537			
Multiple R	0.957			

The prediction fomula for M_{max} is obtained by regression analysis above, $M_{max}= 7635.966-38.09(Ap)-70.42(D/t)+9.33(f_y)$, the coeffiecient -38.09 means when the other factor remain unchanged, once the maximum moment increase one unit, the corresponding imperfection should also decrease 38.09 units, at the same time D/t should also decrease 70.42 units, while f_y has a different situation, it should increase 9.33 units as maximum moment increase one unit. The the percentage of total variation explained by the regression formula is 91.6%, the value of significance is 4.293E-30, which is much less than 0.05, it means that the maximum moment has significant relation with imperfection, D/t and yield strength. It is concluded that the influence of imperfection on maximum moment is much less than the other two factor by observing the predicting P-value, the P-value of influence of imperfection is quite high, almost lost its referential capability since it is close to 0.15. The standard error of predicting fomula is 685.1kNm, less than 10% of average tube capacity, when the extent of combined variables is enlarged to much higher or lower level, it lose its accuracy of perdicting the final results.

The P-value of other two factors are extremely small, it is almost equal to zero, which means that once there is chance to change these factor, the probability to obtain the same result by the other factor like imperfection is equal to zero, indicating the parameter play significant role in influence the maximum moment of tubes.

Based on this regression, the expected values of the M_{max} for every combination of imperfection, f_y,and D/t can be plotted by this regression formula. The results are shown in Figure 145. The x-axis shows the results predicted by the regression model, while the y-axis shows the value calculated from numerical model. The dashed orange line shows the line to compare the accuracy of predicting model. Since the data point of accuracy of regression model for predicting combined parameters features one curved-shape which indicates that there might be other factors should be involved in predicting formula, this problem should be resloved in the future research.

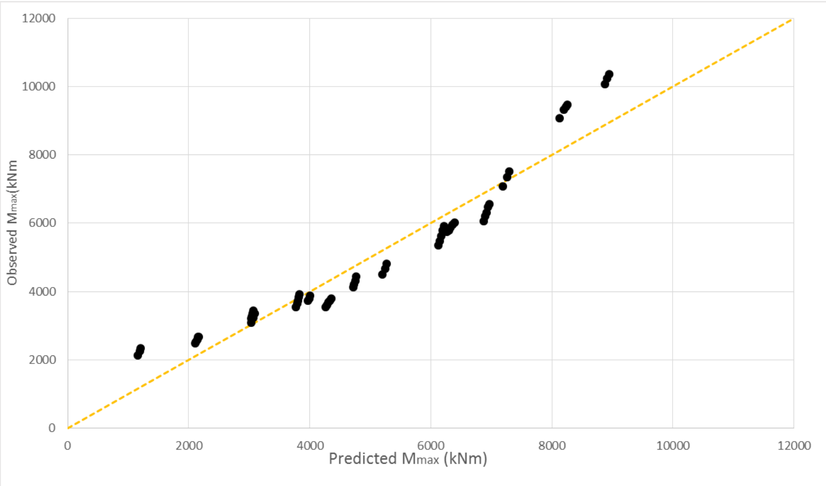

Figure 145: Accuracy of regression model for predicting combined parameters M_{max}

A similar analysis is also performed for $k_{crit.}$ However, the relation between critical curvature and these three parameters is not linear, therefore, logarithm is used to transform the relation into linear as following, the prediction formula has been transformed to exponential equation：

$$k_{crit} = 5.296Ap^{a1} \bullet D/t^{a2} \bullet f_y^{a3} \tag{46}$$

Regression analysis for k_{crit} is similar, the predicting formula is significant because the correlation is found to be 0.908, which indicated that the critical curvature is highly correlated with these three paramters, unlike situation in predicting maximum moment, the influence of imperfection on k_{crit} is much more great than influence of maximum moment, but it is still has less potential to influence the results compare with other two paramters. The P-value of imperfection in predicting k_{crit} is only 5.56E-14, much less than the P-value of D/t and f_y. The accuracy decrease when the tube goes to higher stength tubes.

Table 46: Regression analysis for k_{crit}

	a_0	a_1	a_2	a_3
Coefficient	1.666912	-0.12116	-0.85946	0.627062
Standard Error	0.335961	0.012874	0.04029	0.04934
P-Value	0.009526	1.72E-14	5.61E-30	5.92E-19
Upper 95%	1.571208	-0.09542	-0.7789	0.725724
SignificanceF	1.23E-31			
F	202.1222			
$SS_{Regression}$	5.988382	0.602427	6.590809	
df	3	61	61	
R^2	0.908			
SE	0.099			
Multiple R	0.953			

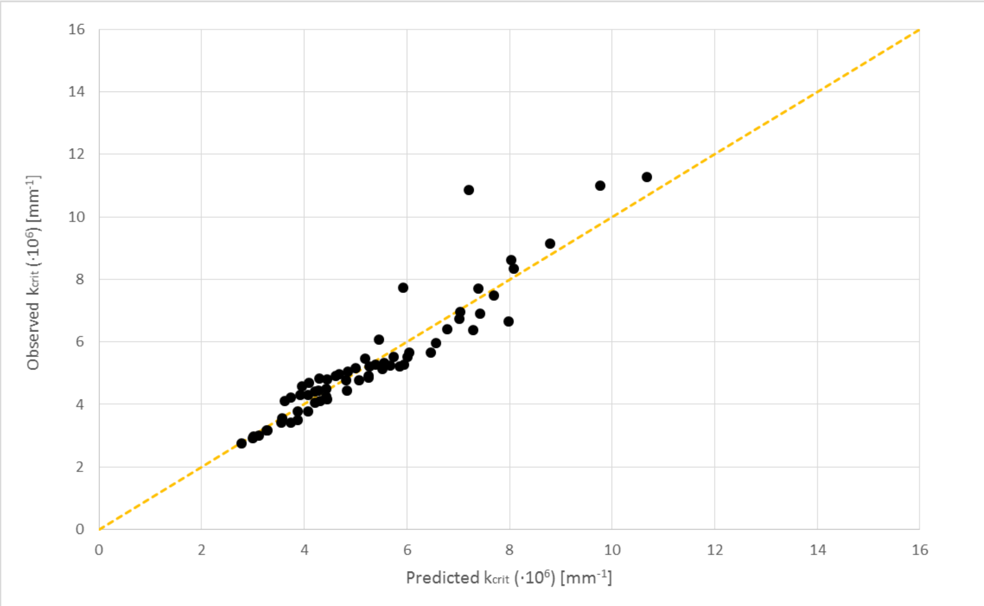

Figure 146: Accuracy of regression model for predicting combined parameters k_{crit}

6.7 Chapter conclusions

It is noticeable that even some problems like the exact impact of residual stress on behavior of buckle are not very clear but main influence tendency of basic parameter can be obtained and summarized through parameter study. By means of simulation and data analysis of tubes in experiments, it is concluded that residual stress have great impact on equilibrium path and the impact on tube with lower D/t is more significant. Residual stresses do not greatly affect the maximum moment.

In the first part of this study, the impact of initial imperfection value Ap on k_{crit}/k_y and the M_{max}/M_p are investigated among various tubes. It is obvious that the impact of imperfection on critical curvature is significant. Curvature is normalized by k_{crit}/k_y, and it decreases logarithmically upon increasing imperfection to thickness ratio which means a small change in imperfection will lead to significant drop in k_{crit}/k_y. When it comes to tubes with lower D/t ratio and low yield strength, this behavior is more pronounced. With regard to the M_{max}/M_p, the relation between the M_{max}/M_p and imperfection can be described as a linear relation, the impact on critical curvature is greater than the impact on the M_{max}/M_p, because the shape of the equilibrium path depends on not only f_y but also on other factors like D/t. Meanwhile, the other two factors of D/t and imperfection value Ap are also investigated.

In the second section, the impact of D/t on k_{crit}/k_y and M_{max}/M_p is investigated, it is found that k_{crit}/k_y decreased with power function as D/t increased. By calculating the derivative, it can be seen that the slope between the lowest D/t to lower D/t is the biggest, it decreases faster with lower D/t. However, with lower yield strength, the impact is more significant and k_{crit}/k_y decrease rapidly. In terms of M_{max}/M_p, there is different situation, the M_{max}/M_p decreased faster with higher strength tubes, it is less pronounced with lower D/t ratio.

Finally, the yield strength is varied in the third section. Yield strength non-linearly influence k_{crit}/k_y which can be described with a power model, the impact on k_{crit}/k_y is more significant with lower D/t ratios. With regard to the M_{max}/M_p, it has a linear relation with varied f_y. It is known that when there is demand for high ductility, D/t should decrease in order to meet the requirement. However, tubes with lower D/t is easily effected by the factor of imperfection or yield strength.

7 Overall Conclusions and recommendations

7.1 Conclusions

This report analyzes the spirally welded tubes under 4-point bending which lead to the tube formed in local buckling in the middle part. To simulate the tube under large deformation in the finite elements analysis, nonlinear geometrical and nonlinear material properties are adopted. Calculated nonlinear material properties of the tube are averaged based on four directions considering the engineering stress strain relationship in material tests which is shown in Appendix A.

The step of adding the initial imperfection is essential for the tubes that have local buckling. Without any geometrical imperfection in non linear analysis, local buckling occurs near the middle supports, the final targeting deformed shape can not be achieved. When initial imperfection is added into non-linear buckling analysis, final buckling occurs in the middle. By moving the curvature and ovalization curvature along the neutraline of the tube in consistent with the physical test configuration, the results obtained from neutral line model is comparable with the experimental data.

Neutral line model can predict critical curvature better than the analytical formula, when all the tubes are considered, the standard error of the analytical solution gets improved. However, in terms of the plain tubes, analytical solution performs better than neutral line model. When comparing with model without ovalization, critical curvature have been improved by neutral line model for all tubes. It is interesting that when all tubes are considered, neutral line performed the best among all model in aspects of critical curvature and maximum moment. Neutral line model has the best prediction in terms of maximum moment when all tubes are compared. It is concluded that free ovaliation end support will obtain more accurate results in aspects of critical curvature and maximum moment for tubes with welded features and the critical curvature is overestimated with tube allowing ovalization at supports.

There are four parameters which affect the capacity of the tubes, residual stress, imperfection, diameter to thickness ratio and yield strength. Residual stresses were found to affect k_{crit} significantly, especially at low D/t ratios. The shape of equilibrium path after yielding is changed greatly and k_{crit} is moved back with lower residual stress. It is a significant parameter because it is very difficult to estimate the magnitude of the stress because they come from several sources and varies depending on how it is manufactured. D/t and yield strength has non-linear impact on k_{crit} and a small change will lead to a large impact on the changing of k_{crit}, especially for tubes featured by lower D/t and lower strength. It has largest impact on deformation capacity of tubes. However, D/t is also one of the most certain parameters because it is directly controlled by the manufacturing process. The most uncertain parameter by far is imperfection value which is found to have a significant impact on k_{crit}, and it is difficult to relate the measured imperfections to the imposed imperfections. In terms of M_{max}/M_p, all parameters were found to affect capacity linearly. The effect of imperfection on the M_{max}/M_p is less significant than the effects of f_y or D/t. In reality, the imperfection is not so large, it might have less impact than other parameters do.

Finally, a finite element analysis model with the correct properties, boundary conditions and parameter settings will have the similiar reaction and results in the experimental test. Considering both the moment curvature relationship and the ovalization curvature relationship, the results from tests and numerical models generally conform with each other. Through investigating the full scale tests results, the developed numerical model is validated.

7.2 Recommendations for further study

Experimental data already deviated from the linear elastic branch before the results from numerical model to show plasticity. This indicates some inpact that is not correct or not accurately modeled in the numerical models. The reason could be geometrical imperfections or residual stresses. It is thought that the most important one of these influence factors is the residual stresses because there exists the largest uncertainty in this factor. It is very difficult to estimate the magnitude of these stresses because they come from several sources and varies depending on how it is manufactured, therefore, residual stress should be studied further and applied to numerical model more concretely and comprehensively.

An improved model could be built considering incoporating the girth weld at the corresponding positions. However it still needs some model designing method before putting into practice. Thermal mechanical simulation is suggested in future study to fully represents the interations of either side for girth welds and coil connection welds. It is suggested that simplified material models can be developed based on f_y to increase certainty in this parameter. Material model has a profound impact on M_{max} and on the shape of the equilibrium path itself, a material model can be created which simulates the true material properties.

It is recommended to use yield strength to tensile strength ratio as one evaluating metics in parameter study. In reality, cold-formed steel structure increase the ratio of yield strength to tensile strengh which will correspondingly lead to lower ductility and toughness, in the meantime, the resistance to fracture and weldability also deteriorates. Post-buckling residual strength for each tube is also suggested to investigate in future study, because the failure of spirally welded tubes does not lead to the final collapse. Being primary structural system, the residual strength plays an important role in strcutural resisting system.

Apart from material model which greatly affect the result should modified, new scaling factor of introducing imperfections into the neutral line models should be modified. To investigate different factors of relating the size of the imposed imperfections to the height of the actual imperfections in the tubes is the main task in future research which will not only produce more representative results but also improve the accuracy of predicting formula. The approach for further calibrating the numerical model can be seen in Appendix D, it is clearly described the relationship how diffenrent section interacting each other, by adjusting the scaling factor multiplied with initial imperfection value and residual stress, the numerical model could be futher modified.

References

Van Es, S. H. J., Gresnigt, A. M., Kolstein, M. H., and Bijlaard, F. S. K. (2013). "Local Buckling of Spirally Welded Tubes–Analysis of Imperfections and Physical Testing." The proceedings of the Twenty-third (2013) International Offshore and Polar. Engineering Conference Anchorage, Alaska, June 30-July 5, 2013.

Gresnigt, A. M. (1986). "Plastic Design of Buried Pipelines in Settlement Areas." HERON, 31(4), 1–113.

Gresnigt, A. M., Williams, C. A., and Karamanos, S. A. (2010). "Local Buckling Limits of Tubular Sections in Bending and Compression." Tubular Structures XII: Proceedings of the 13th International Symposium on Tubular Structures, University of Hong Kong, Hong Kong.

EN 1993-1-1, (2006) Eurocode 3: Design of steel structures – Part 1-1: General rules and rules for buildings.

EN 1993-1-6, (2007) Eurocode 3: Design of steel structures – Part 1-6: General – Strength and Stability of Shell Structures.

Van Es, S. H. J., Gresnigt, A. M., Kolstein, M. H., and Bijlaard, F. S. K. (2013). "Strain Based Design of Spirally Welded Pipes, Local Buckling in 4-point Bending". International Society of Offshore and Polar Engineers (2014).

S.H.J. van Es., A.M. Gresnigt, (2014) "Design of test setup and results of four point bending tests on spiral-welded tubes" COMBITUBE – WP2 Task 2.1 WP3 Task 3.1 Research Fund for Coal and Steel: RFSR-CT-2011-00034.

S.H.J. van Es., A.M. Gresnigt, (2014) "Measurements of imperfections and residual stresses" COMBITUBE – WP2 Task 2.4 Research Fund for Coal and Steel: RFSR-CT-2011-00034.

S.H.J. van Es., Daniel Vasilikis, A.M. Gresnigt,(2014). "Material testing of tube material" COMBITUBE – WP2 Task 2.3 Research Fund for Coal and Steel: RFSR-CT-2011-00034.

Wierzbicki, T., and Sinmao, M. V. (1997). "A Simplified Model of Brazier Effect in Plastic Bending of Cylindrical Tubes." International Journal of Pressure Vessels and Piping, 71(1), 19–28.

Vasilikis, D., and Karamanos, S. A. (2014). Bending Resistance of Steel Tubes in CombiWalls Task 4.2: Modeling of the Spiral-Welded Pipe. Research Report, University of Thessaly.

Reddy, B. D. (1979). “An Experimental Study of the Plastic Buckling of Circular Cylinders in Pure Bending.” International Journal of Solids and Structures, 15(9), 669–683.

Poonaya, S., Teeboonma, U., and Thinvongpituk, C. (2009). “Plastic Collapse Analysis of Thin-Walled Circular Tubes Subjected to Bending.” Thin-Walled Structures, 47(6-7), 637–645.

Guarracino, F., Walker, A. C., and Giordano, A. (2008). “Effects of Boundary Conditions on Testing of Pipes and Finite Element Modeling.” International Journal of Pressure Vessels and Piping, 86, 196–206.

Houliara, S., and Karamanos, S. A. (2006). “Buckling and Post-Buckling of Long Pressurized Elastic Thin-Walled Tubes under In-Plane Bending.” International Journal of Non-Linear Mechanics, 41, 491–511.

Houliara, S., and Karamanos, S. A. (2011). “Buckling of Thin-Walled Long Steel Cylinders Subjected to Bending.” Journal of Pressure Vessel Technology, 133(1), 011201.

Gellin, S. (1980). “The Plastic Buckling of Long Cylindrical Shells under Pure Bending.” International Journal of Solids and Structures, 16(5), 397–407.

Zimmerman, T. Timms, C., Xei, J., Asante, J. (2004) “Buckling resistance of large diameter spiral welded linepipe:” Proceedings of International Pipeline Conference, Calgary, Canada Zimmermann, S., Karbasian, H., Knoop, F.M. (2013) “Helical Submerged Arc Welded Line Pipe Engineered For Strain Based Design” Proceedings of the International Offshore and Polar Engineering Conference (ISOPE), Anchorage, Alaska, U.S.A.

Brazier, L. G. (1927). “On the Flexure of Thin Cylindrical Shells and Other ‘Thin’ Sections.” Proceedings of the Royal Society A: Mathematical, Physical and Engineering Sciences, 116(773), 104–114.

Ades, C. S. (1957). “Bending Strength of Tubing in the Plastic Range.” Journal of the Aeronautical Sciences (Institute of the Aeronautical Sciences), 24(8).

Karamanos, S. A. (2002). “Bending Instabilities of Elastic Tubes.” International Journal of Solids and Structures, 39(8), 2059–2085.

Appendix A: Material Data

The stress-strain curves are averaged based on 4 measured tests in four direction.

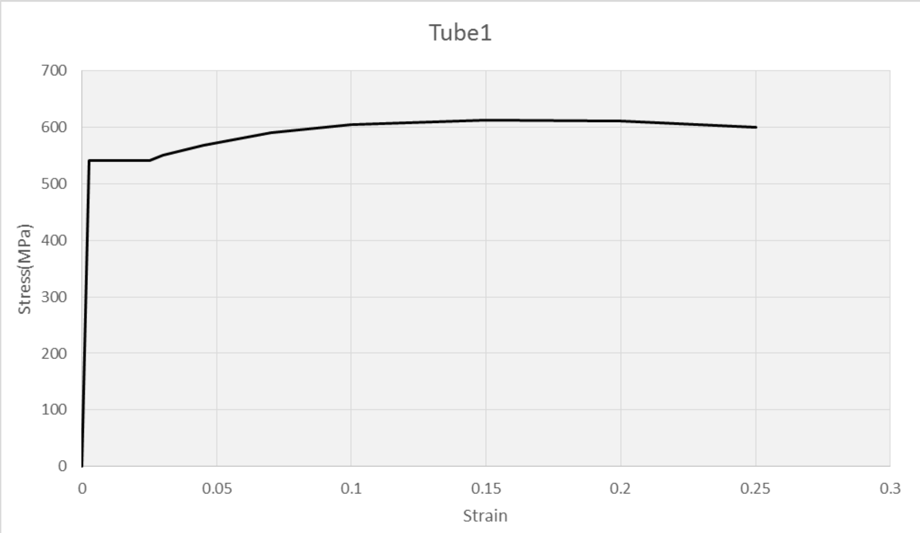

Figure166: Nominal stress-strain curve of Tube 1

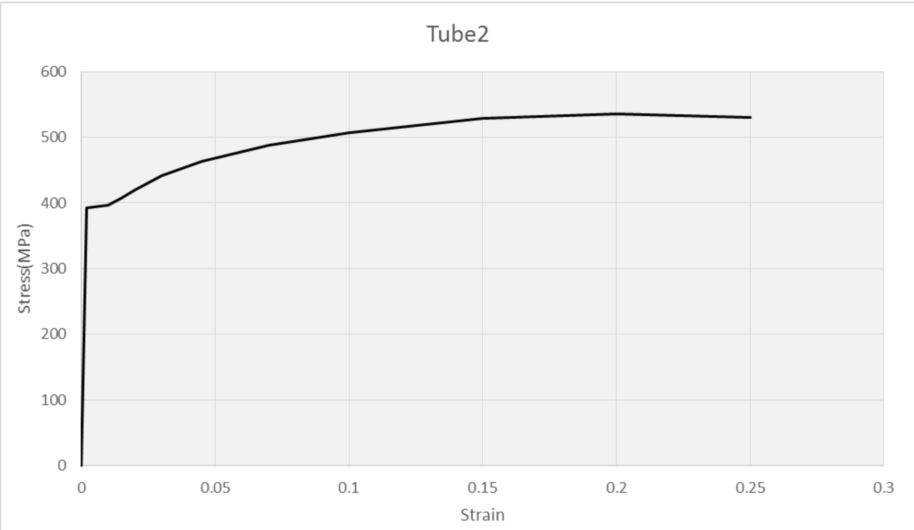

Figure167: Nominal stress-strain curve of Tube 2

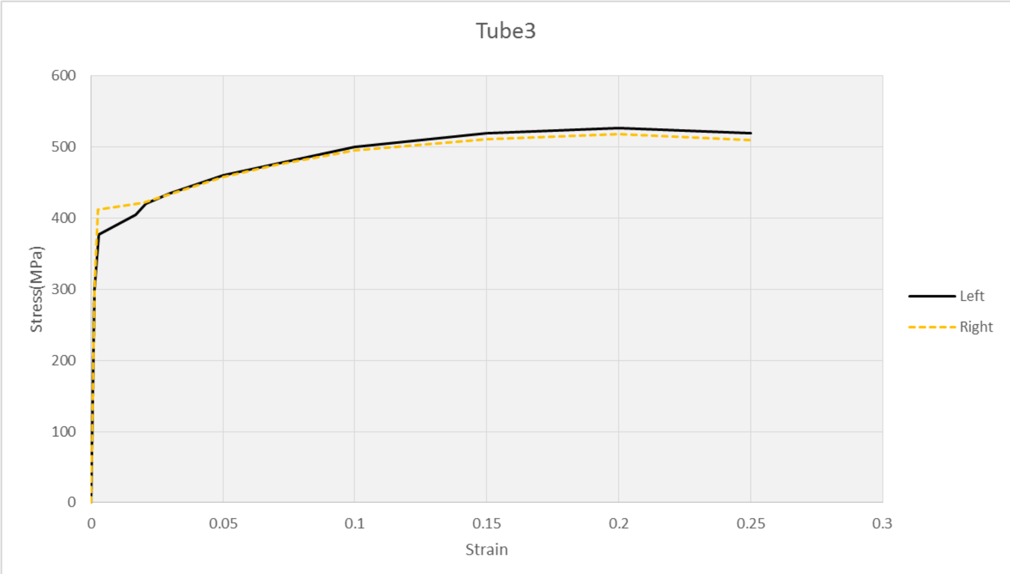

Figure168: Nominal stress-strain curves of Tube 3

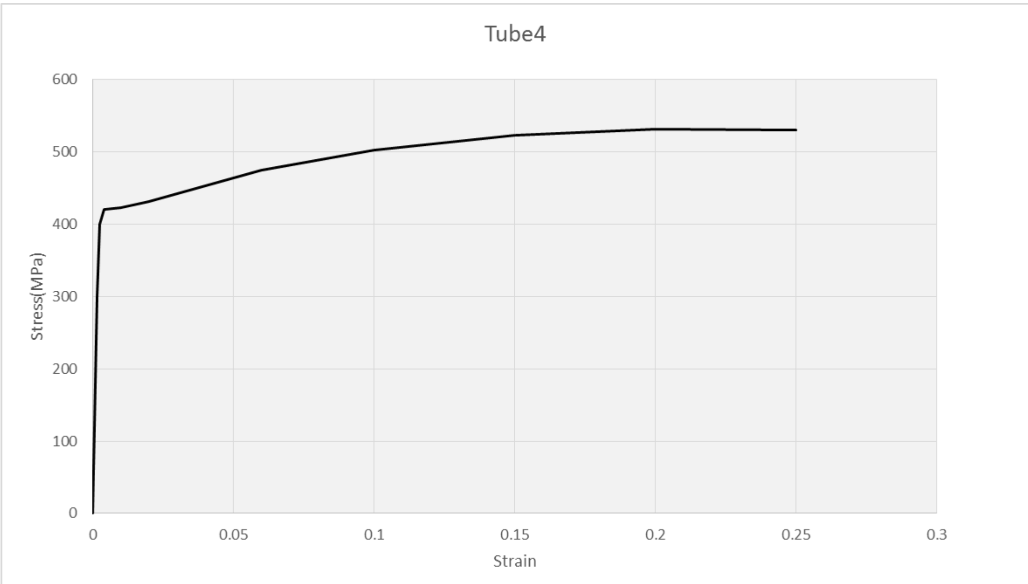

Figure169: Nominal stress-strain curve of Tube 4

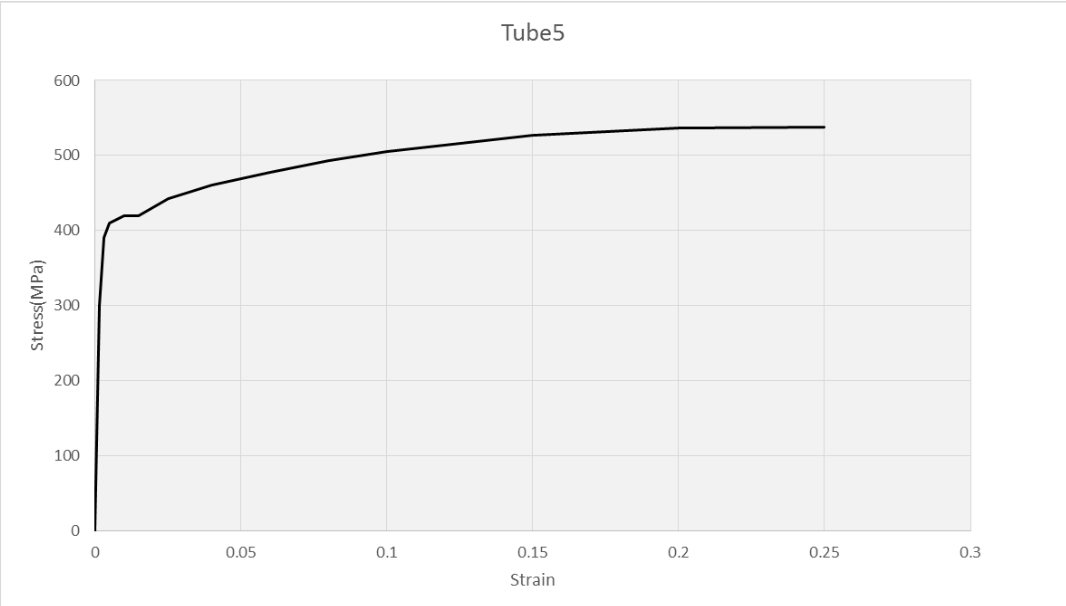

Figure170: Nominal stress-strain curve of Tube 5

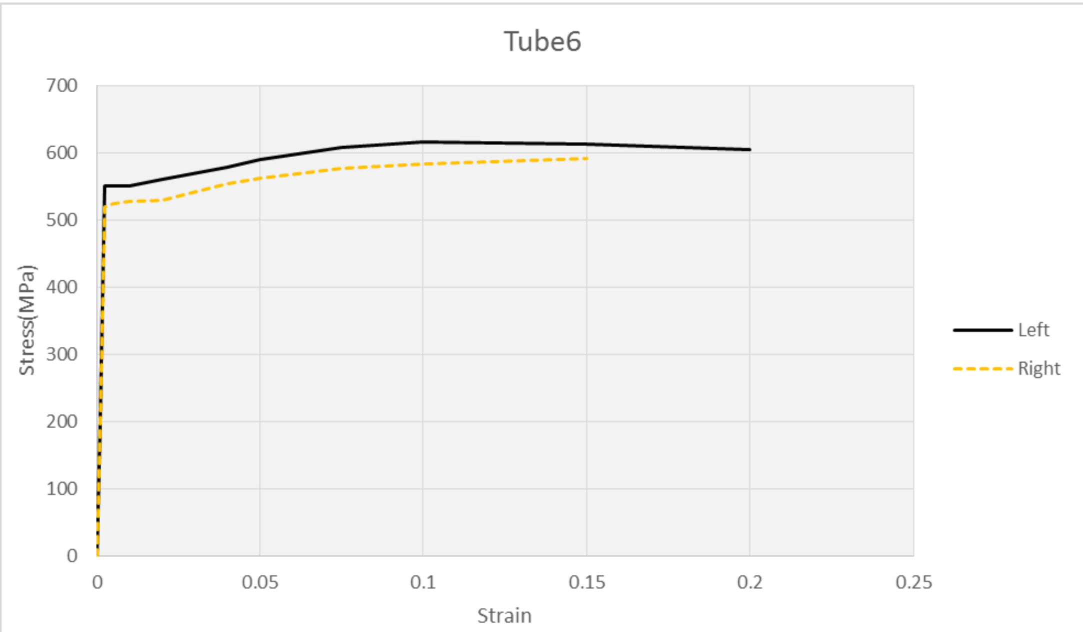

Figure171: Nominal stress-strain curves of Tube 6

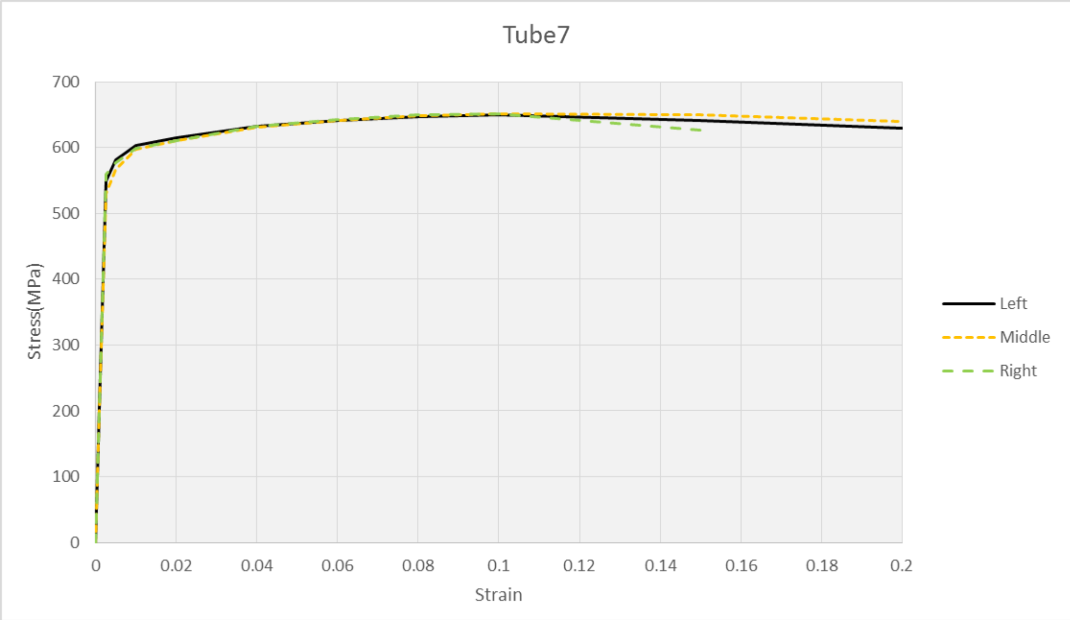

Figure172: Nominal stress-strain curves of Tube 7

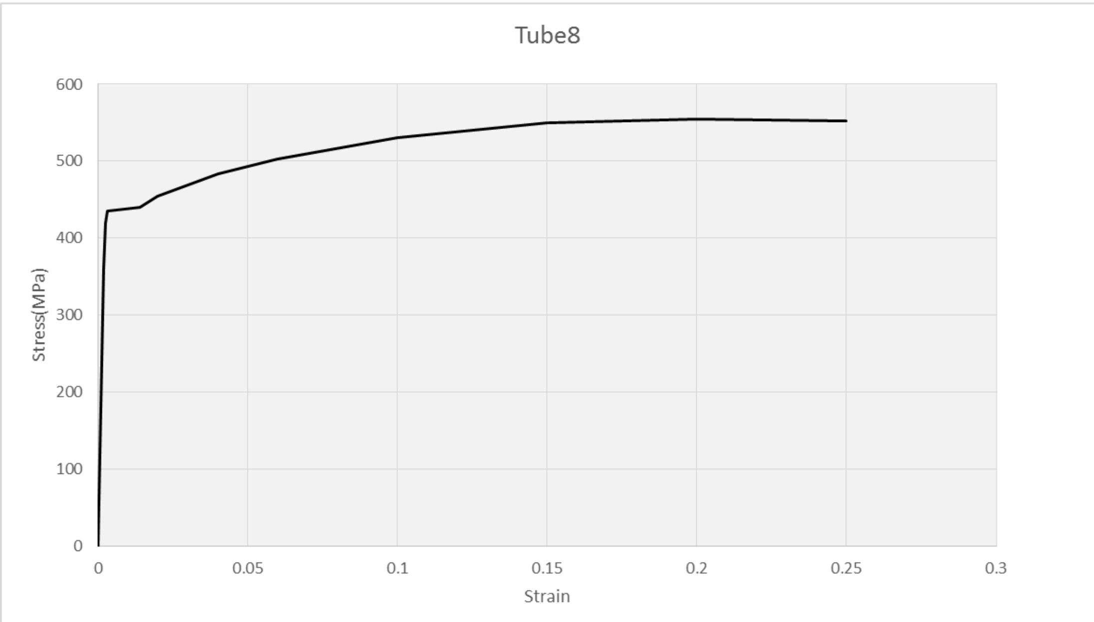

Figure173: Nominal stress-strain curve of Tube 8

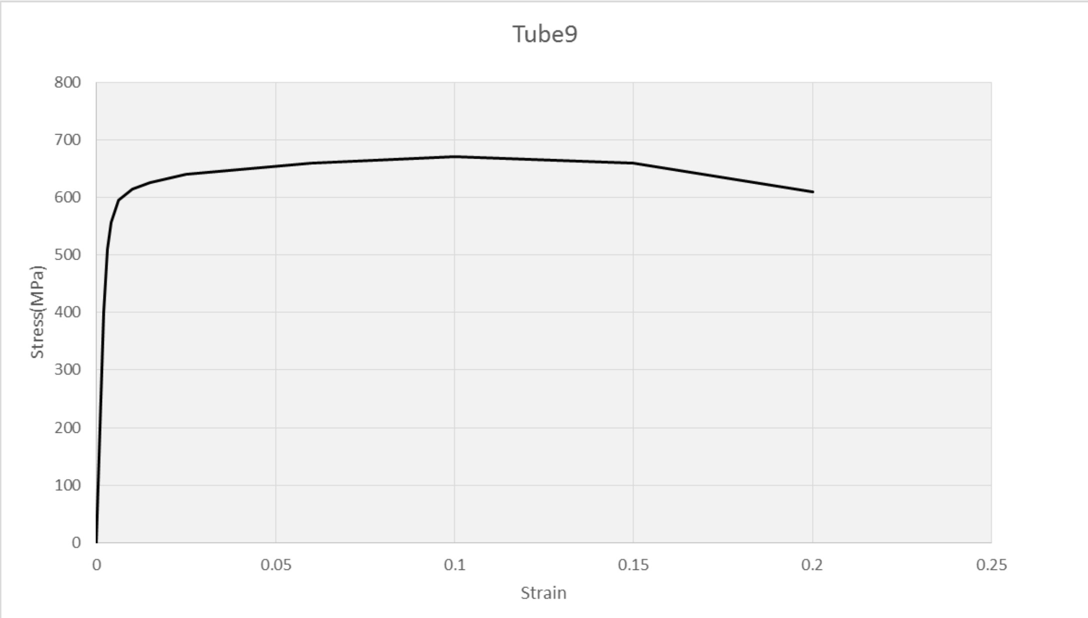

Figure174: Nominal stress-strain curve of Tube 9

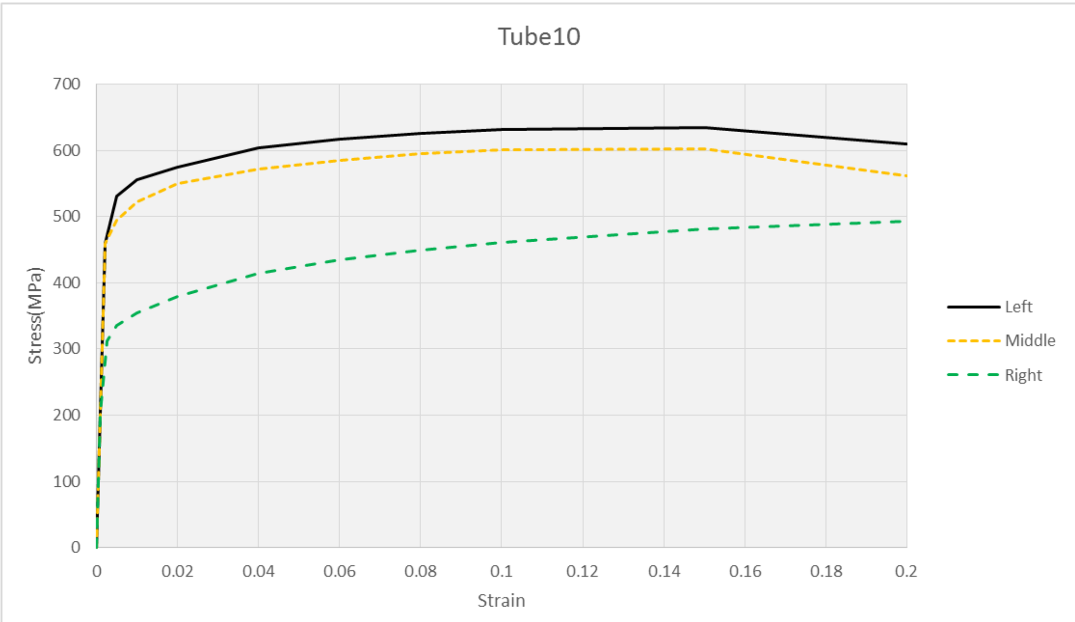

Figure175: Nominal stress-strain curves of Tube 10

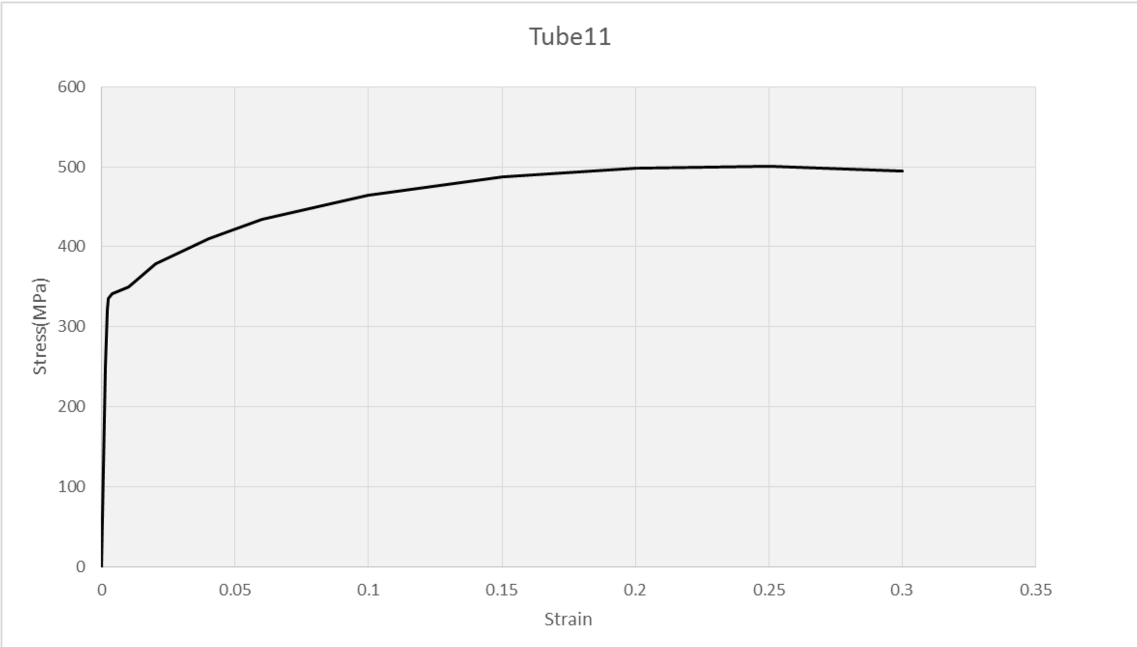

Figure176: Nominal stress-strain curve of Tube 11

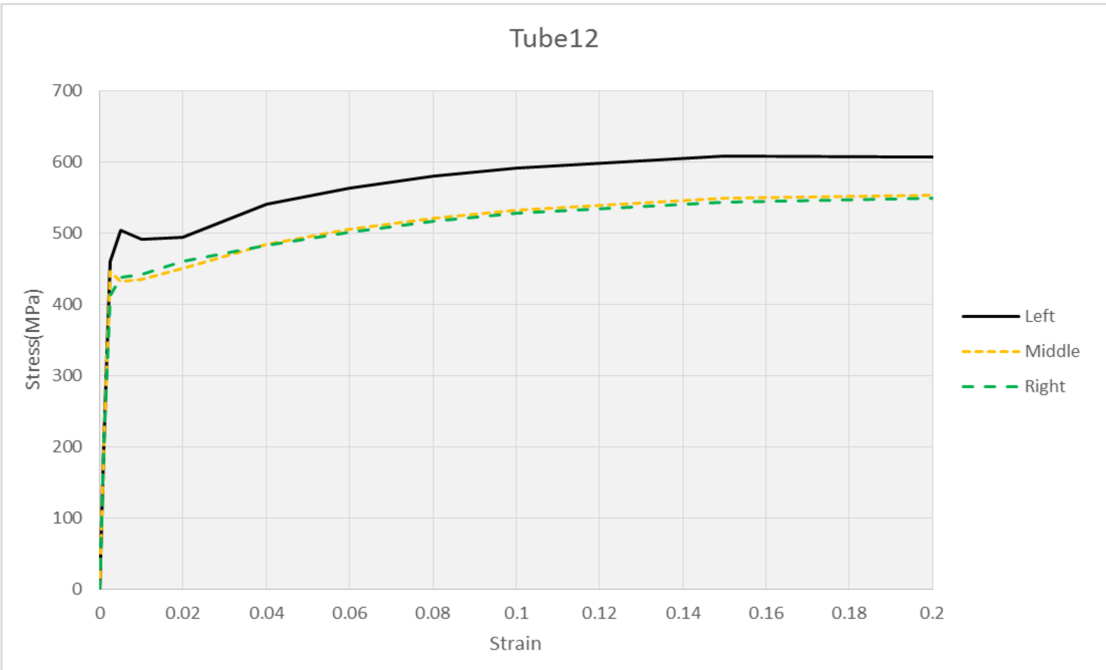

Figure177: Nominal stress-strain curves of Tube 12

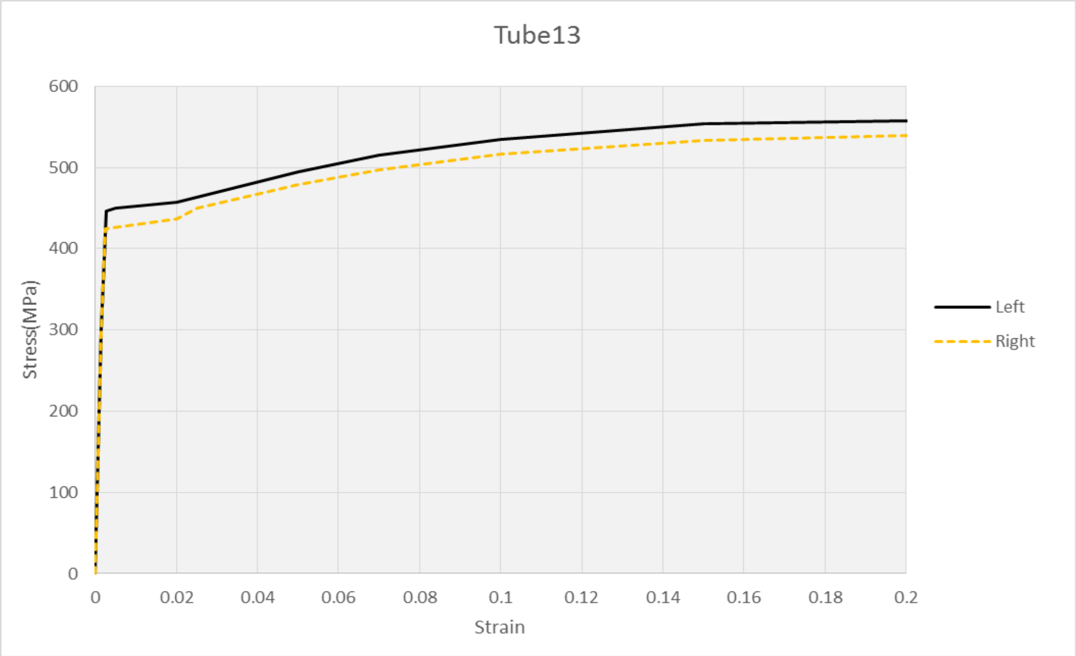

Figure178: Nominal stress-strain curves of Tube 13

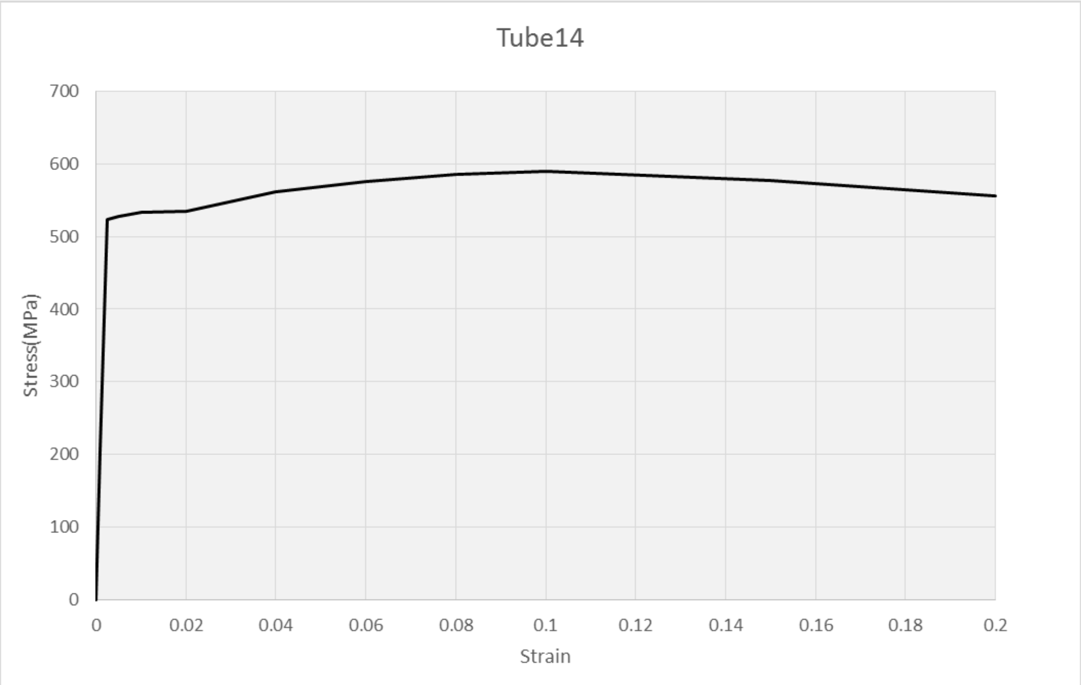

Figure179: Nominal stress-strain curve of Tube 14

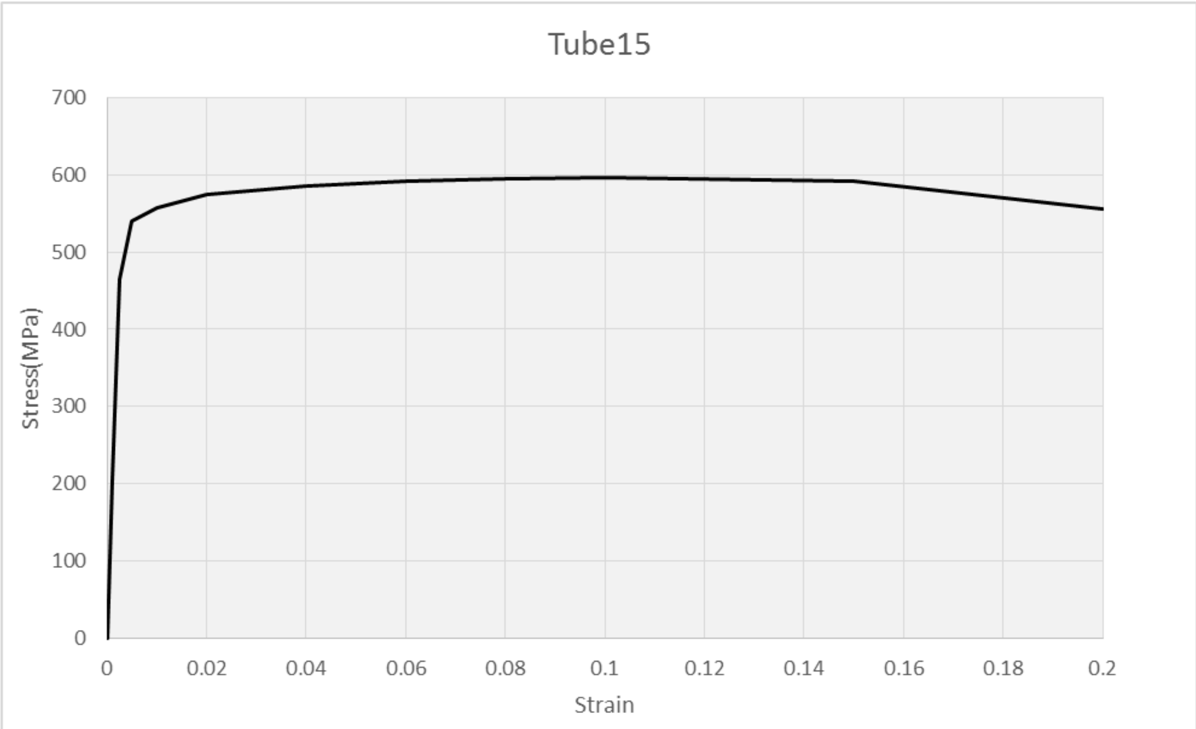

Figure180: Nominal stress-strain curve of Tube 15

Appendix B: Model creation in Abaqus

The first step for creating a tube model is to create the geometry according to the real dimensions. The geometry can be created by sketching the cross section of tube and extruding it to the required length. The geometry should be created based on the outside diameter of the tube if shell offset is defined as top surface, if it is defined as middle surface, the diameter of the tube should be input as radius of tube minus half thickness.

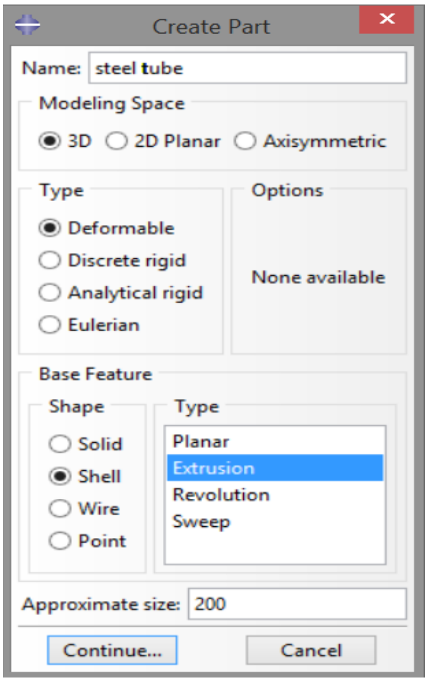

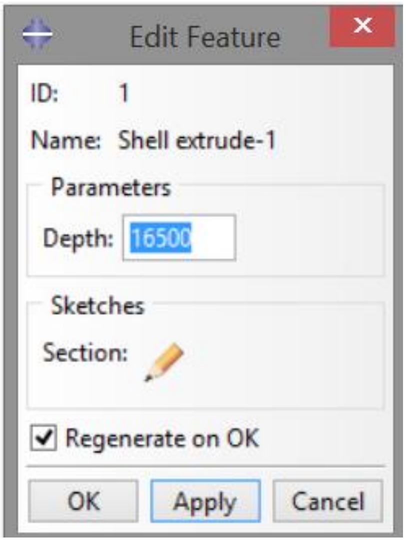

Secondly, material model can be defined. For an elastic analysis, only the elastic modulus needs to be defined. For a nonlinear analysis, the full stress-strain curve should be defined, in terms of true stress-plastic strain.

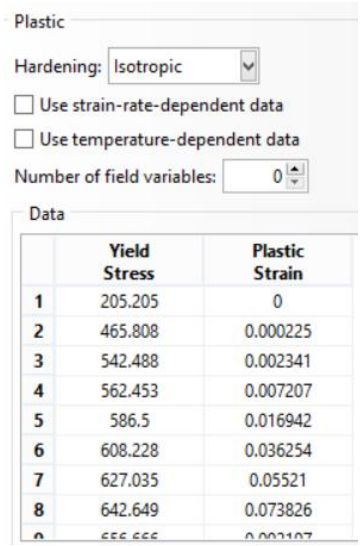

The section can also be defined. The section type 'homogeneous shell' should be used, and the shell thickness, number of integration points, and material model should be assigned appropriately:

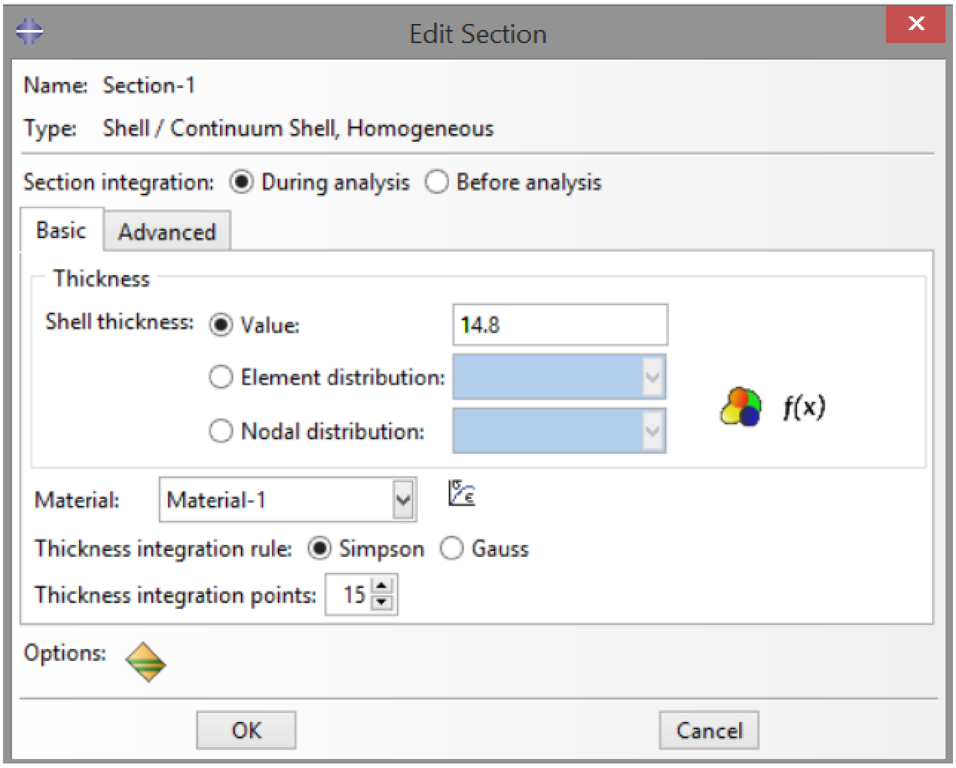

Now the section can be assigned to the geometry, by selecting "Section Assignments" from within the parts manager. The top surface should be selected for the shell offset definition. It should be noted that the author originally used middle surface as shell offset, however, it is more difficult to corvengence than top surface. Therefore top surface is defined:

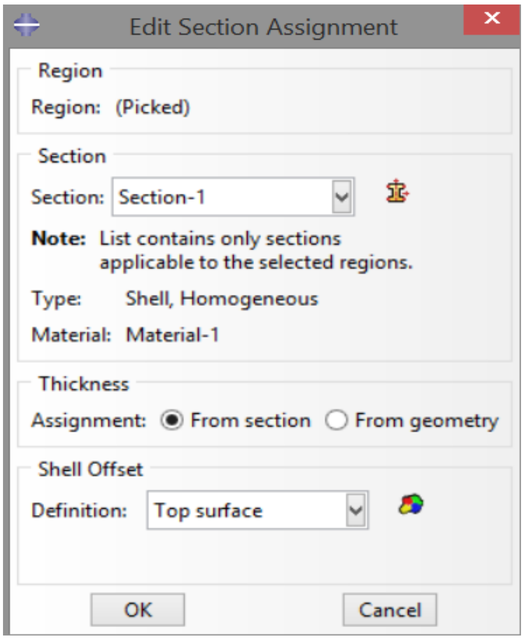

In order to define residual stress, a local cylindrical oordinate system has to be defined, because the residual stresses are given in terms of hoop stress and axial stress. The local system can be defined by going to the "Create Datum CSYS 3 Points" function, while in the parts manager. A cylindrical coordinate system should be created with the origin at the origin of the tube.Next, the material orientation is defined by going to Assign->Material Orientation. The new coordinate system should be selected, and then the correct axis should be selected as the normal direction. Direction 1 should correspond to the axial direction of the tube and direction 2 should correspond with the hoop direction. This is important for defining the residual stresses correctly:

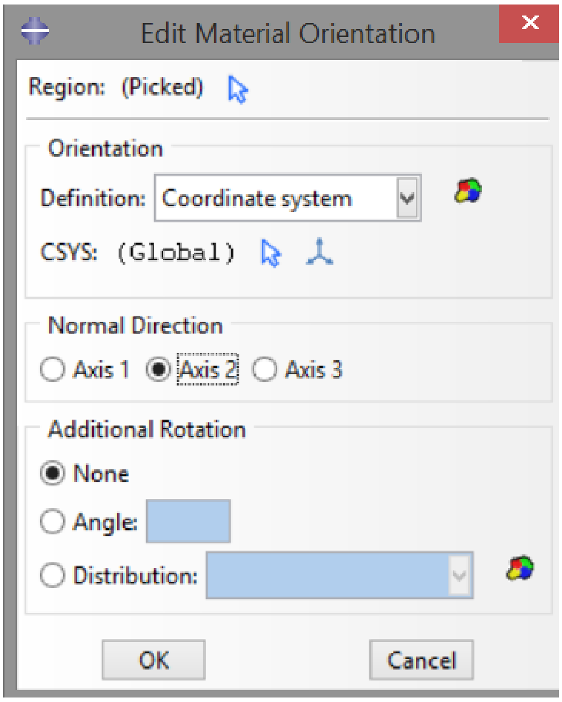

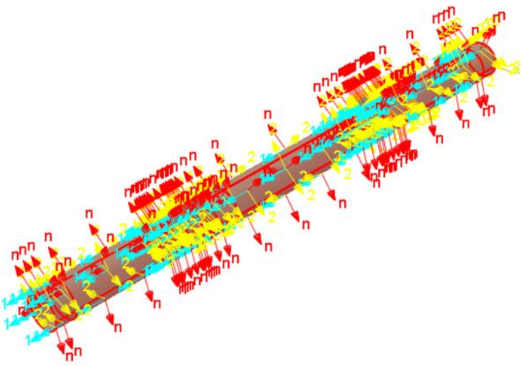

The assembly can now be created and meshed. First, global seeds are created by selecting "Seed Part"Instance" from the mesh toolbar. In this case, a 25mm mesh will be created:

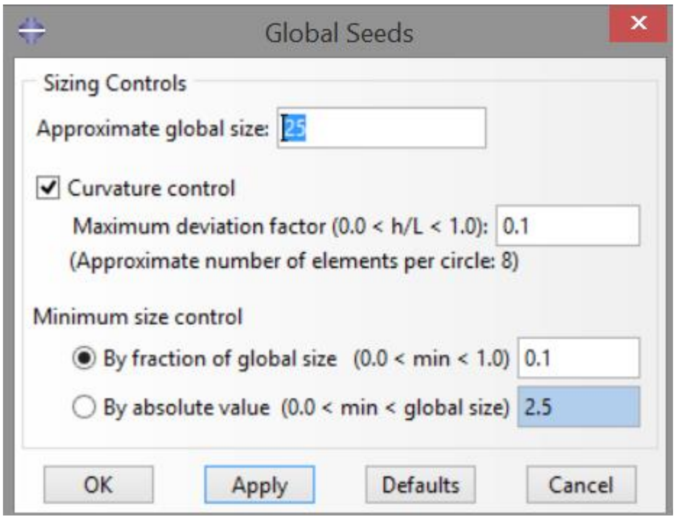

The mesh controls should be checked, because author originally used free mesh, but it show difficult in convergency, therefore, structural mesh is prefered.
If quadrilateral elements were selected, a quad element shape is appropriate. The element type can be chosen by clicking on "Select Element Type". Linear finite-strain elements should be selected. Reduced integration can be used to control the possibility of shear locking, but the stiffness of the element will also be reduced slightly.

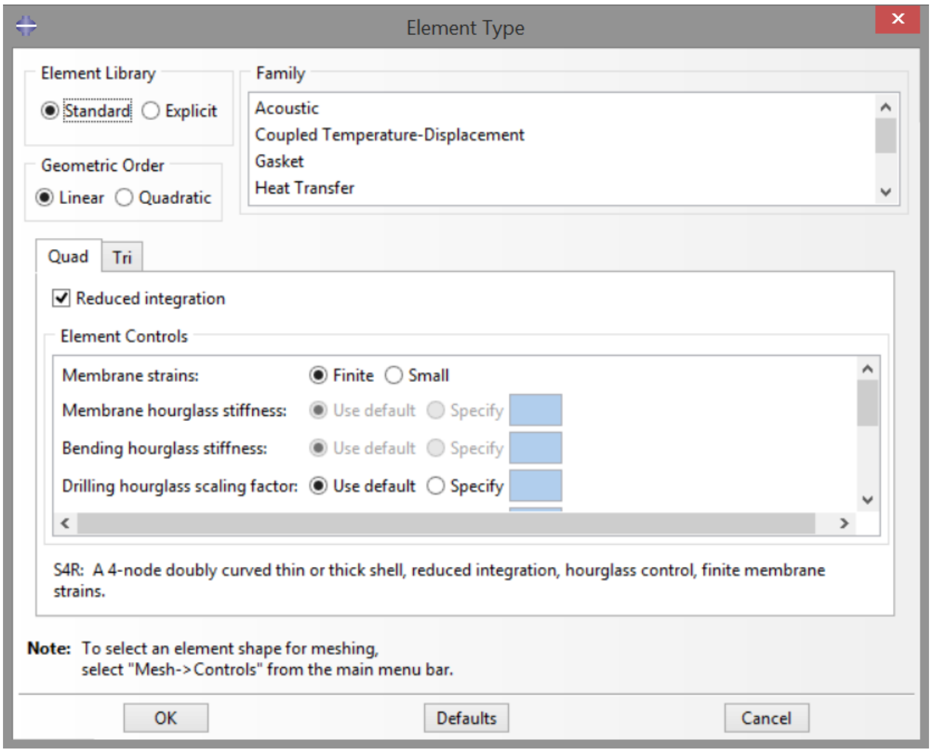

The next step is to define the analysis steps. If residual stresses are applied, an empty static general step has to be applied in order to check for equilibrium before analysis. Next, a static riks step has to be defined. A stopping criteria can be specified by specifying the maximum displacement at the end supports:

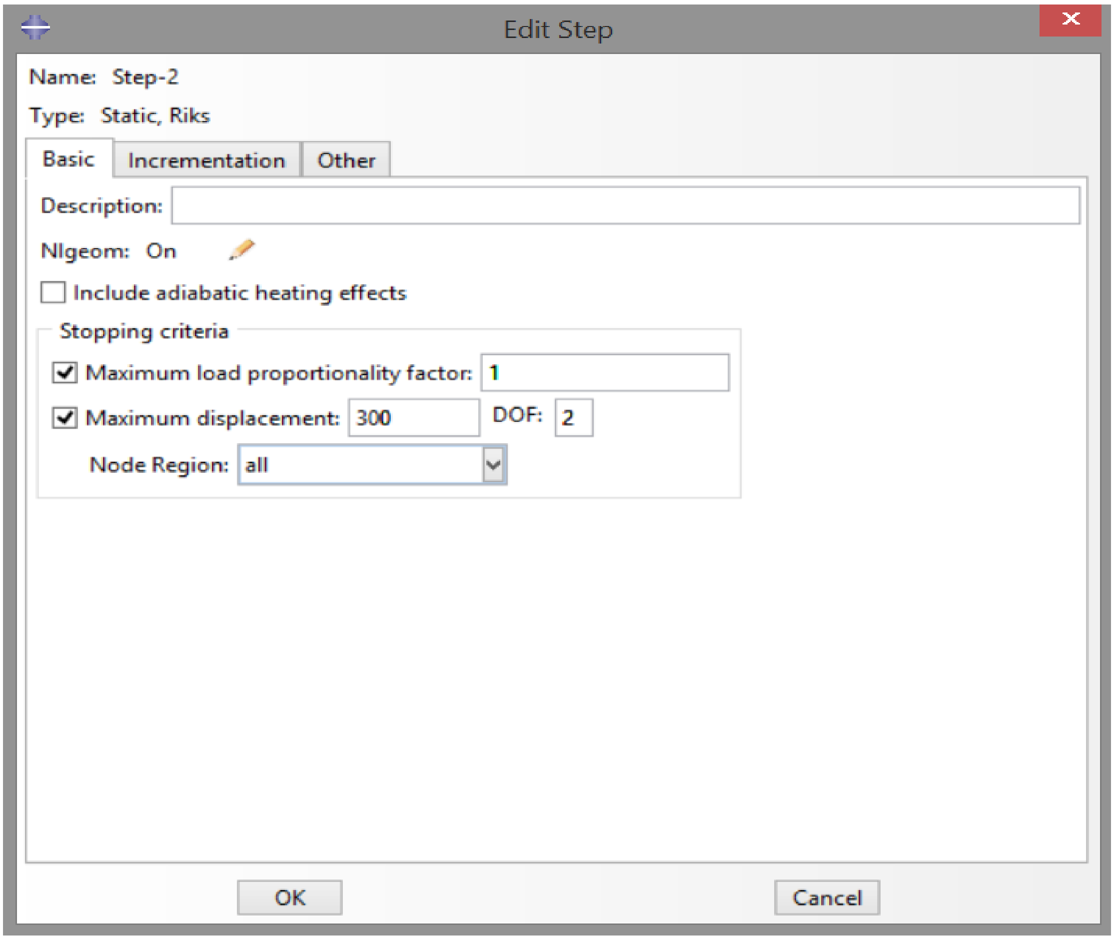

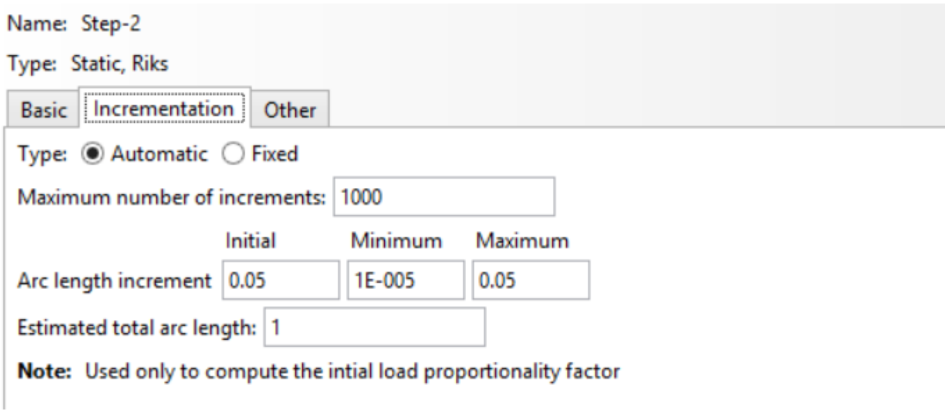

The incrementation is important because it controls the smoothness of the analysis, and can influence whether or not the solution converges close to buckling. A maximun and initial step size of 0.05 is a good initial guess, and the minimum step size can also be decreased if the solution does not converge.

Next the constraints should be defined, which is alos the most important part in this report, in terms of linear buckling analysis, kinematic coupling should be defined at support which will reslut in reasonble imperfection shape, the reason is explained before:

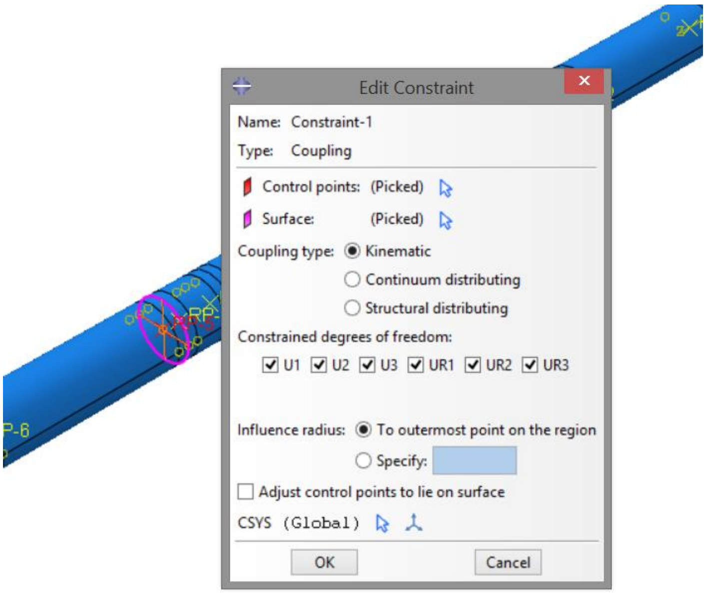

With regard to the linear buckling analysis, in order to avoid stress concentration which negatively increase the possibility that buckle occurs near support, the buckle is defined above with continuum coupling, which allows displacement:

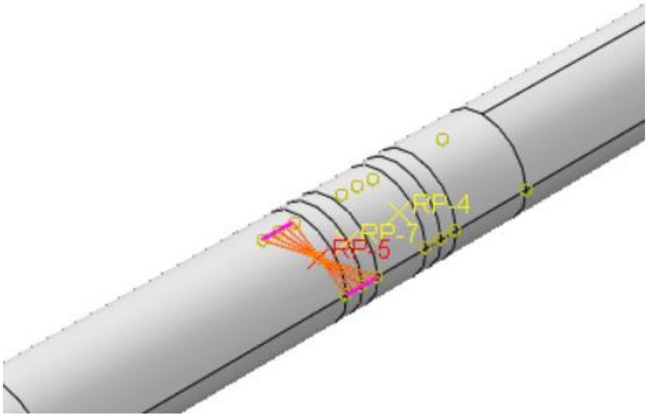

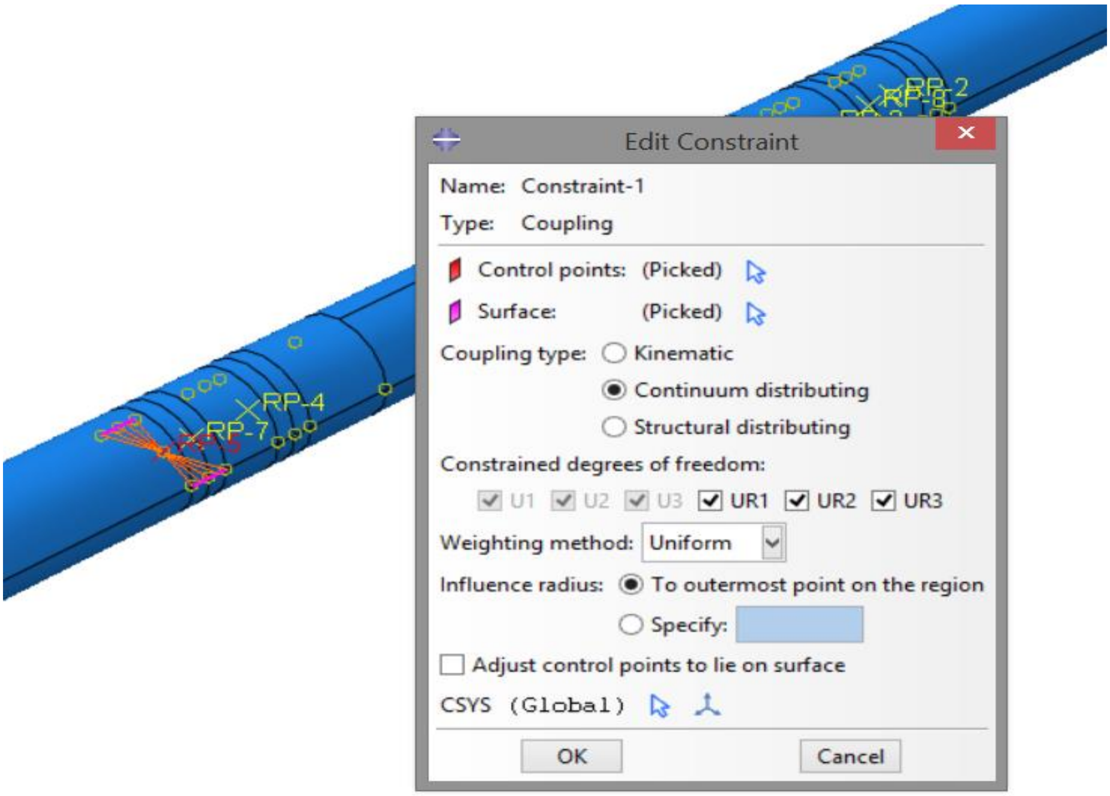

Then the boundary conditions can be defined. One end should be constrained in the directions U1, U2, UR2, and UR3, and the other end should be constrained in U1, U2, U3, UR2, and UR3. These conditions prevent the tube from rotating or moving, but allow one end of the tube to slide along the tube axis, in order to meet the requirment that the model has to keep equilibrium in three dimensions.

The loads can also be applied to the same points. The loads should be symmetric. In the static riks analysis, these loads are defined in form of displacement.

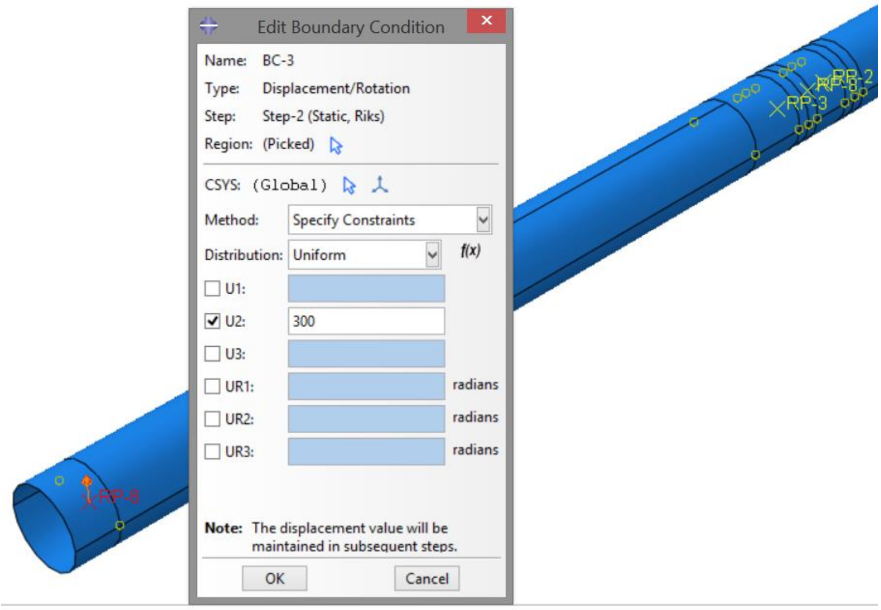

Next, the initial imperfections and initial conditions are applied by editing the input file. Within the graphical user interface, this can be done by right-clicking the name of the model and clicking "Edit Keywords".

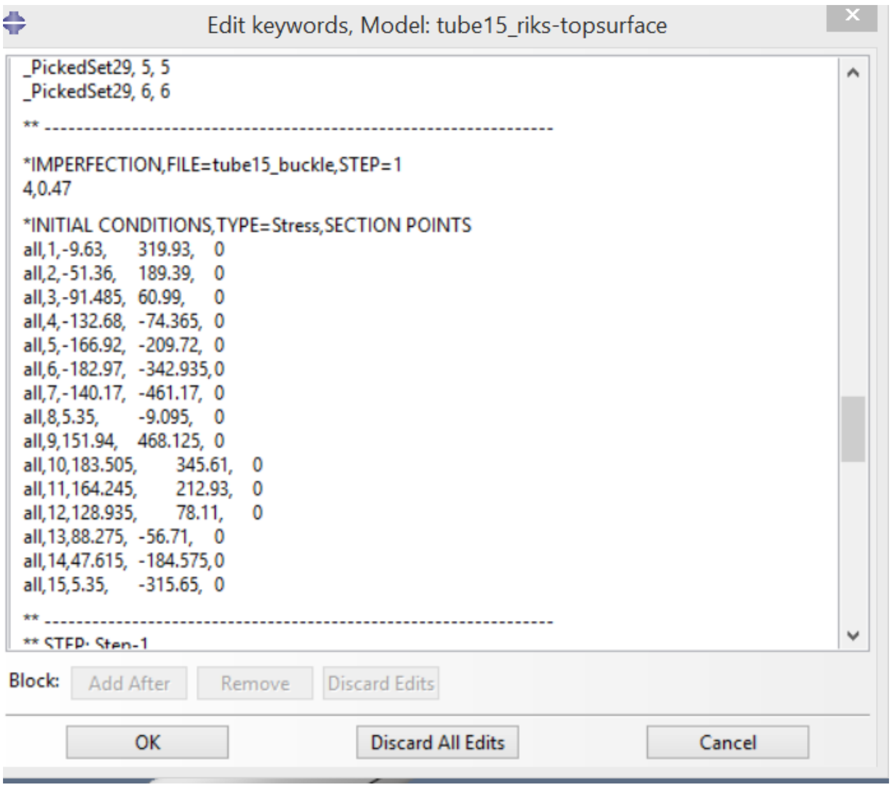

The sytax to input initial imperfection is introduced below:

*IMPERFECTION, FILE = name of buckling analysis, STEP=1
mode number, scale factor

For the residual stresses:

*INITIAL CONDITIONS, TYPE = Stress, SECTION POINTS
element set name, thickness integration point, s11, s22, s12

```
*IMPERFECTION,FILE=tube15_buckle,STEP=1
4,0.47
```

```
*INITIAL CONDITIONS,TYPE=Stress,SECTION POINTS
all,1,-9.63,     319.93,   0
all,2,-51.36,    189.39,   0
all,3,-91.485,   60.99,    0
all,4,-132.68,   -74.365,  0
all,5,-166.92,   -209.72,  0
all,6,-182.97,   -342.935,0
all,7,-140.17,   -461.17,  0
all,8,5.35,      -9.095,   0
all,9,151.94,    468.125,  0
all,10,183.505,      345.61,   0
all,11,164.245,      212.93,   0
all,12,128.935,      78.11,    0
all,13,88.275,   -56.71,   0
all,14,47.615,   -184.575,0
all,15,5.35,     -315.65,  0
```

Now the buckling analysis can be submitted. After the buckling analysis is complete, the static analysis can be submitted in the same way.
The jobs can be monitored by right clicking on the job and clicking on "Monitor", and the results can be viewed by clicking on "Results".
One way to export the output is to go to Tools->XY Data->Manager, in the results viewer. XY data can be created based on the ODB field output.
It is very important that the name of the job must match the name of the job from which the initial imperfections will be taken.

The model tube15_buckle-topsurface is the model from linear buckling analysis. The tube model is simply copied and the following changes are made:
1. The static steps are suppressed and a Linear perturbation->Buckle step is added. The subspace solver can be used and a maximum eigenvalue can be specified.
2. Boundary condition could be applied. The loaction to apply boundary condition could adjust to meet the requirement.
3. The following keyword should be added to the input file right before the keyword *End Step:
*NODE FILE
U

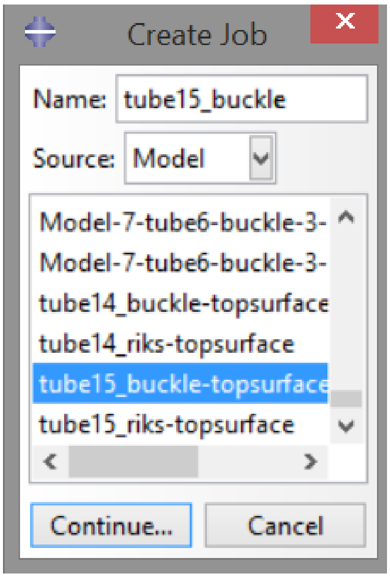

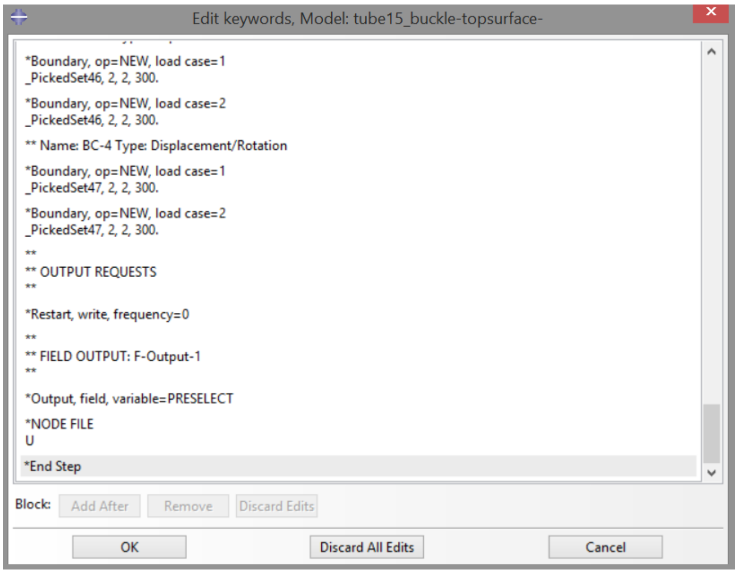

In order to do parameter study, the way of running multiple analyses is to use batch files. An input file can be created from within the graphical interface by right clicking on the job and selecting "Write Input".
Next a batch file has to be created to call this input file. The syntax is as follows:
abaqus job=name of input file cpu=number, interactive
Multiple batch files can be created which correspond to different input files. In order to call them the batch file should create in form of following:
call abaqus job=name of input file cpu=number, interactive

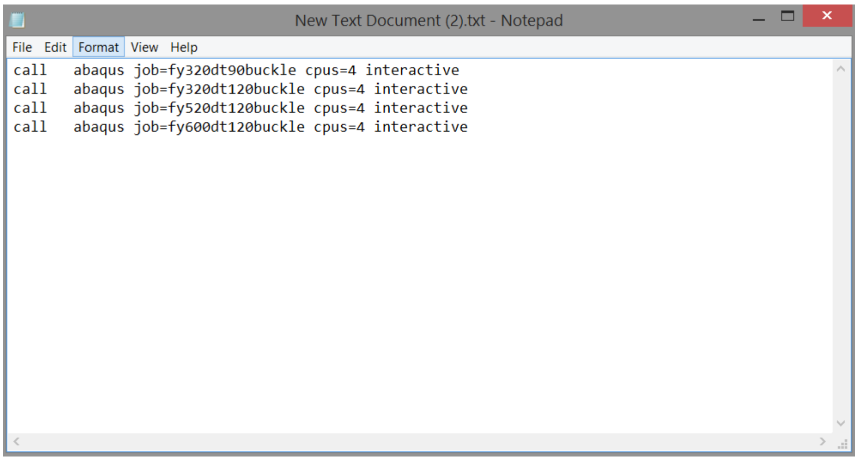

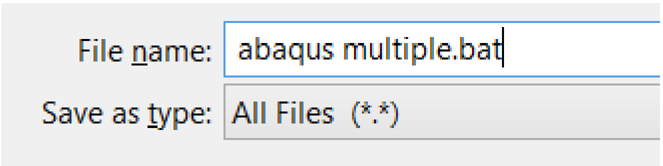

The saved batch file has to be place with abaqus job file.

Appendix C: Material model implementation by Matlab

The syntax here can be used to smoothening the material result based on four directions.

```
clear
clc
format long
strain=xlsread('Material data All tubes_New','A:A');
stress=xlsread('Material data All tubes_New','B:B');
val=strain(1);
count=1;
for i =1: length(strain)
    if val ~= strain(i)
%           strain(i)
%           val
%           val-strain(i)
        count=count+1;
        val=strain(i);
    end
end
Nstrain=zeros(count,1);
Nstress=zeros(count,1);

val=strain(1);
sum=stress(1);
num=1;
count=1;
Nstrain(count)=val;
for i=1:length(strain)
    if val ~= strain(i)
        sum=sum/num;
        Nstress(count)=sum;
        sum=stress(i);
        num=1;
        count=count+1;
        val=strain(i);
        Nstrain(count)=val;
    else
        sum=sum+stress(i);
        num=num+1;
    end
end
sum=sum/num;
```

```
Nstress(count)=sum;
subplot(1,2,1);
plot(Nstrain,Nstress);
xlabel('Nstrain','FontSize',12,'FontWeight','bold','Color','b') % x-axis label
ylabel('Nstress','FontSize',12,'FontWeight','bold','Color','b') % y-axis label

%SMOOTH THE WAVE
interval=0.0001;%Change the interval here
NCount=floor((Nstrain(end)-Nstrain(1))/interval);
Avgstrain=zeros(NCount,1);
Avgstress=zeros(NCount,1);
start=1;
for i=1:NCount
    sum=0;
    for j=start:length(Nstrain)
        if Nstrain(j)>=Nstrain(1)+interval*(i-1) &&
Nstrain(j)<Nstrain(1)+interval*(i)
            sum=sum+Nstress(j);
        else
            Avgstrain(i)=Nstrain(1)+interval*(i-1);
            if(j==start)
                Avgstress(i)=Avgstress(i-1);
            else
                sum=sum/(j-start);
                Avgstress(i)=sum;
            end
            start=j;
            break;
        end
    end
end
subplot(1,2,2);
plot(Avgstrain,Avgstress);
xlabel('Avgstrain','FontSize',12,'FontWeight','bold','Color','b') % x-axis label
ylabel('Avgstress','FontSize',12,'FontWeight','bold','Color','b') % y-axis label
```

Appendix D: Flow chart of analysis procedure

As discussed in the chapters before, the imperfection value and residual stress incoporated into non-linear analysis might not fully representitave. The numerical model could be modified and calibrated by adjusting the magnitude of imperfection and residual stress. The model can be calibrated with the help of the flow chart.